Charles University
Faculty of Science

Study programme: Developmental and Cell Biology
Branch of study: Developmental and Cell Biology

RNDr. Věra Lukášová

Cell-free scaffolds functionalized with bioactive compounds in bone tissue engineering
Funkcionalizace bezbuněčných nosičů pro kostní tkáňové inženýrství pomocí bioaktivních látek

Dissertation

Supervisor: Mgr. Michala Rampichová, Ph.D.

Prague, 2019

PROHLÁŠENÍ O AUTORSTVÍ PRÁCE

Prohlašuji, že jsem doktorskou práci na téma *Funkcionalizace bezbuněčných nosičů pro kostní tkáňové inženýrství pomocí bioaktivních látek* vypracovala samostatně na základě prvoautorských a spoluautorských publikací. Dále prohlašuji, že jsme uvedla všechny použité informační zdroje a literaturu. Tato práce ani její podstatná část nebyla předložena k získání jiného nebo stejného akademického titulu.

COPYRIGHT STATEMENT

I hereby declare that the PhD thesis named *Cell-free scaffolds functionalized with bioactive compounds in bone tissue engineering* is my own work and I have written it independently based on my first-author publications and publications I have co-authored. To the best of my knowledge, I have introduced all the information sources and literature used. This work or a substantial part of it has not been submitted to obtain another or the same academic title.

Prague, 29.9.2019 .....

ACKNOWLEDGEMENT

I would like to express my sincere thanks to those who enabled me to work independently on my PhD thesis, giving valued advice and direction. Mgr. Michala Rampichová, Ph.D. has been an excellent supervisor. I am also to Mgr. Eva Filová, Ph.D., for providing me grateful for providing me with work space and materials in the Laboratory of Tissue Engineering, the Institute of Experimental Medicine of the CAS.

This thesis was supported by the Czech Science Foundation, grants no. 15-15697S and 18-09306S.

ABSTRACT

There are good prospects for bone tissue engineering and therefore researcher is aimed towards the development of cell-free scaffolds. A cell-free scaffold serves as a temporal filling for critical size defects that do not heal spontaneously. Nevertheless, a suitable scaffold composition is yet to be discovered. Moreover, modifications of cell-free scaffolds with a drug delivery system activate the internal healing capacity. Platelets occur in the healing cascade as a natural source of growth factors (GFs), chemokines and cytokines. This autologous source of bioactive compounds enables the substitution of synthetic GFs. The aim of this thesis is to develop a bioactive cell-free scaffold with a drug delivery system supporting the physiological healing of bone defects. The centrifugal spinning method was used to produce nanofibrous poly-ε-caprolactone (PCL) scaffolds. PCL scaffolds were functionalized with different platelet concentrations. Bioactive compounds released from activated platelets were trapped within the formed fibrin net, enabling their gradual release. Improved metabolic activity, proliferation and alkaline phosphatase activity of MG-63 cells and human mesenchymal stem cells (hMSCs) were detected. The release of compounds lasted for two weeks and nearly reached the plateau phase, therefore lyophilized platelet lysate (lyophilisate) was encapsulated in the core of the PCL nanofibers to prolong the bioavailability of encapsulated compounds. An amphiphilic copolymer Pluronic F-68 was used to protect the bioactivity of the lyophilisate. The release lasted for three weeks and did not reach the plateau phase. However, released concentrations of proteins were three times lower compared to platelet adhesion with no observed effect on the osteogenic differentiation of cultured cells. In view of this, further encapsulation of diverse concentrations of osteogenic supplements; β-glycerol phosphate, dexamethasone and ascorbate-2-phosphate was performed in order to induce osteogenic differentiation. The release of these supplements lasted for a month. Induced osteogenic differentiation of cultured hMSCs and promoted osteogenic marker production in Saos2 osteosarcoma cell line were detected. Such drug delivery systems, with gradual drug release, are promising for bone tissue engineering. Moreover, the 3D fibrous morphology of the PCL scaffold ensures the maintenance of natural morphology, compared to flat 2D surfaces.

KEY WORDS: drug delivery system, cell-free scaffold, centrifugal spinning, osteogenic differentiation, osteogenic supplements, platelets

ABSTRAKT

Velká očekávání kladena na oblast tkáňového inženýrství směřují vědecké úsilí směrem k vývoji bezbuněčných nosičů. Bezbuněčné nosiče slouží jako dočasná výplň defektů kritické velikosti, které se nehojí spontánně. Doposud však nebyl vyroben nosič o vhodném složení. Modifikace bezbuněčných nosičů pomocí systému řízeného uvolňování léčiv aktivuje přirozené hojící procesy. Trombocyty jsou přírodním zdrojem růstových faktorů, chemokinů a cytokinů, které se účastní léčebné kaskády. Tento autologní zdroj bioaktivních látek je náhradou syntetických růstových faktorů. Cílem této doktorské práce je otestování bioaktivního bezbuněčného nosiče se systémem řízeného uvolňování léčiv, který by podpořil fyziologické hojení kostních defektů. Metoda odstředivého zvlákňování byla použita k výrobě vlákenných nosičů z poly-ε-caprolactonu (PCL). PCL nosiče byly funkcionalizovány různou koncentrací trombocytů. Bioaktivní látky uvolněné z aktivovaných trombocytů byly zachyceny ve vznikající trombinové síti, což následně umožnilo jejich postupné uvolňování. Bylo pozorováno zlepšení metabolické aktivity, proliferace a aktivity alkalické fosfatázy u MG-63 osteosarkomových buněk a lidských mesenchymálních kmenových buněk (hMSCs). Uvolňování bioaktivních látek po dvou týdnech dosáhlo fáze plató. Následně bylo testováno uzavření lyofilizovaného trombocytárního lyzátu do vlákenného nosiče s cílem prodloužit uvolňování bioaktivních látek. Amfipatický kopolymer Pluronik F-68 byl použit pro ochranu bioaktivity proteinů. Uvolňování látek trvalo tři týdny a nebylo dosaženo fáze plató, ovšem koncentrace uvolněných látek byla nižší v porovnání s povrchovou adhezí trombocytů. Navíc zde nebyl prokázán vliv na navození osteogenní diferenciace kultivovaných buněk. Z tohoto důvodu byly do vláken uzavřeny osteogenní suplementy, β-glycerol fosfát, dexametazon a askorbát-2-fosfát. Uvolňování suplementů trvalo měsíc. V průběhu experimentu bylo pozorování navození osteogenní diferenciace hMSCs a podpora produkce osteogenních markerů u Saos2 osteosarkomové buněčné linie. Navrhované systémy řízeného uvolňování léčiv, které postupně uvolňují bioaktivní látky, jsou slibné pro kostní tkáňové inženýrství. Navíc 3D vlákenná struktura PCL nosiče zajišťuje zachování přirozené buněčné morfologie v porovnání s morfologicky rovnými 2D kultivačními povrchy.

KLÍČOVÁ SLOVA: systém s řízeným uvolňováním léčiv, bezbuněčné nosiče, odstředivé zvlákňování, osteogenní diferenciace, osteogenní suplementy, trombocyty

TABLE OF CONTENTS

LIST OF ABBREVIATIONS

3D Three dimensional
ADP Adenosine diphosphate
ALP Alkaline phosphatase activity
asc-2-P Aascorbate-2-phosphate
bFGF Basic fibroblast growth factor
BGP Bone Gla protein
BMP-2 Bone morphogenetic protein 2
BSP Bone sialoprotein
C Carbon
cAMP Cyclic adenosine monophosphate
COX-2 Cyclooxygenase-2
CS Centrifugal spinning
CSF-1 Colony-stimulating factor-1
CSF-1R CSF-1 receptor
dex Dexamethasone
DiOC6(3) 3,3′-diethyloxacarbocyanine iodide
DMEM Dulbecco's Modified Eagle's Medium
DNA Deoxyribonucleic acid
ECM Extracellular matrix
EEF Eucaryotic elongation factor
ELISA Enzyme-linked immunosorbent assay
EMA European Medicines Agency
ES Electrospinning
FBS Fetal bovine serum
FDA Food and Drug Administration
FTIR-ATR Fourier transform infrared-attenuated total reflectance
G-CSF Granulocyte-colony stimulating factor
GF Growth factor
GM-CSF Granulocyte-macrophage colony-stimulating factor
HGF Hepatocyte growth factor
HIF-1 Hypoxia-inducible factor-1
hMSC humans mesenchymal stem cell
HRP Horseradish peroxidase
IFN-γ Interferon-γ
IGF Insulin growth factor
IL Interleukin
IL-1ra interleukin-1 receptor antagonist
IP-10 Interferon-gamma-inducible protein 10
JNK c-Jun N-terminal kinase
KGF Keratinocyte growth factor
LOQ Limit of quantification
MCP-1 Monocyte Chemoattractant Protein-1
M-CSF Macrophage colony-stimulating factor
MEM Minimum Essential Medium
MIP-1a Macrophage inflammatory protein-1a
MMP Matrix metalloproteinases
mRNA Messenger ribonucleic acid
MTS 3-(4,5-dimethylthiazol-2-yl)-5-(3-carboxymethoxyphenyl)-2-(4-sulfophenyl)-2H-tetrazolium)
NF-κB Nuclear factor kappa B

NPP1 Nucleotide pyrophosphatase phosphodiesterase

O Oxygen

OCIF Osteoclastogenesis inhibitory factor

ODAR Osteoclast differentiation and activation receptor

ODL Osteoclast differentiation factor

OPGL Osteoprotegerin ligand

OS Osteogenic supplements

P Phosphate

p42/44 ERK

P42/44 MAPK p42/p44 mitogen-activated protein kinase

PBS Phosphate buffered saline

PCL Poly-ε-caprolactone

PDGF Platelet-derived growth factor

PEG Polyethylene glycol

PEO Polyethylene oxide

PF-68 Pluronic F-68

PGA Poly-glycolic acid

PGE2 Prostaglandin E2

PI3K

PI3K Phosphatidylinositol 3-kinase

PLA Polylactic acid

PLA Poly-lactic acid

PLLA Poly-l-lactic acid

PNNP p-Nitrophenyl Phosphate

PPO Polypropylen oxide

PRF Platelet rich fibrin

PRP Platelet rich platelets

PTH Parathyroide hormone

qPCR quantitative polymerase chain reaction

RANK Receptor Activator of Nuclear Factor Kappa B

RANKL RANK ligand

RGD Arginine, Glycine, and Aspartate

RNA Ribonucleic acid

RunX2 Runt-related transcription factor 2

SD Standard deviation

SDF-1 Stromal cell-derived factor-1

SEM Scanning electron microscopy

SERCA Sarcoplasmic endoplasmic reticulum calcium ATPase

SPP1 Secreted phosphoprotein 1

TAFI Thrombin-activatable fibrinolysis inhibitor

TBS Tris buffered saline

TGF-β Transforming growth factor β

Tie2 tunica internal endothelial cell kinase 2

TNAP Tissue non-specific alkaline phosphatase

TNF Tumor necrosis factor

TRAF TNF receptor associated factor

TRAIL TNF related ligand

TRANCE TNF-related activation-induced cytokine

TRAP Tartrate resistant acid phosphatase

VEGF Vascular endothelial growth factor

W/O water in oil

w/v Weight/volume

wt% Weight percentage

β-GP β-glycerol phosphate

ABBREVIATIONS OF EXPERIMENTAL GROUPS

CSP1-CSP5 Centrifugally spun scaffold with adhered platelets, platelets concentrations were P1 - 3,000 × 10^9, P2 - 900 × 10^9, P3 - 300 × 10^9, P4 - 10 × 10^9 and P5 - 3 × 10^9 platelet/L

CSC Centrifugally spun scaffold with no adhered platelets, control group

CSNP1-P5 Centrifugally spun scaffold with adhered platelets cultivated in a growth media, platelets concentrations were P1 - 3,000 × 10^9, P2 - 900 × 10^9, P3 - 300 × 10^9, P4 - 10 × 10^9 and P5 - 3 × 10^9 platelet/L

CSNC Centrifugally spun scaffold cultivated in a growth media, control group

CSDP1-P5 Centrifugally spun scaffold with adhered platelets cultivated in a growth media with osteogenic supplements, platelets concentrations were P1 - 3,000 × 10^9, P2 - 900 × 10^9, P3 - 300 × 10^9, P4 - 100 × 10^9 and P5 - 30 × 10^9 platelet/L

CSDS Centrifugally spun scaffold cultivated in a growth media with osteogenic supplements, control group

ESNP1-P5 Electrospun scaffold with adhered platelets cultivated in a growth media, platelets concentrations were P1 - 3,000 × 10^9, P2 - 900 × 10^9, P3 - 300 × 10^9, P4 - 100 × 10^9 and P5 - 30 × 10^9 platelet/L

ESNC Electrospun scaffold cultivated in a growth media, control group

ESDP1-P5 Electrospun scaffold with adhered platelets cultivated in a growth media with osteogenic supplements, platelets concentrations were P1 - 3,000 × 10^9, P2 - 900 × 10^9, P3 - 300 × 10^9, P4 - 100 × 10^9 and P5 – 30 × 10^9 platelet/L

ESDC Electrospun scaffold cultivated in a growth media with osteogenic supplements, control group

5%-20%PF-LYO Centrifugally spun scaffolds with encapsulated lyophilisate using Pluronic F-68 in the concentrations of 0%, 5% and 10% (w/v)

PCL blend Lyo Centrifugally spun scaffolds with encapsulated lyophilisate without using Pluronic F-68

C Centrifugally spun scaffold, control group

OS1-10 Centrifugally spun scaffold with encapsulated osteogenic supplements using once (OS1), two times (OS2), five times (OS5) and ten times (OS10) concentrated osteogenic

supplements compared to generally used *in vitro* concentrations, cultivated in a growth media

CGM Centrifugally spun scaffolds cultivated in a growth media

COM Centrifugally spun scaffolds cultivated in a growth media with osteogenic supplements

INTRODUCTION

Tissue engineering is an interdisciplinary field that unites engineering and life sciences. Combined scientific and medical knowledge has led to the development of tissue replacements that improve regenerative therapies. Apart from auto- and allografts, tissue engineering is centered on cell-based therapies utilizing manufactured scaffolds. However, these methods are connected with invasive procedures and the *ex vivo* manipulation of cells. On the other hand, cell-free scaffolds could address these challenges.

In bones, critical size defects do not heal spontaneously and require filling material, namely a scaffold that would temporarily bridge the created gap. Migrating cells in the defect site could adhere on the surface of the scaffold. During the healing period, cells produce an appropriate extracellular matrix (ECM) that gradually replaces the biodegradable scaffold with the proper tissue. An ideal scaffold for bone tissue engineering should meet certain criterions, among which biocompatibility, sufficient porosity together with osteoinductivity, osteogenicity and osteoconductivity are all important.

ECM has a fibrillar structure and therefore offers contact points for cell adhesion. In addition to superior cell adhesion, fibrous scaffolds are highly porous and offer the possibility of further functionalization. Several techniques for the production of fibrous scaffolds exist. Centrifugal spinning (CS) and electrospinning (ES) are methods that produce porous nanofibrous layers with a fiber diameter ranging from hundreds of nanometers to tens of micrometers. The ES method uses a high electric field to produce fibrous layers with limited pore diameters. Alternatively, the CS method uses centrifugal force to produce scaffolds resembling three dimensional (3D) fluffy structures, enabling cells to migrate deep within the scaffold. In this thesis, both types of scaffolds were tested as a potential scaffold for bone tissue engineering.

In addition, the investigation of a suitable drug delivery system is of interest in order to specifically control bone tissue regeneration. Functionalization of the scaffolds surface and encapsulation of bioactive compounds into the core of fibers were investigated in this thesis. Both methods lead to the prolonged and sustained release of bioactive compounds. Different compounds can be used for drug delivery systems. Apart from the synthetic growth factors (compounds unlikely to be approved for medical use), synthetic molecules that could be obtained in medical grade or natural compounds such as autologous platelets could be used. Platelets are a natural source of growth factors, cytokines and chemokines that participate during bone healing - hematoma formation and inflammatory phase and

promote cell migration, adhesion and proliferation. The application of a drug delivery system into the site of the defect would help to mimic physiological healing, resulting in an improved regeneration. This system eliminates the need for repeated drug administration in supraphysiological concentrations that could be harmful for the organism. Furthermore, by eliminating the negatives related with cell-based therapies, there is potential for a more rapid application in medical practice.

The aim of the thesis is to combine the 3D structure of PCL scaffolds, produced by the CS method, with a drug delivery system in order to develop an osteoinductive and biomimicking scaffold that would be conducive to the healing of bone defects. In order to fulfill these aims, produced PCL scaffolds were used for platelets adhesion and subsequent activation. The effect of released factors was tested on the MG-63 osteosarcoma cell line and on human mesenchymal stem cells (hMSCs). For the purpose of prolonging the release of bioactive compounds either lyophilized platelet lysate (lyophilisate) or osteogenic supplements were encapsulated into the core of the PCL fibers to further promote osteogenic differentiation of seeded Saos2 osteosarcoma cell line and hMSCs.

This PhD thesis is divided into two parts, starting with the chapter *Literature review* that summarizes knowledge of bone tissue, bone healing, platelets and bone tissue engineering. The second part contains the chapter *Materials and methods*, where the procedures by which the results were achieved are described. The chapter *Results* is the output of the PhD thesis. The results from each of the experiments are summarized and accompanied with tables, graphs and figures to complete the *Results* chapter. All of the conclusions are summarized and commented on in the chapters *Discussion* and *Conclusion*.

1 LITERATURE REVIEW

1.1 BONE TISSUE

In vertebrates the mineralized connective tissue is bone. Bones enable locomotion, give the body its shape, weight support and protect internal organs against external forces. As the bones contain bone marrow, they hold the source of healing cells and are the location of hematopoiesis. Bone is a type of hard tissue. Unlike soft tissue, significant amount of water is substituted with an inorganic component of bones - crystals of hydroxyapatite which is a type of calcium phosphate. Therefore, bones maintain mineral homeostasis.

Bone formation occurs in two distinct ways, either by intramembranous ossification or by endochondral ossification. Both ossification models start with the condensation of mesenchymal stem cells (MSCs) that form the shape of the arising bone. During the intramembranous ossification, the MSCs differentiate directly to osteoblasts, this type occurs mainly in the head region [1]. Endochondral ossification occurs in the long bones and during bone regeneration. Endochondral ossification begins with the formation of cartilage template that is subsequently replaced by bone [1, 2].

Bone is composed from bone extracellular matrix (ECM) and bone cells. Two main bone cell lineages are presented in the bones, bone forming cells - osteoblasts, osteocytes and bone lining cells and bone resorbing cells – osteoclasts. These cells are responsible for the continuous remodeling of bones which continue throughout adulthood.

1.1.1 BONE FORMING CELLS

During bone formation several maturational stages of osteoblasts occur: osteoprogenitors, preosteoblasts, mature osteoblasts and osteocytes or bone lining cells (Figure 1). The distinct stages can be distinguished based on the changes in the expression pattern of specific molecules, e.g. collagen type I, osteocalcin (or bone Gla protein (BGP)), osteopontin (also called secreted phosphoprotein 1 (SPP1)), osteonectin, bone sialoprotein (BSP or IBSP) and alkaline phosphatase (ALP) activity [3].

Osteoprogenitors are committed from MSCs. MSCs are multipotent cells, of a spindle or round shape [4], with the ability to differentiate into various types of connective tissue such as osteoblast, chondroblasts, myoblasts, fibroblasts, adipoblasts or neuroblasts [4, 5]. Osteoprogenitors of a spindle shape are capable of dividing and are highly proliferative [3, 6]. Preosteoblasts of a polygonal shape typically occur in the juxtaposition

and synthetize osteopontin and in some cases also low levels of BSP that is typical for differentiated osteoblasts [3, 7]. During the proliferative phase, the expression of collagen type I also occurs, which is necessary for the later deposition of minerals within the ECM [6]. Additionally the interaction between preosteoblasts and collagen type I is mediated by α2β1 integrin, this interaction is necessary for further maturation, as this signaling activates mitogen activated protein kinase (MAPK) [8].

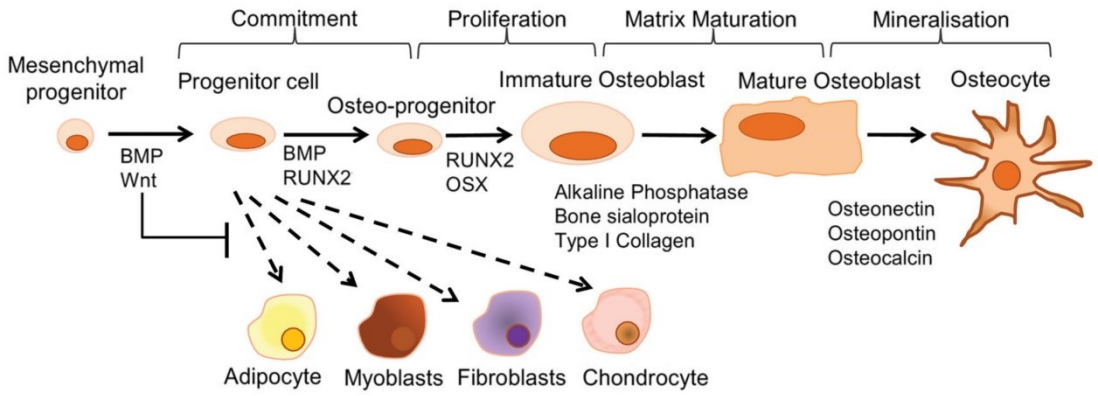

Figure 1: Osteoblast maturation - Osteoblasts undergo several maturational stages during osteogenic differentiation. Each stage is characterized by shape, cellular behavior, ECM and protein synthesis and is governed by certain signaling molecules e.g. BMPs, RunX2 or osterix. Figure taken from [9]. Abbreviations: BMP, bone morphogenetic proteins; OSX, osterix; RunX2, Runt-related transcription factor 2.

Late preosteoblasts express ALP and BSP but no osteocalcin. Furthermore an increase in ALP expression and its enzymatic activity is coupled with a decrease in proliferation [3, 6]. The expression of osteocalcin does not appear until the loss of proliferative capacity occurs, which is connected with the loss of H4 histone mRNA expression. However, a significant amount in osteocalcin expression occurs together with ECM mineralization [6]. Further differentiation results in cuboidal shaped osteoblasts that do not proliferate [3]. It would seem that either an accumulation of collagen type I or a modification of collagen type I is associated with the decline in proliferation. Moreover, a downregulation of proliferation is associated with the induction in expression of some markers associated with mature osteoblast phenotype, e.g. ALP but not osteocalcin as the expression of genes associated with mineralization can be induced after mineral accumulation [6].

Osteoblasts typically have large Golgi apparatus and rough endoplasmic reticulum. This enables them to heavily synthetize ECM proteins such as osteocalcin, BSP and osteopontin [3, 6, 7]. As mentioned in the proliferative phase, osteopontin is also expressed,

however the expression during this phase is about 4 times lower compared to the mineralization phase. The level of ALP expression and activity decreases prior to the process of ECM mineralization [6]. The last stages are spindle shaped osteocytes that are embedded in mineralized tissue and thin bone lining cells [10]. Bone lining cells are flat shaped osteoblasts covering the surfaces of the bones [11].

Osteoblasts further synthesize bone morphogenetic proteins (BMPs) that are stored within the collagenous ECM and function in activation of BMP receptors on preosteoblasts and osteoblasts. This signaling directs further maintenance of osteoblastic phenotype and the induction of osteoblastic differentiation in the surrounding preosteoblasts and MSCs [8].

Osteocytes are located within the mineralized ECM in the osteocyte lacunae [12]. They are smaller than osteoblasts, are the most abundant cells presented in the bone and they evolve a high number of filopodias and cytoplasmic extensions serving for connections with other osteocytes or bone lining cells [13]. The osteocytes are connected through canaliculi in the system called the lacunar-canalicular network [10, 12]. Osteocytes are mechanosensor cells within the bone. They experience whole bone tissue unidirectional strain (around 0.2 %) due to physiological loading [14, 15]. The strain regulates bone remodeling - osteoclasts resorbing the bone and osteoblasts forming the bone [12]. However, such a low whole tissue strain is not capable of inducing stress signaling in cells. On the other hand, higher strains from ECM deformation would result in bone fracture. Therefore, the other possible explanation is the flow of fluid in the lacunar-canalicular network that causes shear stress on the cell membrane and subsequently induces an alteration in cell signaling [16].

1.1.2 OSTEOCLASTS

Osteoclasts are cells responsible for bone resorption. They are derived from monocyte/macrophage lineage, from hematopoietic precursors. It is not however clear how the osteoclast progenitors distinguish in bone marrow from the macrophage lineage [17, 18]. Mature osteoclasts are large multinucleated cells, typically express a calcitonin receptor, tartrate resistant acid phosphatase (TRAP), cathepsin K, integrin αVβ3, c-Fms receptor, c-src signaling molecule and transcription factor PU.1, and are capable of bone resorption [19]. The process of osteoclastogenesis is driven by a group of molecules, e.g. macrophage colony-stimulating factor (M-CSF), receptor activator of nuclear factor kappa B ligand (RANKL), interleukin-1 (IL-1), -6, and -11, prostaglandin E2 (PGE2) produced mainly by stromal cells [18].

Mature osteoclasts are polarized cells with two typical membrane domains that enable osteoclasts their function in bone resorption (Figure 2). The cell polarization is enabled by a huge cytoskeleton rearrangement [20]. The first membrane structure is the professed sealing zone that is formed by actin cytoskeleton [21, 22]. Actin filaments are interconnected to the cytoskeleton via proteins such as α-actinin, talin and vinculin and also to the integrin receptors that tightly anchor osteoclasts to the bone in order to prevent the leaking of protons from resorption lacunae therefore allowing the bone resorption to occur [20, 22]. The bone resorption only occurs after actin ring and sealing zone formation [20]. The main integrin receptor in osteoclasts is αVβ3 integrin which binds the arginine, glycine, and aspartate (RGD) amino acid sequence, present e.g. in vitronectin, collagen type I, osteopontin or bone sialoprotein [20, 23].

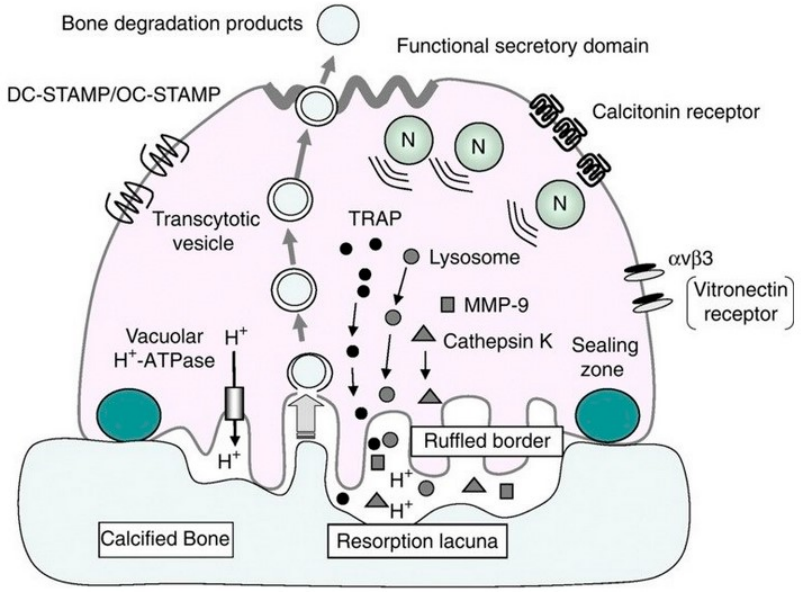

Figure 2: Osteoclast - Osteoclasts are bone resorbing cells. In order to fulfill their role tight anchoring of the osteoclasts to the mineralized bone via the sealing zone is necessary. The sealing zone enables the formation of a non-leaking border and therefore protons can create an acidic environment. An acidic environment is created in the resorption lacunae by V-ATPase and chloride channels presented in a ruffled membrane. In the resorption lacunae the bone resorption occurs either by an acidic environment that dissolves the inorganic phase of bone or by enzymes that dissolve the organic phase of bone. Figure taken from [24].

The second membrane structure is a ruffled membrane. The ruffled membrane is located within the sealing zone. This specialized structure serves as a resorptive organelle that transports the protons into the resorption lacunae, which is mediated by V-ATPases present in the ruffled membrane [21]. The ruffled membrane also has the presence of chloride channels. Vacuolar type H^+-adenosin triphosphatase together with chloride channels, create an acidic environment, ~pH 4, that dissolves the inorganic phase of the

bone and activates secreted enzymes such as TRAP. Proteolytic enzymes, e.g. cathepsin K and matrix metalloproteinases (MMPs) further degrade the organic phase of the bone. The products of degradation are endocytosed by osteoclasts [13].

Early stages of osteoclastogenesis are driven by a set of molecules such as IL-3 and -6 [18, 25]. Interestingly, IL-6 not only stimulates early osteoclastogenesis but also bone resorption in mature osteoclasts [18]. M-CSF, also known as colony-stimulating factor-1 (CSF-1) is a soluble factor produced by stromal cells upon stimulation by parathyroide hormone (PTH) [26]. c-Fms, also called CSF-1 receptor (CSF-1R), is the tyrosine kinase receptor present on osteoclast precursors. This receptor is responsible for the binding of M-CSF [27, 28]. M-CSF regulates proliferation, differentiation and fusion of osteoclast precursors [29]. c-Fms binds M-CSF that results in dimerization of the receptor and activation of its tyrosine kinase activity which leads to autophosphorylation. The autophosphorylation creates binding sites for SH2 or PTB domain containing proteins. Subsequently, phosphatidylinositol 3-kinase (PI3K) and p42/p44 mitogen-activated protein kinase (p42/44 MAPK) and other kinases are activated and further transduce the signaling. M-CSF induces the osteoclastogenesis, however direct contact of osteoclast precursors with either stromal cells or osteoblast is required [17, 19, 30].

Osteoclast precursors or mature osteoclasts have, on their surface, a receptor activator of nuclear factor kappa B (RANK) - also known as an osteoclast differentiation and activation receptor (ODAR). This receptor belongs to a tumor necrosis factor (TNF), a receptor superfamily that binds RANKL [19, 31, 32]. c-Fms and the signaling of M-CSF induce RANK expression [28]. RANK expression is stimulated by PTH, PGE2, dexamethasone, IL-1β and -11, TNFα or 1,25-dihydroxyvitamin D3. The expression is attenuated by transforming growth factor β (TGF-β) or estrogen [30, 33, 34]. In the promoter region of the RANKL gene, there is a responsive element for Runt-related transcription factor 2 (RunX2) present, indicated on osteoblastogenesis coupled with osteoclastogenesis [34]. RANK binds RANKL that is also called osteoprotegerin ligand (OPGL) or osteoclast differentiation factor (ODF) or TNF-related activation-induced cytokine (TRANCE) [19, 26, 31]. RANKL is important for osteoclastogenesis mediated by osteoblasts; RANKL signaling also inhibits osteoclasts from apoptosis [34]. RANKL exists either in soluble or transmembrane form [19, 33]. The soluble form is derived post-translationally by cleavage from the transmembrane form [34]. Upon binding of RANKL to RANK the bipotential early precursors undergo osteoclastogenesis, therefore if RANKL is not present then a macrophage is obtained [28]. Upon binding of RANKL, RANK

associates with several cytoplasmic TNF receptor associated factors (TRAFs) that subsequently activate c-Jun N-terminal kinase (JNK), nuclear factor kappa B (NF-κB), PI3K/Akt or c-src activation [32, 34]. Although, both osteoblasts and osteocytes express receptors for PTH and 1,25-dihydroxyvitamin D3, osteocytes synthesize RANKL to a greater extent compared to osteoblasts or MSCs, therefore osteocytes support osteoclastogenesis more than osteoblasts [35].

1.1.3 EXTRACELLULAR MATRIX

Bone tissue is composed of 70% inorganic components – mainly from nanocrystals of hydroxyapatite, 10% is formed of water and 20% consists of organic components that are connected with hydroxyapatite [36]. The organic phase of bone ECM is composed of 90% collagen type I that is responsible for tensile stiffness and, following mineralization, also for biomechanical properties such as load bearing [37]. The organic phase of bone ECM is composed of 10% non-collagenous proteins, e.g. osteocalcin, osteonectin, BSP or osteopontin, all of which are mainly synthesized by osteoblasts [8, 38].

In general, the interconnection of bone ECM is mediated through collagen fibrils. Collagen has a slightly positive surface at neutral pH. Non-collagenous acidic proteins, therefore interacts with the collagen surface mainly via electrostatic interactions. More acidic proteins, such as osteocalcin or BSP, have stronger binding capabilities to collagen compared to less acidic proteins, for example osteonectin [39]. The ECM is further linked to cells mainly via RGD peptide sequence that serves for αVβ3 integrin binding [40]. In the space between collagen triple helices, bone ECM mineralization occurs [41]. The nucleation process of hydroxyapatite is moderated by acidic non-collagenous proteins [42].

PROTEIN COMPOSITION

Collagen type proteins have a typical triple-helical structure with three left handed chains supercoiled into the right handed helical axis. Each of these helices has the characteristic glycine in every third position, allowing the close proximity of helices, as glycine is a small amino acid. Typically in the repeats is the presence of proline and hydroxyproline amino acids that offer stabilizing intramolecular hydrogen bounds to the triple helix. The further modification of lysine to hydroxylysine offers the possibility of intermolecular crosslinking of collagen fibrils [37]. Triple-helical structured procollagen is secreted extracellularly. Following the secretion, carboxy- and amino-propeptides are cleaved off. Hydrophobic and electrostatic interactions assist the triple-helical collagen monomer association, resulting in the formation of long fibrils (with 67 nm long repeated areas called D-period) [37, 43]. The

fibrils further occur periodically axially and laterally, forming larger fibrils of 25 - 400 nm in diameter. The MMP binding and cleavage site is presented on collagens. Collagen type I is typically formed from two α1 chains and one α2 chain [37, 43, 44].

RunX2 is a transcription factor, induction of its transcription activity is mediated by MAPK pathway which results in phosphorylation of RunX2. RunX2, upon phosphorylation, promotes the expression of osteocalcin, osteopontin and collagen type I, however represses expression of BSP [8, 45]. Upon collagen accumulation, osteoblasts start to express BMP2, -4 and -7 that are important for the induction of osteoblastic gene expression. BMPs bind to BMP receptor type II that subsequently interacts with BMP receptor type I. BMP receptors are serine/threonin kinases. Upon BMP binding, type II receptor phosphorylates type I receptor that subsequently phosphorylates Smad proteins. Smad proteins form active complexes that transduce the signal in the nucleus. As a result, transcription activation of genes, such as osteocalcin or BSP is induced [8, 46].

In general, the majority of non-collagenous proteins are acidic and phosphorylated in order to support binding to the collagen fibrils and also to enhance hydroxyapatite deposition. In addition, some of them have cell binding RGD motifs that enable cell adhesion via αVβ3 integrins. The most abundant protein in bone ECM is osteonectin, and glutamic acid residues presented on this protein serve for calcium binding [40, 47].

On the surface of osteocalcin γ-carboxyglutamic acid residues are present that are post-translationally modified, while vitamin K is necessary for its synthesis. These residues serve for calcium binding, upon which osteocalcin appears in the conformation of three alpha-helices [40]. The synthesis of osteocalcin is stimulated by 1,25-dihydroxyvitamin D3 [47].

BSP has sialic acid containing oligosaccharides. In the BSP there are also phosphorylated serine residues present, and glutamic acid residues serving for the binding of calcium and nucleation of hydroxyapatite [40]. N-terminal zone on BSP mediates binding to collagen fibrils via hydrophobic interactions. BSP also provides cells with RGD sequence for cell binding. The synthesis of BSP is stimulated by dexamethasone and is inhibited by 1,25-dihydroxyvitamin D3 [47].

Osteopontin has RGD tripeptide sequence for cell binding, phosphorylated serine and threonine residues and negatively charged aspartic acid residues, rather than glutamic acid residues present on BSP. Upon thrombin cleavage, a binding site for hyaluronate receptor (CD44) is revealed [40]. Osteopontin synthesis is stimulated by 1,25-dihydroxyvitamin D3. Osteopontin can be found in the sealing zone of osteoclasts and, as

this protein contains RGD sequence, it can serve for the adhesion of osteoclasts. Phosphorylation of osteopontin inhibits the growth of hydroxyapatite crystals, in contrast to the nucleation activity of BSP [40, 47].

PROCESS OF ECM MINERALIZATION

During the process of bone ECM mineralization the mineral-organic composite bone material is produced. Basically, hydroxyapatite crystals, composed of $Ca_{10}(PO_4)_6(OH)_2$, are deposited over the fibrillary collagen. The apatite crystals are on average 50 nm long, 28 nm wide and 2 nm thick [44, 48]. Prior to collagen mineralization, there is mineral formation [49]. This process is connected with matrix vesicles. These vesicles are small and bound to the plasma membrane of osteoblasts, chondroblasts and odontoblasts. In the membrane there are tissue non-specific alkaline phosphatases (TNAP) and nucleotide pyrophosphatase phosphodiesterases (NPP1) present, both are important for the process of mineralization. The matrix vesicles also contain annexins [50].

Pyrophosphate is an inhibitor of the mineralization process. It is produced from nucleoside triphosphate by NPP1. However, the formed pyrophosphate is hydrolyzed by the function of TNAP that decreases the pyrophosphate concentration, therefore increasing the inorganic phosphate concentration, and this then promotes the process of mineralization [50]. The phospholipids from the matrix vesicles are able to bind calcium and phosphate and thus could serve as a nucleation sites for hydroxyapatite formation. The vesicles also contain MMP-2, -3 and -13 that enable ECM remodeling prior to the mineralization process. The precise mechanism of the mineralization process occurring within the matrix vesicles and the role of collagen is still unknown, however the proposed model suggests that calcium and phosphate are transported into the vesicles and initiate the mineral formation [49, 50].

The carboxyl and carbonyl groups on the collagen are the nucleation sites for hydroxyapatite [51, 52]. *In vitro* studies suggest that firstly amorphous calcium phosphate is deposited within the collagen and subsequently it is transformed into a crystalline phase [53]. However, collagen is not capable of inducing nucleation of hydroxyapatite crystals [41, 44]. Non-collagenous proteins sequestrate and stabilize the calcium phosphate in order to initiate the nucleation of hydroxyapatite and its deposition within the gaps occurring in the collagen fibrils. For example BSP, upon binding to collagen, increases its hydroxyapatite binding potential [41, 48].

1.1.4 BONE ANATOMY

Bone is composed from collagens, non-collagenous proteins and hydroxyapatite. The complex structure of bone is important to fulfill different functional demands. Microscopically we can divide the bone into woven and lamellar [13, 44]. Hierarchically the bone is divided into macrostructures (cortical, cancellous bone), microstructures ranging from 10 μm - 500 μm (osteons, Haversian systems, trabeculaes), sub-microstructures ranging from 1 μm - 10 μm (lamellae), nanostructures ranging from 100 nm - 1 μm (collagen fibrils) and subnanostructures below 100 nm (minerals, collagen molecule) (Figure 3) [54, 55].

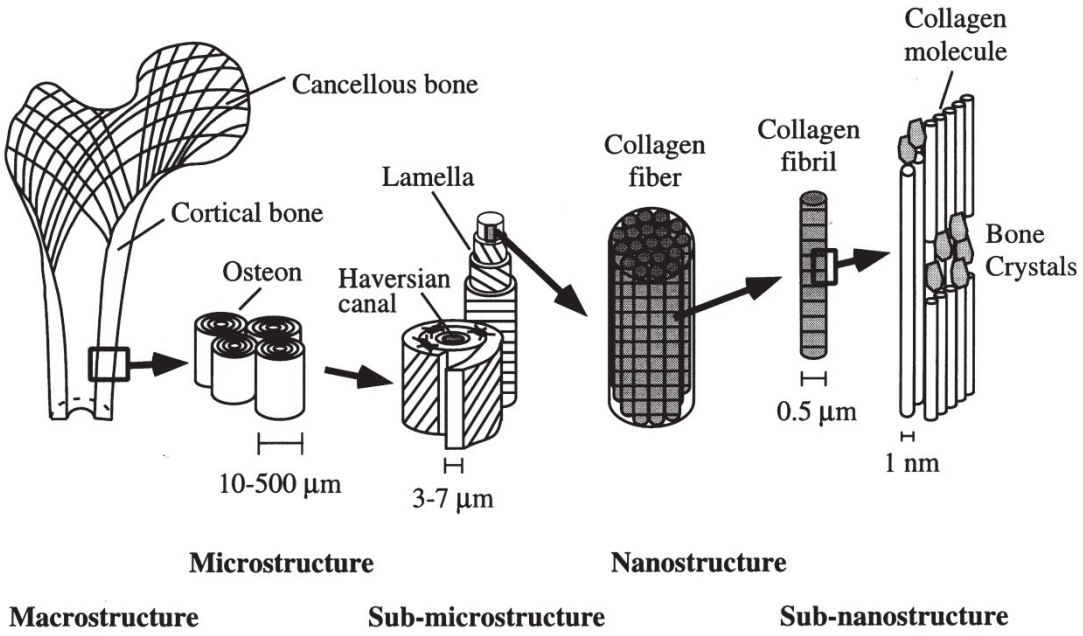

Figure 3: Bone hierarchy – Complex structure of bone is divided into macro-, micro-, submicro, nano- and subnanostructures including cortical bone, osteons, lamellae, collagen and minerals, respectively. Figure taken from [54].

WOVEN BONE

The woven bone is typical for embryonic and fetal development but it can be found in adult tissue as well, in the ligaments and tendon insertions. Furthermore, the woven bone in adults could be provisionally present after bone fracture healing when a temporary callus is formed, yet the woven bone is replaced within a few weeks by the lamellar bone [13]. In pathophysiological conditions the woven bone is present in osteogenic tumors and metastasis. The woven bone is less structurally designed compared to the lamellar bone. The collagen fibrils within the woven bone are disorganized, therefore the hydroxyapatite crystals are also less ordered [13, 44].

LAMELLAR BONE

Remodeling of the woven bone upon mechanical stimulation leads to lamellar bone formation [13]. From mechanically stimulated bone the prostaglandins are released. As a consequence, β-catenin is active through PI3K/Akt pathway which is activated by released PGE2 and the bone mass therefore increases [56]. The lamellar bone is a mature bone, consisting of the lamellae of calcified extracellular matrix. It can be found in both the cortical (compact) and cancellous (spongy or trabecular) bone [13, 57]. The cortical bone is composed from osteons that consists of layers of lamellae coaxially arranged around the Haversian canal that contains a blood vessel [13, 58]. Primary and secondary osteons can be distinguished. Primary osteons are formed de novo from the woven bone while secondary osteons are formed as a consequence of bone remodeling [13].

Alternatively, cancellous bone is a 3D porous network composed of trabeculae (lamellae) that group as they reflect the stress lines. The bone marrow and the vessels are situated between the trabeculae. The trabecular bone also contains less hydroxyapatite compared to the compact bone [57, 59].

1.1.5 BONE REMODELING

Bone is a dynamic tissue and therefore bone remodeling is a naturally occurring process. It takes part during the longitudinal bone growth in the region of metaphysis and diaphysis [13]. Throughout adulthood, the bone remodeling also deals with the removal of old bone tissue by the osteoclasts while new bone formation is provided by the function of the osteoblasts. As a consequence, the microcracks within the bones, originated from the natural bone loading forces, are repaired [60]. The bone remodeling further serves to adapt the bones to the loading changes or to react to the metabolic demands [13]. In the trabecular bone every year approximately 25% of bone tissue is remodeled as the trabecular bone poses a high volume to surface ratio while it is only 3% of the cortical bone [18]. A mature osteoclast is able to resorb 200,000 μm^3 of bone mass per day. The process of bone remodeling is orchestrated by a set of GFs, cytokines and hormones. As a consequence of signaling dysregulation, the pathophysiological state, e.g. osteoporosis, can evolve [13].

RANKL can be bound not only by RANK but also by a soluble glycoprotein receptor called osteoprotegerin (OPG or osteoclastogenesis inhibitory factor (OCIF)) (Figure 4) [26, 30]. OPG is secreted by stromal cells and osteoblasts [30, 61]. Its expression is stimulated by IL-1α and -1β, TNF-α and –β, 1,25-dihydroxyvitamin D3, BMP-2 or by estrogen and TGF-β and decreased by glucocorticoids and PGE2 [34]. It belongs to the TNF receptor

superfamily [62]. OPG binds to RANKL and therefore competes with RANK concerning binding to RANKL. This OPG-RANKL interaction prevents RANKL from binding to RANK and induces the inhibition of osteoclast terminal differentiation, activation and apoptosis [34, 63]. Therefore, OPG increases the bone density. OPG also binds TNF-related ligand (TRAIL) and blocks its antiosteoclastogenic activity [26].

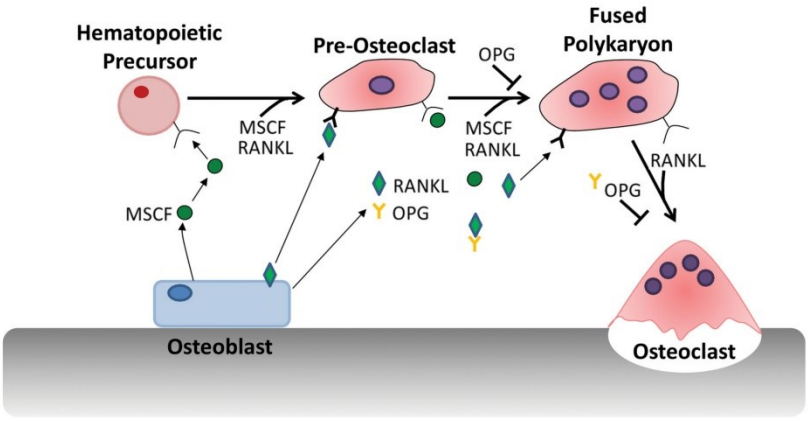

Figure 4: Osteoclast differentiation – Osteoclasts are differentiated from hematopoietic precursors. The whole process is driven by a set of molecules that induce osteoclastogenesis. Between these molecules belong M-CSF, RANKL and OPG. RANK and OPG are both capable of binding RANKL which results in the dynamic regulation of the osteoclast differentiation. Figure taken from [9].

OPG was shown *in vitro* to be upregulated by PGE2 and downregulated by IL-1α and TNF-α and –β. PTH has a calcemic effect as it regulates serum calcium. PTH stimulates mRNA expression for RANKL and inhibits mRNA expression of OPG [26, 30]. As a consequence of estrogen deficiency, there is an increase in the production of IL-1, TGF-β, TNF-α, PGE2 and M-CSF. These pro-resorptive cytokines affect osteoclast activation and the inhibition of apoptosis [34]. Sclerostin is a secreted glycoprotein secreted by osteoblastic cells, mainly by osteocytes. It is a BMP antagonist with the affinity to bind BMP receptor type I and II. Upon binding, the Wnt signaling pathway is inhibited. As a result, the osteoblastic differentiation and mineralization are inhibited, causing a decrease in bone mass [64].

Osteoclasts are motile cells that transmigrate through blood vessels and migrate through the bone ECM to the site of future bone resorption [23, 65]. Stromal cell-derived factor-1 (SDF-1 or CXCL12) is a chemokine expressed by osteoblasts, stromal marrow cells and endothelial cells lining the blood vessels in the bones. The SDF-1 receptor called CXCR4, is expressed on the hematopoietic progenitor cells and its expression decreases, along with cell differentiation. The binding of SDF-1 to its receptor induces chemotaxis, cytoskeletal remodeling and the upregulation of MMPs and integrins, and all of this is

necessary for cell migration [66]. MMPs are zinc dependent endopeptidases crucial for enabling the migration of osteoclasts [25, 67]. For example, MMP-12 cleaves osteopontin and BSP, both involved in osteoclasts adhesion and spreading [67]. During bone resorption, MMP-2, -9 and 13 were mainly shown to be responsible for the resorption of the organic phase of bone. The expression of MMPs is regulated by IL-1 and -6 signaling [25]. Furthermore, PGE2 stimulates the expression of MMP-2 and -13 in periosteoclastic cells, e.g. osteoblasts or mononuclear cells [23]. MMP-9, -12 and -14 are expressed by osteoclasts [25, 65, 67]. MMP-9, -12 and -14 activate TNF-α which is a pro-osteoclastic agent [67]. MMP-9 activity is stimulated by RANKL and SDF-1, therefore its signaling triggers the migration of preosteoclasts. Moreover MMP-9, upon cleaving of ECM, releases vascular endothelial growth factor (VEGF) bounded in ECM, subsequently the capillary invasion is promoted and thus bone remodeling can occur [66].

Bone resorption is mediated by two groups of enzymes; cysteine proteinases produced by osteoclasts and MMPs produced by both osteoblasts and osteoclasts [25, 68]. To begin with, osteoclasts migrate through the bone ECM and degrade collagens by MMPs that function at physiological pH; subsequently the bone resorption occurs [66]. Bone resorption takes place in the extracellular space surrounded by the ruffled border of osteoclasts, in the resorption pit where acidification of the extracellular space is necessary for the function of cysteine proteinases. The presence of protons acidifies and solubilizes minerals in the subosteoclastic resorption zone, leaving the organic phase available for the proteinase degradation [65].

Cathepsin K is a cysteine proteinase, its expression is stimulated by RANKL signaling [65, 66]. Cathepsin K cleaves triplehelical collagen, but only in the presence of glycosaminoglycans associated with collagen [69]. Homodimers of cathepsin K form a high molecular weight complex with glycosaminoglycans and cleave the collagen triple helix [65, 69]. The triple helix of collagen, upon cleaving, is unwound and susceptible for other proteinases, e.g. cathepsin B, H and L [65]. Collagen type I contains various RGD amino acid sequences that accumulate upon cleavage of collagen type I. The RGD peptide accumulation consequently inhibits the bone resorption activity of osteoclasts in an autocrine manner, as the integrin receptors are reorganized and the disruption of the actin ring, forming the sealing zone, occurs [20]. In the absence of glycosaminoglycans, the cathepsin K cleaves only gelatinases and telopeptides [69].

Bone ECM degradation further leads to the release of calcium that inhibits osteoclasts activity via binding to calcium receptors [70]. The degradation of the collagen

network by osteoclasts, leads to the release of insulin growth factor (IGF) that is bound to the ECM. Released IGF later stimulates osteoblastic activity and new bone formation [37].

1.2 Bone Healing

Bone tissue has the regenerative capacity to heal fractures without forming a fibrous scar, thus the bone tissue is restored to its original physical and mechanical properties. However, bone healing is a complex process that can result in delayed healing, non-unions and structural abnormalities [71]. The fracture heals either directly (primary healing) or indirectly (secondary healing). Direct healing is rare and only occurs in the absence of gap formation and with stable fixation, mainly after surgery. On the other hand, indirect healing occurs when bone fragments are unstable and temporary callus from fibro-cartilaginous tissue is formed [71, 72].

The fracture healing process consists of both endochondral and intramembranous ossification [71]. The fracture area can be divided into four zones: medullary canal, area between cortices, sub-periosteal area and surrounding soft tissue. Medullary canal and the area between cortices heal by endochondral ossification as it firstly creates the soft callus. The sub-periosteal area and surrounding soft tissue around the fracture site heals by intramembranous ossification and form hard callus [73]. Bone healing can be divided into distinct stages that occur after trauma and overlap with each other (Figure 5). These stages are initiated by the inflammatory stage followed by the repair stage and lastly the stage of hard callus remodeling occurrence [71, 72]. Weight bearing and motion can enhance healing but only to certain limits, otherwise the process of healing is altered [71].

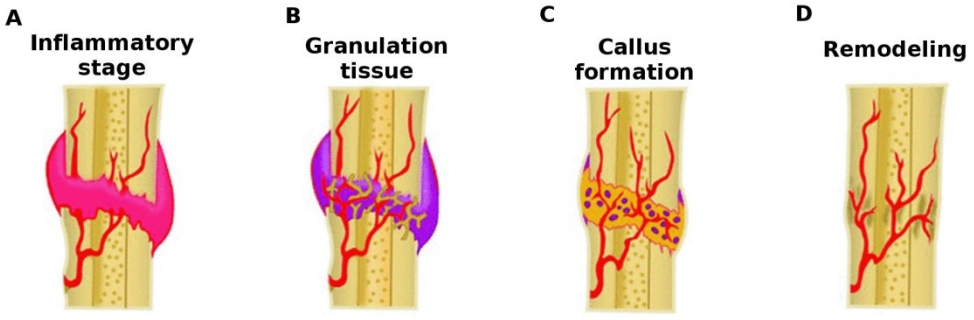

Figure 5: Bone healing: Inflammatory stage (A) – hematoma is formed by immune cells and bone marrow cells. Coagulation cascade is initiated and platelets release their granules. Granulation tissue formation (B) – MSCs and fibroblasts migrate to the fracture site, capillaries start to ingrow and the fibrin rich granulation tissue is formed. Callus formation (C) – MSCs firstly differentiate into chondroblasts and cartilaginous soft callus is formed. Chondroblasts undergo hypertrophy, therefore the soft callus is subsequently replaced by woven bone hard callus. Remodeling (D) – Woven bone

hard callus is replaced by lamellar bone during the orchestrated function of osteoclast resorbing the woven bone and osteoblasts laying the lamellar bone. Adapted from [74].

1.2.1 INFLAMMATORY STAGE

The inflammatory stage is initiated by disrupted blood vessels in the trauma site. Coagulation forms the hematoma from immune cells and bone marrow cells, and at the same time the platelets de-granulate [71-73]. The rapid inflammation response is initially isolated from the rest of the tissues, as the trauma site is avascular, in order not to infect the rest of the body [75]. The same cascade that activates the hematoma formation activates the inflammatory cells as well [72]. The hematoma coagulates at the ends of the fracture preparing the template for callus formation. The migration of MSCs and fibroblasts from the surrounding tissue, e.g. bone marrow, periosteum and circulation, occurs. These cells, together with the capillaries, grow into the hematoma and produce fibrin rich granulation tissue [71]. All of these events are orchestrated by a number of produced cytokines and growth factors (GFs).

Platelets present in the hematoma are a source of variety of GFs and at the fracture site they are activated either by sub-endothelial collagen or by tissue factor and thrombin [76]. Platelets mainly release TGF-β and platelet-derived growth factor (PDGF). These initiate MSCs migration and proliferation, induce angiogenesis by the stimulated secretion of VEGF by pericytes, and serve as chemotactic agents for inflammatory cells and help platelets to aggregate [75, 76]. Therefore, these GFs are important for the initiation of fracture repair. Furthermore, platelets release IGF-1 and -2 or EGF that stimulate MSCs and osteoblasts proliferation and differentiation [73]. In the 24 hours following the trauma, the secretion of pro-inflammatory molecules reaches its peak and declines within a week [71, 72]. Moreover, neutrophils, and subsequently macrophages migrate to the fracture site 24-96 hours after the injury. These cells serve as phagocytic cells in the debridement process that also prevents infection occurrence in the wound. Macrophages produce TNF-α, TGF-β, IL-1, -6, -8, -12, TGF-β, PDGF, IGF-1 and nitric oxide [72]. At the same time BMPs are released from migrated MSCs and from the surrounding bone ECM [76].

TNF-α is expressed by inflammatory cells (macrophages, monocytes and lymphocytes), it is a chemoattractant for the cell migration to the site of injury. Macrophages produce IL-1 that induces the production of IL-6 in the osteoblasts [71]. IL-6 then stimulates VEGF and IL-17 production, angiogenesis and the differentiation of both osteoblasts and osteoclasts [71, 77, 78]. IL-1β has been shown to stimulate proliferation and mineralization in preosteoblasts but inhibit these processes in MSCs [79]. Moreover,

activated T-lymphocytes produce TGF-β, interferon-γ (IFN-γ), IL-4, -10 and -17 that inhibit osteoclastogenesis. IL-4 also serves as a chemoattractant for osteoblasts [72]. IL-17 stimulates osteoblast maturation [78, 80]. IFN-γ induces the expression of inducible nitric oxide synthases that produce nitric oxide in macrophages [72].

The inflammation also induces the expression of cyclooxygenase-2 (COX-2). This enzyme, together with COX-1, is responsible for converting prostaglandins from arachidonic acid that is released by phospholipases from the membrane phospholipids. The COX-1 enzyme is expressed constitutively by many tissues. On the other hand, COX-2 is mainly expressed after pro-inflammatory stimuli [81]. The receptors for prostaglandins, G protein-coupled receptors, are expressed on MSCs, osteoblasts and osteoclasts. These receptors stimulate the production of cyclic adenosine monophosphate that activates signaling by protein kinase A [81, 82]. COX-2 together with PGE2, inhibits OPG secretion and stimulates RANKL and RANK expression; moreover IL-6 stimulates PGE2 production and prostaglandin receptor expression (specifically EP4 subtype) [82]. Therefore, a deficiency in COX-2 results in delayed fracture healing as the prostaglandins stimulate both bone formation as well as bone resorption [81, 83].

Hypoxia, occurring after the bone fracture induction, is also responsible for the homing of MSCs to the fracture site. The homing is mediated by an increase in the expression of SDF-1 [71]. SDF-1 expression is regulated by the transcription factor hypoxia-inducible factor-1 (HIF-1) in endothelial cells, as a result of reduced oxygen tension [84].

1.2.2 REPAIR STAGE

Following the inflammation, intramembranous and endochondral ossification take place. The intramembranous ossification comprises of direct osteogenic differentiation of the osteoprogenitor cells which remain in the periosteum [85]. In general, the osteogenic differentiation of cells is directed by BMPs (mainly BMP-2, -4, -6, -7 and -9) [73] that are produced by MSCs and also further by inflammatory cytokines such as TNF-α, TGF-β, IFN-γ [85].

During endochondral ossification, the cartilage is formed first. MSCs differentiate into chondroblasts that produce the cartilaginous ECM (mainly consisting of collagen type II). Cartilaginous ECM then replaces the fibrin rich granulation tissue [85, 86]. These events are triggered by TGF-β2 and –β3, FGF-1, IGF and BMP-2, -4, -5 and -6 [86]. The fracture is mechanically supported by the cartilage, the soft callus. Chondrocytes undergo

hypertrophy and the ECM becomes consistently preferential of collagen type X and undergoes calcification and invasion by blood vessels [85]. Hypertrophic chondrocytes are removed by chondroclasts and MSCs migrate to the sites of hypertrophy.

Subsequent to the endochondral ossification, MSCs undergo osteogenic differentiation and form woven bone [85]. The woven bone hard callus formation occurs from peripheral callus where stability of the fracture is secured. The previous soft callus is removed as angiogenesis begins. This stage is also referred to as primary bone formation. In the places where no soft callus is formed, hard callus is formed by intramembranous ossification [86].

The angiogenesis is an important event in the process of bone healing as the vessels maintain the oxygen homeostasis, enable recruitment of the cells and deliver the nutrients and ensure the removal of waste products. VEGF, produced by osteoblasts under the control of RunX2 transcription factor, is bound by the VEGF receptor 2 and angiopoietin 1 is bound by tunica internal endothelial cell kinase 2 (Tie2). Both receptors are expressed on the endothelial cells and they secure cell proliferation, angiogenesis, survival and endothelium integrity. Angiopoietins mainly regulates larger vessels and branching. The signaling can be negatively regulated by VEGF receptor 1 or by angiopoietin 2 [87]. In addition to these two factors, FGF-1 and -2, BMPs, TGF-β and cysteine-rich protein 61 also promote angiogenesis [86].

The formation of woven bone is triggered by highly active osteoblasts. The presence of blood vessels is crucial as the osteogenic differentiation of osteoblasts is triggered by increased oxygen tension. The process of mineralization of hard callus ECM begins from the periphery, from the sites with the stability [86].

1.2.3 REMODELING STAGE

The remodeling stage is important for woven bone hard callus to be converted into original lamellar bone. This stage is also called secondary bone formation. The migrating osteoprogenitors most likely originate from bone marrow and periosteum and they migrate into forming hard callus [86]. Therefore, it is not mature osteoblasts but progenitors that migrate to the callus site [88]. The bone remodeling includes bone resorption, performed by osteoclasts, and then followed by lamellar bone formation, at the same time angiogenesis still proceeds [86].

1.3 PLATELETS

Platelets are anucleated, approximately 2-3 μm in diameter small circulating cells. They are derived in bone marrow from giant precursor cells – mature megakaryocytes, in a process called thrombopoiesis [89, 90]. Each megakaryocyte is able to release 10^2–10^3 of platelets. Consequently each megakaryocyte undergoes apoptosis and is engulfed by macrophages [89, 91]. The apoptotic events, such as cytoskeletal reorganization, membrane condensation and ruffling, seem to be important for platelet production [92]. The main role of platelets is during the hemostasis, however platelets have a broad scale of other functions, e.g. the initiation of inflammation, angiogenesis or immune related functions. The platelets lifespan is 8-10 days. In human the average platelet concentration is 150-400 × 10^9 per liter of blood [93, 94].

Megakaryocytes are myeloid cells that can preferably be found in bone marrow. Megakaryopoiesis is a process of megakaryocyte maturation from hematopoietic stem cells [92]. Thrombopoietin (also named megakaryocyte growth or development factor) not only supports the maturation and fragmentation of megakaryocytes but also the proliferation and survival of hematopoietic stem cells; all carried out together with erythropoietin, IL-11 or stem cell factor [93]. During the megakaryocyte maturation the cells are enlarged, up to 100 μm in diameter, and filled with ribosomes which enable the production of platelet specific proteins. During maturation megakaryocytes pass several rounds of endomitosis to amplify their DNA which is regulated by thrombopoietin. Therefore, the mature megakaryocyte is a polyploid cell with DNA content in the range from 4N to 128N [92]. The last stage of megakaryocyte maturation is the thrombopoiesis.

1.3.1 THROMBOPOIESIS

The exact mechanism, how the platelets are released, has not yet been proposed. However, there are several theories including megakaryocytes fragmentation and proplatelet formation.

FRAGMENTATION

The formation of platelets by the process of fragmentation is an older theory compared to proplatelet formation. Megakaryocytes are extended towards the vasculature in the bone marrow, however the platelets are formed individually and do not form proplatelets. The surface of the megakaryocyte is increased and the cytoplasmic membrane, after internalization, forms together with membranes of Golgi apparatus and endoplasmic

reticulum, the demarcation membrane system. The demarcation membrane system defines the evolving platelets [95].

PROPLATELET FORMATION

The more recent theory suggests that megakaryocytes form proplatelets (Figure 6) [89, 91]. Proplatelets are formed as the megakaryocytes elongate towards the bone marrow where they access the vasculature under stimulation by thrombopoietin [89, 90]. Thrombopoietin is an acidic glycoprotein, responsible for thrombopoiesis. This hormone is produced in kidney and the liver, but also by bone marrow stromal cells. Megakaryocytes and platelets have c-Mpl receptors for thrombopoietin. IL-6, FGF2 and PDGF increase the level of thrombopoietin, while platelet factor 4, thrombospondin and TGF-β decrease its level [93].

During the process of proplatelet formation, the cytoskeleton is highly reorganized. Microtubules move to the cortex of megakaryocytes causing local bulging of the cytoplasm. As a consequence, pseudopodia emerge and further elongate and subsequently bend and re-enter the formed shaft of proplatelets and then loop again. The goal of this repeated bending is to multiply the proplatelet ends that are formed from the majority of megakaryocytes cytoplasm. The process of bending is dependent on actin filaments [89, 91]. Finally, the proplatelets are fragmented and platelets are formed [93]. Along the microtubules there is a transport of organelles and granules specific for platelets. The appearance of this transport is necessary before the platelets are released from the proplatelets into the blood stream [92].

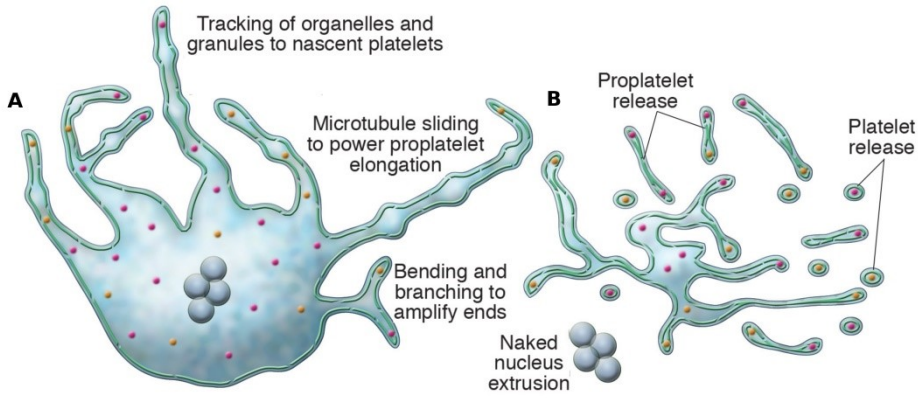

Figure 6: Platelet formation – During platelet formation the megakaryocyte elongates, forming proplatelets, which is stimulated by thrombopoietin (A). Due to enormous cytoskeleton reorganization the proplatelets are multiplied and fragmented, forming platelets. As a consequence, the majority of megakaryocyte's cytoplasm is remodeled into the platelets and the remaining megakaryocyte undergoes apoptosis (B). Figure adapted from [92].

1.3.2 PLATELET CONTENT

Platelets are composed from cytoplasmic part and granules. Platelets evince a complex structure divided into four parts. The first zone is called the peripheral zone. It is composed from inert and extracellular membranes and is covered by glycocalyx [94]. There is an open canalicular system present, it is an internal membranous system that is responsible for the exchange of molecules, mainly in the phase of platelets activation [94, 96]. The platelet membrane is rich in glycoproteins and receptors that serve for adhesion and activation events [94].

The second zone is the sol-gel zone. It is composed form actin cytoskeleton and microtubules beneath the peripheral zone. Microtubules preserve the discoid shape of platelets, while actin cytoskeleton acts in the change of the platelets shape during activation [94].

The third zone is the membrane zone, consisting of an endomembrane system called a dense tubular system which stores calcium ions and enzymes, including adenylate synthase, which are necessary during the platelets activation [94, 96]. The membrane zone originates from the megakaryocyte endoplasmic reticulum. It is located near the microtubules. It is the location of thromboxane A2 synthesis by thromboxane synthase which is dependent on COX-1 function [96].

In the center of the platelets is the organelle zone. It contains α-granules, dense granules (δ-granules) and cellular content such as lysosomes (λ-granules), which contain digestive enzymes and mitochondria necessary to maintain the platelets energy (Figure 7) [94, 96]. Dense granules are the smallest types of granules (92). They are non-proteins as they contain adenosine triphosphate, adenosine diphosphate (ADP), serotonin, and calcium ions [94]. However, the calcium ions in the dense granules are not mobilized for the platelet activation, but they interact with serotonin and adenine nucleotides [96].

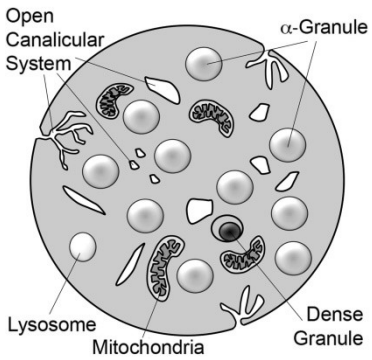

Figure 7: Platelet's granules – Platelets within its organelle zone contain α-granules, dense granules (δ-granules), lysosomes (λ-granules) and mitochondria - all of these are necessary to

execute their function during the hemostasis, initiation of inflammation or angiogenesis. Figure taken from [97].

α-GRANULES

α-granules are the major type of granules within platelets. They are 200-400 nm spherical single membrane granules. α-granules are originally presented as small and immature in the megakaryocytes and they are enlarged together with megakaryocyte maturation. Some of the protein content is synthesized by megakaryocytes and some of the proteins are endocytosed from the plasma, either by megakaryocytes or by the platelets. The low concentration proteins such as albumins or immunoglobulins are endocytosed passively, and the rest by receptor mediated endocytosis [96].

α-granules contain proteins necessary for providing platelets with important roles during inflammation, hemostasis, and wound healing [96]. As the platelets lack the nucleus, their proteome is stable with more than 5,000 different proteins [98]. For example α-granules contain proteoglycans, adhesive proteins, coagulation factors, mitogens, chemokines, cytokines, angiogenic factors as well as anti-angiogenic factors or inhibitors of proteases [96, 99]. Proteoglycans secure the α-granules stability [96]. GFs contained in the α-granules are e.g. PDGF, VEGF, EGF, IGF, TGF-β, FGF, HGF or endothelial cell growth factor [96, 98, 100]. Among the adhesive proteins are von Willebrand factor, fibrinogen, fibronectin, thrombospondin, albumin [98, 99]. Protease inhibitors are plasminogen activator inhibitor 1, α_1-protease inhibitor, the tissue factor pathway inhibitor, the platelet-derived collagenase inhibitor and the platelet inhibitor of factor XI [96]. In the membrane guanosine triphosphate binding proteins important for the regulation of secretion are present. P-selectin, a major protein is further presented in the membrane along with vitronectin, osteonectin, a platelet endothelial cell adhesion molecule or glucose transporter GLUT3 [96].

1.3.3 PLATELET ACTIVATION

As mentioned in the chapter *Bone healing*, platelets are an important part of the inflammation stage occurring right after the bone fracture injury. The coagulation cascade is a series of steps including several enzymatic conversions. It is composed of three phases: initiation, amplification and propagation [101].

INITIATION PHASE

The initiation of the coagulation cascade begins with the exposure of damaged tissue to the blood. Tissue factor is a transmembrane glycoprotein expressed constitutively by

extravascular tissue mainly in the perivascular tissue [101]. Tissue factor forms an extrinsic tenase complex with factor VIIa which could be neutralized by the tissue factor pathway inhibitor [102]. The neutralization particularly occurs on free circulating complexes, therefore preventing initiation of coagulation from the places where no cells expressing tissue factor are present. The complex of tissue factor and factor VIIa activates zymogens - factor X and factor IX. Factor Xa then generates serine protease thrombin (factor IIa) from prothrombin (factor II) [101, 102]. Damaged tissue further exposes subendothelium collagens that bind to the receptors on the platelet surface and which then result in the activation of integrin αIIbβ3 that binds fibrinogen and α2β1 integrin that binds collagen [94, 103].

AMPLIFICATION PHASE

The amplification phase is important for accelerated thrombin production. Factor XIa forms an intrinsic tenase complex with factor VIIIa, this increases the production of factor Xa. As a result more thrombins are activated. Thrombin then binds to its membrane receptor GpIb on platelets which interacts with protease-activated protein-1 which causes the degranulation of the α-granules, expression of membrane bound factor Va and activation of GIIb/IIIa receptor (receptor for fibrinogen) [101]. Following this, the platelets start to aggregate and negatively charged phosphatidylserine is exposed in the outer cell membrane. Thrombin further liberates factor VIIIa from the complex with von Willebrand factor and also activates additional factor XIa [101]. Platelets binds the exposed laminin, fibrin, collagen (receptors GPVI, α2β1 integrin), von Willebrand factor (receptor GpIb), thrombin, ADP and thromboxane A2, which activate other integrin receptors and initiate the remodeling of cytoskeleton, platelet activation and release of ADP and calcium ions (Figure 8) [94, 104].

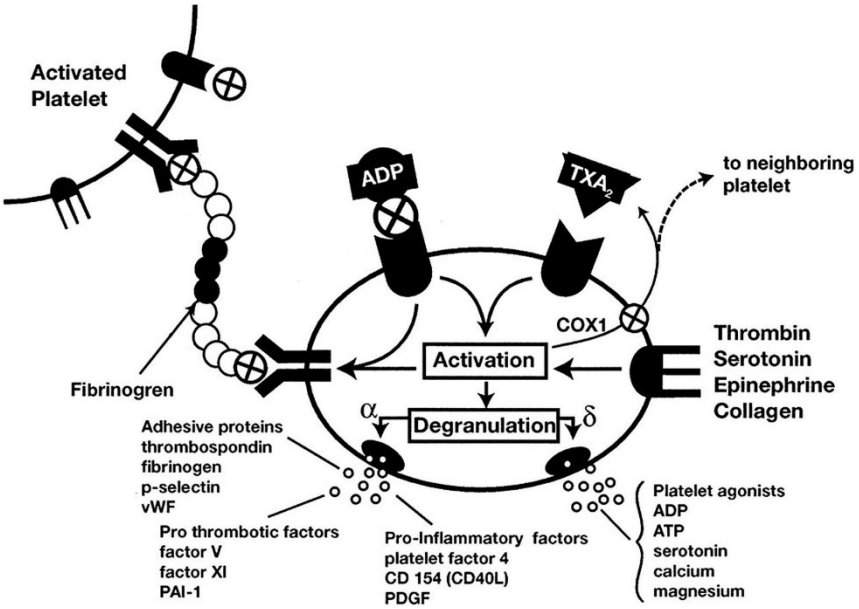

Figure 8: Platelet activation – Platelets circulate in the blood stream intact. However, the platelets are activated after the damaged tissue occurs. The exposure of platelets to the tissue factor or by sub-endothelium laminin, fibrin and collagen, lead to the binding to the platelets surface receptors which result in the platelets activation. Activated platelets release their granules that among other proteins contain von Willebrand factor, thrombin, ADP and thromboxane A2 which further amplifies the activation. Released coagulation factors start the coagulation cascade that activates thrombin which initiates the fibrin clot formation. Figure adapted from [105].

The rupture of the membrane is not necessary for the release of granules. During the release, the membrane integrity is maintained [94]. The myosin light chains, upon phosphorylation, direct the release of granules from the platelets through an open canalicular system or by the fusion of the granules with a plasma membrane [94, 100]. Thromboxane A2 is released during platelet activation and, after binding to its receptor on the platelet surface, it triggers further platelet activation. Calcium ions stored in a dense tubular system after mobilization, which is controlled by a sarcoplasmic endoplasmic reticulum calcium ATPase (SERCA), activates phospholipase A2, light myosin chain kinase and calpain, all of which are important for platelet activation. SERCA is coupled with plasma membrane calcium ATPase that is controlled by cyclic adenosine monophosphate (cAMP) level. When the cytosolic concentration of cAMP decreases it causes the liberation of calcium ions during the platelet activation [96]. Activated platelets express P-selectin on the surface, an adhesion molecule that interacts with P-selectin glycoprotein-1 on immune cells which induces a pro-inflammatory response [100, 104].

PROPAGATION PHASE

During the propagation phase it is important to recruit other platelets into the site of the injury and to specifically localize the platelets. This is secured by the production of thrombin, calcium and a specific phospholipid composition of the outer membrane. After sufficient amplification of platelets in the site of injury, thrombin generates fibrin from fibrinogen, therefore a fibrin clot is formed [101, 102]. Factor XIIIa then covalently crosslinks the fibrin monomers. Thrombin also activates a thrombin-activatable fibrinolysis inhibitor (TAFI) that serves as a regulator of fibrin clot formation. TAFI proteolytically excise lysine residues that serve for the binding of plasmin. Therefore, plasmin is unable to bind to the fibrin clot and proceeds to its lysis [101, 102].

1.4 BONE TISSUE ENGINEERING

Bone tissue engineering is a multidisciplinary field that is concerned with alternative strategies to the gold standard – use of bone autografts (from fibula, iliac crest or ribs), to restore the bone tissue after the injury. The bone has the capacity to self-regenerate, however the bone defects originated from tumor reconstructions, chronic infections, neoplasm, failed arthroplasty or trauma can exceed the critical size of the defect [44, 106]. The critical sized defect is defined as 2.5 times bigger than the bone radius. The spontaneous bone remodeling which results in the restoration of the original bone tissue does not occur during the critical size defect healing [44, 107].

The negatives of using the bone autografts are mainly in the limited source, risk of morbidity accompanied by the scarce, pain, infection or hematoma in the donor site together with prolonged surgery time [44, 108]. Also, the size of the defect could be limiting while using autografts, as large autografts could be resorbed by the cells before osteogenesis is completed [108]. An alternative is the use of allografts, however they lack the cellular component and also carry the risk of disease transmission and possible infections, so these are disadvantages of this method [44, 106]. Therefore, alternatives to the use of auto- and allografts are being extensively researched.

A suitable scaffold material, for bone tissue engineering should meet several criterions in order to aid the bone regeneration, e.g. controlled biodegradability allowing time for the deposit of ECM and replacement by new bone tissue, biocompatibility of the material and of the breakdown products, sufficient porosity with interconnected pores favoring cell migration, vascularization, diffusion of oxygen, nutrients and waste products,

proper mechanics, 3D nature, osteoconductivity, osteoconectivity and osteogenic capability [44, 106]. The scaffolding material could either be rigid or injectable. The host organisms should further provide responsive cells and a viable vascularized host bed [108].

From the mechanical point of view, the proper scaffold should meet the criterion that is most similar to the original tissue. As the bone is a complex structure with a hierarchical arrangement, the mechanical properties of bone are made by each of its components. Important factors are its compressive and bending strength together with fracture toughness. The porosity of cortical bone is 10-30%, porosity of cancellous bone is 30-90% [55]. Also different bones should withstand different demands, e.g. ribs are involved in tensile stress while talus is under heavy compressive strength [55]. The ideal porosity of the scaffold is between 60%-90% and an average pore size of 100-400 μm [106, 109]. Scaffold porosity is an important factor for bone tissue engineering but with porosity the mechanical properties of the material are decreased. Therefore, the balance between mechanical properties and porosity must be taken into account as mechanically relevant materials often fail *in vivo* due to insufficient vascularization [110].

The development of an ideal bone tissue engineered scaffolds is, because of demanding requirements, very challenging. Also the manufacturing of the scaffold must be of a scalable manufacturing process [110]. Scaffolds can be divided into cellular or cell-free [108]. Cellular scaffolds require another operational procedure where cells are aspirated for the subsequent cell seeding. This must be done prior the scaffold implantation. Also during *ex vivo* expansion of aspirated cells unwanted phenotypic changes during the manipulation can occur [110]. Cellular scaffolds are extensively studied and the results are often positive, however in animals, the defect size is smaller and bone remodeling capacity is higher [111-113]. Moreover, cells pre-seeded on the cellular scaffold can suffer, upon implantation, from cell death due to lack of vascularization in bigger bone defects [114]. Cell-free scaffolds on the other hand are meant to be placed in the defect site immediately after the injury. These scaffolds are often modified in order to deliver bioactive compounds into the defect site. These compounds then serve to induce migration, proliferation and differentiation in the migrating cells [115].

From the material point of view, metals, synthetic or natural polymers, and bioactive glass or ceramics are often tested for bone tissue engineering applications. However, each type has negatives and positives and therefore the use of composite scaffolds could be advantageous.

1.4.1 METALS

Metal implants such as stainless steel or titanium and its alloys are light, with good mechanical properties, however a high Young's modulus means stress shielding and therefore it prevents osseointegration as mechanical stimulation of new bone tissue formation is limited [107]. The big disadvantage of the titanium alloys is that they are not biodegradable and also corrosion can result in the release of toxic ions that can cause inflammation. Titanium and its alloys inhibit cell proliferation. In view of these disadvantages, new modification approaches are being tested in order to improve the bioactivity of the metals [55].

Surface adhesive properties could be improved by introducing TiO_2 nanotubes by the process of anodic oxidation [116]. Improved biocompatibility or mechanics can be reached by combination of titanium with either nickel - the alloy is called nitinol (NiTi alloy) [117] or in a combination with aluminium and vanadium (TiAlV alloy), however negative effect on cell viability could be detected due to their release [118, 119]. Cobalt-chrome-molybdenum alloys (CoCrMo alloy) were shown to possess biocompatible properties and induce a less inflammatory response compared to TiAlV alloy [119]. The incorporation of GFs or ECM proteins on the surface of the titanium alloy [120], hydroxyapatite coating [121] or use of porous titanium foam [122] can improve osteoinductivity and the ingrowth of new bone tissue. Biodegradable magnesium alloy was tested *in vivo* on a rabbit model [123]. In general, titanium alloys are preferred over stainless steel or cobalt scaffolds due to their better mechanical properties and biocompatibility.

1.4.2 CERAMICS

Ceramic scaffolds are excellent in terms of biocompatibility, osteoinductivity and osteoconductivity as the composition mimics bone tissue and provides the cells with good adhesive properties. Widely used options are hydroxyapatite ($Ca_{10}(PO_4)_6(OH)_2$) and related calcium phosphates (α- (α-triclacium phosphate (Ca_3PO_4) or β-tricalcium phosphate (β-Ca_3PO_4) ceramic scaffolds) [55]. The ceramic scaffolds are prepared by mixing a calcium phosphate based powder with a liquid phase. The mechanics of ceramic scaffolds are superior to the polymers, however it is still not similar to the bone [55, 124]. The elasticity of the ceramics is very low and their surface is hard and brittle. As the ceramic scaffolds cannot sustain the mechanical loading, they are only approved for use in non-load bearing applications [110, 124]. The ceramics are relatively slow degrading materials that are degraded by phagocytosis or osteoclast related degradation. Between ceramic scaffolds

belongs also bioactive glass. The glass has good biocompatibility properties but low mechanics [125]. The dissolution of 45S5 Bioglass releases ions that induce a gene expression related to osteogenic differentiation [126]. Available commercial products are e.g. Novabone or PerioGlass [125, 127].

In order to increase comprehensive strength, tricalcium phosphate can be doped with additives such as SiO_2 or ZnO [128]. Examples of ceramic scaffolds approved for clinical use are products like ChronOS^{TM} Inject or Norian SRS [124].

1.4.3 POLYMERS

Polymeric scaffolds are of interest as they are controllable in terms of physiochemical characteristics, solubility and enzymatic reaction [55]. These materials are of good biocompatibility, biodegradability and can be manufactured in diverse shapes but the mechanical characteristic is weak [55, 110]. There are different methods for how to fabricate scaffolds from polymers. It could be done by e.g. 3D printing method [129] or by freeze drying technique [130]. Also other methods for production of polymeric fibrous scaffolds exist. Fibrous scaffolds are porous, have high surface to volume ratio which is advantageous for cell adhesion and adsorption of compounds to the fibrous surface. These scaffolds can be produced by centrifugal spinning (CS) [131], electrospinning (ES) [132], phase separation [133], electro-blowing [134] or self-assembly [135].

Synthetic polymers such as saturated aliphatic polyesters, e.g. poly-lactic acid (PLA), poly-l-lactic acid (PLLA), poly-glycolic acid (PGA), PCL or their copolymers are more commonly used for tissue engineering applications [55]. Biodegradation occurs by water uptake with subsequent hydrolysis of ester bounds [125]. Hydrolysis of PLLA or PGA produces CO_2 that acidifies the environment and can lead to necrosis [110]. Other polymers, such as poly hydroxyl butyrate, polyethylene or polypropylene are rapidly degraded *in vivo* and creates an acidic environment that can lead to inflammation processes [55].

PCL was used in this thesis for the production of the scaffolds by the ES and CS methods. PCL is a widely used material and was reported to be tested for bone [136] cartilage [137] or cardiac [138] tissue engineering. PCL was approved by FDA for certain applications, e.g. in commercial product Monocryl (poliglecaprone 25) Suture [139]. PCL degrades within several months or years depending on the molecular weight or degree of crystallinity, that can be controlled during the manufacturing of the scaffold [140]. Products of PCL degradation are *in vivo* degraded in the Krebs cycle or by renal secretion [141].

Natural polymers are derived either from proteins (e.g. collagen fibrinogen, gelatin or silk) or polysaccharides (e.g. glykosaminoglykans, cellulose, chitin, starch, alginate and hyaluronic acid derivatives) [55, 110]. Scaffolds derived from ECM are similar to the original tissue. Unlike autogenic ECM scaffolds, that conatin cellular components, allogenic ECM scaffolds must be decellularized [55]. These materials are biologically active and favor cell adhesion and proliferation. However, the reproducibility of natural polymers is questionable [110].

ELECTROSPINNING METHOD

ES is a method which enables the production of fibrous scaffolds with fiber diameters ranging from nano- to micrometers, high surface to volume ratio and interconnected pores. The process involves the application of a high electrical field into the polymeric solution to the tip of the syringe needle (Figure 9A). An increasing electric field results in protruding the polymeric droplet until it becomes conical, creating a Taylor cone [142]. When the charge, accumulated on the surface of the droplet, overcomes the surface tension, the critical voltage is reached and an elongated polymeric jet flows towards a collector. During the elongation, the solvent is evaporated. On the collector the fibrous scaffold is deposited. Morphology of the scaffold can be modified by e.g. different types of collectors, distance between the collector and the polymeric droplet, humidity or polymeric solution [142].

The ES method is a widely used technique for the production of fibrous scaffolds; however there are a few negatives e.g. the necessity of a high voltage electrical field, the variability in polymers conductivity, a low production rate or limits in the production of 3D scaffolds [143].

CENTRIFUGAL SPINNING METHOD

The CS method uses centrifugal forces to create fibrous scaffolds. During CS, the polymeric solution is placed into the rotation reservoir with small orifices that are connected to a rotational motor (Figure 9B). As the motor rotates at high speed, the centrifugal force applied to the polymeric solution induces the ejection of polymer jets through the orifices. Due to the rotation, the polymeric jets travel in a curly trajectory, and this stretching is important for the reduction of the polymeric jet diameter. During this time, the solvent evaporates. The polymeric jets are deposited on the collector placed around the reservoir. The whole process could be affected by the rotational speed, used solvent and its evaporation rate, collector type and radius or humidity [143].

Unlike ES, CS is a rapid technique with simple apparatus that does not require a high voltage field and is able to produce higher quantities of scaffolds. Moreover, the resulting meshes are porous with a 3D morphology [143].

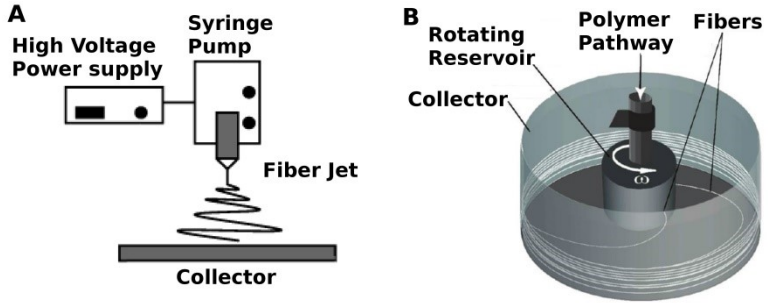

Figure 9: Spinning methods –ES method (A): A high electric field is applied to the polymeric solution in the syringe pump. When the critical voltage is reached, the elongated fiber ejects from the polymeric droplet and is deposited on the collector. CS method (B): During CS, the centrifugal force is applied on the solution placed in the rotational reservoir with orifices. During the rotation, the polymeric jets are ejected from the orifices, elongated and afterwards deposited on the surrounding collector. Figure adapted from [142, 143].

MODIFICATION OF SPUN SCAFFOLDS

Scaffolds prepared by spinning could be modified in different ways in order to deliver the susceptible bioactive compounds. One such approach is blend spinning where a mixed solution of bioactive compounds and polymer is spun (Figure 10A) [115]. If the mixed solution is prepared by sonication or homogenization, it is called emulsion spinning [144]. In the scaffolds prepared by blend or emulsion spinning, the compounds are distributed within the fibers. The negative of this approach is potential damage of the compounds during the mixing of the solution and possible loss of activity after contact with the polymer solution [115]. In order to protect the bioactive compounds, they can be encapsulated prior to mixing with the solution. For example TGF-β was protected from degradation by encapsulation into chitosan nanoparticles [145] or the use of pluronic copolymers protected the activity of protease K [146]. Typically blend spinning materials have an initial burst release, after which an almost linear release of compounds is obtained [147]. Additionally, the release kinetics depend on the polymer used for the scaffold preparation, e.g. PLGA is a quickly degrading polymer, while PCL is a slowly degraded polymer [115]. Blend centrifugal spinning have been used to incorporate VEGF [147], lysozyme [147], BMP-2 [148], EGF [149], TGF-β [145] or osteogenic supplements (OS) (155).

Coaxial spinning produces scaffolds with a core-shell fiber morphology (Figure 10B). During this procedure, two solutions are spun coaxially at the same time. For example, during the ES procedure, the bioactive compounds within the inner solution are

protected from electrical charge degradation. During coaxial spinning the compounds are distributed homogenously inside the core of the fibers. There is also an initial burst release, however in lower concentrations as compared to blend spinning [115]. Scaffolds were prepared coaxially with encapsulated BMP-2 and IGF-1 [150], PDGF-bb [151] and BSA or lysozyme [152]. CS method was used in this thesis not only because it is a promising method but also because not many research was done in the field of production drug delivery CS fibrous systems.

During physical adsorption, the bioactive compounds are attached via electrostatic interactions to the surface of the scaffold. A high surface to volume ratio, typical for spun scaffolds, makes physical adsorption effective compared to macro-structured scaffolds. Physical adsorption does not degrade the bioactive compounds, however the efficiency of a controlled long term release is limited [115]. EGF was for example conjugated to the scaffolds [153]. Alternatively, covalent immobilization serves to bind bioactive compounds to the surface of the scaffolds via chemical bounds [115]. In this case, the release of the compounds could be controlled for example by enzyme degradation, e.g. by MMPs [154]. However, this approach is complex and the surface properties could be changed during the covalent modification of the scaffold [115].

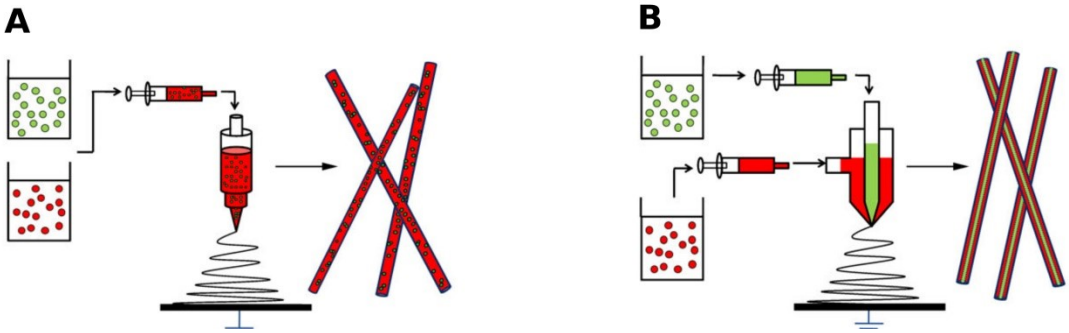

Figure 10: Scaffold modifications - Blend ES procedure (A): During blend spinning the polymer solution is mixed with the bioactive compounds which is then spun. Coaxial ES procedure (B): During coaxial spinning two polymeric solutions are spun coaxially at the same time which results in the forming of fibers with core-shell morphology. The core of the fibers contain bioactive compounds. Figure adapted from [115].

1.4.4 COMPOSITES

The bone is a composite material which consists from a hydroxyapatite and organic phase of ECM proteins. Compose scaffolds can combine more materials in order to profit from the advantages of individual materials [55]. A composite of PLGA with hydroxyapatite can overcome the limits of ceramic brittleness [155]. PLGA with titanium nanoparticles can lead to a reduction of the pH while PLGA is degraded [156]. Other investigated composed

scaffolds are e.g. hydroxyapatite and titanium [157, 158], calcium phosphate scaffold with collagen [159] or strontium together with hydroxyapatite and chitosan [160]. These composite features improved either the biocompatibility, osteointegration, osteoinductivity or osteoconductivity of the scaffolds.

1.4.5 BIOACTIVE COMPOUNDS

Scaffolds provide physical support to the cells in the defect site. Moreover, scaffolds could be modified, with suitable bioactive compounds, to produce drug delivery systems which provide morphogenetic signals to the surrounding tissue.

GFs are extensively studied as bioactive compounds that induce different cell signaling pathways in combination with scaffolds [145, 147, 148, 150, 151]. However, large quantities of recombinant GFs are necessary which is expensive and there is also a limited stability of GFs [115]. Moreover, this raises safety concerns regarding the adverse effects of GFs used for clinical purposes [161]. Although, BMP-2 and -7 are approved for clinical use, this is only in combination with collagen scaffolds under the product names Infuse and OP-1, respectively [162]. An alternative to GFs are short peptide sequences, derived from receptor binding sequences of GFs. An example being in a clinical trial, where a peptide derived from collagen type I was used, is called peptide P-15 [163]. Amino acid sequences derived from other ECM proteins are extensively studied, such as fibrinogen, fibronectin, BMP-2 and -7 [164-166]. Another approach is the delivery of gene encoding GFs; the transfection of targeted cells is important in order to produce GFs in the defect site [167]. In this thesis, alternatives to GFs such as platelets and osteogenic supplements (dexamethasone, β-glycerol phosphate and ascorbate-2-phosphate) were tested.

PLATELETS

Alternatives to the recombinant GFs are platelets as a natural source of GFs. Platelets store numerous GFs within its α-granules, cytokines and chemokines, which are important for the healing processes. During bone healing, the first stage is a characteristic for hematoma formation, platelets coagulate and activate, at the same time releasing their contents which are entrapped within the formed fibrin clot [76]. As the platelets could be used autologously from the blood aspirated preoperatively, the research in bioactive bone tissue engineered scaffold is centered on their usage. Alternative possibilities are available on platelet preparation for subsequent usage. They can be used e.g. as a platelet gel, platelet concentrate, platelet rich plasma (PRP), platelet lysate, concentrated GFs or Choukroun's platelet-rich fibrin (PRF) [168].

During PRP production, blood is collected in the presence of anticoagulants, e.g. citrate, phosphate and dextrose, to prevent coagulation. Then it is fractioned in the density cell separator to distinguish erythrocytes, platelet poor plasma and PRP (also called buffy coat) [168]. If the PRP is further concentrated, platelet concentrate is obtained which can be re-suspended either in the plasma or in saline solution. Platelet gel is produced by mixing the PRP with thrombin or $CaCl_2$ in order to induce the activation of platelets [168]. PRF is produced in a similar way as PRP, however the procedure is without anticoagulants [169]. Platelet lysate is prepared from platelet concentrate by either repeating freeze thaw cycles, sonication or by detergent usage [170]. These platelet derivatives differ in terms of platelet activation state, presence of leukocytes, and in the bioactive compounds concentration between individuals.

After coagulation, a fibrin clot is formed. Within this natural scaffolding material, released GFs are trapped and gradually released as the fibrin clot degrades, thus serving as a drug delivery system [171]. However, the fibrin clot is a quickly degrading material, therefore it is beneficial to combine it with a longer lasting scaffolding material. Rai et al. adsorbed PRP in the presence of thrombin and $CaCl_2$ on the PCL-tricalcium phosphate scaffold and observed accelerated bone healing *in vivo* [172]. Sarkar et al. used collagen scaffolds loaded with PRP *in vivo*, however no enhanced bone formation was observed [173]. Chang et al. tested *in vivo* collagen/hydroxyapatite beads with weakly injecting PRP; they observed only fibrous tissue formation without injecting PRP [174]. Cerruti et al. performed a dental clinical study with bone graft mixed with MSCs, and PRP mixed with $CaCl_2$ and thrombin, and observed an improved healing process due to the presence of MSCs [175]. The conflicting results in the efficiency of the platelet derivatives used can be caused by inter-individual differences between donor age, gender or physiological state [98]. However, soft tissue injuries, caused by sport activity, are often healed with re-injections of PRP [176]. Moreover, the positive effect of platelets *in vitro* on cell proliferation and metabolic activity has been proven [177-179]. In addition, improved ALP activity as a marker of osteogenic differentiation was observed [180].

OSTEOGENIC SUPPLEMENTS

Apart from GFs, other bioactive compounds tested for bone tissue engineering applications are osteogenic supplements. Between these supplements belong dexamethasone, β-glycerol phosphate, ascorbate-2-phosphate or 1,25-dihydroxyvitamin D (1,25(OH)2 D). These compounds are generally used for the *in vitro* induction of osteogenic differentiation of MSCs [5]. Unlike GFs, osteogenic supplements are longer lasting molecules with prolonged *in vivo* half-life [181]. Dexamethasone is a synthetic glucocorticoid that induces the transcription of bone sialoprotein or integrin α which leads to the RunX2 dependent transcription activation. β-glycerol phosphate is a substrate for ALP. Ascorbate-2-phosphate is a cofactor in the process of proline and lysine hydroxylation during collagen maturation. 1,25-dihydroxyvitamin D interacts with its receptor and, together with dexamethasone and BMP-2, induces expression of genes, such as ALP or osteocalcin, associated with osteogenic differentiation [5].

The encapsulation of osteogenic supplements into diverse scaffold types was used in order to induce osteogenic differentiation. Shi et al. fused PLGA microsphere scaffolds loaded with dexamethasone, β-glycerol phosphate and ascorbate-2-phosphate and tested them *in vitro* on cultured MSCs. The results indicated an induced osteogenic activity of cells cultured on the scaffolds compared to the control group where solely dexamethasone was encapsulated [181]. Kim et al. incorporated dexamethasone and ascorbate-2-phosphate into a PLGA scaffold. The released osteogenic supplements induced *in vitro* mineralization of MSCs cultured on the scaffolds [182]. Subsequently they tested this scaffold *in vivo* and detected an enhanced mineralization [183]. Yoon et al. produced a PLGA scaffold with encapsulated dexamethasone and they detected a decrease in proliferation of lymphocytes and smooth muscle cells *in vitro* [184]. Martins et al. used the ES method to produce PCL scaffolds with encapsulated dexamethasone, and an increase in the osteogenic differentiation of *in vitro* cultured MSCs was detected [185]. These studies clearly proved the positive effects of released osteogenic supplements on proliferation and osteogenic differentiation in both *in vitro* and *in vivo* conditions.

2 AIMS OF THE THESIS

The main aims of the PhD thesis are as follows:

1. To verify that platelets as a natural source of growth factors and osteogenic supplements as compounds, are capable of inducing the osteogenic differentiation which could be combined with a fibrous scaffold in order to design cell-free scaffold for bone tissue engineering.
2. The characterization of proposed drug delivery systems.
3. The *in vitro* evaluation of drug delivery systems on the biological response of cells cultured on the scaffolds.

This PhD thesis was written based on the following four articles that have been published in impacted journals:

1. Rampichova M., Buzgo M., Mickova A., Vocetkova K., Sovkova V., **Lukasova V.**, Filova E., Rustichelli F., Amler E., Platelet-functionalized three-dimensional poly-ε-caprolactone fibrous scaffold prepared using centrifugal spinning for delivery of growth factors. International Journal of Nanomedicine, 2017. 12: p. 347-361. (IF 4.471)

2. Buzgo, M., Rampichova, M., Vocetkova, K., Sovkova, V., **Lukasova V.**, Doupnik M., Mickova A., Rustichelli F., Amler E., Emulsion centrifugal spinning for production of 3D drug releasing nanofibres with core/shell structure. RSC Advances, 2017. 7(3): 1215-1228. (IF 3,049)

3. **Lukasova V.**, Buzgo M., Vocetkova K., Kubikova T., Tonar Z., Doupnik M., Blahnova V., Litvinec A., Sovkova V., Voltrova B., Staffa A., Svora P., Kralickova M., Amler E., Filova E., Rustichelli F. and Rampichova M., Osteoinductive 3D scaffolds prepared by blend centrifugal spinning for long-term delivery of osteogenic supplements. RSC Advances, 2018, 8, 21889 – 21904. (IF 3,049)

4. **Lukasova V.**, Buzgo M., Vocetkova K., Sovkova V., Doupnik M., Himawanf E., Staffa A., Sedlacek R., Chlup H., Rustichelli F., Amler E., Rampichova M., Needleless electrospun and centrifugal spun poly-ε-caprolactone scaffolds as a carrier for platelets in tissue engineering applications: A comparative study with hMSCs. Materials Science and Engineering: C, 2019, 4, 567-575. (IF 4.959)

Apart from these articles, I am first author or co-author of further publications:

• **Lukasova V.**, Buzgo M., Sovkova V., Dankova J., Rampichova M., Amler E., Osteogenic differentiation of 3D cultured mesenchymal stem cells induced by bioactive peptides. Cell Prolif, 2017. 50(4): p. e12357-n/a.

• Sovkova V., Vocetkova K., Rampichova M., Mickova A., Buzgo M., **Lukasova V.**, Dankova J., Filova E., Necas A., Amler E., Platelet lysate as a serum replacement for skin cell culture on biomimetic PCL nanofibers. Platelets, 2017: p. 1-11.

• Vocetkova K., Buzgo M., Sovkova V., Rampichova M., Staffa A., Filova E., **Lukasova V.**, Doupnik M., Fiorif F. and Amler E., A comparison of high throughput core–shell 2D electrospinning and 3D centrifugal spinning techniques to produce platelet lyophilisate-loaded fibrous scaffolds and their effects on skin cells. RSC Adv., 2017, 7, 53706. DOI: 10.1039/c7ra08728d

• Rampichova M., Chvojka J., Jencova V., Kubikova T., Tonar Z., Erben J., Buzgo M., Dankova J., Litvinec A., Vocetkova K., Plencner M., Prosecka E., Sovkova V., **Lukasova V**., Kralickova M., Lukas D., Amler E., The combination of nanofibrous and microfibrous materials for enhancement of cell infiltration and in vivo bone tissue formation. Biomed Mater. 2017 Oct 31. doi: 10.1088/1748-605X/aa9717.

• Gregor A., Filova E., Novak M., Kronek J., Chlup H., Buzgo M., Blahnova V., **Lukasova V.,** Bartos M., Necas A., Hosek J., Designing of PLA scaffolds for bone tissue replacement fabricated by ordinary commercial 3D printer. J Biol Eng. 2017 Oct 16;11:31. doi: 10.1186/s13036-017-0074-3. eCollection 2017.

• Buzgo M., Filova E., Staffa A.M., Rampichova M., Doupnik M., Vocetkova K., **Lukasova V**., Kolcun R., Lukas D., Necas A., Amler E., Needleless emulsion electrospinning for the regulated delivery of susceptible proteins. Journal of Tissue Engineering and Regenerative Medicine: p. n/a-n/a.

3 MATERIALS AND METHODS

Tables 1, 2, 8, 9 and 11 are mentioned in *Materials and methods* section. These tables state the sample naming list and their characterization. However, these tables are located in the *Results* section in order to make easier the orientation during the reading of the results.

3.1.1 CENTRIFUGAL SPINNING

CENTRIFUGAL SPINNING OF PCL SCAFFOLD

CS was performed on a machine Cyclone 1000 L/M Forcespinning® (Fiberio, McAllen, TX, USA) 40% (weight/volume; w/v) PCL (45,000 Da, Sigma Aldrich St. Louis, USA) was dissolved in a mixture of chloroform and ethanol solution. The volume ratio was 9:1. An orifice G30 was used at a rotation speed of 10,000 rpm (6,000 × g) to prepare the nanofibrous scaffolds. Collector distance was 10 cm and static voltage used was of 48 V. The nanofibers were deposited on a spunbond textile with vacuum-assisted deposition.

EMULSION CENTRIFUGAL SPINNING

The general approach for emulsion CS technology is based on a double emulsification procedure. Firstly, 30% (w/v) Pluronic F-68 (PF-68, Sigma-Aldrich) is dissolved in 90% ethanol and mixed with protein, that should be encapsulated, dissolved in 50% ethanol and pure ethanol to achieve solutions of 0, 5, 10 or 20% PF-68 and encapsulated protein in 70% ethanol. The emulsification process was executed by dropwise mixing of the components with subsequent sonification. The emulsion of PF-68 with proteins was afterwards emulsified with 50% PCL (45,000 Da, Sigma-Aldrich, St. Louis, USA) dissolved in chloroform to obtain 40% PCL dissolved in chloroform : ethanol in the ration of 4:1. The ethanol phase was added drop-wise under stirring. The prepared emulsion was then processed by CS on Cyclone 1000 L/M Forcespinning® device using G30 orifice at 11,000 rpm and collector distance 10 cm and static voltage of 48 V. The nanofibers were deposited on a spunbond textile with vacuum-assisted deposition.

To evaluate the bioactivity of encapsulated compounds, we prepared scaffolds as described previously that contained 300 μg ml^{-1} of horseradish peroxidase (HRP) in the core of the nanofibers. Prepared were scaffolds containing 0% PF-68 and HRP dispersed in 40% PCL (0%PF-HRP), 5% PF-68 and HRP dispersed in 40% PCL (5% PF-HRP), 10% PF-68 and HRP dispersed in 40% PCL (10%PF-HRP), 20% PF-68 and HRP dispersed in 40%

PCL (20%PF-HRP). The control sample was prepared by directly dissolving the corresponding HRP in 40% PCL solution (PCL blend HRP) (Table 8).

To prepare the nanofibers with encapsulated platelet lyophilisates, scaffolds were prepared as described previously and contained 2 mg mL^{-1} of platelet lyophilisates in the core of the nanofibers. Prepared were scaffolds containing 0% PF-68 and platelet lyophilisate dispersed in 40% PCL (0%PF-LYO), 5% PF-68 and platelet lyophilisate dispersed in 40% PCL (5% PF-LYO), 10% PF-68 and platelet lyophilisate dispersed in 40% PCL (10%PF-LYO), 20% PF-68 and platelet lyophilisate dispersed in 40% PCL (20%PF-LYO). The control sample was prepared by directly dissolving the corresponding amount of platelet lyophilisate in 40% PCL solution (PCL blend LYO) (Table 9).

CENTRIFUGAL SPINNING OF SCAFFOLDS WITH ENCAPSULATED OSTEOGENIC SUPPLEMENTS

Nanofibrous scaffolds with encapsulated osteogenic supplements were prepared as follows. 13% w/v PCL (molecular weight 8,0000 Da, Sigma Aldrich, St. Louis, USA) and 16% w/v PCL (molecular weight 45,000 Da) were dissolved in a mixture of acetic acid and formic acid in the volume ratio of 1:1 (v/v). This solution was afterwards blended with osteogenic supplements (namely β-glycerol phosphate, dexamethasone and ascorbate-2-phosphate). Scaffolds with 4 different concentrations of osteogenic supplements were prepared: once concentrated osteogenic supplements (OS1), two times concentrated (OS2), five times concentrated (OS5) and ten times concentrated (OS10) (Table 11). Plain PCL fibers were used for control samples (CGM, COM). The spinning conditions for all groups were constant to evaluate the effect of polymeric blend properties on scaffold performance. The nanofibers were processed using a CS device Cyclone 1000 L/M Forcespinnig device at 10,000 rpm using a G30 orifice, collector distance 10 cm and static voltage of 48 V. Nanofibres were deposited on a spunbond textile with vacuum-assisted deposition.

3.1.2 ELECTROSPINNING METHOD

ES was performed using 24% (w/v) PCL (45,000 Da, Sigma Aldrich St. Louis, USA) that was dissolved in a mixture of chloroform and ethanol solution, volume ratio 9:1. The ES was performed using a needleless wire electrode on Nanospider NS500 (Elmarco, Czech Republic) at a potential difference of 50 kV. Distance of the collector was 2o cm. The process was performed at room temperature and the nanofibers were deposited on a spunbond textile.

3.1.3 CHARACTERIZATION OF FIBROUS SCAFFOLDS

SCANNING ELECTRON MICROSCOPY

The prepared scaffolds were visualized using SEM. The samples were coated with thin layer of platinum using a Quorum 150R S Device (3 cycles, Quorum Technologies, Lewes, UK) or using a Quorum SC7620 device (1 cycle, Quorum Technologies, Lewes, UK). Subsequently SEM (Vega 3, Tescan, Brno, CZ or Phenom G5 Pure, Eindhoven, Netherlands) was used to visualize the samples. The acceleration voltage for the samples ranged from 5 KV to 15 kV. The analysis of the images was done using the ImageJ program.

FTIR-ATR SPECTROSCOPY

Fourier Transform Infrared-Attenuated Total Reflectance (FTIR-ATR) spectroscopy was used to for the analysis of the chemical composition of produced scaffolds in order to evaluate the encapsulation of osteogenic supplements within the fibers. Plain PCL scaffolds and PCL scaffolds with encapsulated osteogenic supplements were pelleted on a manual press. The pellets were further analyzed using FTIR-ATR (IRAffinity-1, Shimazu with ZnS ATR). The measurement was performed with Happ-Ganzel apodization, at a resolution of 8 cm^{-1} and 20 scans per spectrum.

3.1.4 DRUG RELEASE STUDIES ON MODEL OF HORSERADISH PEROXIDASE

The HRP activity, after the release on day 1 from the fibers, was measured colorimetrically using tetramethylbenzidine assay (TMB, Sigma Aldrich) with tetramethylbenzidine as the substrate. The reaction of enzyme-substrate was after 30 s terminated with 50 ml of 2 N H_2SO_4. The HRP activity was measured on a fluorescence reader (Biotec, Synergy HT) at 450 nm. The enzyme activity was calculated as a percent ratio of active enzyme concentration measured by the tetramethylbenzidine assay and enzyme concentration measured by the Quant IT Protein Assay (Life Technologies, Carlsbad, CA, USA).

3.1.5 CHARACTERIZATION OF PHOSPHATE RELEASE

In order to quantify the release of β-glycerol phosphate and ascorbate-2-phosphate from the prepared scaffolds, the phosphate was quantified using ammonium molybdate. The samples with a size of 1 cm^2 were placed in an Eppendorf tube. Subsequently 1 mL of tris-buffered saline was added to each sample. On the day of measurement, the supernatant was collected and immediately frozen until the analysis was performed. Then 1 mL of tris-buffered saline

was added to the samples until the next experimental day. For the analysis, the samples were dissolved in chloroform and re-suspended in tris-buffered saline. The samples were placed into Eppendorf tubes with 0.25 mL of 2.5% ammonium molybdate solution followed by addition of 0.25 mL of 10% ascorbic acid solution. The samples were mixed thoroughly and heated for 5 min in a bath with boiling water. After that, the samples were cooled down for 5 min in a cold-water bath. Afterwards the optical density was measured using a Synergy H1 microplate reader at 820 nm. Parallel determinations of the blank values of the reagent solution and a standard preparation were made.

3.1.6 PREPARATION OF PLATELET SOLUTION

Fresh human leukocyte-depleted platelets derived from buffy coat in additive solution were obtained from the Transfusion Station at Šumperk hospital. The bags contained platelets from 4 donors. According to the Czech legislation of blood transfusion, related to the time the experiments were proceeding, blood products that are not used for therapy could be used for scientific purposes. Thus, approval from an ethics committee was not required. All donors signed an informed agreement about using their blood for scientific purposes. Two different bags were used, the bags contained either 900 × 10^9 platelets/L or 968× 10^9 platelets/L. Platelets were centrifuged at 120 × g for 7 min for sedimentation of residual erythrocytes. Afterwards, the supernatant was transferred into a new tube and centrifuged at 2200 × g for 10 min in order to retrieve the pellet of platelets. The pellet was resuspended in Platelet Additive Solution SSP+ (Macopharma, Tourcoing, France). The platelets were further diluted to required concentrations in SSP solution: 3,000 × 10^9/L (P1), 900 × 10^9/L (P2), 300 × 10^9/L (P3), 100 × 10^9/L (P4) and 30 × 10^9/L (P5) (**Table *1***Table 1 and Table 2).

3.1.7 PREPARATION OF PLATELET LYOPHILISATE

Fresh human leukocyte-depleted platelets derived from buffy coat in additive solution were obtained from the Transfusion Station at Šumperk hospital. The bag contained blood of 16 donors, the platelet concentration in the bag was 1020 × 10^9 platelets/L. By the freeze/thaw method the platelet lysate was prepared. First, the whole bag was frozen at -80°C and then thawed at 37°C, the whole procedure was three times repeated in order to disrupt the cellular membranes. The solution was centrifuged at 4100 × g for 15 min to remove the cellular debris. Afterwards, the lysate was lyophilized for 24 h under 480 mT (VirTis BenchTop Pro Freeze Dryer, SP Scientific, PA, USA). Until use, the platelet lyophilisate was stored at -80°C.

3.1.8 QUANTIFICATION OF SELECTED MOLECULES RELEASED FROM PLATELETS

To quantify the concentrations of cytokines, chemokines and GFs contained in the platelets, a Bio-Plex 200 Multiplex System (Bio-Rad Laboratories, Hercules, CA, USA) and enzyme-linked immunosorbent assay (ELISA, DuoSet®; R&D Systems, Minneapolis, MN, USA) were used. Platelets at a concentration of 900×10^9/L were lysed using 3 freeze/thaw cycles (−80°C and 37°C) and then centrifuged at 3422 × g for 10 min to rid of the cell membranes.

To analyze the cytokine content of the platelet lysate, commercially available cytokine panel (Bio-Plex ProTM Human Cytokine 27-plex Assay; Bio-Rad Laboratories) was used according to the instructions. The assay allows multiple cytokines quantification simultaneously in 1 well. The platelet lysate was incubated with a set of color-coded magnetic beads, each of them conjugated with an antibody directed against a specific mediator. Biotinylated detection antibody was added to bind to streptavidin–phycoerythrin. The unbound protein was removed by thorough washing series that were performed between each step by an automatic wash station (Bio-Plex ProTM II). The data were analyzed using a BioPlex 200 instrument fitted with BioManager analysis software (5-parameter curve fitting).

To observe the distribution of GFs released from platelets, a sandwich ELISA was used. GFs were determined in accordance with the guidelines (Peprotech, Rocky Hill, NJ, USA or DuoSet).

3.1.9 RELEASE OF PROTEINS

RELEASE OF PROTEINS FROM PLATELETS ADHERED ON FIBERS

To quantify the released proteins from platelets, overall protein quantification by the QuantIT Protein assay was performed. Scaffolds of 11 mm diameter were punched out of the produced nanofibrous layers. The scaffolds, functionalized with different concentrations of platelets, were incubated in 500 µL of phosphate buffered saline (PBS) at 37°C. On the day of analysis, the PBS was collected, stored at -20°C until the day of analysis and fresh 500 µL PBS was added again to the same samples. On the day of analysis, 10 µL of the sample was mixed with 200 µL of fluorescent probe from the QuantIT Protein assay. The fluorescence intensity was measured using a fluorescence reader (Synergy HT; Biotek, Winooski, VT, USA) at λex=470 nm and λem=570 nm.

RELEASE OF OVERALL PROTEINS FROM CORE OF THE FIBERS

In order to determine the release of proteins from the fibers, the samples were cut into pieces (~50 mg). 1 mL of TBS buffer was added to each sample and incubated at room temperature. At given time points, the TBS buffer was collected and replaced with fresh TBS. Fluorescent Quant-IT Protein Assay Kit was used, as described previously, to determine the release of HRP or platelet lyophilisate from the fibers.

3.1.10 QUANTIFICATION OF THROMBOSPONDIN

In order to determine the release profile of GFs from the platelet functionalized samples, the thrombospondin was used as a model drug. Scaffolds of 11 mm diameter were punched out of the produced nanofibrous layers. The scaffolds, functionalized with different concentrations of platelets, were incubated in 500 μL of PBS. At given time points, the PBS buffer was collected and replaced with fresh PBS and the samples were stored at −20°C until the day of analysis. The thrombospondin quantification was performed using the ELISA in accordance with the protocol (DuoSet).

3.1.11 CELL SEEDING

EXPERIMENTS WITH PLATELET ADHESION

Prior to cell seeding, PCL nanofibers were cut into round patches of 6 mm in diameter. The scaffolds were sterilized by ethylene oxide at 37°C, The Military University Hospital Prague. Scaffold were put into 96 well plate and were seeded with either 10 $\times 10^3$ MG-63 cells (Cell Lines Service GmbH, Eppelheim, Germany) in 30 μL of culture medium that consisted of Dulbecco's Modified Eagle's Medium (DMEM) supplemented with 2% fetal bovine serum (FBS) and 1% penicillin/streptomycin. Alternatively, the scaffolds were seeded with 25 × 10^3 hMSC (human bone marrow derived MSCs; ScienCell, San Diego, California, USA) in 30 μL of medium. The samples seeded with hMSCs were cultured either in a growth medium or in a growth medium supplemented with osteogenic supplements. Growth medium consisted of a Minimum Essential Medium (MEM α medium), 5% FBS and 1% penicillin/streptomycin. Growth medium supplemented with osteogenic supplements was enriched with 10 mM β-glycerol phosphate, 100 nM dexamethasone and 40 μg mL^{-1} ascorbate-2-phosphate.

Cells were let to adhere to the surface of the scaffolds for 2 hours. Subsequently, 20 μL of platelet solution in different concentrations was added and let to adhere for 1 hour. Finally, 250 μL of appropriate culture medium was added. Culture medium was not changed

during the experiment to avoid loss of released compounds from platelets after their activation.

Six different samples were prepared: five groups with different platelets concentrations adhered on PCL scaffolds (P1–P5), and PCL scaffold without platelets as a control sample (PCL) (Table 1 and Table 2). Scaffolds with adhered platelets in different concentrations (P1–P5) without cells were used as controls. The results from these samples were used as a control to the platelets interaction with the methods used in this experiment and were deducted from the values measured on the samples seeded with cells.

EXPERIMENT WITH EMULSION CS OF PLATELETS LYOPHILISATE

Prior to cell seeding, PCL nanofibers were cut into round patches of 6 mm in diameter. The scaffolds were sterilized by ethylene oxide. Scaffolds were placed in the 96 well plate and seeded with 10×10^3 MG-63 cells (Cell Lines Service GmbH, Germany). Cells were let to adhere to the surface of the scaffolds for 2 hours in 30 mL of culture media that consisted of DMEM supplemented with 2% FBS and 1% Penicillin/Streptomycin. Afterwards, medium was added to the total volume of 300 µL per well. Culture medium was not changed during the experiment to avoid loss of released compounds from platelets after their activation. Three different scaffolds were used for *in vitro* evaluation. Two different concentrations of encapsulated lyophilizate were tested and plain PCL scaffold was used as a control group (Table 9).

EXPERIMENT WITH ENCAPSULATED OSTEOGENIC SUPPLEMENTS

Prior to cell seeding, PCL nanofibers were cut into round patches of 6 mm in diameter. The scaffolds were sterilized by ethylene oxide. Scaffolds were placed in the 96 well plate and seeded either with 25×10^3 hMSCs or with 10×10^3 Saos2 osteosarcoma cell line (Cell line service, Germany). Scaffolds with encapsulated different concentrations of osteogenic supplements seeded with hMSCs were cultivated in growth medium consisted of MEM α medium supplemented with 10% FBS and 1% Penicillin/Streptomycin, those seeded with Saos2 cells were cultivated in medium that consisted of McCoy's 5A Medium supplemented with 15% FBS and 1% Penicillin/Streptomycin. Two types of controls were used; plain PCL scaffolds cultivated in growth medium (CGM) and plain PCL fibers cultivated in Growth medium supplemented with osteogenic supplements was enriched with 10 mM β-glycerol phosphate, 100 nM dexamethasone and 40 µg mL^{-1} ascorbate-2-phosphate (COM), see Table 11. Half of the culture medium was changed on days 7 and 14. Minimal changing of

medium was performed in order not to wash out the osteogenic supplements released from the scaffolds to the culture medium.

3.1.12 METABOLIC ACTIVITY MEASUREMENT

Cells metabolic activity was measured using an MTS assay (CellTiter 96® AQueous One Solution Cell Proliferation Assay; Promega, Madison, WI, USA). On specific time points, the scaffolds were put into new clean well. 20 µL of 3-(4,5-dimethylthiazol-2-yl)-5-(3-carboxymethoxyphenyl)-2-(4-sulfophenyl)-2H-tetrazolium) (MTS solution) together with 100 µL of the medium was added to each well with the scaffold and incubated for 2 hours at 37°C. Afterwards, 100 µL of the solution was transferred to a new clean well and the absorbance was measured using a microplate reader Synergy HT at 490 nm. The background absorbance measured at 690 nm together with the absorbance of the medium without cells were subtracted from the measured absorbance.

3.1.13 QUANTIFICATION OF DNA AMOUNT

Cells proliferation was determined from the amount of deoxyribonucleic acid (DNA) using Quant-iT™ dsDNA Assay Kit (Life Technologies, Carlsbad, CA, USA). The scaffolds seeded with cells, after the MTS measurement, were placed in 200 µL of cell lysis solution (0.2% v/v Triton X-100, 10mM Tris (pH 7.0), and 1mM EDTA) and frozen. Samples were further processed threw 3 freeze/thaw cycles with vortexing performed between each cycle. Subsequently 10 µL of each of the samples was mixed with 200 µL of the buffer with fluorescent PicoGreen probe and measured using a multiplate fluorescence reader Synergy HT with λex=485 nm and λem=525 nm.

3.1.14 DETECTION OF ALKALINE PHOSPHATASE ACTIVITY

ALP activity was detected using a 1-Step™ PNPP kit (Thermo Scientific, Waltham, MA USA). The scaffolds were transferred into new clean well and 100 µL of p-Nitrophenyl Phosphate (PNPP) was added to each well and incubated for 10 min. Afterwards, the reaction was stopped by adding 50 µL of 2 N NaOH. Subsequently, 100 µL of the solution was transferred into new clean well. The absorbance at 405 nm was measured using a microplate reader Synergy HT. The absorbance of the solution incubated with the scaffolds without cells was subtracted from the measured absorbance.

3.1.15 VISUALIZATION OF CELL ADHESION ON SCAFFOLDS

CONFOCAL MICROSCOPY

Cell distribution on the scaffolds was visualized using the confocal microscopy. The cells were stained using 3,3′-diethyloxacarbocyanine iodide (DiOC6(3), D273, Invitrogen, Molecular Probes) and propidium iodide (Sigma Aldrich, Germany). First, scaffolds were fixed with frozen methanol (−20°C) for 10 min and then incubated with DiOC6(3) at concentration of 1 μg mL^{-1} in PBS (pH 7.4) for 45 min at room temperature. Afterwards, the samples were incubated with propidium iodide at concentration of 5 μg mL^{-1} in PBS for 10 min. The samples were scanned using a ZEISS LSM 5 DUO confocal microscope (propidium iodide: λex=561 nm, λem=630–700 nm and DiOC6(3): λex=488 nm, λem=505–550 nm).

SCANNING ELECTRON MICROSCOPY

The cells morphology or formed fibrin mesh, after platelets adhesion, were visualized using SEM (Vega 3 Tescan). First, scaffolds were washed in PBS and fixed in 2.5% glutaraldehyde for 2 hours at 4°C. Afterwards, the scaffolds were dehydrated in ethanol ranging from 35–100%. In order to dry the scaffolds hexamethyldisilazane (Sigma-Aldrich) was added. Scaffolds were coated with platinum and analyzed using the SEM as described previously (Chapter 3.1.3).

3.1.16 RNA ISOLATION AND QPCR ANALYSIS

The total ribonucleic acid (RNA) was isolated using a Qiagen RNeasy Mini Kit (Qiagen, Hilden, Germany) in accordance with the manufacturer's protocol. Reverse transcription was executed using a RevertAid H Minus First Strand cDNA Synthesis Kit (Thermo Scientific, Waltham, MA, USA). Level of transcripts was evaluated using quantitative polymerase chain reaction (qPCR). qPCR was performed using the Light Cycler 480 II real-time PCR system (Roche, Basel, Switzerland) with TaqMan Master Mix and TaqMan probes (Thermo Scientific, Waltham, MA USA) according to the manufacturer's protocols. The analyzed genes were: RunX2 (86 bp, RUNX2, Hs01047973_m1, Thermo Scientific), osteocalcin (138 bp, BGLAP Hs01587814_g1, Thermo Scientific), collagen type I (66 bp, COL1A1 Hs00164004_m1, Thermo Scientific) and eukaryotic elongation factor (EEF1 Hs00265885_g1, Thermo Scientific). The thermo cycling parameters were 95°C for 10 min; 95°C for 10 s, 60°C for 10 s (45 cycles); and 40°C for 1 min. All samples were scale bard

relative to the median of the EEF1 expression level, an endogenous control gene. Gene expression data were analyzed using the relative quantification $2^{(-\Delta Ct)}$ method.

3.1.17 INDIRECT IMMUNOFLUORESCENCE STAINING

To detect osteocalcin, indirect immunofluorescence staining was performed. Samples were fixed with frozen methanol (-20°C) for 10 min and washed with PBS. Afterwards, incubated in 3% FBS in PBS/0.1% Triton X-100 for 30 min at room temperature. Subsequently, primary monoclonal antibody against osteocalcin (either Rabbit anti-osteocalcin IgG, Peninsula Laboratories, dilution 1:20, San Carlos, CA USA or OCG3, Abcam, Cambridge, UK, dilution 1:20) was incubated overnight at 2–8°C with the samples. After three washes with PBS/0.05% Tween 20, the samples were further incubated with secondary antibody Alexa Fluor 488 (either Alexa Fluor 488 conjugated anti-rabbit antibody or Alexa Fluor 488 conjugated anti-mouse antibody) at a dilution of 1:300 for 45 min. Subsequently, a solution of propidium iodide was added for 5 min to visualize cell nuclei (5 μg mL^{-1} in PBS). After that, the samples were washed three times with PBS/0.05% Tween 20. A confocal microscope ZEISS LSM 5 DUO was used to detect the present osteocalcin with Alexa Fluor 488: λex=488 nm, λem=505–550 nm and propidium iodide: λex=561 nm, λex=630–700 nm.

3.1.18 STATISTICAL ANALYSIS

Quantitative data are presented as mean values ± standard deviation (SD). The averaged values were determined from at least 3 independently prepared samples. The data were statistically evaluated using SigmaStat (SigmaStat 12.0, Systat). The normality of the data was tested by Kolmogorov-Smirnov test. The equality of variances was tested using Levene's test. If the data passed the normality test and the test of equality of variances, statistical significance between a pair of groups was determined by ANOVA test and Tukey's comparative test for post-hoc analysis. If the data were without normal distribution, statistical significance between a pair of groups was determined using Kruskal-Wallis test and Dunn's multiple comparisons test for post hoc analysis. All results were considered statistically significant if $p < 0.05$.

4 RESULTS

The results section is divided into three parts according to the experimental design. Firstly, the effect of platelets adhered on the PCL scaffold was evaluated. Next, we encapsulated the lyophilized platelet lysate (lyophilisate) in the core of the PCL nanofibers. The third experimental trial was the encapsulation of osteogenic supplements in the core of PCL nanofibers. The design was settled in order to design a bioactive cell-free scaffold with drug a delivery system suitable for bone tissue engineering.

Each step in the design of the cell-free scaffolds was tested *in vitro* with the aim being to either support superior cell adhesion and viability together with cell proliferation, or promote osteogenic differentiation of the cells. We used standard cell models for bone tissue engineering: cell lines such as MG-63 and Saos2 osteosarcoma cell line and also primary hMSCs derived from bone marrow. Osteosarcoma cell lines are osteoblasts where alteration in the production of osteogenic markers can be monitored. hMSCs are primary cells that are tested in order to follow the induction of osteogenic differentiation. These cells were chosen to accurately test the potential of designed scaffolds to induce osteogenic differentiation, superior cell adhesion and fostered proliferation.

In *in vitro* conditions, the cells are generally cultured on cultivation plastic that is intended for cell cultures and therefore supports cell adhesion and proliferation. However, for our research the controls are plain PCL scaffolds with no modification, only the culture conditions are modified in order to introduce negative or positive controls.

4.1 PLATELET ACTIVATION EXPERIMENT

Ideal cell-free scaffold for tissue engineering should not only serve as a filling material that is meant to support the adhesion of migrating cells. The scaffold should also have the ability to actively induce the migration of the surrounding cells that take part in the healing process, resulting in a shorter and more effective healing process. Platelets, that could be used autologously, are an ideal source of natural GFs stored in the α-granules. Among the GFs, anti- and pro-inflammatory cytokines and chemokines are also present.

In this set of experiments the effect of bioactive compounds, released from platelets after their activation, was studied. The activation of platelets was induced by the adhesion on the PCL scaffold, prepared by the CS method. The process of activation causes the content of the platelets to release and a fibrin net is formed. Subsequently, the bioactive compounds are trapped within this net. As the PCL scaffold is used as a support for the

deposited fibrin net, the GFs, cytokines and chemokines are stored in the net and available to be gradually released, therefore, prolonging their bioavailability and the overall effect on the healing process.

Furthermore, differently prepared PCL scaffolds were tested with hMSCs. Scaffolds prepared by ES method are more planar. In contrast, the CS method produces 3D porous fluffy-like structures with bigger pores that promote cell migration deeper into the scaffolds, thus allowing proliferation of the cells. Moreover, differently prepared scaffolds affect the adhesion of platelets and therefore the release kinetics of bioactive compounds is altered.

Different concentrations of platelets (see Table 1 and Table 2) were tested in order to optimize the optimal platelet concentration regarding the influence on adhesion, metabolic activity, proliferation, and ALP activity of cultured cells. In order to accurately test the influence of released proteins from platelets, cells were cultured in only 2% FBS (MG-63 cells) or 5% FBS (hMSCs) instead of the generally used 5% or 10% FBS, respectively. Furthermore, the culture media was not changed for the whole experiment in order not to aspirate released bioactive compounds. The model of MG-63 osteosarcoma cell line and primary hMSCs were used to confirm the overall effect.

Table 1: MG-63 osteosarcoma cell line was tested in the presence of five different platelet's concentrations. Platelets were adhered on the CS PCL scaffold. Control group was plain PCL scaffold with no platelets. Abbreviation: CS, centrifugal spinning.

Sample	Scaffold type	Cell type	Media	Platelet concentration [platelets/L]
CSP1	CS	MG-63	Growth	$3{,}000 \times 10^9$
CSP2	CS	MG-63	Growth	900×10^9
CSP3	CS	MG-63	Growth	300×10^9
CSP4	CS	MG-63	Growth	100×10^9
CSP5	CS	MG-63	Growth	30×10^9
CSC	CS	MG-63	Growth	-

Table 2: hMSCs were, unlike MG-63 cells, cultured on two different types of PCL scaffolds, either CS or ES scaffolds. Platelets of five different concentrations were adhered on these scaffolds. Moreover, two different types of media were used – growth medium and growth medium with osteogenic supplements (namely 10 mM β-glycerol phosphate, 40 μg mL^{-1} ascorbate-2-phosphate and 100 nM dexamethasone). Control groups were chosen as a CS or ES scaffold in the corresponding media without platelets. Abbreviations: CS, centrifugal spinning; ES, electrospinning; D, growth medium with osteogenic supplements (differentiation medium); N, growth medium (non-differentiation media); OS, osteogenic supplements; P, platelets.

Sample	Scaffold type	Cell type	Media	Platelet concentration [platelets/L]
CSNP1	CS	hMSC	Growth	$3{,}000 \times 10^9$
CSNP2	CS	hMSC	Growth	900×10^9
CSNP3	CS	hMSC	Growth	300×10^9
CSNP4	CS	hMSC	Growth	100×10^9
CSNP5	CS	hMSC	Growth	30×10^9
CSNC	CS	hMSC	Growth	-
CSDP1	CS	hMSC	Growth + OS	$3{,}000 \times 10^9$
CSDP2	CS	hMSC	Growth + OS	900×10^9
CSDP3	CS	hMSC	Growth + OS	300×10^9
CSDP4	CS	hMSC	Growth + OS	100×10^9
CSDP5	CS	hMSC	Growth + OS	30×10^9
CSDC	CS	hMSC	Growth + OS	-
ESNP1	ES	hMSC	Growth	$3{,}000 \times 10^9$
ESNP2	ES	hMSC	Growth	900×10^9
ESNP3	ES	hMSC	Growth	300×10^9
ESNP4	ES	hMSC	Growth	100×10^9
ESNP5	ES	hMSC	Growth	30×10^9
ESNC	ES	hMSC	Growth	-
ESDP1	ES	hMSC	Growth + OS	$3{,}000 \times 10^9$
ESDP2	ES	hMSC	Growth + OS	900×10^9
ESDP3	ES	hMSC	Growth + OS	300×10^9
ESDP4	ES	hMSC	Growth + OS	100×10^9
ESDP5	ES	hMSC	Growth + OS	30×10^9
ESDC	ES	hMSC	Growth + OS	-

4.1.1 THE CHARACTERIZATION OF PCL SCAFFOLDS

The different preparation methods of PCL scaffolds resulted in a different morphology of the produced scaffolds (Figure 11 and Table 3). While the mean fiber diameter for ES scaffolds is 232 ± 129 nm it slightly increased for CS scaffold to 572 ± 330 nm. Also, the mean pore size is lower for ES scaffold, only 0.783 ± 1.521 μm^2. For the CS scaffold we detected bigger pores with a mean pore size of 13.36 ± 33.4 μm^2. Additionally, the porosity

of CS scaffolds is over 16% higher in comparison with the ES scaffold. This result is important as bigger pores enable deeper penetration of cells within the scaffolds volume.

Table 3: Characterization of prepared scaffolds.

Parameter	CS	ES
Fiber diameter ± SD	572 ± 330 nm	232 ± 129 nm
Pore size ± SD	13.36 ± 33.4 μm^2	0.783 ± 1.521 μm^2
Porosity ± SD	62.4 ± 3.67%	46.0 ± 0.27%

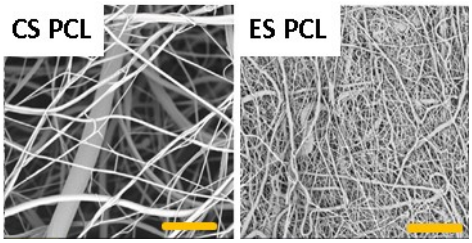

Figure 11: Images taken by SEM showing different morphologies of PCL scaffolds prepared either by CS or ES method. Scale bar 20 μm, magnification 3,000 ×. Abbreviations: CS, centrifugal spinning; ES, electrospinning

4.1.2 THE CHARACTERIZATION OF PLATELET LYSATE

The platelet's content differs inter-individually in terms of the concentration of GFs, chemokines and cytokines. Therefore, a platelet lysate was prepared from each leukocyte-depleted platelets derived from buffy coat used in experiments and further characterized. The platelet lysate was prepared by the freeze/thaw method, this was performed three times using a multiplex protein assay and ELISA (see Tables 4-7). The characterization was performed three times, twice from a bag derived from 4 donors (number of platelets in the bag were 900 × 10^9/L - experiment with platelet adhesion and MG-63 evaluation; and 968 × 10^9/L - experiment with platelet adhesion and hMSC evaluation) and once with a bag derived from 16 donors (number of platelets in the bag was 1020 × 10^9/L – experiment with lyophilizate encapsulation).

The pro-inflammatory cytokines presented in higher concentrations were IL-8, -9, -12, -15, -17, IFN-γ and TNF-α. The other measured pro-inflammatory cytokines, IL-1b, -2, -6 and -7 were below 50 pg mL^{-1}. The anti-inflammatory cytokine present in a higher concentration was IL-1ra. In the case of other anti-inflammatory cytokines, the concentrations were below 50 pg mL^{-1} for IL-4. For IL-10 the concentrations were in the range of 50-100 pg mL^{-1} and once was not detected. In the case of IL-13 the concentrations were below 20 pg mL^{-1} and once was not detected. From chemokines, higher concentrations of IP10, MIP-1b and RANTES were detected. The other chemokines, Eotaxin, MCP-1 and

MIP-1a were below or approximately 100 pg mL^{-1}. However, from a tissue engineering point of view, the GFs have the highest importance for stimulating cell proliferation and differentiation. TGF-β and PDGF-BB were the most abundant GFs identified. Moreover, in high concentrations bFGF, G-CSF, VEGF, EGF and HGF were also present. IGF-1 and KGF were detected in lower concentrations. Furthermore, P-selectin as a marker of release α-granules was detected in a high concentration and thrombospondin, an antiangiogenic factor was also present in a high concentration. Concentrations of some of the tested GFs are not stated in Table 7, they were not measured due to the financial issues.

There were detected differences between platelet lysates prepared from different leukocyte-depleted platelets. These differences reflect the interindividual variabilities between individuals and also between the obtained human leukocyte-depleted platelet derivate from buffy coat.

Table 4: List of pro-inflammatory cytokine concentrations in different leukocyte-depleted platelets derived from buffy coat measured by multiplex protein assay. Abbreviations: LOQ, Limit of quantification; SD, standard deviation. Note: Lower limits of quantification for IL-2, IL-5 and IL-12 are 1.29 pg mL^{-1}, 3.63 pg mL^{-1} and 1.43 pg mL^{-1}, respectively.

Pro-inflammatory cytokine	**Platelet adhesion – MG-63 pg mL^{-1} ± SD**	**Platelet adhesion – hMSC pg mL^{-1} ± SD**	**Lyophilisate encapsulation pg mL^{-1} ± SD**
IL-1b	11.92 ± 0.55	1.6 ± 0.1	7.26 ± 0.21
IL-2	32.61 ± 1.98	7.7 ± 0.4	<LOQ
IL-5	28.52 ± 1.26	41.2 ± 2.8	<LOQ
IL-6	31.13 ± 1.26	15.6 ± 3.5	21.17 ± 2.54
IL-7	52.87 ± 1.8	14.8 ± 0.9	46.28 ± 2.15
IL-8	133.65 ± 12.43	19.2 ± 1.1	116.05 ± 2.16
IL-9	139.18 ± 2.82	95.4 ± 2.7	129.61 ± 2.86
IL-12	228.88 ± 9.17	<LOQ	128.05 ± 5.56
IL-15	108.34 ± 9.17	239.7 ± 15.1	OOR < ± 3.52
IL-17	1774.22 ± 16.27	17.7 ± 1.0	1042.66 ± 27.55
IFN-γ	298.71 ± 13.57	9.1 ± 0.4	164.83 ± 4.15
TNF-α	204.01 ± 7.23	57.2 ± 3.0	145.12 ± 3.41

Table 5: List of anti-inflammatory cytokine concentrations in different leukocyte-depleted platelets derived from buffy coat measured by multiplex protein. Abbreviations: LOQ, Limit of quantification; SD, standard deviation. Note: Lower limits of quantification for IL-10 and IL-13 are 1.06 pg mL^{-1} and 0.31 pg mL^{-1}, respectively.

Anti-inflammatory cytokine	Platelet adhesion – MG-63 pg mL^{-1} ± SD	Platelet adhesion – hMSC pg mL^{-1} ± SD	Lyophilisate encapsulation pg mL^{-1} ± SD
IL-1ra	340.09 ± 15.98	214.0 ± 11.3	235.87 ± 15.25
IL-4	16.75 ± 0.38	1.2 ± 0.1	14.9 ± 0.15
IL-10	109.26 ± 4.95	<LOQ	58.39 ± 1.27
IL-13	13.0 ± 4.0	<LOQ	9.0 ± 0.5

Table 6: List of chemokines concentrations in different leukocyte-depleted platelets derived from buffy coat measured by multiplex protein assay. Abbreviations: SD, standard deviation.

Chemokine	Platelet adhesion – MG-63 pg mL^{-1} ± SD	Platelet adhesion – hMSC pg mL^{-1} ± SD	Lyophilisate encapsulation pg mL^{-1} ± SD
Eotaxin	122.29 ± 3.68	23.3 ± 0.7	78.3 ± 1.29
IP10	383.43 ± 3.64	225.0 ± 4.6	315.08 ± 3.44
MCAF	113.68 ± 12.09	12.3 ± 1.1	58.01 ± 9.95
MIP-1a	25.31 ± 0.34	1.3 ± 0.1	13.09 ± 0.36
MIP-1b	176.95 ± 2.33	1427.1 ± 91.1	156.58 ± 3.34
RANTES	14721.88 ± 342.48	16082.4 ± 1498	11131.75 ± 270.89

Table 7: List of GFs concentrations in different leukocyte-depleted platelets derived from buffy coat measured by ELISA or by multiplex protein assay (G-CSF, GM-CSF, PDGF-BB, VEGF). Abbreviations: SD, standard deviation.

Growth Factor	Platelet adhesion – MG-63 pg mL^{-1} ± SD	Platelet adhesion – hMSC pg mL^{-1} ± SD	Lyophilisate encapsulation pg mL^{-1} ± SD
IGF-1	283.2 ± 27.03	32.4 ± 0	
TGF-β1	76817.0 ± 6384.0	17569.9 ± 1507.8	
bFGF	379.44 ± 10.29	67.6 ± 4.1	273.88 ± 1.64
G-CSF	219.43 ± 12.32	79.0 ± 5.9	138.66 ±7.78
GM-CSF	163.5 ± 6.2	6.5 ± 0.4	98.33 ± 3.26
PDGF-BB	9218.12 ± 164.9	1125.8 ± 29.8	14655.93 ± 115.58
VEGF	521.67 ± 9.34	275.0 ± 29.8	509.83 ± 0.7
KGF	127.94 ± 11.52		49.5 ± 5.5
EGF	403.3 ± 67.51		591.3 ± 123.0

HGF	529.78 ± 12.1	514.6 ± 49.2
SDF-1α	66.5 ± 54.75	33.8 ± 55.9
Thrombospondin	94200.0 ± 11823.2	
P-selectin	4667.0 ± 87.34	

4.1.3 THE RELEASE KINETICS OF PROTEINS FROM ADHERED PLATELETS

The release kinetics of GFs, from platelets adhered on ES and CS PCL scaffolds in five different concentrations were evaluated on the model protein thrombospondin. Thrombospondin, an antiangiogenic factor, was chosen as it is contained in high concentrations in the platelets. On days 1, 3, 7 and 14 the concentrations of released thrombospondin were detected. PCL scaffolds with adhered platelets were incubated in PBS and collected on the experimental days. The thrombospondin concentrations of the two least concentrated samples (CSP4 and ESP4 and CSP5 and ESP5) were below the detection limit of ELISA, therefore, in Figure 12, only the concentrations of CSP1-CSP3 and ESP1-ESP3 are summarized as a cumulative release of thrombospondin.

Clearly, based on the relative release of thrombospondin, this model protein was released for up to 14 days on the most concentrated group CSP1 then plateau phase was reached (Figure 13). The group CSP2 reached the plateau on day 7 and the rest of the tested groups reached the plateau phase on day 1. The plateau phase was reached in dependence on the platelet concentration. Moreover, the scaffolds morphology affected the release kinetics. As a consequence, higher concentrations of thrombospondin were detected on CS scaffolds compare to ES scaffolds as ESP1 group reached the plateau phase on day 3.

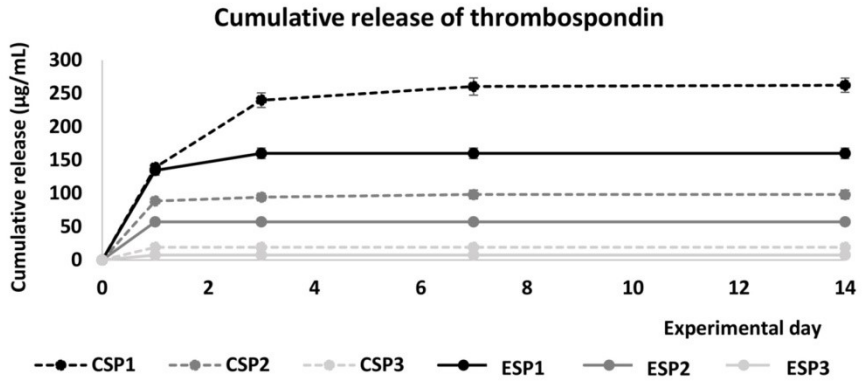

Figure 12: Release kinetics of thrombospondin from platelets adhered on CS and ES PCL scaffolds. Thrombospondin was used as a model protein. Data are presented as the cumulative release. Abbreviations: CS, centrifugally spun scaffold; ES, electrospun scaffold; P1 - 3,000 × 10^9, P2 - 900 × 10^9, P3 - 300 × $10^9$of adhered platelets

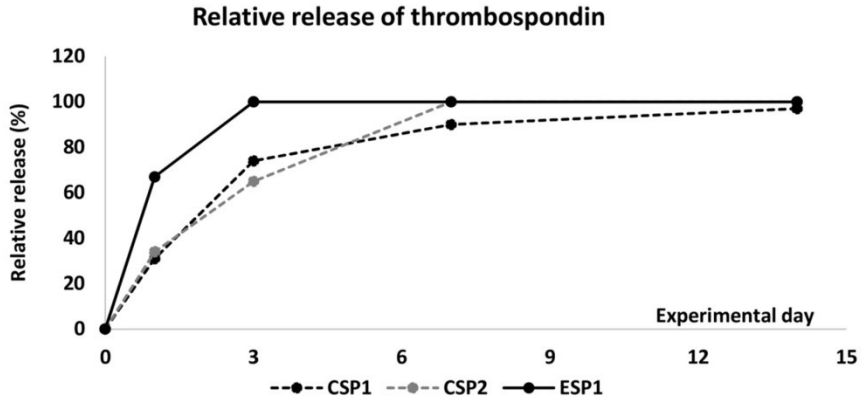

Figure 13: Release kinetics of thrombospondin from platelets adhered on CS and ES PCL scaffolds. Thrombospondin was used as a model protein. Data are presented as the relative release. Only data for samples CSP1, CSP2 and ESP1 are presented, as the rest of the samples released thrombospondin until day one and the curves would overlap. Abbreviations: CS, centrifugally spun scaffold; ES, electrospun scaffold; P1 - 3,000 × 10^9, P2 - 900 × 10^9 platelet/L of adhered platelets

The overall protein release, detected from the same samples as with the release of thrombospondin, is stated in Figure 14. A fluorescent probe was used for the detection of all proteins, thus, the sensitivity of the colorimetric ELISA assay was overcome and release kinetics from all the samples were detected. Based on the results we observed, the release of overall proteins lasted for 14 days. However, as the protein assay measures all the proteins in the samples, the result is influenced by the presence of plasma proteins. Therefore, the differences between the samples are minimal. Group CSP1 showed the highest release of overall proteins.

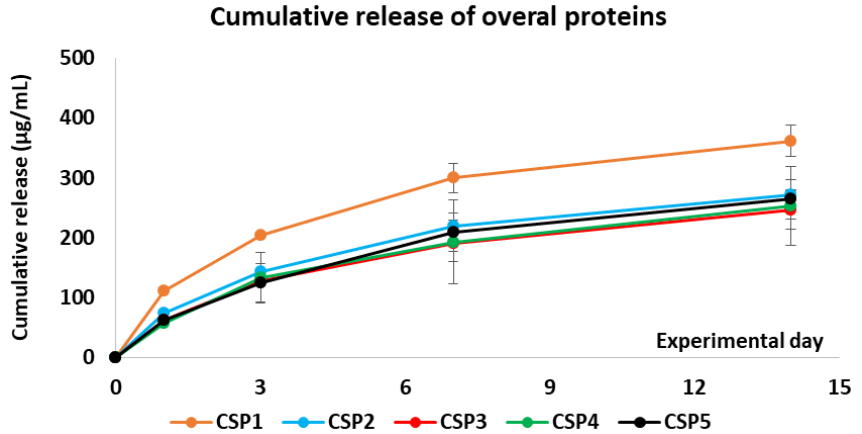

Figure 14: Total protein release from platelets adhered on CS PCL scaffolds measured by Quant-IT Protein assay, data are presented as the cumulative release. Abbreviations: CS, centrifugal spun scaffold; CS, centrifugal spun scaffold; CS, centrifugally spun scaffold; P1 - 3,000 × 10^9; P2 - 900 × 10^9; P3 - 300 × 10^9; P4 - 100 × 10^9; P5 – 30 × 10^9 platelet/L of adhered platelets

Formed fibrin net was visualized by SEM (Figure 15A-15H). The fibrous fibrin net was formed on the surface of the CS PCL scaffolds when the three highest concentrations of platelets (3,000 × 10^9 platelet/L (P1), 900 × 10^9 platelet/L (P2) and 300 × 10^9 (P3)) were used. On the contrary, when the platelets adhered on the surface of the ES PCL scaffold, the fibrin net lacked the fibrous structure and was more dense and visible also for the three highest concentrations of platelets (P1-P3). These results suggest that the differences in the morphology of differently produced PCL scaffolds led to the formation of a different fibrin net. In the case of cell seeding, the observed results are similar. The formed fibrin net is seen as a confluent layer formed over the seeded hMSCs (Figures 15I-K and 15M-O). No fibrin net was visible on the group CSNP4 and ESNP4 (Figures 15L and 15P).

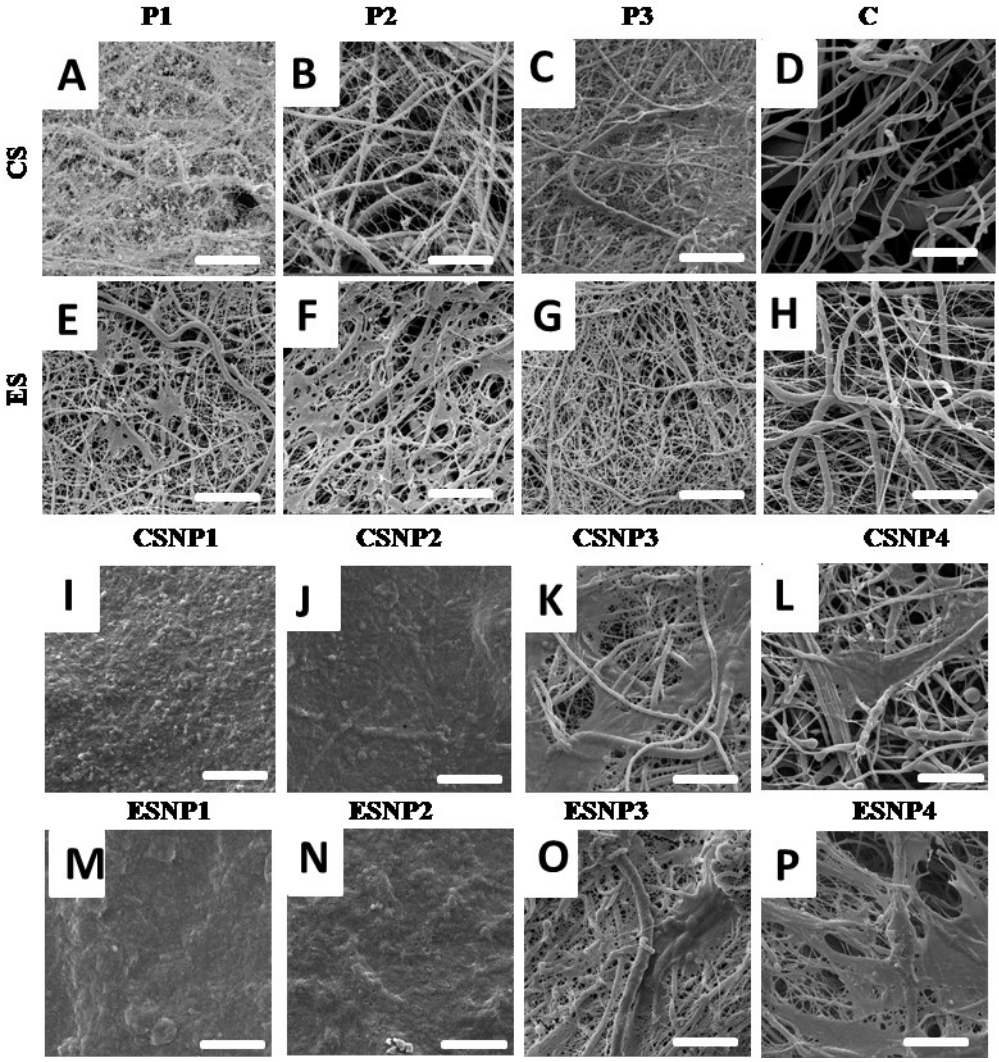

Figure 15: Images taken by SEM of formed fibrin net, after platelet adhesion, on the surface of plain PCL scaffolds without cell seeding (**A-H**). Magnification 4000 ×, scale bar 20 µm. Images taken by SEM of seeded hMSCs with adhered platelets (**I-P**). Magnification 5000 ×, scale bar 10 µm. Abbreviations: CS, centrifugal spinning; ES, electrospinning; N, growth media; P1, 3,000 × 10^9; P2, 900 × 10^9; P3, 3,000 × 10^9 platelet/L; P4, 100 × 10^9; C, control group (no platelets).

4.1.4 CELL PROLIFERATION

A DNA concentration of cells seeded on PCL scaffolds was measured on days 1, 3, 7, 10 and 14 using Quant-iT™ dsDNA Assay Kit. In Figure 16, the proliferation rate of MG-63 cells is stated. The amount of DNA on all tested groups on day 1 is similar. This indicates a comparable cell adhesion, 24 hours after the seeding of the scaffolds. Over the course of the 14 days experiment, the differences in the proliferation became significantly different.

On day 3, we detected higher amount of DNA on groups CSP1 and CSP2 compared to groups CSP4, CSP4 and CSCS. Moreover, group CSP1 had higher amount of DNA in comparison to group CSP3. On day 7, the highest amount of DNA from all the tested groups was detected on group CSP1. Furthermore, DNA amount detected on groups CSP2 and CSP3 was statistically higher compared to groups CSP4, CSP5 and CSC. On day 10, we detected higher amount of DNA on group CSP2 compared to group CSP5. On days 10 and 14, the amount of DNA detected on group CSP1 was statistically higher in comparison to the groups CSP4, CSP5 and CSC. Between groups CSP4, CSP5 and the CSC control group, there were no differences observed during the whole experiment. The highest rate of cell proliferation was observed on group CSP1, followed by groups CSP2 and CSP3. The decline in DNA concentration was probably caused by not changing the media for the whole experiment and in the presence of such an amount of cells, the media was exhausted.

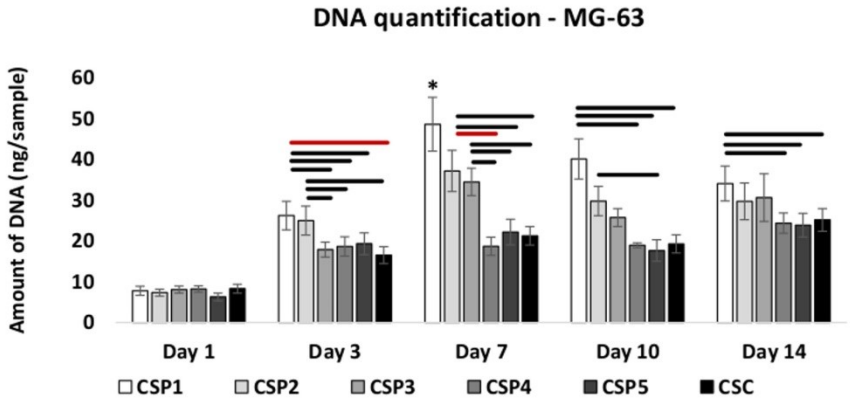

Figure 16: MG-63 osteosarcoma cell line adhesion and proliferation measured using Quant-iT™ dsDNA Assay Kit to quantify DNA. Statistical significance is shown by bars above the columns (* means statistically the highest value versus all tested groups that day, $p < 0.05$ in black and $p < 0.001$ in red).

In the case of scaffolds prepared using the CS method, hMSCs cultured in growth media showed the highest rate of cell proliferation in groups CSNP1 and CSNP2 (Figure 17). The increase in the DNA amount was constant throughout the whole culture period. On day 1, the detected amount of DNA on group CSNP3 was higher in comparison to groups CSNP5 and CSNC and also the higher amount of DNA was detected on group CSNP4 compared to CSNC. On day 3, the amount of DNA in groups CSNP3 and CSNP4 was higher than on group CSNP5. On day 7, we detected higher amount of DNA in group CSNP3 compared to groups CSNP4, CSNP5 and CSNC and also in group CSNP4 compared to group CSNC. On day 10, the amount of DNA in group CSNP3 was higher in comparison to group CSNC. Also higher amount of DNA was detected in group CSNP4 in comparison to groups CSNP5 and CSNC. On day 14, higher amount of DNA was detected in group CSNP3 compared to groups CSNP5 and CSNC and in group CSNP4 compared to group CSNC. No statistical differences were detected between groups CSNP5 and CSNC. In groups CSNP4, CSNP5 and the CSNC control group the increase in the amount of DNA was slower and in lower amounts.

The results from the hMSCs cultivated on the CS scaffold in growth culture media with osteogenic supplements also showed on a positive effect in the two most concentrarted groups, CSDP1 and CSDP2, on the detected amount of DNA while hMSCs were cultivated on the scaffolds in the presence of different platelet concentrations (Figure 18). On days 3 and 7, the amount of DNA in group CSDP3 was higher compared to groups CSDP4, CSDP5 and CSDC. On days 10 and 14, the amount of DNA detected in group CSDP3 was higher in comparison to groups CSDP5 and CSDC. The group CSDP4 showed higher amount of DNA on days 3, 10 and 14 compared to the CSDC control group and on day 10 also in comparison to group CSDP5.

hMSCs cultured in a growth media on ES PCL scaffolds showed in groups ESNP1 and ESNP2 a statistically significant higher amount of DNA compared to groups ESNP4, ESNP5 and the ESNC control group on day 1 (Figure 19). Moreover, higher amount of DNA was also detected in group ESNP2 in comparison to group ESNP1 and in group ESNP3 compared to groups ESNP4, ESNP5 and ESNC. On day 3 and 7, the highest amounts of DNA were detected in groups ESNP1 and ESNP2 compared to groups ESNP3-ESNP5 and ESNC. On day 3, higher amount of DNA was further detected in group ESNP3 in comparison to groups ESNP5 and ESNC. Further cultivation led to a decrease in DNA amount in group ESNP2, while group ESNP1 still statsitically contained the highest amount

of DNA in compariosn to group ESNP4, ESNP5 and ESNC on day 10 and in comparison to all tested groups on day 14. Moreover, the amount of DNA, detected on the ES scaffold with seeded hMSCs in a growth media, was the lowest from all of the tested conditions.

The observed trend was distinct while culturing hMSCs on ES scaffolds in a growth media with osteogenic supplements (Figure 20). An increase in the amount of DNA was observed, even in groups ESDP2 and ESDP3. On day 1, the amount of detected DNA in group ESDC was significantly lower compared to ESDP1-ESDP3 groups. On day 3, the highest amount of DNA was detected in group ESDP1 compared to all tested groups, in group ESDP2 the amount of DNA was higher in comparison to groups ESDP3-ESDP5 and ESDC and in group ESDP3 the amount of DNA was higher in comparison to the groups ESDP5 and ESDC. On day 7, the highest amount of DNA from all tested groups was detected in group ESDP2. In group ESDP1 the amount of DNA was significantly higher in comparison to groups ESDP3-ESDP5 and ESDC and in group ESDP3 the amount of DNA was higher compared to group ESDC. On day 10, in groups ESDP1 and ESDP2 the amount of DNA was higher compared to groups ESDP3-ESDP5 and ESDC and also in group ESDP3 the higher amount of DNA was detected in comaprison to groups ESDP4, ESDP5 and ESDC. On day 14, the highest amount of DNA was detected in group ESDP1 and in group ESDP2 the detected amount of DNA was higher in comparsion to groups ESDP3-ESDP5 and ESDC. Further, a decrease in the amount of DNA was detected on group ESDP3. In group ESDP4 the amount of DNA was higher compared to groups ESDP3, ESDP5 and ESDC.

Similarly to the experiment with MG-63 cells, in the case of seeding hMSCs a statistically significant influence on the amount of DNA was also proven for the two highest concentrations of adhered platelets, regardless of the used culture medium or type of scaffold. Therefore suggesting that the bioactive compounds contained in the platelets showed a positive effect on the amount of DNA. Moreover, we observed positive effect of adhered platelets in synergy with osteogenic supplements, as differences in the amount of DNA were even observed for groups CSDP3 and CSDP4 in contrast to the CSDC control group.

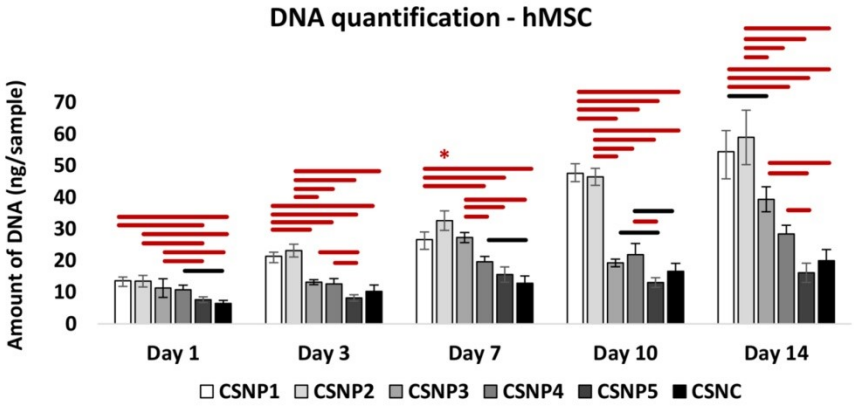

Figure 17: hMSC proliferation measured using Quant-iT™ dsDNA Assay Kit to quantify the amount of DNA. hMSCs cultivated on CS scaffolds in growth media. Statistical significance is shown by bars above the columns (* means statistically the highest value versus all tested groups that day, $p < 0.05$ in black and $p < 0.001$ in red).

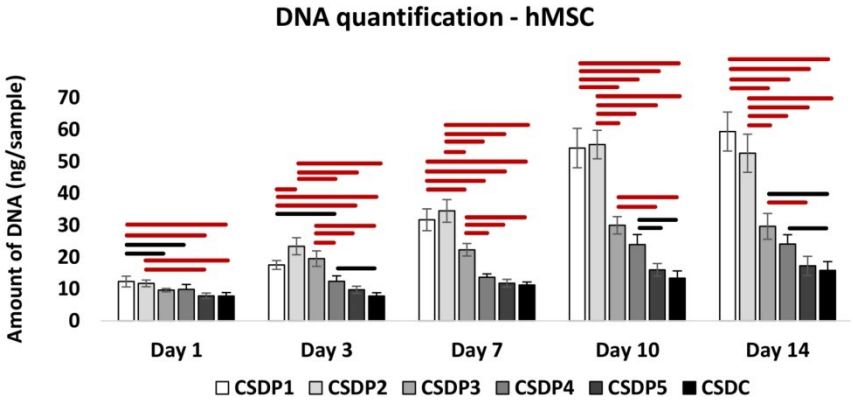

Figure 18: hMSC proliferation measured using Quant-iT™ dsDNA Assay Kit to quantify the amount of DNA. hMSCs cultivated on CS scaffolds in growth media with osteogenic supplements. Statistical significance is shown by bars above the columns ($p < 0.05$ in black and $p < 0.001$ in red).

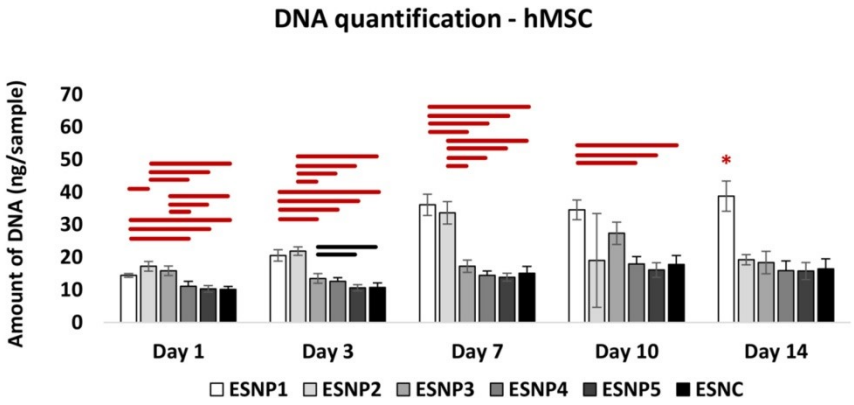

Figure 19: hMSC proliferation measured using Quant-iT™ dsDNA Assay Kit to quantify the amount of DNA. hMSCs cultivated on ES scaffolds in growth. Statistical significance is shown by

bars above the columns ((* means statistically the highest value versus all tested groups that day, $p < 0.05$ in black and $p < 0.001$ in red).

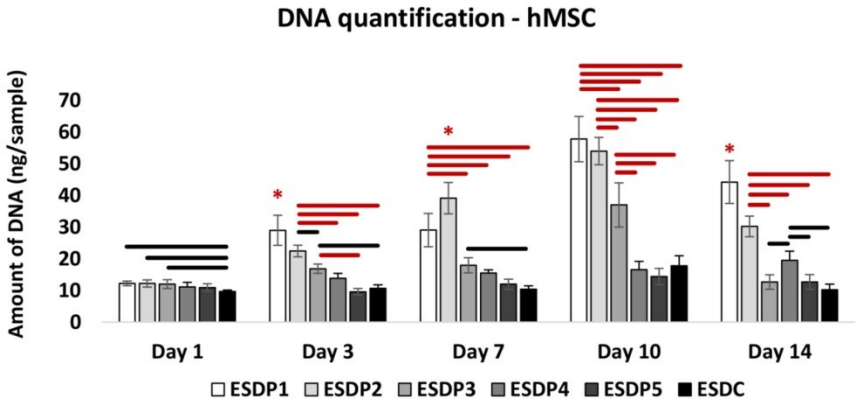

Figure 20: hMSC proliferation measured using Quant-iT™ dsDNA Assay Kit to quantify the amount of DNA. hMSCs cultivated on ES scaffolds in growth media with osteogenic supplements. Statistical significance is shown by bars above the columns (* means statistically the highest value versus all tested groups that day, $p < 0.05$ in black and $p < 0.001$ in red).

A comparison of the tested groups from the point of view of the used scaffolds, showed that the best cell adhesion occurred on samples ESNP1, ESNP2 and ESNP3. Proliferation was comparable on the scaffolds until day 7. After this time point the detected amount of DNA differed; in general groups CSNP1, CSNP2, CSDP1 and CSDP2 contained the highest amount of DNA. This means that the different morphology of scaffolds led to different platelets activation that subsequently influenced hMSC proliferation. In the lower concentrations of adhered platelets the differences were not so distinct.

4.1.5 METABOLIC ACTIVITY

The metabolic activity of MG-63 cells, stated in Figure 21, rose steadily over period of 14 days. No statistically significant differences were detected between the CSC control group and groups CSP3-CSP5. In groups CSP1 and CSP2 we observed a statistically significant rate of metabolic activity that was dose dependent with used platelet concentrations. Group CSP1 showed the best metabolic activity from all of the tested groups on days 1, 3, 7 and 10. On day 14, the metabolic activity between groups CSP1 and CSP2 was comparable.

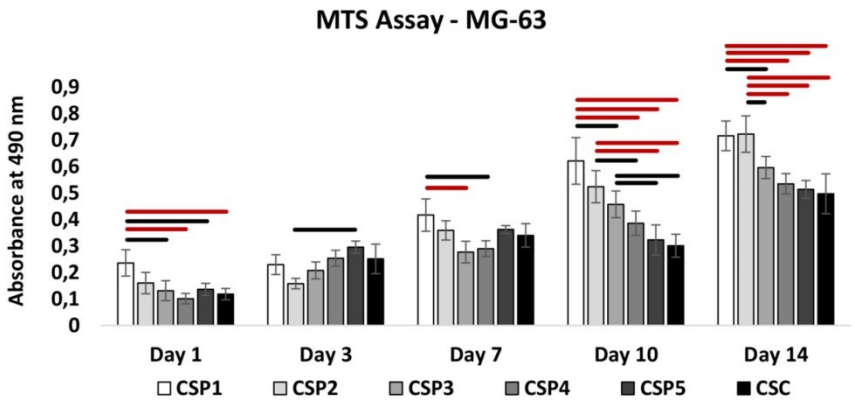

Figure 21: Metabolic activity of MG-63 osteosarcoma cell line seeded on scaffolds was determined using the MTS assay. Statistical significance is shown by bars above the columns ($p < 0.05$ in black and $p < 0.001$ in red).

A positive effect on metabolic activity of hMSCs was observed in the groups with the three highest concentrations of platelets, regardless of the scaffold and culture media (Figure 22-25). In general, the culture media enriched with osteogenic supplements had the most positive effect on metabolic activity of the hMSCs.

In some experimental groups, there was an observed decrease in cell metabolic activity during the experiment. This phenomenon could be caused by the fact that the culture media was not changed during the experiment and that a lower amount of FBS was used while the cells were seeded in the higher amount. On the contrary, there was hardly any decrease in metabolic activity observed in the case of MG-63 cells, but the amount of seeded MG-63 cells was 2.5 times lower compared to seeded hMSCs. Based on the results we observed a positive platelets concentration dependent effect on the cell metabolic activity.

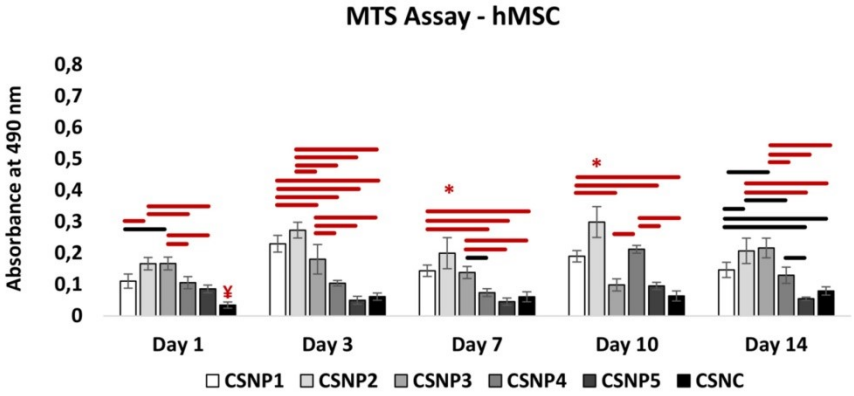

Figure 22: Metabolic activity of hMSC seeded on scaffolds was determined using the MTS assay. hMSC cultivated on CS scaffolds in growth media. Statistical significance is shown by bars above the columns (* means statistically highest value versus all tested groups that day, $p < 0.05$ in black and $p < 0.001$ in red).

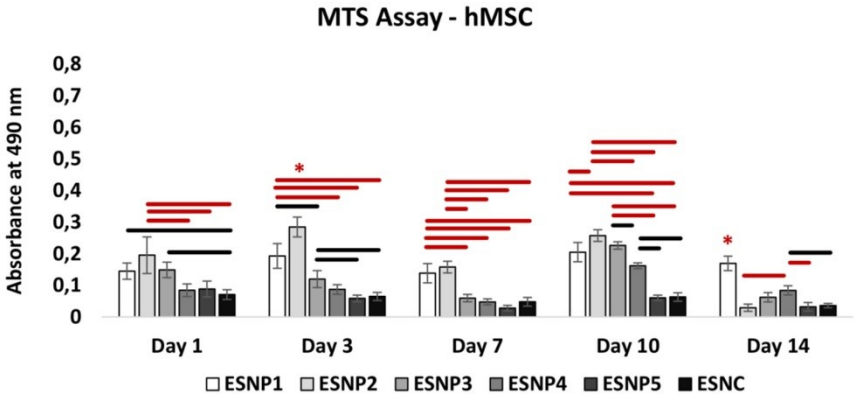

Figure 23: Metabolic activity of hMSC seeded on scaffolds was determined using the MTS assay. hMSC cultivated on ES scaffolds in growth media. Statistical significance is shown by bars above the columns (* means statistically highest value versus all tested groups that day, $p < 0.05$ in black and $p < 0.001$ in red).

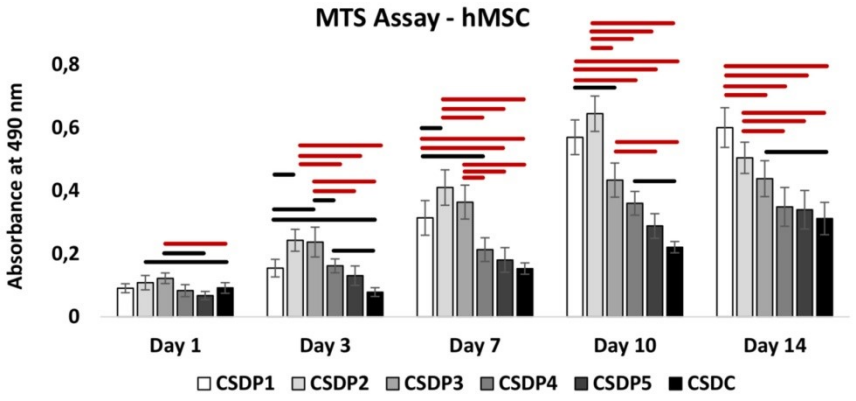

Figure 24: Metabolic activity of hMSC seeded on scaffolds was determined using the MTS assay. hMSC cultivated on CS scaffolds in growth media with osteogenic supplements. Statistical significance is shown by bars above the columns ($p < 0.05$ in black and $p < 0.001$ in red).

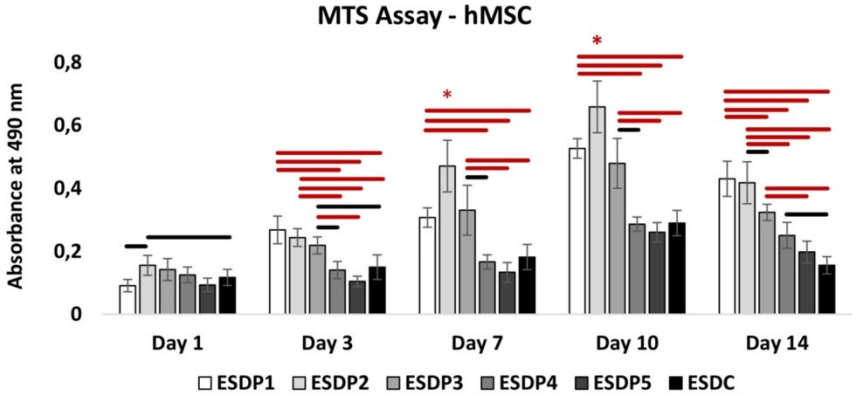

Figure 25: Metabolic activity of hMSC seeded on scaffolds was determined using the MTS assay. hMSC cultivated on ES scaffolds in growth media with osteogenic supplements. Statistical significance is shown by bars above the columns (* means statistically highest value versus all tested groups that day, $p < 0.05$ in black and $p < 0.001$ in red).

4.1.6 Alkaline phosphatase activity

ALP activity is a marker of osteogenic differentiation; therefore it was evaluated in order to test the effect of platelets on days 1, 7 and 14. The ALP activity of MG-63 osteosarcoma cell line (Figure 26) seeded on the scaffolds in the presence of different concentration of platelets showed a similar trend to the metabolic activity of the cells. Between groups CSP3-CSP5 and the CSC control group there were no statistical differences detected. However, the CSP1 group showed significantly higher ALP activity from all of the tested groups. The ALP activity of the MG-63 cells on group CSP2 was statistically higher compared to groups CSP3-CSP5 and the CSC control group.

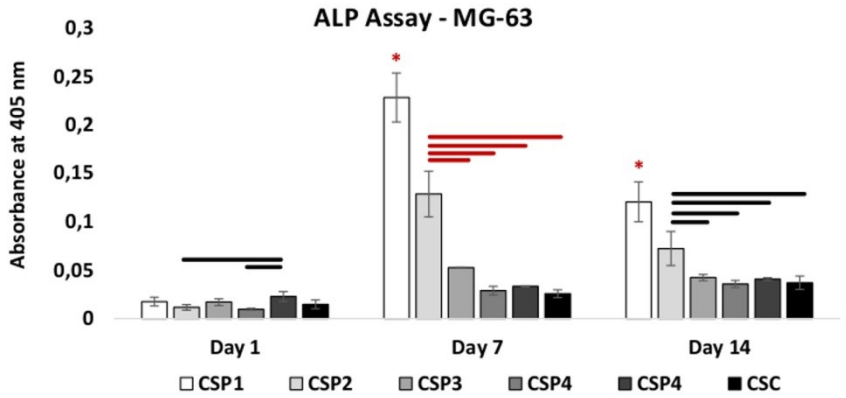

Figure 26: ALP activity of MG-63 osteosarcoma cell line seeded on scaffolds was determined using 1-Step™ PNPP kit. Statistical significance is shown by bars above the columns (* means statistically highest value versus all tested groups that day, $p < 0.05$ in black and $p < 0.001$ in red).

Unlike the MG-63 osteosarcoma cell line, hMSCs seeded on both type of scaffolds in a growth media showed a less strong effect of platelets on the ALP activity. In the case of CS scaffolds, on day 1, higher ALP activity was detected on group CSNP1, CSNP2 and CSNP5 in comparison with CSNC group (Figure 27). On day 14, higher ALP activity was detected on group CSNP2 in comparison with groups CSNP1, CSNP4, CSNP5 and CSNC. While hMSCs were cultivated on ES scaffolds in growth media, increased ALP activity was detected on day 1 on group ESNP2 in comparison with groups ESNP4, ESNP5 and ESNC (Figure 28). On day 14, higher ALP activity was detected on group ESNC in comparison with groups ESNP1 and ESNP4.

The situation was different when the hMSCs were cultivated in a growth media with osteogenic supplements. We observed a synergistic effect of osteogenic supplements together with adhered platelets on the enhanced ALP activity of hMSCs. In case when hMSCs were cultured on CS scaffolds, higher ALP activity was detected on groups CSDP1, CSDP2 and CSDP4 in comparison with CSDC on day 1 (Figure 29). On day 7, statistically higher ALP activity was detected on group CSDP3 in comparison with groups CSDP1, CSDP1 and CSDC. Furthermore, higher ALP activity was detected also on groups CSDP2 and CSDP4 compared to groups CSDP5 and CSDC. On day 14, three highest concentrations of platelets led to statistically higher ALP activity in comparison to the CSDP4, CSDP5 groups and the CSDC control group. On CSDC control group was further detected higher ALP activity in comparison with CSDP5 group.

In the case of ES PCL scaffolds seeded with hMSCs and cultivated in growth media with osteogenic supplements, on day 7, higher ALP activity was detected on group ESDP3 compared to groups ESDP4, ESDP5 and ESDC (Figure 30). On day 14, the ESDP3 group showed higher ALP activity in comparison to groups ESDP4, ESDP5 and ESDC. Higher ALP activity was further detected on group ESDP2 compared to groups ESDP5 and ESDC and also on group ESDP1 in comparison to group ESDC.

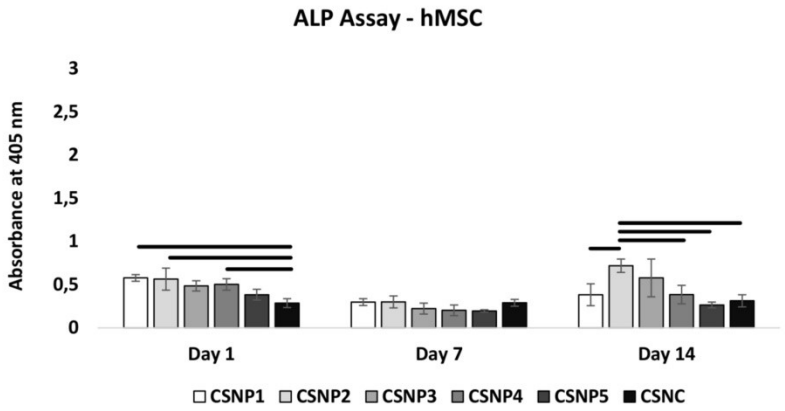

Figure 27: ALP activity of hMSC on scaffolds was determined using 1-Step™ PNPP kit. hMSC cultivated on CS scaffolds in growth media. Statistical significance is shown by bars above the columns ($p < 0.05$).

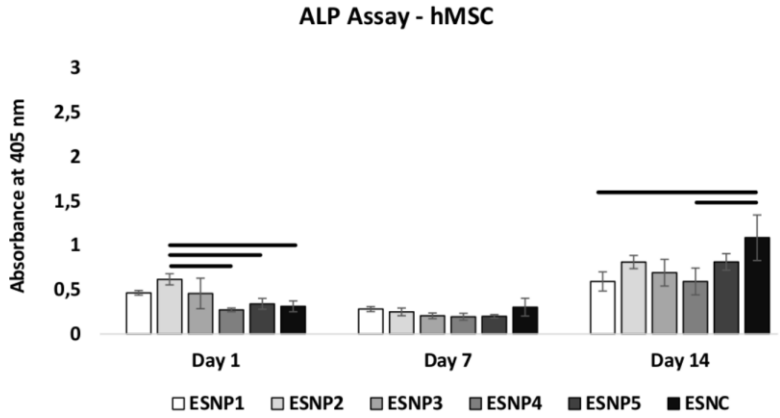

Figure 28: ALP activity of hMSC on scaffolds was determined using 1-Step™ PNPP kit. hMSC cultivated on ES scaffolds in growth media. Statistical significance is shown by bars above the columns ($p < 0.05$).

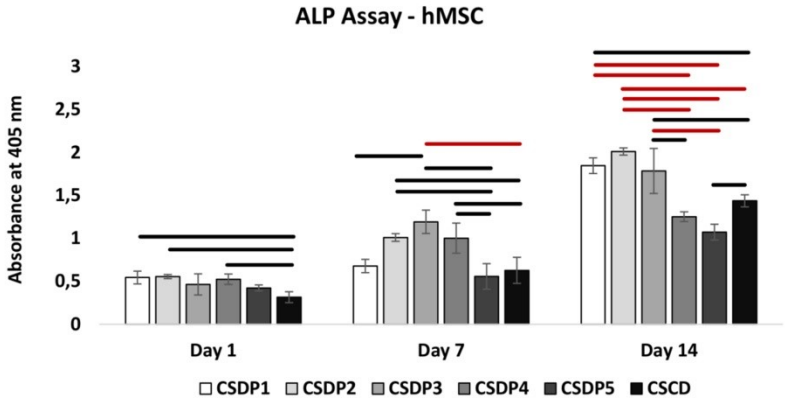

Figure 29: ALP activity of hMSC on scaffolds was determined using 1-Step™ PNPP kit. hMSC cultivated on CS scaffolds in growth media with osteogenic supplements. Statistical significance is shown by bars above the columns ($p < 0.05$ in black and $p < 0.001$ in red).

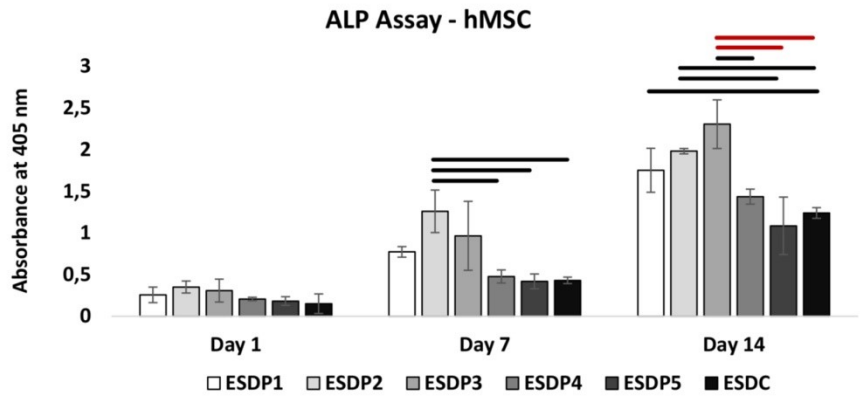

Figure 30: ALP activity of hMSC on scaffolds was determined using 1-Step™ PNPP kit. hMSC cultivated on ES scaffolds in growth media with osteogenic supplements. Statistical significance is shown by bars above the columns ($p < 0.05$ in black and $p < 0.001$ in red).

These results suggest that bioactive molecules contained in the platelets have the effect to further promote the osteogenic activity of osteosarcoma cell line MG-63 cells. The effect on hMSCs was only observed in synergy with the osteogenic supplements added into the growth media. It means that solely GFs and other factors contained in the platelets are not sufficient to induce the osteogenic differentiation of hMSCs. Interestingly, the highest concentration of platelets showed the best ALP activity for cultured MG-63 cells. Yet in the case of hMSCs in a growth media with osteogenic supplements, groups CSDP2 and ESDP3 showed the best results, meaning that the induction of osteogenic differentiation could be achieved with a lower amount of bioactive molecules in stem cells, while a further promotion of osteogenic activity in already differentiated cells was achieved with higher concentrations of adhered platelets.

4.1.7 CELL MORPHOLOGY AND SPREADING ON THE SCAFFOLDS

A confocal microscopy observation was performed to verify the adhesion on the first day and also to examine the cell interaction with the scaffolds through further experimental days. DiOC6(3) and propidium iodide were used to visualize cell membranes and cell nuclei, respectively. MG-63 cells adhered on the scaffolds similarly in all of the tested groups (Figure 31, Figure 32). Throughout the cell culture period the number of MG-63 cells increased. The highest amount of cells was observed on days 7 and 14 in group CSP1 which is in agreement with the DNA amount quantified (Figure 16). Moreover, MG-63 cells were well spread on all scaffolds to a similar extent as they were adhered on the polymeric fibers.

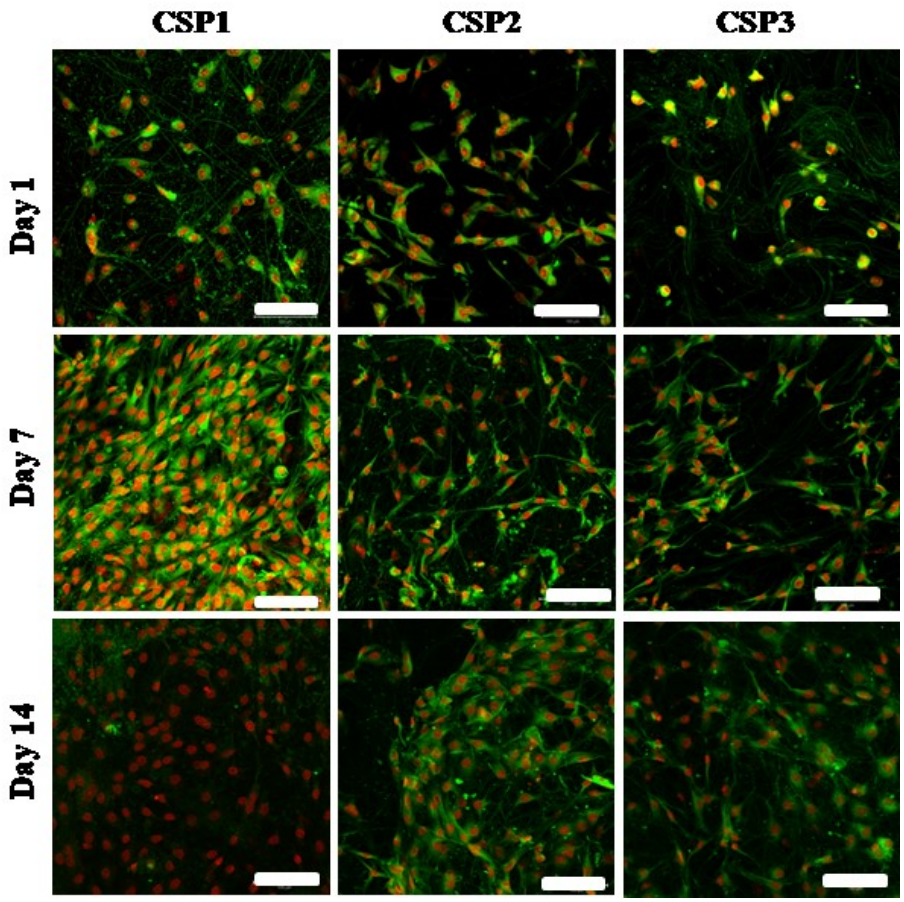

Figure 31: Visualization of MG-63 osteosarcoma cell line adhesion and distribution on CSP1-CSP3 scaffolds using a confocal microscope. Cell nuclei were stained using propidium iodide (red color) and cell membranes using DiOC6(3) (green color). Magnification 200 ×, scale bar 100 μm. Abbreviations: CS, centrifugally spun scaffold; P1 - 3,000 × 10^9; P2 - 900 × 10^9; P3 - 300 × 10^9 platelet/L.

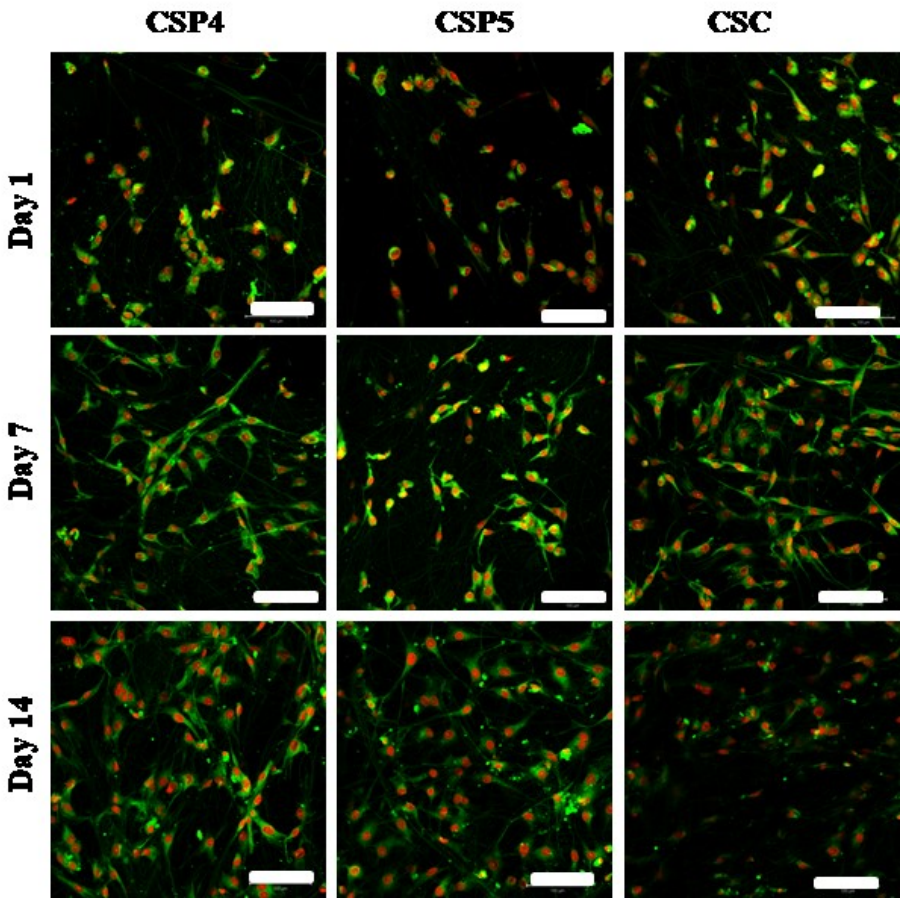

Figure 32: Visualization of MG-63 osteosarcoma cell line adhesion and distribution on CSP4, CSP and CSC scaffolds using a confocal microscope. Cell nuclei were stained using propidium iodide (red color) and cell membranes using DiOC6(3) (green color). Magnification 200 ×, scale bar 100 µm. Abbreviations: CS, centrifugally spun scaffold; P4 - 100 × 10^9; P5 – 30 × 10^9 platelet/L; C, control group (no platelets).

A confocal microscopy observation of hMSCs seeded on PCL scaffolds (Figure 33-36), showed adhered and spread cells even on day 1 on the surface of the scaffold. As the cultivation period proceeded we observed confluent layers of hMSCs on day 14. A lower amount of cells was apparent in the control groups and the groups with a lower amount of adhered platelets which is in agreement with DNA quantification (Figure 17-20).

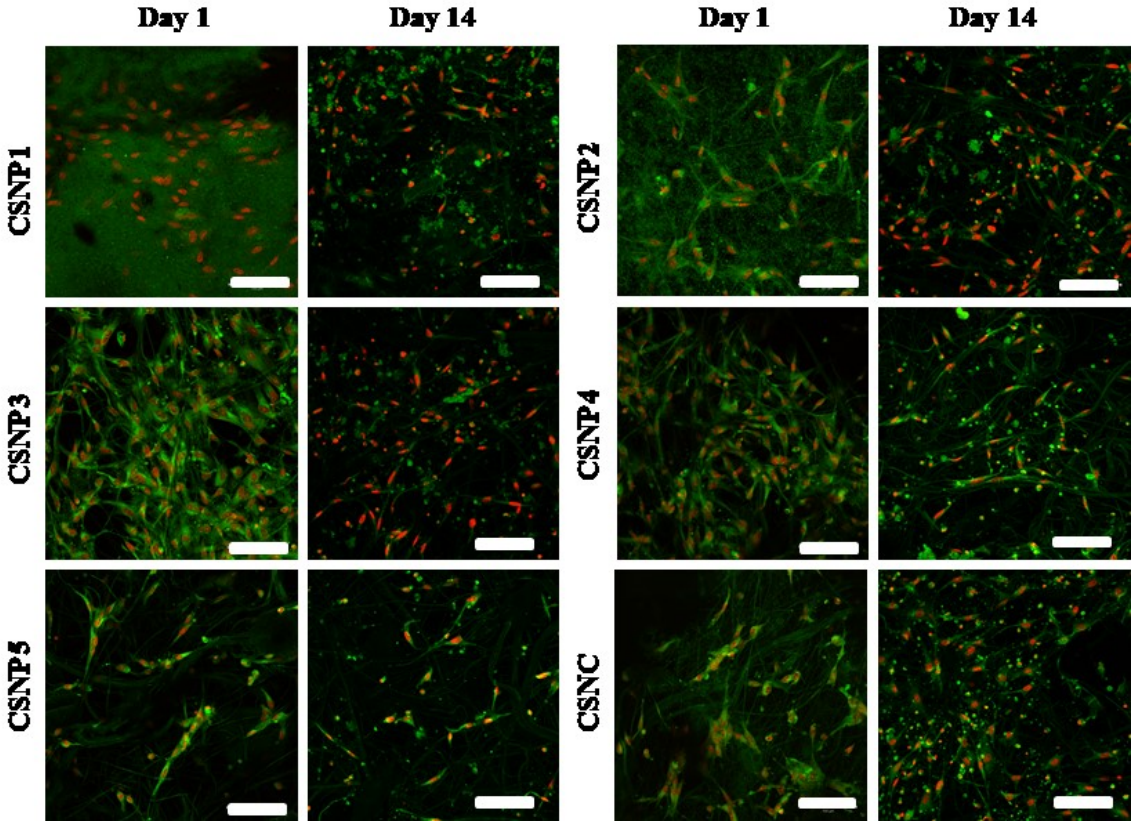

Figure 33: Visualization of hMSC adhesion and distribution on CS scaffolds using a confocal microscope. hMSCs were cultured in growth media. Cell nuclei were stained using propidium iodide (red color) and cell membranes using DiOC6(3) (green color). Magnification 200 ×, scale bar 100 µm. Abbreviations: CS, centrifugally spun scaffold; N, growth media; P1 - 3,000 × 10^9; P2 - 900 × 10^9; P3 - 300 × 10^9; P4 - 100 × 10^9; P5 – 30 × 10^9 platelet/L; C, control group (no platelets).

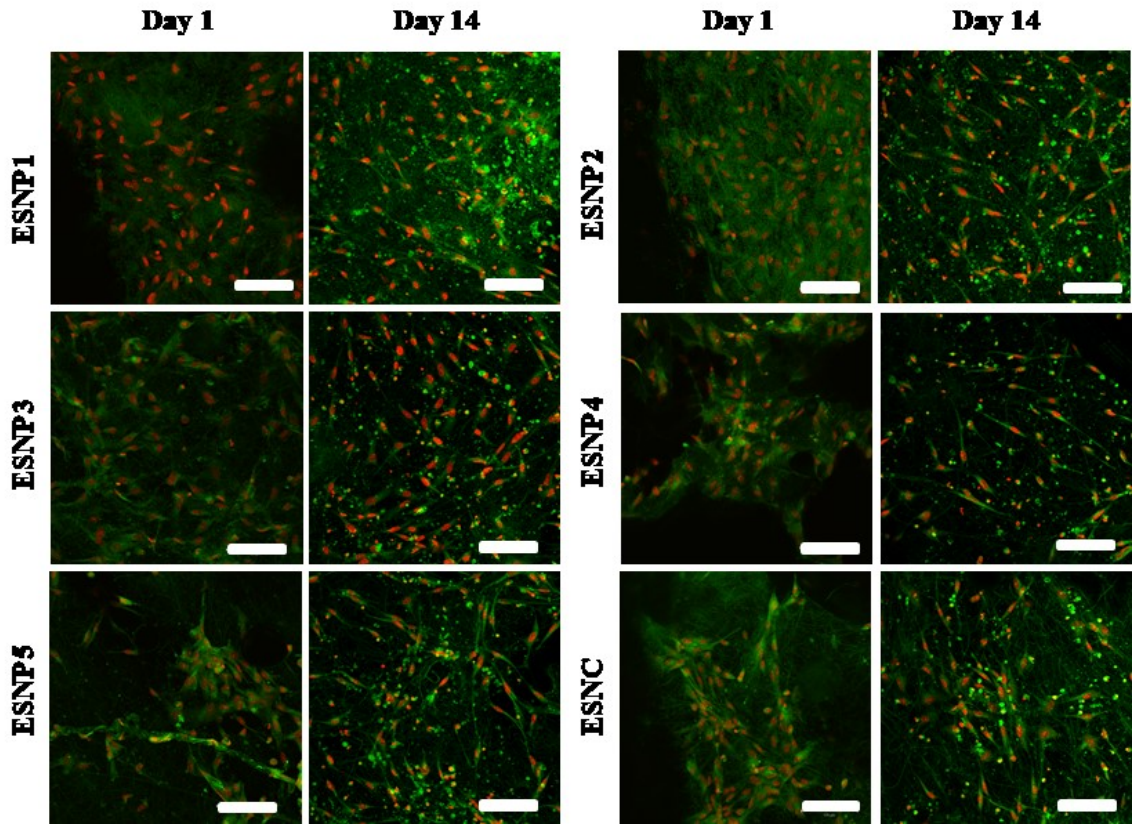

Figure 34: Visualization of hMSC adhesion and distribution on ES scaffolds using a confocal microscope. hMSCs were cultured in growth media. Cell nuclei were stained using propidium iodide (red color) and cell membranes using DiOC6(3) (green color). Magnification 200 ×, scale bar 100 µm. Abbreviations: ES, electrospun scaffold; N, growth media; P1 - 3,000 × 10^9; P2 - 900 × 10^9; P3 - 300 × 10^9; P4 - 100 × 10^9; P5 – 30 × 10^9 platelet/L; C, control group (no platelets).

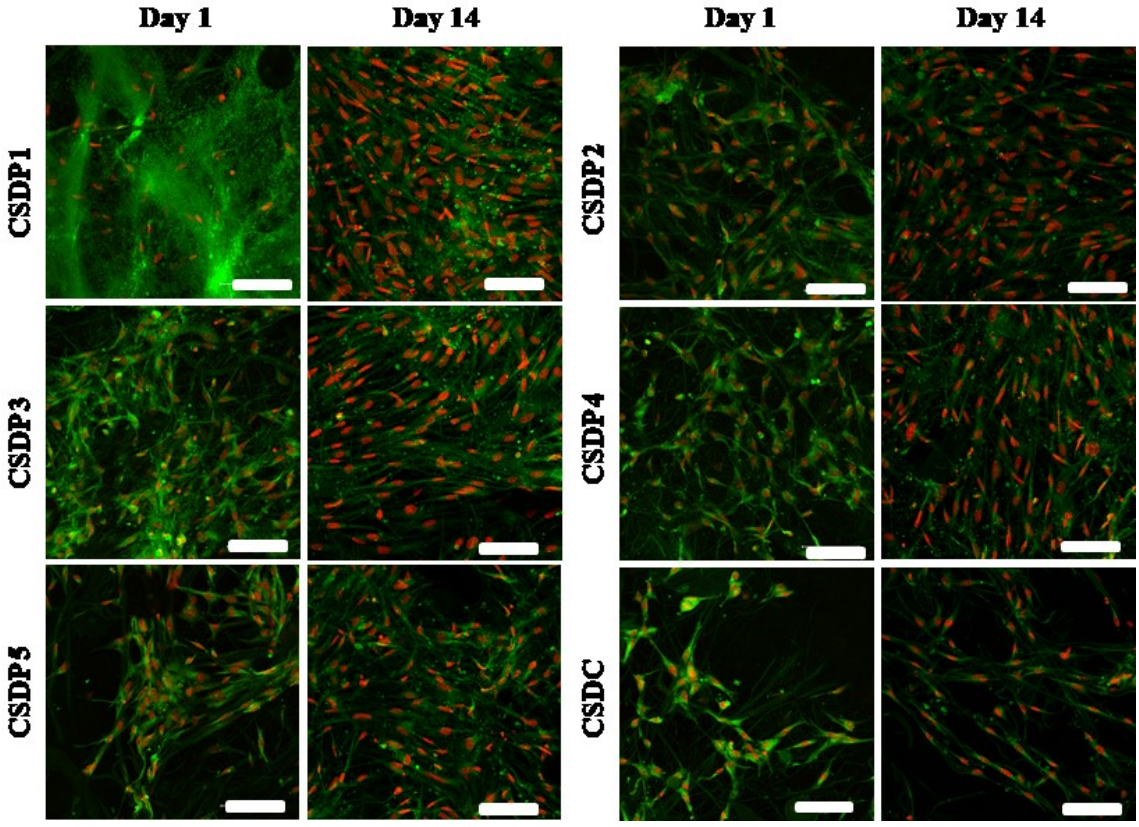

Figure 35: Visualization of hMSC adhesion and distribution on CS scaffolds using a confocal microscope. hMSCs were cultured in growth media with added osteogenic supplements. Cell nuclei were stained using propidium iodide (red color) and cell membranes using DiOC6(3) (green color). Magnification 200 ×, scale bar 100 µm. Abbreviations: CS, centrifugally spun scaffold; D, growth media with OS; P1 - 3,000 × 10^9; P2 - 900 × 10^9; P3 - 300 × 10^9; P4 - 100 × 10^9; P5 – 30 × 10^9 platelet/L; C, control group (no platelets).

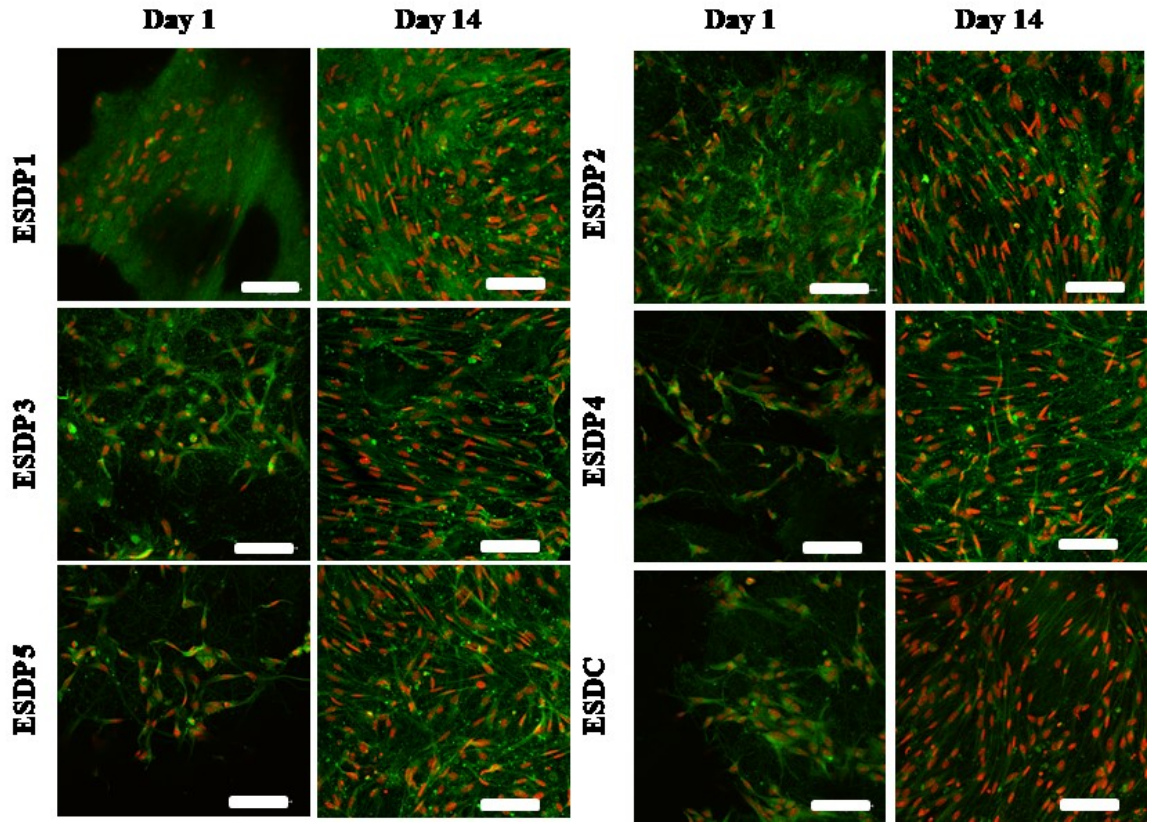

Figure 36: Visualization of hMSC adhesion and distribution on ES scaffolds using a confocal microscope. hMSCs were cultured in growth media with added osteogenic supplements. Cell nuclei were stained using propidium iodide (red color) and cell membranes using DiOC6(3) (green color). Magnification 200 ×, scale bar 100 μm. Abbreviations: ES, electrospun scaffold; D, growth media with OS; P1 - 3,000 × 10^9; P2 - 900 × 10^9; P3 - 300 × 10^9; P4 - 100 × 10^9; P5 – 30 × 10^9 platelet/L; C, control group (no platelets).

4.2 PLATELET LYOPHILISATE ENCAPSULATION EXPERIMENT

In the previous set of experiments, we demonstrated the positive effect of released bioactive compounds, from activated platelets, on metabolic activity, proliferation and enhanced ALP activity of MG-63 osteosarcoma cell line and hMSCs. Due to the fact that this system allows only a short-term delivery of released molecules, encapsulation of lyophilized platelet lysate (lyophilisate) into the core of PCL nanofibers was performed. As a result of the emulsification CS method, core/shell fibers, in other words coaxial nanofibers, are produced. In this way, the release of bioactive compounds from the core of nanofibers would be prolonged.

Different concentrations of lyophilisate were used for the preparation of coaxial PCL nanofibers. The overall characterization of GFs, cytokines and chemokines content of platelets are listed above (see Tables 4-7). During the emulsion approach of the coaxial PCL fibers with encapsulated lyophilisate, it is necessary to protect the lyophilisate from

degradation in order to preserve the bioactivity of the GFs, cytokines and chemokines. Therefore, PF-68, an amphiphilic polymer, was used. The efficiency of lyophilisate encapsulation and preservation of its bioactivity were verified using the model molecule HRP, see Table 8 for the composition and naming of the samples. The blend encapsulation of HRP or lyophilisate was always used as a control for the emulsion approach of the PCL scaffold preparation.

The most promising scaffolds, with platelet lyophilisate in the core of the PCL fibers, were biologically evaluated on the model of MG-63 osteosarcoma cell line in terms of cell proliferation and viability, and a plain PCL scaffold was used as a control (Table 9). In order not to wash out the bioactive compounds released from the PCL scaffolds, the culture medium was not changed during the 14 days experiment. Furthermore, the MG-63 cells were cultured in a medium with only 2% of FBS, instead of generally used 5%, to accurately test the overall effect of released platelet lyophilisate on cultivated MG-63 cells.

Table 8: Sample naming list of scaffolds with encapsulated HRP. Abbreviations: CS, centrifugal spinning; HRP, horseradish peroxidase; PF-68, Pluronic F-68; w/v, weight/volume.

Sample	Scaffold type	PF-68	HRP
0%PF-HRP	CS	0% (w/v)	300 μg mL^{-1}
5%PF-HRP	CS	5% (w/v)	300 μg mL^{-1}
10%PF-HRP	CS	10% (w/v)	300 μg mL^{-1}
20%PF-HRP	CS	20% (w/v)	300 μg mL^{-1}
PCL blend HRP	CS	-	300 μg mL^{-1}

Table 9: Sample naming list of scaffolds with encapsulated platelet lyophilisate, Abbreviations: C, control; CS, centrifugal spinning; PF-68, Pluronic F-68; w/v, weight/volume.

Sample	Scaffold type	Cell type	PF-68	Platelet lyophilisate
0%PF-LYO	CS	No cell testing	0% (w/v)	2 mg mL^{-1}
5%PF-LYO	CS	MG-63	5% (w/v)	2 mg mL^{-1}
10%PF-LYO	CS	MG-63	10% (w/v)	2 mg mL^{-1}
20%PF-LYO	CS	No cell testing	20% (w/v)	2 mg mL^{-1}
PCL blend LYO	CS	No cell testing	-	2 mg mL^{-1}
C	CS	MG-63	-	-

4.2.1 THE CHARACTERIZATION OF COAXIAL FIBERS

Different PCL scaffolds were prepared by CS using the emulsion approach. It resulted in the formation of PCL fibers in the range of micro- to nanofibers (Table 10). A high number of defects in the shape of droplets were present (Figure 37). The mean microfiber diameter was comparable between each group. The smallest diameter of nanofibers was measured in the PCL blend LYO group, this group was also connected with the highest percentage of pores larger than 10 μm^2.

Table 10: Characterization of prepared scaffolds. Abbreviations: SD, standard deviation.

Sample	Microfiber dimeter ± SD	Nanofiber diameter ± SD	Mean pore size	Pores larger than 10 μm^2
0%PF-LYO	1.6 ± 0.6 µm	440 ± 110 nm	38 ± 47 μm^2	32 %
5%PF-LYO	2.4 ± 1.9 µm	470 ± 103 nm	30 ± 29 μm^2	24 %
10%PF-LYO	2.1 ± 0.9 µm	453 ± 95 nm	32 ± 21 μm^2	20 %
20%PF-LYO	2 ± 1.2 µm	537 ± 168 nm	29 ± 39 μm^2	21 %
PCL blend LYO	2.7 ± 1.5 µm	338 ± 90 nm	47 ± 56 μm^2	36 %

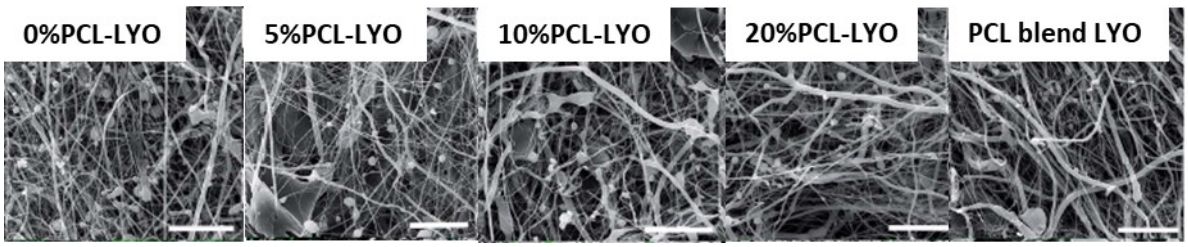

Figure 37: Images taken by SEM from prepared PCL scaffolds with encapsulated lyophilisate, scale bar 50 µm.

THE DETECTION OF ACTIVITY AND RELEASED KINETICS OF ENCAPSULATED HRP

In order to evaluate the protective effect of PF-68 on the bioactivity of proteins encapsulated in the core of the PCL fibers, we encapsulated a model enzyme, HRP (Table 8), to measure its biological activity (Figure 38). PCL fibers with PF-68 showed > 60% activity of released HRP in comparison to fibers without PF-68 that showed only < 30% activity of HRP. These results indicate a protective activity of PF-68 on encapsulated HRP due to its amphiphilic structure.

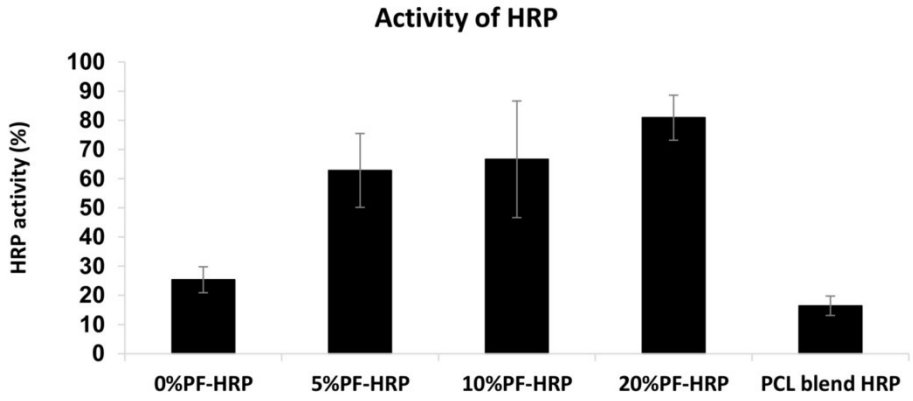

Figure 38: Activity of HRP released from the core of the PCL fibers. Abbreviation: HRP, horseradish peroxidase.

RELEASE KINETICS OF PROTEINS FROM SCAFFOLDS WITH ENCAPSULATED PLATELET LYOPHILISATE

The quantification of released overall proteins from encapsulated lyophilisate (Figure 39) indicated that proteins were released for a period of 14 days and the plateau phase was not reached, as it was when platelet adhesion was performed (Figure 14), however, released concentrations of bioactive compounds were much lower. The highest released rates were detected in groups 10%PF-LYO and 20%PF-LYO. Scaffolds with lower or no concentration of PF-68 (0%PF-LYO and 5%PF-LYO) showed a slower release comparable to the PCL blend LYO scaffold, indicating a low efficiency of the encapsulation procedure.

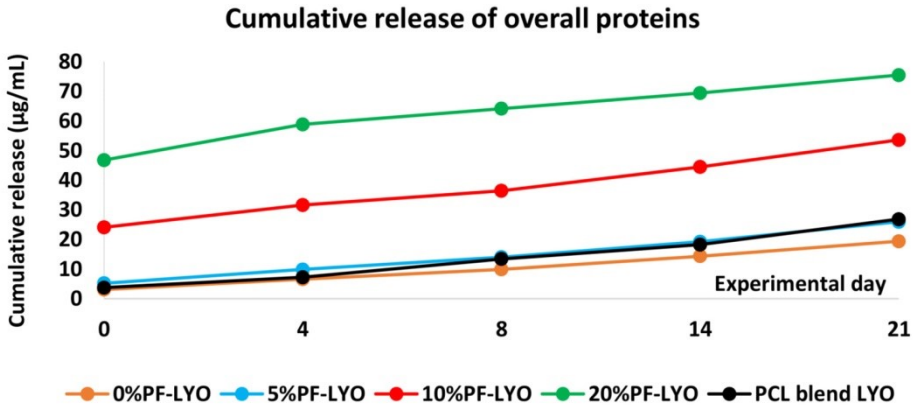

Figure 39: Release kinetics of lyophilisate from the core of PCL fibers, data are presented as the cumulative release.

4.2.2 CELL PROLIFERATION

Based on the results obtained by the Quant-iT™ dsDNA Assay Kit, the DNA amount was comparable on all three tested groups on the first day, suggesting that cell seeding was uniform (Figure 40). We observed an ingrowth of MG-63 cells towards day 3, however, a significantly lower DNA amount was detected in the control group. Throughout further cultivation days, the differences between the samples united.

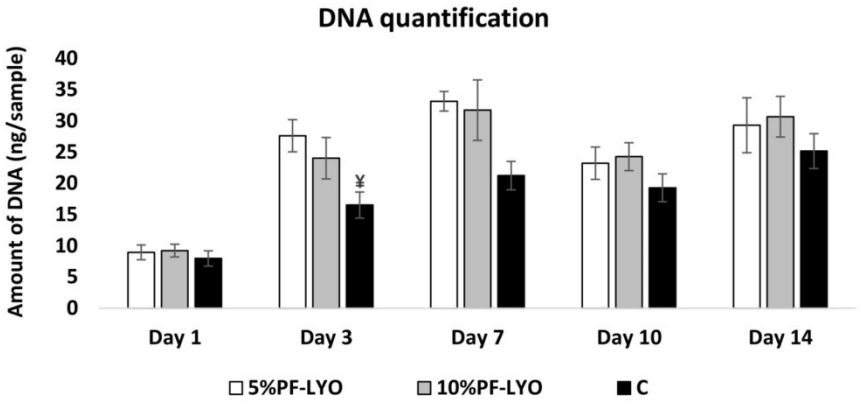

Figure 40: MG-63 osteosarcoma cell line adhesion and proliferation measured using Quant-iT™ dsDNA Assay Kit to quantify DNA. Statistical significance is shown above the columns (¥ means statistically lowest value versus all tested groups that day with $p < 0.05$).

4.2.3 METABOLIC ACTIVITY

Unlike DNA quantification, the metabolic activity of seeded MG-63 cells revealed that from day 1 to day 10, the control group showed the significantly lowest metabolic activity compared to both groups with an encapsulated platelet lyophilisate (Figure 41). On day 14, there were no differences detected between the 5%PF-LYO group and the control group, however, the 10%PF-LYO group showed the statistically highest metabolic activity from all of the tested groups.

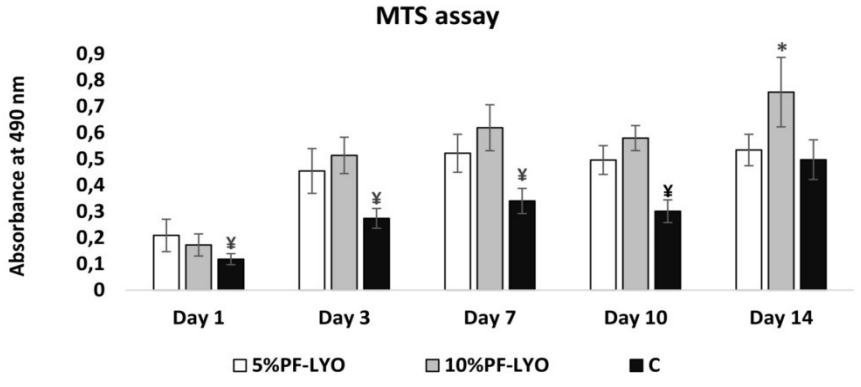

Figure 41: Metabolic activity of MG-63 osteosarcoma cell line seeded on scaffolds was determined based on the MTS assay. Statistical significance is shown above the columns (* means statistically

highest value versus all tested groups that day, ¥ means statistically lowest value versus all tested groups that day, $p < 0.05$).

4.2.4 CELL MORPHOLOGY AND SPREADING ON THE SCAFFOLDS

The confocal microscopy observation (Figure 42) is in agreement with the DNA quantification (Figure 40). Differences between the groups were not observed, and the cell number was comparable between the three tested groups. Cells were spread confluently on the scaffolds. The possible differences seen in the amount of cells could be caused by the number of washing steps performed during the cell staining method.

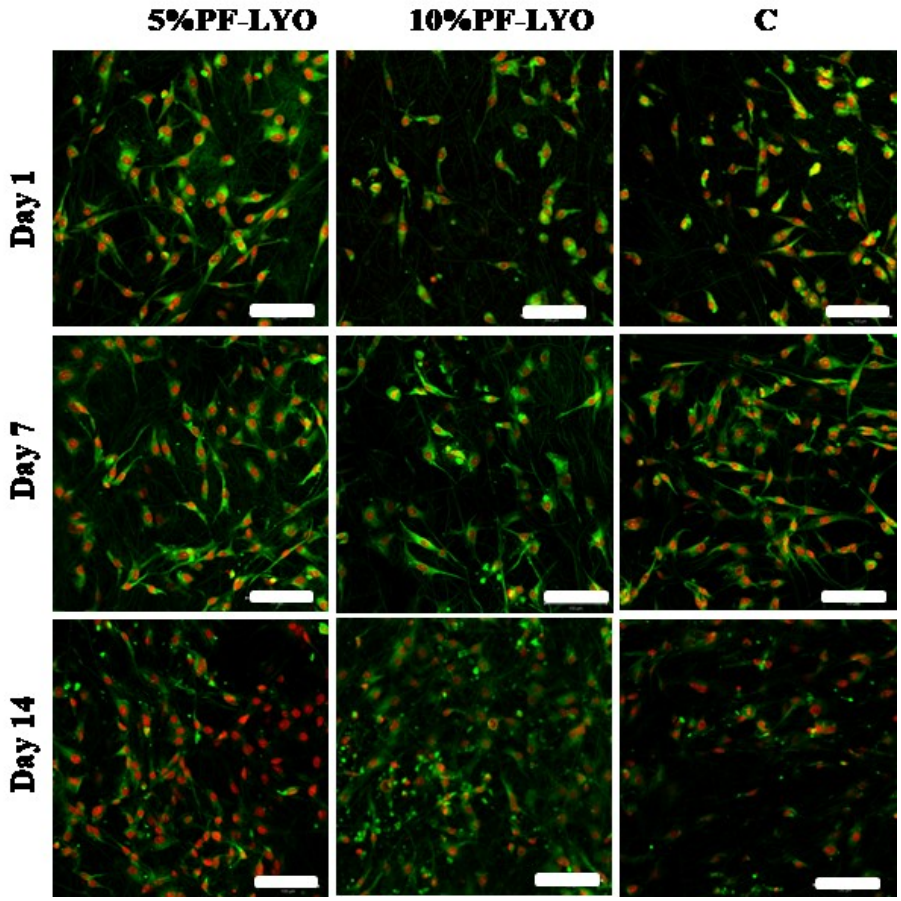

Figure 42: Visualization of MG-63 osteosarcoma cell line adhesion and distribution on scaffolds using a confocal microscope. Cell nuclei were stained using propidium iodide (red color) and cell membranes using DiOC6(3) (green color). Magnification 200 ×, scale bar 100 μm.

4.3 OSTEOGENIC SUPPLEMENT ENCAPSULATION EXPERIMENT

In the previous set of experiments, the encapsulation of platelet lyophilisate was performed in order to prolong the effect of bioactive compounds. The encapsulation led to a sustained release of bioactive molecules for up to 14 days and preserved their bioavailability.

However, the effect was not so distinct compare to activated platelets by adhesion on the surface of PCL scaffold.

The idea of a scaffold that serves as a drug delivery system in the site of a defect is caused by the positive effect of the active stimulation of the healing process. Therefore, we chose to encapsulate osteogenic supplements. For these experiments we decided not to use synthetic GFs, which are widely tested, as they are more expensive, unstable and medical approval is problematic. Osteogenic supplements are compounds generally used to induce the osteogenic differentiation of cells in *in vitro* conditions. Namely these compounds are β-glycerol phosphate, ascorbate-2-phosphate and dexamethasone. Commonly used concentrations for cell culturing are 10 mM and 40 μg mL^{-1} and 100 nM, respectively.

The aim of the experiment was to verify the different concentrations of osteogenic supplements encapsulated in the core of the PCL scaffold (Table 11) by the blend CS method. This scaffold could serve as a cell-free scaffold with osteo-inductive properties due to its released bioactive compounds. A Saos2 osteosarcoma cell line as well as hMSCs, were cultured on prepared PCL scaffolds for a period of three weeks. In this experiment we used Saos2 cells instead of MG-63 cells, as Saos2 cells evince a stronger production of osteogenic markers *in vitro*. Two control groups were chosen to thoroughly assess the effect of released osteogenic supplements. Plain PCL scaffolds cultured in a growth media, or in a growth media with added osteogenic supplements, were evaluated as negative and positive controls. The exchange of the media was minimal during the experiment in order not to aspirate the released osteogenic supplements. However, for the three week incubation period it was necessary, thus, half of the media was changed on days 7 and 14.

Table 11: Sample naming list, osteogenic supplements concentrations used for preparation of PCL scaffolds by blend centrifugal spinning method and type of the media used for cell culture experiments. Abbreviations: asc-2-P, ascorbate-2-phosphate; β-GP, β-glycerol phosphate; dex, dexamethasone; OS, osteogenic supplements.

Sample	β-GP (mM)	asc-2-P (μg mL^{-1})	Dex (nM)	Media
OS1	10	40	100	Growth
OS2	20	80	200	Growth
OS5	50	200	500	Growth
OS10	100	400	1,000	Growth
CGM	-	-	-	Growth
COM	-	-	-	Growth + OS

4.3.1 THE CHARACTERIZATION OF A PCL SCAFFOLD WITH ENCAPSULATED OS

The blend CS method resulted in the production of a fibrous PCL scaffold with encapsulated osteogenic supplements (Figure 43). The scaffolds were porous. The fiber diameters and pore sizes are listed in Table 12. Based on the analysis, the mean fiber diameter increased, with an increase in the concentrations of used osteogenic supplements. However, on the sample OS10 we detected a decrease in the mean fiber diameter. The difference could be caused by the presence of defects on the OS10 sample. In addition, the maximal pore size detected on the OS10 sample was 33.3 μm^2 which is in contrast to samples OS1-OS5 and PCL, where detected maximal pores were 205, 157.9, 204.5 and 326 μm^2 respectively.

Table 12: Characterization of prepared scaffolds.

Sample	Fiber diameter ± SD	Mean pore size ± SD	Pores larger than 5 μm^2
OS1	739.7 ± 159.3 nm	11.7 ± 20.5 μm^2	51.1 %
OS2	824.9 ± 271.2 nm	10.1 ± 18.9 μm^2	43.3 %
OS5	1569.7 ± 1067.7 nm	16.3 ± 25.9 μm^2	58.0 %
OS10	697.8 ± 527.7 nm	2.6 ± 5.9 μm^2	39.3 %
PCL	974.6 ± 299.1 nm	13.7 ± 29.8 μm^2	46.6 %

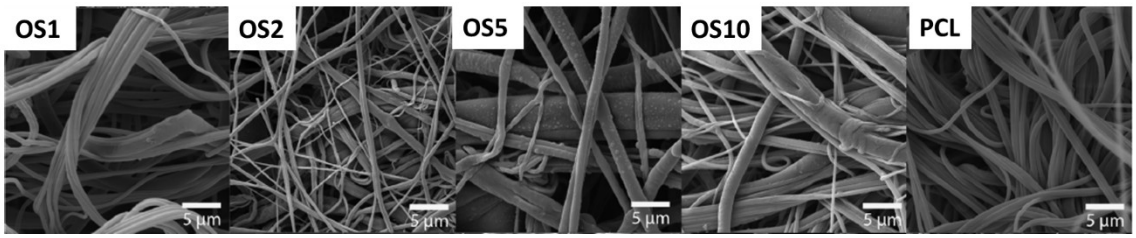

Figure 43: Images from SEM of prepared PCL scaffolds. Scale bar 5 µm.

THE VERIFICATION OF OSTEOGENIC SUPPLEMENT ENCAPSULATION

The incorporation of osteogenic supplements into the PCL scaffold was verified using ATR-FTIR spectroscopy (Figure 44). The spectra of plain PCL scaffold revealed peaks for C=O groups at 1700 cm^{-1} and for C-H groups at 2800-2950 cm^{-1}. The incorporation of osteogenic supplements resulted in an increase of a peak at 3200-3500 cm^{-1} typical for the O-H group that is present in all added osteogenic supplements. Moreover, β-glycerol phosphate and ascorbate-2-phosphate have typical -PO_4 group. This peak was visible at 1,000 cm^{-1}. Dexamethasone was further proved by the peak at 1,600 cm^{-1}, typical for C=C groups.

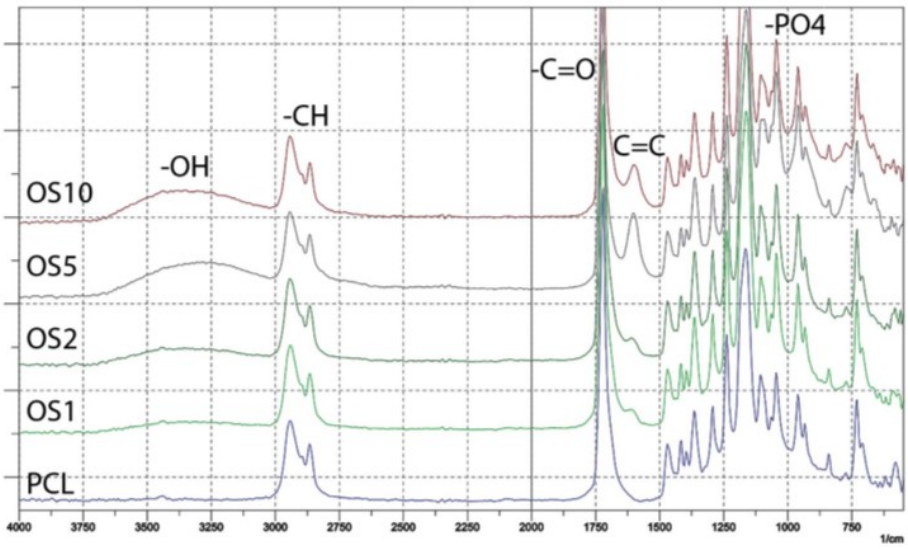

Figure 44: Spectra of prepared scaffolds measured by FTIR-ATR spectroscopy

We also evaluated the release of phosphate from β-glycerol phosphate and ascorbate-2-phosphate, encapsulated into the core of PCL fibers over a period of 31 days. A cumulative phosphate release (Figure 45) indicates a faster release from the OS1 and OS2 samples in comparison to OS5 and OS10 samples. The half-time of phosphate release was reached on the sample OS2 on day 8 and on day 14 on the OS1 sample. The half time of phosphate released for the OS5 and OS10 samples was 24 and 23 days respectively. The release kinetics of osteogenic supplements from fibers was dose dependent and lasted for a period of 31 days. The encapsulation efficiency calculated from the total release of phosphate was highest for the OS1 sample (98.2 ± 62.1%), however, the OS5 and OS10 samples had the encapsulation efficiency 40.1 ± 22.4% and 35.9 ± 0.9% respectively.

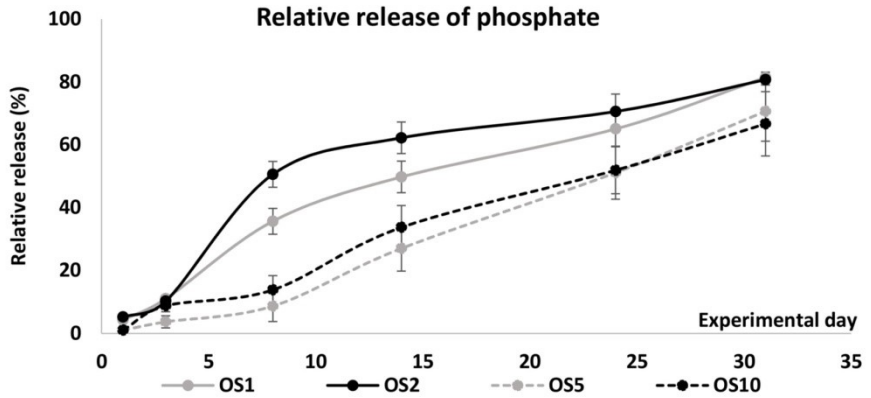

Figure 45: Release kinetics of phosphate from PCL scaffolds. Data are presented as the cumulative release.

4.3.2 CELL PROLIFERATION

Cell proliferation of hMSCs on the scaffolds was detected on days 1, 3, 7, 14 and 21 (Figure 46). The cell proliferated gradually throughout the whole experiment. On day 7, the higher amount of DNA was detected in groups OS10 and COM in comparison to groups OS5 and CGM. On day 14, a decrease in the amount of DNA was detected in the COM group, it was statistically lower compared to the group OS10. On the last day of the experiment, a decrease in the DNA amount was observed on OS5 group, the amount of DNA was statistically lower in comparison to groups OS1, OS2 and the control groups.

Based on the results, confirmed by the DNA quantification of Saos2 cells (Figure 47). On day 3, in both the CGM and COM control groups the amount of DNA was lower compared to groups OS1-OS5. Unlike hMSCs, Saos2 osteosarcoma cells showed a higher increase in the amount of DNA between days 7 and 21 of the experiment on the groups OS1-OS10 and CGM group. On day 14, in the groups OS1 and OS5 detected amount of DNA was higher compared to group COM. In groups OS2 and OS10 the amount of DNA was higher in comparison to both control groups. The amount of DNA on day 21 was significantly the lowest in the COM group and further the amount of DNA detected in groups OS1 and OS2 was higher in comparison to group CGM.

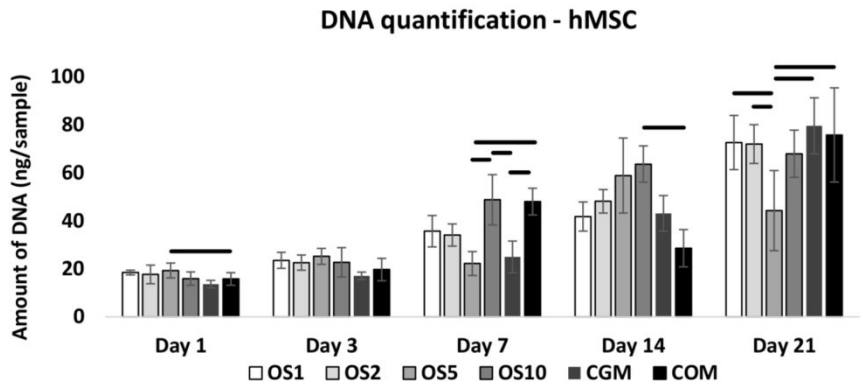

Figure 46: hMSCs adhesion and proliferation measured using Quant-iT™ dsDNA Assay Kit to quantify DNA. Statistical significance is shown by bars above the columns ($p < 0.05$).

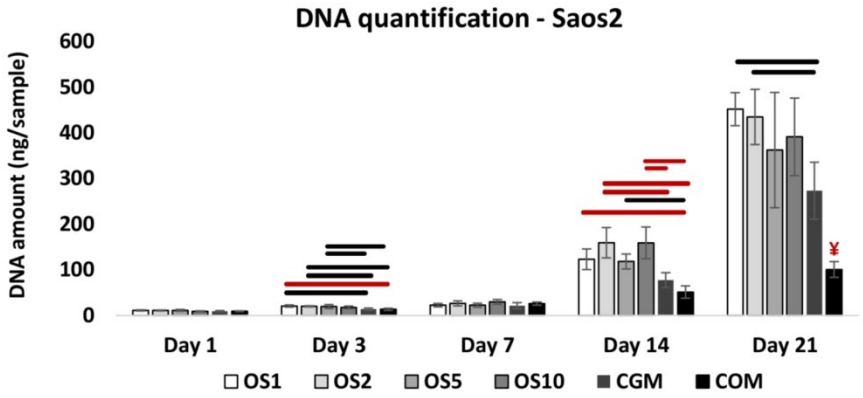

Figure 47: Saos2 osteosarcoma cell line adhesion and proliferation measured using Quant-iT™ dsDNA Assay Kit to quantify DNA. Statistical significance is shown by bars above the columns (¥ means statistically lowest value versus all tested groups that day, $p < 0.05$ in black and $p < 0.001$ in red).

4.3.3 METABOLIC ACTIVITY

The metabolic activity was measured using MTS assay on the same days as we quantified the amount of DNA. On day 1, the metabolic activity of hMSCs cultivated in the OS5 group was higher in comparison to OS1, OS10, CGM and COM groups (Figure 48). Also in OS2 group, the metabolic activity was higher compared to COM group. No statistically significant differences in metabolic activity of hMSCs were measured on days 3 and 21. On day 7, metabolic activity detected in the COM group was higher compared to OS1-OS5 groups and in OS10 group was the detected metabolic activity higher in comparison to OS5 group. On Day 14, the OS10 and CGM groups showed a higher metabolic activity in comparison to the group OS2. Osteogenic supplements are routinely used in *in vitro* and are intended for the induction of osteogenic differentiation. Based on the results, we observed no detrimental or highly positive effect of these supplements, either added into the culture media or released from the PCL scaffolds, on metabolic activity or the proliferation of hMSCs.

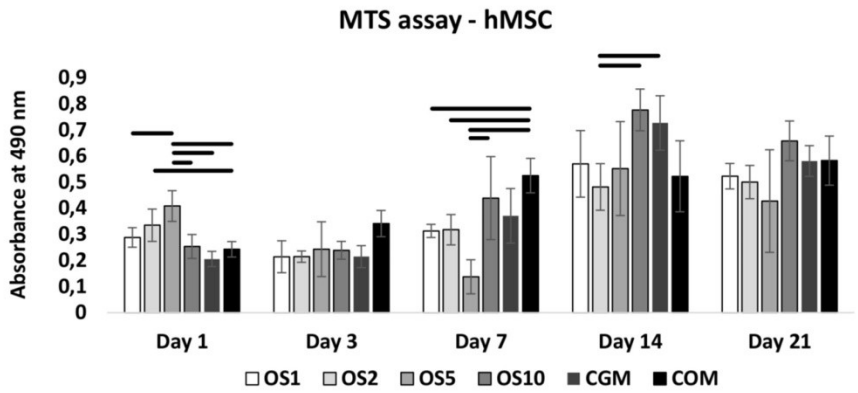

Figure 48: Metabolic activity of hMSCs on scaffolds was determined based on the MTS assay. Statistical significance is shown by bars above the columns ($p < 0.05$).

The metabolic activity of Saos2 cells revealed (Figure 49) a constant value of absorbance in the case of the COM group. The metabolic activity was in COM group lowest from all tested groups on days 14 and 21, however, increase in the amount of DNA was detected on this sample according to the DNA amount quantified (Figure 47). On day 3, the metabolic activity in group CGM was significantly lower in comparison to groups OS1, OS2, OS10 and COM. On day 7, the metabolic activity detected in the OS1 group was higher compared to CGM and COM groups. Also, the metabolic activity in the OS5 group was lower compared to groups OS2 and OS10. On day 14, metabolic activity in group OS10 was higher compared to groups OS1, OS5, CGM and COM. Detected metabolic activity in group OS2 was higher compared to OS5, CGM and COM groups and in group OS1 the metabolic activity was higher in comparison to CGM and COM groups. On day 14, the metabolic activity detected in groups OS1 and OS5 was higher compared to groups OS10, CGM and COM. Further, the metabolic activity in groups OS2 and OS10 was higher in comparison with CGM and COM groups. As Saos2 cells are normally cultivated without osteogenic supplements, this possibly indicates, that higher concentrations of osteogenic supplements negatively affect cell proliferation and metabolic activity but in lower concentrations this positively influences these measured characteristics.

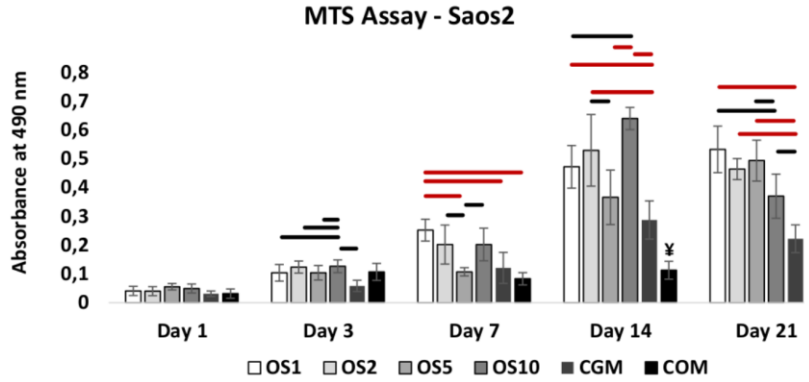

Figure 49: Metabolic activity of Saos2 osteosarcoma cell line on scaffolds was determined based on the MTS assay. Statistical significance is shown by bars above the columns (¥ means statistically lowest value, $p < 0.05$ in black and $p < 0.001$ in red).

4.3.4 CELL ADHESION AND SPREADING ON SCAFFOLDS

The confocal microscopy observations (Figure 50, Figure 51) are in agreement with the DNA amount quantified (Figure 46, Figure 47). Saos2, as well as the hMSCs adhered on all types of the scaffolds. The spreading of cells occurred from day 1. The ingrowth of the cells was observed throughout the cell culture period and confluent layers of cells were observed on day 14 suggesting that cell differentiation, typically occurring at the confluent layers of cells, could have started. Moreover, the spreading of hMSCs on the fibers of the PCL scaffold occurred from day 1, based on the SEM observation (Figure 52).

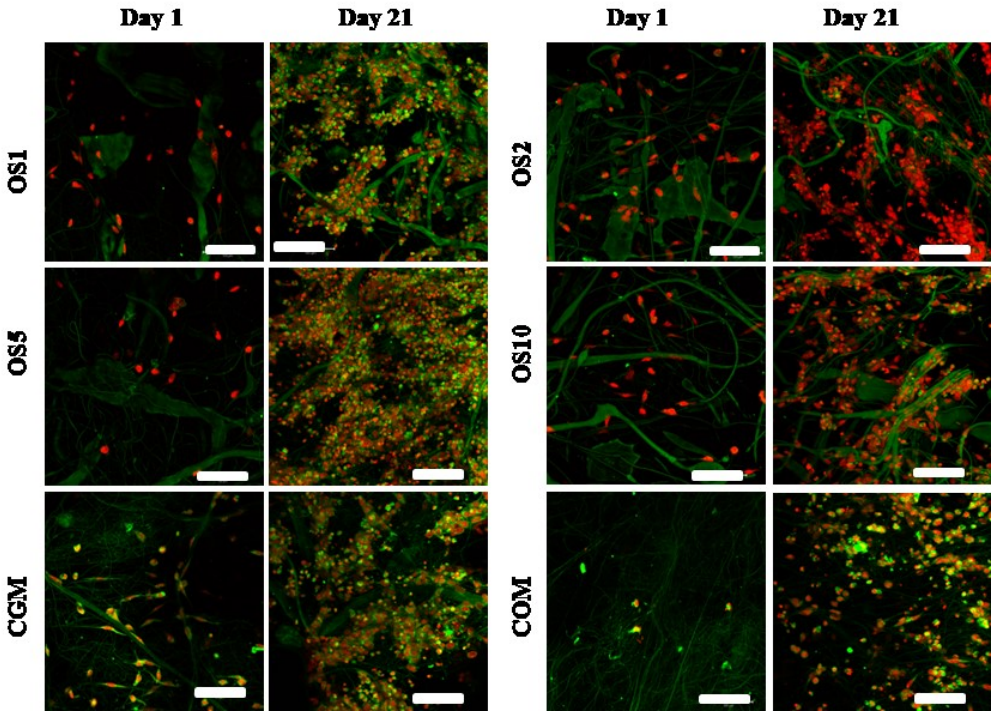

Figure 50: Visualization of Saos2 osteosarcoma cell line adhesion and distribution on scaffolds using a confocal microscope. Cell nuclei were stained using propidium iodide (red color) and cell membranes using DiOC6(3) (green color). Magnification 200 ×, scale bar 100 µm. Abbreviations: CGM, control group cultivated in a growth media; COM, control group cultivated in a growth media with osteogenic supplements.

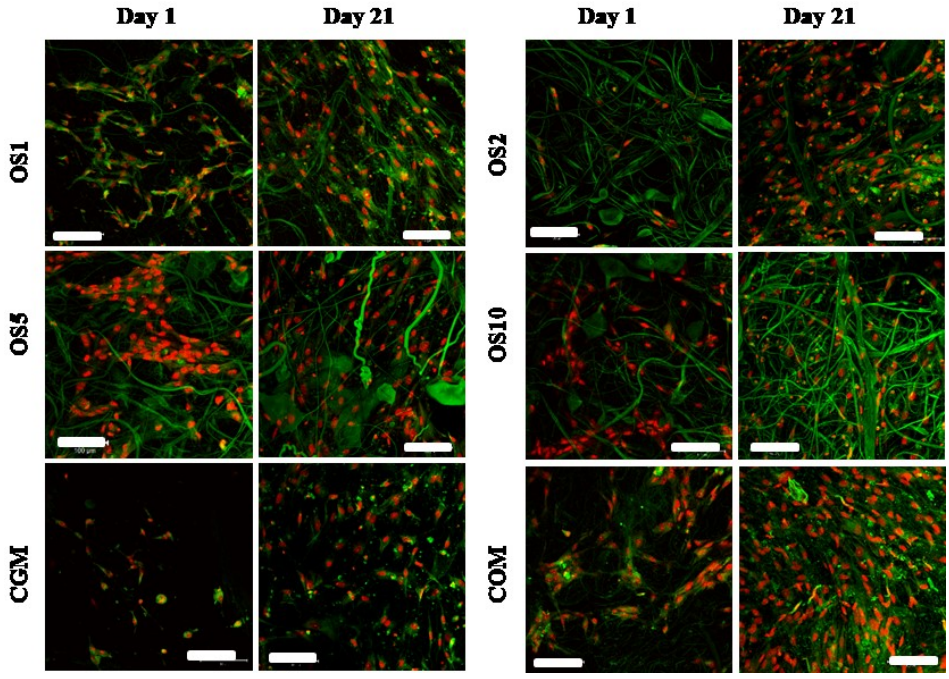

Figure 51: Visualization of hMSC adhesion and distribution on scaffolds using a confocal microscope. Cell nuclei were stained using propidium iodide (red color) and cell membranes using DiOC6(3) (green color). Magnification 200 ×, scale bar 100 µm. Abbreviations: CGM, control group cultivated in a growth media; COM, control group cultivated in a growth media with osteogenic supplements.

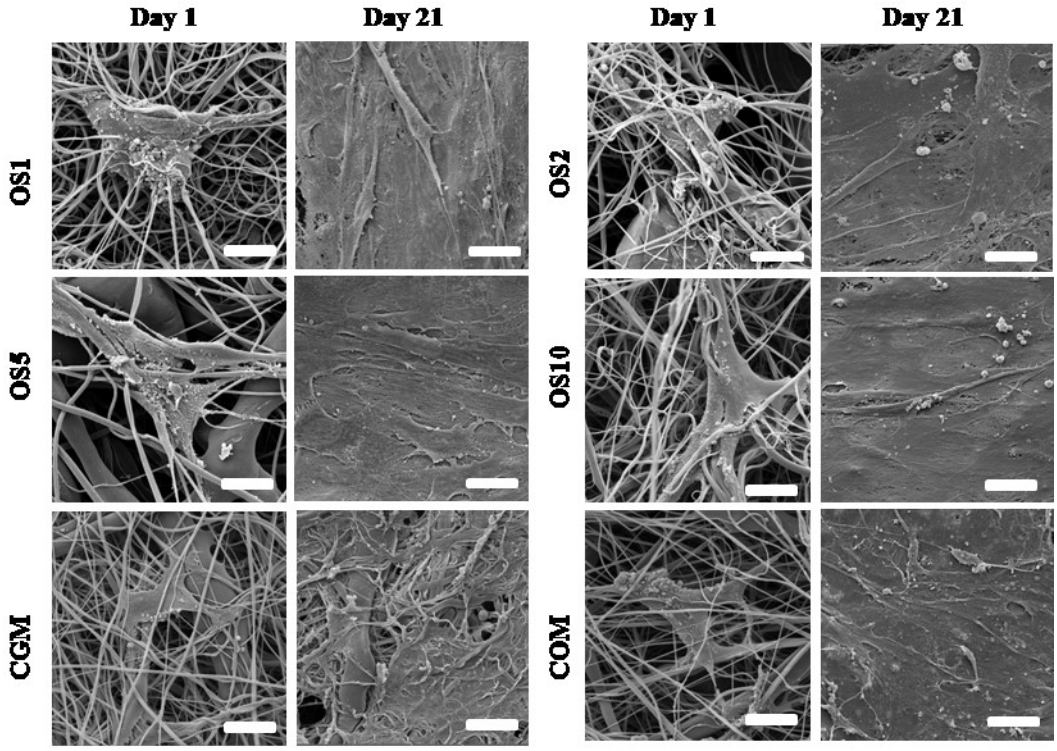

Figure 52: hMSCs adhesion and interaction on scaffolds visualized using SEM. Magnification 3,000 ×, scale bar 20 µm. Abbreviations: CGM, control group cultivated in a growth media; COM, control group cultivated in a growth media with osteogenic supplements.

4.3.5 ALKALINE PHOSPHATASE ACTIVITY

ALP activity is an early marker of osteogenic differentiation. In *in vitro* conditions the activity is enhanced by the osteogenic supplements freely added into the growth media. On day 7 the highest ALP activity was detected in the COM group compared to the OS1 and OS2 groups (Figure 53). A higher ALP activity was also detected in the OC10 group in comparison with the OS1 group. On days 14 and 21 only statistical differences were observed between the COM group compared to the OS2 and CGM groups, the rest of the tested groups were comparable.

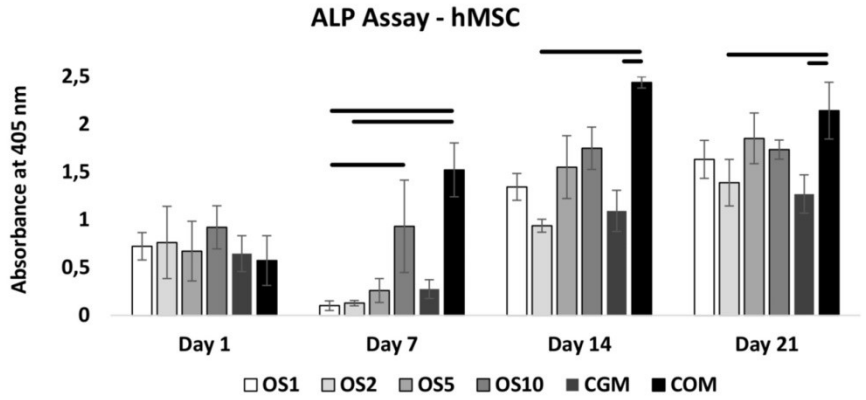

Figure 53: ALP activity of hMSC on scaffolds was determined using 1-Step™ PNPP kit. Statistical significance is shown by bars above the columns ($p < 0.05$).

4.3.6 THE EXPRESSION OF OSTEOGENIC MARKERS DETECTED BY QPCR

A relative mRNA expression of type I collagen, an early marker of osteogenic differentiation, was performed on days 1, 7 and 14 for both of the tested cell types. Saos2 cultured in the group OS10 expressed the statistically highest amount of collagen type I from all of the tested groups on day 1 (Figure 54). On day 7 the normality test failed, thus a one-way analysis of variance on the ranks revealed that only the OS5 group promoted a type I collagen expression, statistically more in comparison to the COM group, however, the trend that also the OS2 and OS10 groups promoted the expression was observed. On day 14, the COM group promoted the expression statistically, at least from all of the tested groups. Moreover, the OS5 group was statistically the best in supporting the expression of collagen type I, followed by the OS2 group. The expression of collagen type I, detected in the case of the cultivated hMSCs, revealed the highest expression on day 1 in the OS2 group (Figure 55). Further cultivation on day 7, led to the highest expression of mRNA for collagen type I in groups OS5 and OS10 and the lowest rate of expression was measured in the OS2 group. The expression of mRNA for collagen type I decreased on day 14 in all of the samples with the exception of the CGM control sample. The expression of collagen type I mRNA in OS1 and OS2 groups was statistically the lowest.

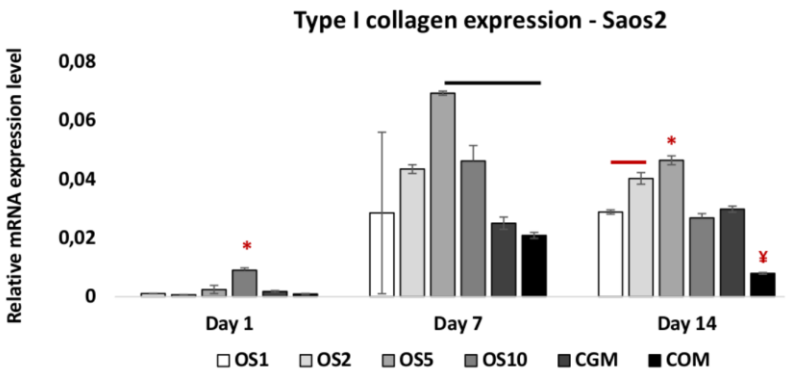

Figure 54: Osteogenic differentiation of Saos2 osteosarcoma cell line determined by qPCR analysis of osteogenic markers. Relative expression of type I collagen. Statistical significance is shown by bars above the columns (* means statistically highest value versus all tested groups that day, ¥ means statistically lowest value versus all tested groups that day, $p < 0.05$ in black and $p < 0.001$ in red).

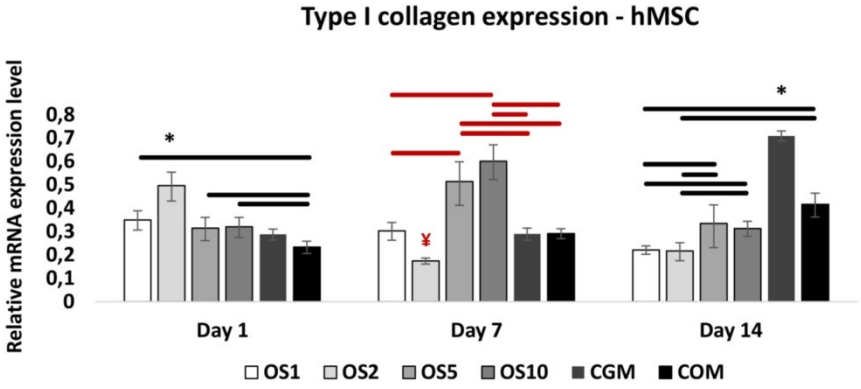

Figure 55: Osteogenic differentiation of hMSCs determined by qPCR analysis of osteogenic markers, relative expression of type I collagen. Statistical significance is shown by bars above the columns (* means statistically highest value versus all tested groups that day, ¥ means statistically lowest value versus all tested groups that day, $p < 0.05$ in black and $p < 0.001$ in red).

RunX2 is an early marker of osteogenic differentiation. A relative expression of mRNA in hMSC was statistically higher on day 1 in the OS2 group in comparison to the OS5, COM and CGM groups (Figure 56). On day 7, the OS5 group expressed a statistically higher amount of mRNA for RunX2 compared to the OS2 and CGM groups. On the last day of measurement, day 14, the CGM group expressed a statistically higher amount of RunX2 mRNA in comparison to the OS1 and OS2 groups. A late marker of osteogenic differentiation is osteocalcin, an extracellular matrix protein. On day 7 the lowest expression was detected in the OS1 and CGM groups (Figure 57). The highest relative expression was observed in the OS5 and COM groups. On day 14 the highest relative expression remained on group OS5 followed by the OS10 and COM groups.

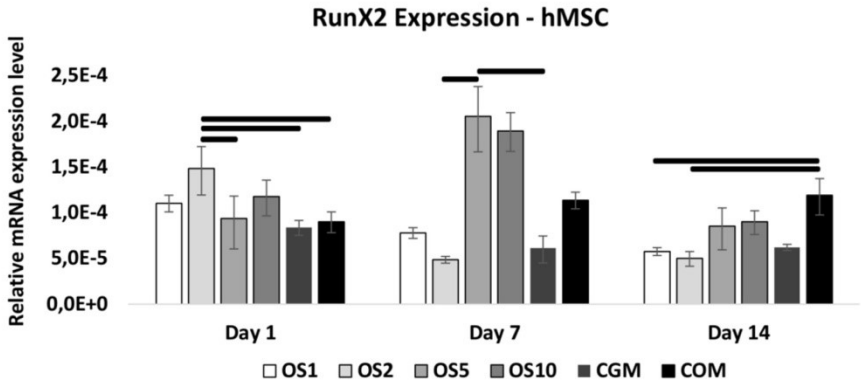

Figure 56: Osteogenic differentiation of hMSCs determined by qPCR analysis of osteogenic markers, relative expression of RunX2. Statistical significance is shown by bars above the columns ($p < 0.05$).

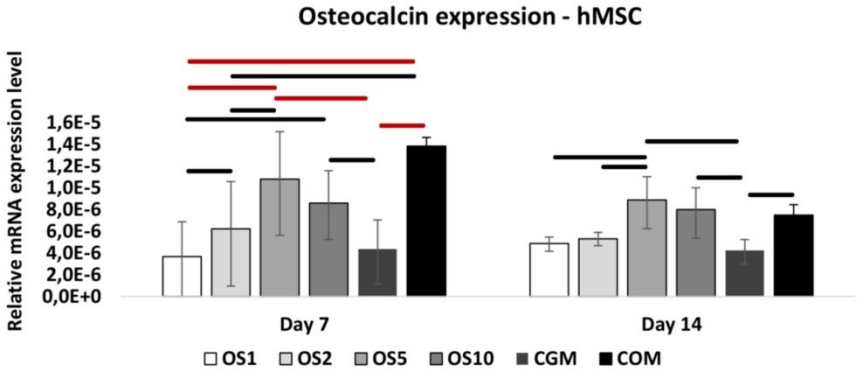

Figure 57: Osteogenic differentiation of hMSCs determined by qPCR analysis of osteogenic markers, relative expression of osteocalcin. Statistical significance is shown by bars above the columns (* means statistically highest value, ¥ means statistically lowest value, $p < 0.05$ in black and $p < 0.001$ in red).

4.3.7 THE IMMUNOFLUORESCENT STAINING OF OSTEOCALCIN

Osteocalcin is an extracellular matrix protein, its relative expression was verified by the qPCR method (Figure 57). Moreover, the presence of osteocalcin was confirmed by indirect immunofluorescence staining on day 21. Osteocalcin was present in all of the tested groups in the case of Saos2 cells (Figure 58) as this protein is typically expressed by this osteosarcoma cell line. The strongest staining of this protein was observed in groups OS1-OS5. Moreover, the staining of osteocalcin in the case of hMSC on day 14, showed the presence of osteocalcin in the groups with the highest concentrations of osteogenic supplements, meaning in groups OS5, OS10 and COM (Figure 59).

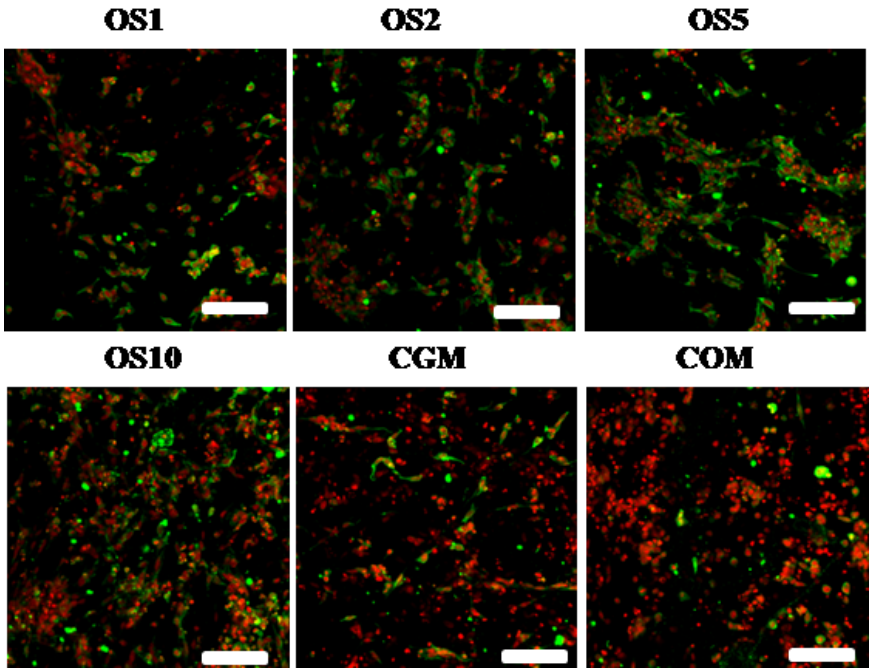

Figure 58: Immunofluorescence staining of osteocalcin. Saos2 osteosarcoma cell line stained on day 21. Osteocalcin was stained using indirect immunofluorescence (green color) and cell nuclei using propidium iodide (red color) and visualized using a confocal microscope. Magnification 200 ×, scale bar 100 µm. Abbreviations: CGM, control group cultivated in a growth media; COM, control group cultivated in a growth media with OS.

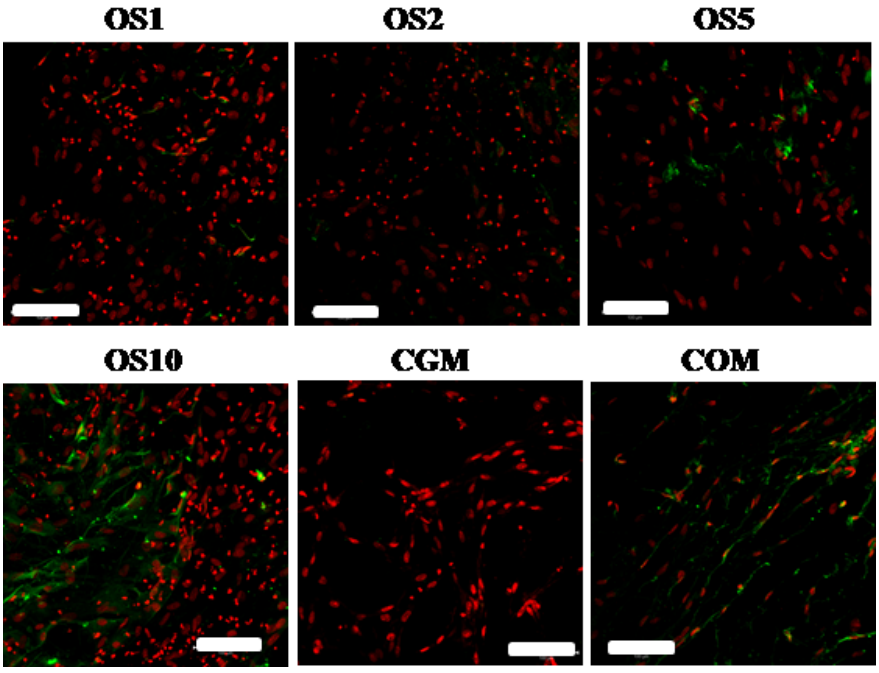

Figure 59: Immunofluorescence staining of osteocalcin. hMSC stained on day 14. Osteocalcin was stained using indirect immunofluorescence (green color) and cell nuclei using propidium iodide (red color) and visualized using a confocal microscope. Magnification 200 ×, scale bar 100 µm. Abbreviations: CGM, control group cultivated in a growth media; COM, control group cultivated in a growth media with OS.

5 DISCUSSION

These days organ and tissue transplantations continue to be the most important but also very complicated, with the possibility of damaged organs recovering in order to prolong and improve life expectancy [186-188]. For example, US Transplant Patient Registers keep a record of more than 100,000 patients every year but no more than a quarter of them are satisfied [189, 190]. In the European Union the population is 512.6. millions and the demands for organ and tissue transplantation are estimated to be of a factor 5/3 higher. As the increase in life expectancy continues, the gap between the need and possibility for transplantation will extend [191]. In the case of bone defects, four millions operations worldwide are necessary to be done annually to aid healing and stability to the critical size bone defects [159]. Therefore, the aim of this thesis is to design and *in vitro* evaluate a bioactive cell-free scaffold for the healing of critical sized bone defects to offer a solution for the expected improvement in the patient's prospects for quality of movement after bone defect repair.

The main causes for disability in the population include bone and cartilage defects. If the size of the bone defect overcomes the critical size, meaning that the defect is 2.5 times larger than the bone radius, fixation does not lead to proper bone tissue restoration [107]. As cells migrating into the defect lack the matrix to overcome the formed gap, non-unions occur. In order to properly heal the defect, a scaffolding material is necessary to be introduced into the formed gap to provide the migrating cells with support to overcome the created gap. To integrate the scaffold into the surrounding bone tissue it is necessary that osteoprogenitor cells adhere on the scaffold surface, differentiate and produce the bone ECM. The mostly commonly used scaffolds for the healing of bone defects are autologous or allogenic grafts that have many disadvantages. Therefore, alternatives to bone grafts are being investigated.

Several kinds of manufactured scaffolds have been tested both *in vitro* and *in vivo* for bone tissue engineering purposes. In general, two main approaches are tested. Either osteogenic scaffolds seeded with pre cultured cells [112, 192, 193] or cell-free scaffolds designated as drug delivery systems that serve as bioactive scaffolds to stimulate bone healing [194-198]. The use of cell-free scaffolds is privileged nowadays as these possess several advantages in comparison to scaffolds that are seeded with cells prior to implantation. The aspiration of cells is connected with extra surgical procedures that can

lead in the donor side to the morbidity, pain or inflammation. Moreover, during the *ex vivo* expansion and cultivation, the cells can undergo unwanted phenotypic changes.

In this thesis, PCL was used for the manufacturing of fibrous scaffolds by either the CS or ES method. The fibrous morphology of scaffolds mimics the natural fibrillary environment of cells and therefore offers superior cell adhesion. Moreover, fibrous scaffolds pose further advantages in terms of morphology as these scaffolds have a large surface area-to volume ratio and are highly porous with fully interconnected pores [199]. PCL is biodegradable polyester, therefore ECM produced by cells during the healing period eventually replaces the scaffold [200]. Furthermore, PCL is biocompatible and has been approved for medical application by the FDA. Many studies have pointed out the positive effect of PCL fibrous scaffolds *in vitro* [132, 201, 202] and *in vivo* [113, 203, 204] suggesting the potential for bone tissue engineering applications.

Both CS and ES methods utilize different procedures to manufacture fibrous scaffolds with nano- to micro-fibrous morphology that is desired for superior cell adhesion and the ability to modulate cell behavior in terms of cell signaling. However, different CS and ES procedures resulted in different stereology of the scaffolds. CS scaffolds resembled a 3D structure and fulfilled the demands on bone tissue engineering scaffolds to a higher extent than ES scaffolds that had the sheet like 2D morphology. A 3D nature of bone defect emphasizes the need of 3D porous scaffolds. Many studies confirmed the superior cell attachment to 3D scaffolds compared to 2D scaffolds [205, 206]. Moreover, CS eliminates the necessity of a high electric field, the production rate is higher [207]. In this thesis, the produced PCL scaffolds showed a fibrous morphology with interconnected pores. ES scaffolds showed a planar structure and were more compact compared to CS scaffolds as the mean fiber diameter along with mean pore size, were smaller in the case of ES scaffolds. Moreover, CS scaffolds had a higher mean pore size, open morphology and loose packing that is preferable for cell migration and the process of vascularization [208]. Optimal porosity of the scaffold is tissue specific. A pore size smaller than 100 µm does not support bone and tissue ingrowth [209]. For bones the optimal range in pore diameter is between 100 – 400 µm [109]. However, *in vivo* testing of new bone formation revealed no differences in the pores ranging from 350 µm to 800 µm [210].

For the production of a suitable drug delivery system, we were centered on a CS procedure as it produced scaffolds shown to be 3D, with larger pores and open morphology. The release of active molecules from the scaffolds could be applied to substitute the osteoinductive properties of bone grafts. Surface modifications [211-213] as well as the

encapsulation of bioactive compounds in the core of the scaffolds [150, 214-216] have been tested with the aim to produce a drug delivery system that prolongs and sustain bioavailability of the specific compounds in proper concentrations. Such a system is beneficial as it avoids the need of repeating drug administration in supraphysiological ranges.

The current thesis deals with three different modifications of the PCL scaffolds. Firstly, platelet adhesion to the surface of the scaffolds was applied to deliver natural GFs, cytokines and chemokines, contained in the α-granules. In physiological healing, platelets are immobilized and subsequently activated, and as a result fibrin net formation occurs. The fibrin net is a natural scaffolding material that traps the active compounds, released from platelets and further serves as a reservoir of active agents to affect the healing for a distinct period of time. As the fibrin net progresses to degradation, the compounds trapped within the net are gradually released [171]. Five different concentrations of platelets were used to test the concentration dependence on the release and bioavailability of the GFs, cytokines and chemokines. Based on the SEM observations, we detected the formation of a fibrin net for the three highest platelets concentrations used. The release of molecules, from platelets adhered on the surface of the PCL scaffold, lasted for up to 14 days, was gradual and was dependent on the platelet concentration. Moreover, we detected differences between the amount of released molecules when CS and ES scaffolds were compared. CS scaffold supported the release of molecules to a greater extent, possibly due to the different stereological properties; the platelets were activated in a distinct manner. The 14 days release followed by the plateau phase is consistent with the *in vitro* evaluation of fibrin net degradation as it was shown that the initial degradation occurred between the first three to five days and the degradation was completed in two weeks [171, 217, 218]. Fibrin gels made from platelets favor cell adhesion, proliferation and osteogenic differentiation *in vitro* [169] and bone healing *in vivo* [219, 220], however the lack of the fibrin gel stability does not fulfill the demands for a long term temporal scaffolding material. The stability of a fibrin gel could be prolonged by e.g. PEGylation, but the fibrin fibers are more packed and the porosity of the gel is minimal [221]. Therefore, the combination of a fibrin net formation with PCL scaffolds that has a controlled degradation rate is beneficial [204].

The second modification of a PCL scaffold, aiming to obtain a drug delivery system for bone tissue engineering, was the encapsulation of lyophilized platelet lysate (lyophilisate) into the core of PCL fibers. The main aim was to further prolong the release and bioavailability of bioactive compounds. PCL is a hydrophobic polymer that is dissolved

in organic solvents. Therefore, the water in oil (W/O) emulsion was processed by CS in order to protect the bioactivity of encapsulated compounds. Blend CS could not be used for encapsulation of lyophilisate as the direct mixing of organic solvents with lyophilisate would result in denaturation of the proteins. PF-68 was used as a surfactant for stabilizing the proposed W/O emulsion. PF-68 is the amphiphilic polymer that consists of polypropylen oxide (PPO) hydrophobic segments and polyethylene oxide (PEO) hydrophilic segments [222]. PF-68 is used to protect the proteins from degradation [223]. Li et al. used PF-68 to protect the activity of protease K during the ES emulsification of PLA-PEG nanofibers [146]. In this thesis, PF-68 was dissolved in ethanol and mixed with platelet lyophilizate. After exceeding the critical micelle concentration, the micelles of PF-68 were formed consisting of hydrophobic PPO cores with embedded platelet lyophilisate and hydrophilic PEO coronas. Upon mixing with PCL, dissolved in chloroform, the micelles rearranged forming inverse micelles with the lyophilisate in the core of the micelles [222]. As the ethanol is easily mixed with chloroform the resulting emulsion could be processed by the CS method. The use of the PF-68 eliminates the contact of lyophilisate with organic solvents. The protective activity of the PF-68 was tested using the HRP as a model enzyme. When the PF-68 was used for the protection of HRP, the activity of this enzyme was above 60%, however without the PF-68 the HRP activity decreased below 30%. The release of overall proteins encapsulated in the core of PCL fibers showed a burst release and was dependent on the concentration of the used PF-68. The release kinetics of PF-68 (5%PF-LYO) was comparable with 0%PF-LYO and PCL blend LYO. The higher concentrations of PF-68 (10%PF-LYO and 20%PF-LYO) showed higher concentrations of release proteins and faster release kinetics of lyophilisate during the first week. These results were indicated on fostered release kinetics from samples with higher concentrations of PF-68, subsequently followed by a limited diffusion of PF-68 micelles from the areas of non-eroding PCL. The release kinetics showed a prolonged bioavailability of the platelet lyophilisate for a period of three weeks and it did not reach the plateau phase. However, the encapsulation efficiency was not that high as the release experiment detected almost three times lower concentrations of proteins in comparison with the release while platelets where adhered on the surface of the scaffold.

Therefore, the third and last type of PCL scaffold modification, prepared in this thesis, was the blend CS method in order to produce fibers with encapsulated osteogenic supplements, β-glycerol phosphate, ascorbate-2-phosphate and dexamethasone. Osteogenic supplements are generally used to induce osteogenic differentiation *in vitro* [181, 182].

Unlike proteins contained in platelets, osteogenic supplements are compounds readily mixed with organic solvents without altering their structure. During the preparation of a blend solution for CS, the osteogenic supplements are mixed directly with the PCL and dissolved in acetic acid and formic acid. Direct mixing in the liquid phase secures the distributions of the supplements along the PCL fibers. The high loading concentrations of osteogenic supplements (from 40 mg g^{-1} to 400 mg g^{-1} of PCL for β-glycerol phosphate and from 750 mg g^{-1} of PCL to 7500 mg g^{-1} of PCL for ascorbate-2-phosphate) affected the CS procedure. Dexamethasone was present in low concentrations due to its toxic effect when higher concentrations were used for cell culturing [224]. A further increase of osteogenic supplements in polymeric solution resulted in the fibrous scaffold formation, however, the diameter of fibers and their quality slightly decreased. In the case of lower supplements concentrations used (OS1 and OS2 samples), the mean fiber diameter was lower compare to the plain PCL scaffold. This phenomenon possibly occurred due to the increased polymer conductivity when supplements were added into the polymeric solution. With higher supplements concentrations the internal viscosity increased. This resulted in the increase in the mean fiber diameter due to the presence of microfibers (OS5 sample). A further increase in osteogenic supplements concentration (OS10 sample) resulted in a decrease of mean fiber diameter but at the same time a higher amount of defects was present as the cohesion of polymer increased and aberrant fiber formation possibly occurred.

A successful encapsulation of osteogenic supplements was demonstrated by FTIR-ATR spectroscopy. With the increased concentration of supplements, we detected an increase in the resonance typical for PO_4, O-H and C=C groups. The release kinetics of the osteogenic supplements from the PCL scaffolds were evaluated based on the phosphate release from β-glycerol phosphate and ascorbate-2-phosphate. The dexamethasone release was not evaluated as the concentration of dexamethasone encapsulated into the fibers ranged from 3.9 ng (OS1) to 39 ng (OS10). Such low concentrations are below the detection limit of generally used methods: UV-VIS spectroscopy [225] and High performance liquid chromatography [226]. Based on the results of phosphate release, a sustained release of osteogenic supplements for 31 days was observed with no burst release in the first phase. OS5 and OS10 samples released higher amounts of phosphate compared to the OS1 and OS2 samples. None of the tested samples reached the release plateau, indicating that the release of molecules would possibly further continue. As bone healing is a long term event, a drug delivery system releasing the drugs over the one-month period is advantageous for bone tissue engineering.

In general, the release of drugs from the fibers occurs via two main mechanisms. Degradable materials release the drugs as the material degrades [227, 228] while non-degradable or slowly degradable materials releases the drugs via their diffusion through the polymer [229]. PCL, used to prepare the scaffolds for this thesis, is a slowly degradable polymer, therefore, the release of either platelet lyophilisate or osteogenic supplements depend on the diffusion rate of water and drugs through the polymer.

In regenerative therapy, platelets are often studied for their therapeutic potential. A number of publications showed evidence that platelets alone do not enhance bone healing but in combination with bone marrow stromal cells or bone grafts or with manufactured scaffolds permit the acceleration of bone healing [230-233]. A study by Sarkar et al. does not support the evidence for the acceleration of bone healing when platelets with collagen scaffold were used [173]. On the contrary, a study by Kim et al. showed an acceleration in bone healing when platelets were used alone; the results showed the same healing potential when compared to concentrated GFs [234]. The differences in literature concerning the effect of platelets vary, mainly due to the preparation procedure and different platelets concentrations used [235].

The healing of bone fractures is a complex process during which cytokines, chemokines and GFs are crucial. In the first phases of healing, haemostoma and inflammation take place. Macrophage activation is mediated via IL-1 and IL-6 pro-inflammatory cytokines [77, 79]. Osteoblast maturation is activated by IL-17 [80, 236]. IL-1, TNF-α, SDF-1 and GCSF stimulate activation in mesenchymal progenitors [237]. bFGF is responsible for promoting the proliferation of progenitor cells [238]. IGF-1 is an antiapoptotic and pro-osteogenic factor [237, 239]. TGF-β stimulates osteogenic differentiation [239, 240]. PDGF has also been shown to have a positive effect on bone repair as it is a strong chemotactic agent for osteoblasts and stem cells [241]. VEGF is necessary for the neovascularization of bone tissue. RANTES was proven to influence the osteogenic differentiation of MSCs [242].

In this thesis, three different bags, derived from the blood of 4 or 16 donors, were used in order to minimize inter-individual differences that vary in the terms of donors age, gender or physiological state [98]. A multiplex protein assay and ELISA were performed from each of the bags to evaluate the presence of different GFs, cytokines and chemokines. However, these assays have limited sensitivity, therefore, we have identified only part of the factors contained in the platelets as complex proteomic analysis identified more than 500 proteins within the platelets proteome [98]. In higher concentrations pro-inflammatory

cytokines IL-8, -9, -12, -15, -17, IFN-γ and TNF-α were presented. The anti-inflammatory cytokine IL-1ra was also present in higher concentration while the others were below 100 pg mL^{-1}. IP10, MIP-1b and RANTES are chemokines detected in higher concentrations. The most abundant GFs were TGF-β and PDGF-BB. Moreover, detected bFGF, G-CSF, VEGF, EGF and HGF were also present in higher concentrations and IGF-1 together with KGF were also present but in lower concentrations. The antiangiogenic factor thrombospondin was one of the most abundant proteins identified. As platelets contain a mix of proteins, some of them also posess negative role in bone healing. For example, TNF-α is a mediator of the foreign body reaction [202], and was also shown to induce apoptosis of osteoblasts [204, 223]. However, there is evidence that some levels of TNF-α are necessary for bone resorption occurring during the process of bone repair [146]. IL-10 was shown to downregulate TGF-β synthesis in mouse bone marrow cells [243]. Thrombospondin is an angiogenic factor that inhibits neovascularization and was shown to negatively influence the proliferation of osteoblasts, endothelial cells and periodontal ligament cells in concentrations above 2.5 μg mL^{-1} [222]. However, the concentration of thrombospondin detected in this thesis was below 95 ng mL^{-1}.

Prepared scaffolds were tested *in vitro* in order to evaluate the potential of the drug delivery system to provide regeneration promoting substances to the system. MG-63 is a human osteosarcoma cell line frequently used in bone tissue engineering studies [244-248]. However, differences in the proliferative potential or synthesis of ECM proteins between cell lines derived from osteosarcoma and primary cells have been published [249, 250]. Therefore, we also included experiments with hMSCs. Adhered platelets on the surface of PCL scaffolds provided bioactive compounds with a diverse effect to the cultured cells. Based on the results, we observed a positive effect of released compounds on cell proliferation and metabolic activity. The positive effect proved to be dose dependent on the concentration of adhered platelets. In the case of MG-63 osteosarcoma cell line, the two highest concentrations of platelets ($3{,}000 \times 10^9$/L and 900×10^9/L of platelets, groups P1 and P2) had a positive effect on cell metabolic activity and proliferation. In the case of hMSCs we have seen differences in the response to different doses of platelets. Following the concentration of 100×10^9/L of adhered platelets (group P4) a positive effect on metabolic activity and the proliferation of hMSCs was observed. The two highest concentrations of adhered platelets ($3{,}000 \times 10^9$/L and 900×10^9/L of platelets, groups P1 and P2), were shown to be the most promising. Comparable results between groups P1 and P2 were detected, thus, the saturation in the pro-proliferative capacity was demonstrated. No

positive effects of the lowest concentration (30×10^9/L of platelets, group P5) was detected. These results are in agreement with studies that evaluated the effect of platelets on cell proliferation [177-179, 208].

During this experiment different morphology of the scaffolds and the presence of osteogenic supplements in the culture media were also tested. In general, a positive effect on metabolic activity of hMSCs in the presence of platelets was proven, however the coadministration of platelets with osteogenic supplements (10 mM β-glycerol phosphate, 100 nM dexamethasone and 40 μg mL^{-1} ascorbate-2-phosphate) had a supportive effect and resulted in an increase in the rate of metabolic activity. The different morphology of the scaffolds is an additional factor affecting cell behavior. CS scaffolds were shown to promote cell proliferation in comparison with ES scaffolds in the second half of the cultivation period. The ES scaffold had a high packing density, therefore cells did not have the space to further migrate and proliferate after reaching the confluency. On the other hand, the CS scaffolds showed an open morphology enabling cell to penetrate deep within the volume of the scaffold [251]. An increase in ALP activity is connected with the induction of osteogenic differentiation [252, 253]. MG-63 showed fostered ALP activity in the case of the two highest platelets concentrations (P1 and P2). In the case of hMSCs, no effect on ALP activity was observed when the cells were cultured in a growth media. However, upon the addition of osteogenic supplements, an increase in the activity of ALP was detected. Moreover, the three highest platelets concentrations ($3{,}000 \times 10^9$/L - 300×10^9/L of platelets, groups P1-P3), promoted the activity of ALP statistically more, compared to the rest of the groups. These results are in agreement with Herrera et al. who observed the dose dependent effects on stimulation of ALP activity [180]. On the contrary, there are studies that show no stimulatory effect of platelets [178] or even inhibition of platelets on ALP activity [179].

The effect of released encapsulated lyophilisate from the PCL scaffold was tested on the model of MG-63 osteosarcoma cell line. Cell proliferation was influenced during the early phase of cell cultivation, however during the first week the effect of released compounds was diminished and no differences were observed when compared to the control group. Different results were obtained when the effect of release compounds was tested in regard to cell metabolic activity. A significant improvement in the metabolic activity occurred for the whole culture period in comparison with the control group. However, the estimated effect was not observed. In addition to superior cell proliferation and metabolic

activity, we also estimated the onset of the osteogenic differentiation. Therefore, in addition to platelets we decided on the utilization of osteogenic supplements.

Osteogenic supplements, namely β-glycerol phosphate, ascorbate-2-phosphate and dexamethasone, are compounds widely used in a number of *in vitro* protocols. Suggested concentrations for the induction of osteogenic differentiation of MSCs are 10 mM for β-glycerol phosphate, 40-50 μg mL^{-1} of ascorbate-2-phosphate and 10-100 nM of dexamethasone [254-258]. The cultivation of Saos2 osteosarcoma cell line on PCL scaffolds with encapsulated osteogenic supplements revealed a positive effect of released supplements on Saos2 proliferation and improved metabolic activity compared to both the CGM (cell cultured in growth medium) and COM groups (cells cultured in growth medium with added osteogenic supplements). The indirect immunostaining method of osteocalcin revealed the presence of this protein on all of the scaffolds as Saos2 cells typically express osteocalcin, however, the higher doses of osteocalcin were observed on scaffolds OS1-OS10. Furthermore, collagen type I expression showed the highest levels on groups OS2 and OS5. Overall these data suggest that higher doses of osteogenic supplements, present in groups OS10 and COM, had a negative effect on the production of osteogenic markers. Also, the comparison of the tested groups with the CGM group revealed a positive effect of scaffolds loaded with osteogenic supplements. These results clearly demonstrate the positive effect of gradually released osteogenic supplements on Saos2 osteosarcoma cell line, with scaffold OS5 showing the best results. hMSCs were seeded on the same scaffolds, however, the observed trend was distinct to the results obtained while Saos2 were cultured on these PCL scaffolds. From a proliferation and metabolic activity point of view, we observed no positive as well as no detrimental effects of different PCL scaffolds releasing osteogenic supplements compared to both control groups. The results from SEM observation and confocal microscopy are in agreement with this statement. hMSCs adhered similarly on all of the scaffolds and, as proliferated, they confluently covered the whole surface of the scaffolds. This finding is in agreement with the study that followed the effect of released osteogenic supplements from microspheres on hMSC proliferation [181]. The positive effect of osteogenic supplements on fostered cell proliferation and metabolic activity was proven when the cells were seeded in a lower cell density compared to our cell seeding density [255, 259]. Moreover, Peter et al. confirmed that after reaching the confluency of seeded rat MSC, further exposure of cells to the osteogenic supplements had no positive effect on cell proliferation /49/. Those studies suggest that the effect on cells is connected to the initial cell seeding density and after reaching the confluency the effect of supplements is diminished.

However, the osteogenic supplements are used mainly due to their osteoinductive potential which was also evaluated in this thesis. Changes in ALP activity is marker of early osteogenic differentiation, however ALP is also a marker of stemness. Therefore, the trend in ALP activity for ongoing osteogenesis is an increase in the early days followed by a decrease [6]. In this experiment, we observed an increase in ALP activity, which is the osteogenic marker, for all scaffolds, however, the highest measured ALP activity was observed in the COM group. hMSCs in the COM group were cultured in the presence of a constant level of β-glycerol phosphate, which serves as a substrate for ALP. There are several studies that are concerned with different cultivation conditions, however the complete growth medium with osteogenic supplements shows the best effect on cultured hMSCs [255, 258, 259]. The qPCR analysis of markers related with osteogenic differentiation was performed. The key transcription factor, RunX2 is an early marker. The peak in the expression was reached on day 7 in group OS5. Higher amounts of mRNA for collagen type I were expressed on day 7 in groups OS5 and OS10 and in group CGM on day 14. Moreover, indirect immunostaining of extracellular protein osteocalcin was performed. The protein was present on day 21 in groups OS5, OS10 and COM. These results are in agreement with the qPCR analysis of expressed mRNA for osteocalcin. Therefore, the higher doses of osteogenic supplements either released or added to the growth culture medium, mostly influenced the onset of osteogenic differentiation in the cultured hMSCs. These results are similar to those obtained by Shi et al who cultured hMSCs in the presence of released osteogenic supplements from poly(lactic-co-glycolic acid) sintered microsphere scaffolds and detected highest mRNA for osteogenic marker expression on this scaffold [181]. Therefore, groups OS5 and OS10 were comparable with the COM group where hMSCs were incubated with the concentrations of osteogenic supplements sgenerally used *in vitro*.

The author's contribution in each of the published articles: Věra Lukášová made a substantial contribution to the most *in vitro* methods in the listed publications. She participated in the release kinetic testing and in the fabrication of the scaffolds.

Mgr. Michala Rampichová, Ph.D.

6 CONCLUSION

The aim of this thesis was to design and *in vitro* verify the cell-free scaffolds for bone tissue engineering. Fibrous 3D scaffolds fill the critical size bone defects, serve as a scaffolding material for migrating cells and further promote their proliferation. However, modification of these scaffolds is necessary to support the complex healing of bone defects. The CS method is a versatile technique to produce fibrous 3D scaffolds that could be modified to support the healing of a broad scale of target tissue.

Platelets are a natural source of GFs, cytokines and chemokines that participate in the healing process. Platelets adhesion to CS PCL scaffolds, led to their activation and formation of fibrin net on the surface of the PCL scaffold. The fibrin net enables the immobilization of the released bioactive compounds from the platelets. The release studies showed a concentration dependence on the amount of adhered platelets with a platelet concentration of 3,000 × 10^9/L, visibly releasing the highest amount of overall proteins. Moreover, we compared the two scaffolding systems on their ability to immobilize the bioactive compounds. The ES scaffold showed the release of thrombospondin in lower concentrations for just up to 3 days compared to the CS scaffold that released thrombospondin in higher concentrations. The CS scaffold is more porous with a 3D structure and offers more contact points for platelets adhesion. Thus, the prolonged bioavailability of the thrombospondin for up to 7 days was detected. Contained between the released compounds in higher concentrations were TGF-β1, PDFG-BB, thrombospondin, RANTES and P-selectin. However, the number of other GFs and ILs were also released in lower concentrations. The dose dependent effect of these compounds was verified in the model of MG-63 osteosarcoma cell line and hMSCs. Improved metabolic activity, proliferation and ALP activity was detected when concentrations of platelets 900-3,000 ×10^9/L were used. Thus, the potency of this system for bone tissue engineering was proven, however, the prolonged release of active molecules was intended. Therefore, we prepared lyophilized platelet lysate (lyophilisate) that was encapsulated in the core of the PCL fibers by the CS emulsion approach. An amphiphilic molecule PF-68 was used in order to protect the bioactivity of the proteins during the manufacturing of the scaffolds in order not to degrade in the solvent system. A prolonged release of up to 21 days without reaching the plateau phase was observed. In up to 10% of the used PF-68 with platelets lyophilisate, we observed the dose dependent release, but higher concentrations of PF-68 did not further improved encapsulation efficiency. The release of bioactive compounds was three times

lower in concentrations compared to the platelet adhesion. Therefore, only in the first week of the experiment, the improvement in metabolic activity of MG-63 cells was observed.

In order to produce a scaffold with a stronger osteogenic potential, we encapsulated osteogenic supplements, in the core of the PCL fibers. Namely β-glycerol phosphate, dexamethasone and ascorbate-2-phosphate, in the range from once to ten times concentrated, compared to generally used *in vitro* concentrations (10 mM, 100 nm and 40 μg mL^{-1} respectively). The manufacturing of this scaffold was performed based on the blend CS method as the acidic solvent environment does not degrade the osteogenic supplements and enables mixing with high supplements concentrations. The release of osteogenic supplements lasted for up to 31 days and was sustained. The scaffolds with osteogenic supplements showed fostered metabolic activity and proliferation of Saos2 osteosarcoma cell line. OS5 scaffold, with 50 mM β-glycerol phosphate, 500 nM dexamethasone and 200 μg mL^{-1} ascorbate-2-phosphate was also used for the PCL scaffold preparation, promoted osteogenic differentiation of hMSCs and Saos2 the most of all the tested scaffolds.

The proposed bioactive scaffolds could serve as cell-free scaffolds. The immobilization of platelets forming the fibrin net on the PCL scaffold or encapsulation of osteogenic supplements, deliver bioactive molecules to a precise location. Moreover, the sustained release of a bioactive compound in a spaciotemporal manner in proper concentrations is possible. Unlike synthetic GFs, platelets are a natural source of GFs that can be used autologously. Osteogenic supplements could be processed with the qualities applicable in medicine. Furthermore, a PCL scaffold is a material approved by the FDA for medical use, its biodegradability could also be controlled based on the selection of a suitable molecular weight of PCL. Therefore, the proposed future perspective of tested scaffolds is a combination of both systems in order to process a promising material with a high application potential for bone tissue engineering applications.

7 REFERENCES

[1] Ortega N, Behonick DJ, and Werb Z. *Matrix remodeling during endochondral ossification.* Trends in Cell Biology. 2004; 14(2): p. 86-93.

[2] Kelly DJ and Jacobs CR. *The role of mechanical signals in regulating chondrogenesis and osteogenesis of mesenchymal stem cells.* Birth Defects Research Part C: Embryo Today: Reviews. 2010; 90(1): p. 75-85.

[3] Malaval L, Liu F, Roche P, et al. *Kinetics of osteoprogenitor proliferation and osteoblast differentiation in vitro.* Journal of Cellular Biochemistry. 1999; 74(4): p. 616-627.

[4] Valenti MT, Carbonare LD, Donatelli L, et al. *Gene expression analysis in osteoblastic differentiation from peripheral blood mesenchymal stem cells.* Bone. 2008; 43(6): p. 1084-1092.

[5] Vater C, Kasten P, and Stiehler M. *Culture media for the differentiation of mesenchymal stromal cells.* Acta Biomaterialia. 2011; 7(2): p. 463-477.

[6] Owen TA, Aronow M, Shalhoub V, et al. *Progressive development of the rat osteoblast phenotype in vitro: Reciprocal relationships in expression of genes associated with osteoblast proliferation and differentiation during formation of the bone extracellular matrix.* Journal of Cellular Physiology. 1990; 143(3): p. 420-430.

[7] Bianco P, Riminucci M, Bonucci E, et al. *Bone sialoprotein (BSP) secretion and osteoblast differentiation: relationship to bromodeoxyuridine incorporation, alkaline phosphatase, and matrix deposition.* Journal of Histochemistry & Cytochemistry. 1993; 41(2): p. 183-191.

[8] Xiao G, Gopalakrishnan R, Jiang D, et al. *Bone Morphogenetic Proteins, Extracellular Matrix, and Mitogen-Activated Protein Kinase Signaling Pathways Are Required for Osteoblast-Specific Gene Expression and Differentiation in MC3T3-E1 Cells.* Journal of Bone and Mineral Research. 2002; 17(1): p. 101-110.

[9] Collins FL, Rios-Arce ND, Schepper JD, et al. *The Potential of Probiotics as a Therapy for Osteoporosis.* Microbiology spectrum. 2017; 5(4): p. 10.1128/microbiolspec.BAD-0015-2016.

[10] Sugawara Y, Kamioka H, Honjo T, et al. *Three-dimensional reconstruction of chick calvarial osteocytes and their cell processes using confocal microscopy.* Bone. 2005; 36(5): p. 877-883.

[11] Florencio-Silva R, Sasso GRdS, Sasso-Cerri E, et al. *Biology of Bone Tissue: Structure, Function, and Factors That Influence Bone Cells.* BioMed Research International. 2015; 2015: p. 17.

[12] Schneider P, Meier M, Wepf R, et al. *Towards quantitative 3D imaging of the osteocyte lacuno-canalicular network.* Bone. 2010; 47(5): p. 848-858.

[13] Sommerfeldt D and Rubin C. *Biology of bone and how it orchestrates the form and function of the skeleton.* European Spine Journal. 2001; 10(2): p. S86-S95.

[14] Rubin CT and Lanyon LE. *Limb mechanics as a function of speed and gait: a study of functional strains in the radius and tibia of horse and dog.* Journal of Experimental Biology. 1982; 101(1): p. 187-211.

[15] Fritton SP, J. McLeod K, and Rubin CT. *Quantifying the strain history of bone: spatial uniformity and self-similarity of low-magnitude strains.* Journal of Biomechanics. 2000; 33(3): p. 317-325.

[16] You L, Cowin SC, Schaffler MB, et al. *A model for strain amplification in the actin cytoskeleton of osteocytes due to fluid drag on pericellular matrix.* Journal of Biomechanics. 2001; 34(11): p. 1375-1386.

[17] Udagawa N, Takahashi N, Akatsu T, et al. *Origin of osteoclasts: mature monocytes and macrophages are capable of differentiating into osteoclasts under a suitable microenvironment prepared by bone marrow-derived stromal cells.* Proceedings of the National Academy of Sciences. 1990; 87(18): p. 7260-7264.
[18] Manolagas SC and Jilka RL. *Bone Marrow, Cytokines, and Bone Remodeling — Emerging Insights into the Pathophysiology of Osteoporosis.* New England Journal of Medicine. 1995; 332(5): p. 305-311.
[19] Lacey DL, Timms E, Tan HL, et al. *Osteoprotegerin Ligand Is a Cytokine that Regulates Osteoclast Differentiation and Activation.* Cell. 1998; 93(2): p. 165-176.
[20] R. WS, C. P, P. S, et al. *Cathepsin K Activity-dependent Regulation of Osteoclast Actin Ring Formation and Bone Resorption.* Journal of Biological Chemistry. 2009; 11(1): p. 2584-2592.
[21] H.K. V and M. H. *The osteoclast clear zone is a specialized cell-extracellular matrix adhesion structure.* Journal of Cell Science. 1995; 15: p. 2729-2732.
[22] Jurdic P, Saltel F, Chabadel A, et al. *Podosome and sealing zone: Specificity of the osteoclast model.* European Journal of Cell Biology. 2006; 85(3): p. 195-202.
[23] Sato T, Foged NT, and Delaissé J-M. *The Migration of Purified Osteoclasts Through Collagen Is Inhibited by Matrix Metalloproteinase Inhibitors.* Journal of Bone and Mineral Research. 1998; 13(1): p. 59-66.
[24] Takahashi N, Udagawa N, and Suda T. *Vitamin D endocrine system and osteoclasts.* BoneKEy reports. 2014; 3: p. 495-495.
[25] K. K, C. M, M. I, et al. *Regulation of Matrix Metalloproteinases (MMP-2, -3, -9 and -13) by Interleukin-1 and Interleukin-6 in Mouse Calvaria: Association of MMP Induction with Bone Resorption.* Endocrinology. 1998; 139(3): p. 1338-1345.
[26] Lee S-K and Lorenzo JA. *Parathyroid Hormone Stimulates TRANCE and Inhibits Osteoprotegerin Messenger Ribonucleic Acid Expression in Murine Bone Marrow Cultures: Correlation with Osteoclast-Like Cell Formation*.* Endocrinology. 1999; 140(8): p. 3552-3561.
[27] Dai X-M, Ryan GR, Hapel AJ, et al. *Targeted disruption of the mouse colony-stimulating factor 1 receptor gene results in osteopetrosis, mononuclear phagocyte deficiency, increased primitive progenitor cell frequencies, and reproductive defects.* Blood. 2002; 99(1): p. 111-120.
[28] Arai F, Miyamoto T, Ohneda O, et al. *Commitment and Differentiation of Osteoclast Precursor Cells by the Sequential Expression of C-Fms and Receptor Activator of Nuclear Factor κb (Rank) Receptors.* The Journal of Experimental Medicine. 1999; 190(12): p. 1741-1754.
[29] Hodge JM, Kirkland MA, and Nicholson GC. *Multiple roles of M-CSF in human osteoclastogenesis.* Journal of Cellular Biochemistry. 2007; 102(3): p. 759-768.
[30] Morony S, Capparelli C, Lee R, et al. *A Chimeric Form of Osteoprotegerin Inhibits Hypercalcemia and Bone Resorption Induced by IL-1β, TNF-α, PTH, PTHrP, and 1,25(OH)2D3.* Journal of Bone and Mineral Research. 1999; 14(9): p. 1478-1485.
[31] Tsukii K, Shima N, Mochizuki S-i, et al. *Osteoclast Differentiation Factor Mediates an Essential Signal for Bone Resorption Induced by 1α,25-Dihydroxyvitamin D3, Prostaglandin E2, or Parathyroid Hormone in the Microenvironment of Bone.* Biochemical and Biophysical Research Communications. 1998; 246(2): p. 337-341.
[32] Ha H, Bok Kwak H, Woong Lee S, et al. *Reactive oxygen species mediate RANK signaling in osteoclasts.* Experimental Cell Research. 2004; 301(2): p. 119-127.

[33] Wada T, Nakashima T, Hiroshi N, et al. *RANKL–RANK signaling in osteoclastogenesis and bone disease.* Trends in Molecular Medicine. 2006; 12(1): p. 17-25.
[34] Hofbauer LC, Khosla S, Dunstan CR, et al. *The Roles of Osteoprotegerin and Osteoprotegerin Ligand in the Paracrine Regulation of Bone Resorption.* Journal of Bone and Mineral Research. 2000; 15(1): p. 2-12.
[35] Nakashima T, Hayashi M, Fukunaga T, et al. *Evidence for osteocyte regulation of bone homeostasis through RANKL expression.* Nature Medicine. 2011; 17: p. 1231.
[36] Takeuchi A, Ohtsuki C, Miyazaki T, et al. *Heterogeneous nucleation of hydroxyapatite on protein: structural effect of silk sericin.* Journal of The Royal Society Interface. 2005; 2(4): p. 373-378.
[37] Gelse K, Pöschl E, and Aigner T. *Collagens—structure, function, and biosynthesis.* Advanced Drug Delivery Reviews. 2003; 55(12): p. 1531-1546.
[38] Kassem M, Abdallah BM, and Saeed H. *Osteoblastic cells: Differentiation and trans-differentiation.* Archives of Biochemistry and Biophysics. 2008; 473(2): p. 183-187.
[39] Fujisawa K and Kuboki Y. *Affinity of bone sialoprotein and several other bone and dentin acidic proteins to collagen fibrils.* Calcified Tissue International. 1992; 51(6): p. 438-442.
[40] R. F and M. T. *Acidic bone matrix proteins and their roles in calcification.* Frontiers in Bioscience. 2012; 8(1): p. 1891-1903.
[41] Tomoaia G and Pasca R-D. *On the Collagen Mineralization. A Review.* Clujul medical (1957). 2015; 88(1): p. 15-22.
[42] Nudelman F, Pieterse K, George A, et al. *The role of collagen in bone apatite formation in the presence of hydroxyapatite nucleation inhibitors.* Nature Materials. 2010; 9: p. 1004.
[43] Kramer RZ, Bella J, Brodsky B, et al. *The crystal and molecular structure of a collagen-like peptide with A biologically relevant sequence12Edited by I. A. Wilson.* Journal of Molecular Biology. 2001; 311(1): p. 131-147.
[44] Cui F-Z, Li Y, and Ge J. *Self-assembly of mineralized collagen composites.* Materials Science and Engineering: R: Reports. 2007; 57(1): p. 1-27.
[45] Komori T. *Regulation of bone development and extracellular matrix protein genes by RUNX2.* Cell and Tissue Research. 2009; 339(1): p. 189.
[46] Derynck R and Zhang YE. *Smad-dependent and Smad-independent pathways in TGF-β family signalling.* Nature. 2003; 425(6958): p. 577-584.
[47] Heinegård D and Oldberg A. *Structure and biology of cartilage and bone matrix noncollagenous macromolecules.* The FASEB Journal. 1989; 3(9): p. 2042-2051.
[48] Baht GS, Hunter GK, and Goldberg HA. *Bone sialoprotein–collagen interaction promotes hydroxyapatite nucleation.* Matrix Biology. 2008; 27(7): p. 600-608.
[49] Golub EE. *Role of matrix vesicles in biomineralization.* Biochimica et Biophysica Acta (BBA) - General Subjects. 2009; 1790(12): p. 1592-1598.
[50] Bottini M, Mebarek S, Anderson KL, et al. *Matrix vesicles from chondrocytes and osteoblasts: Their biogenesis, properties, functions and biomimetic models.* Biochimica et Biophysica Acta (BBA) - General Subjects. 2018; 1862(3): p. 532-546.
[51] Kikuchi M, Itoh S, Ichinose S, et al. *Self-organization mechanism in a bone-like hydroxyapatite/collagen nanocomposite synthesized in vitro and its biological reaction in vivo.* Biomaterials. 2001; 22(13): p. 1705-1711.

[52] Zhang W, Huang Z-L, Liao S-S, et al. *Nucleation Sites of Calcium Phosphate Crystals during Collagen Mineralization.* Journal of the American Ceramic Society. 2003; 86(6): p. 1052-1054.
[53] Bradt J-H, Mertig M, Teresiak A, et al. *Biomimetic Mineralization of Collagen by Combined Fibril Assembly and Calcium Phosphate Formation.* Chemistry of Materials. 1999; 11(10): p. 2694-2701.
[54] Rho J-Y, Kuhn-Spearing L, and Zioupos P. *Mechanical properties and the hierarchical structure of bone.* Medical Engineering & Physics. 1998; 20(2): p. 92-102.
[55] Ghassemi T, Shahroodi A, Ebrahimzadeh MH, et al. *Current Concepts in Scaffolding for Bone Tissue Engineering.* The archives of bone and joint surgery. 2018; 6(2): p. 90-99.
[56] Lara-Castillo N, Kim-Weroha NA, Kamel MA, et al. *In vivo mechanical loading rapidly activates β-catenin signaling in osteocytes through a prostaglandin mediated mechanism.* Bone. 2015; 76: p. 58-66.
[57] Reznikov N, Shahar R, and Weiner S. *Bone hierarchical structure in three dimensions.* Acta Biomaterialia. 2014; 10(9): p. 3815-3826.
[58] M.G. A and A.K. R. *The osteon: the micromechanical unit of compact bone.* Frontiers in Bioscience. 2012; 8(1): p. 1551-81.
[59] Reznikov N, Chase H, Brumfeld V, et al. *The 3D structure of the collagen fibril network in human trabecular bone: Relation to trabecular organization.* Bone. 2015; 71: p. 189-195.
[60] Khosla S, Westendorf JJ, and Mödder UI. *Concise Review: Insights from Normal Bone Remodeling and Stem Cell-Based Therapies for Bone Repair.* STEM CELLS. 2010; 28(12): p. 2124-2128.
[61] Won KY, Kalil RK, Kim YW, et al. *RANK signalling in bone lesions with osteoclast-like giant cells.* Pathology. 2011; 43(4): p. 318-321.
[62] Simonet WS, Lacey DL, Dunstan CR, et al. *Osteoprotegerin: A Novel Secreted Protein Involved in the Regulation of Bone Density.* Cell. 1997; 89(2): p. 309-319.
[63] Atkins GJ, Bouralexis S, Haynes DR, et al. *Osteoprotegerin inhibits osteoclast formation and bone resorbing activity in giant cell tumors of bone.* Bone. 2001; 28(4): p. 370-377.
[64] Winkler DG, Sutherland MK, Geoghegan JC, et al. *Osteocyte control of bone formation via sclerostin, a novel BMP antagonist.* The EMBO Journal. 2003; 22(23): p. 6267-6276.
[65] Delaissé J-M, Andersen TL, Engsig MT, et al. *Matrix metalloproteinases (MMP) and cathepsin K contribute differently to osteoclastic activities.* Microscopy Research and Technique. 2003; 61(6): p. 504-513.
[66] Yu X, Huang Y, Collin-Osdoby P, et al. *Stromal Cell-Derived Factor-1 (SDF-1) Recruits Osteoclast Precursors by Inducing Chemotaxis, Matrix Metalloproteinase-9 (MMP-9) Activity, and Collagen Transmigration.* Journal of Bone and Mineral Research. 2003; 18(8): p. 1404-1418.
[67] Hou P, Troen T, Ovejero MC, et al. *Matrix metalloproteinase-12 (MMP-12) in osteoclasts: new lesson on the involvement of MMPs in bone resorption.* Bone. 2004; 34(1): p. 37-47.
[68] Everts V, Delaissé J-M, Korper W, et al. *Degradation of collagen in the bone-resorbing compartment underlying the osteoclast involves both cysteine-proteinases and matrix metalloproteinases.* Journal of Cellular Physiology. 1992; 150(2): p. 221-231.

[69] Rucci N and Teti A. *The "love–hate" relationship between osteoclasts and bone matrix.* Matrix Biology. 2016; 52-54: p. 176-190.
[70] Moonga BS, Moss DW, Patchell A, et al. *Intracellular regulation of enzyme secretion from rat osteoclasts and evidence for a functional role in bone resorption.* The Journal of Physiology. 1990; 429(1): p. 29-45.
[71] Marsell R and Einhorn TA. *The biology of fracture healing.* Injury. 2011; 42(6): p. 551-555.
[72] Kolar P, Schmidt-Bleek K, Schell H, et al. *The Early Fracture Hematoma and Its Potential Role in Fracture Healing.* Tissue Engineering Part B: Reviews. 2010; 16(4): p. 427-434.
[73] Phillips AM. *Overview of the fracture healing cascade.* Injury. 2005; 36(3, Supplement): p. S5-S7.
[74] Pountos I and Giannoudis PV. *Fracture healing: Back to Basics and Latest Advances.* In Fracture Reduction and Fixation Techniques: Upper Extremities (Giannoudis PV, Ed.), Springer International Publishing. 2018; pp 3-17.
[75] Caplan AI and Correa D. *PDGF in bone formation and regeneration: New insights into a novel mechanism involving MSCs.* Journal of Orthopaedic Research. 2011; 29(12): p. 1795-1803.
[76] Tsiridis E, Upadhyay N, and Giannoudis P. *Molecular aspects of fracture healing:Which are the important molecules?* Injury. 2007; 38(1, Supplement): p. S11-S25.
[77] Yang X, Ricciardi BF, Hernandez-Soria A, et al. *Callus mineralization and maturation are delayed during fracture healing in interleukin-6 knockout mice.* Bone. 2007; 41(6): p. 928-936.
[78] D. N, E. M, Y. W, et al. *T-Lymphocytes Enable Osteoblast Maturation via IL-17F during the Early Phase of Fracture Repair.* PloS One. 2019; 8.
[79] Lange J, Sapozhnikova A, Lu C, et al. *Action of IL-1β during fracture healing.* Journal of Orthopaedic Research. 2010; 28(6): p. 778-784.
[80] Ono T, Okamoto K, Nakashima T, et al. *IL-17-producing γδ T cells enhance bone regeneration.* Nature Communications. 2016; 7: p. 10928.
[81] Simon AM, Manigrasso MB, and O'Connor JP. *Cyclo-Oxygenase 2 Function Is Essential for Bone Fracture Healing.* Journal of Bone and Mineral Research. 2002; 17(6): p. 963-976.
[82] Liu X-H, Kirschenbaum A, Yao S, et al. *Cross-Talk between the Interleukin-6 and Prostaglandin E2 Signaling Systems Results in Enhancement of Osteoclastogenesis through Effects on the Osteoprotegerin/Receptor Activator of Nuclear Factor-κB (RANK) Ligand/RANK System.* Endocrinology. 2005; 146(4): p. 1991-1998.
[83] Naik AA, Xie C, Zuscik MJ, et al. *Reduced COX-2 Expression in Aged Mice Is Associated With Impaired Fracture Healing.* Journal of Bone and Mineral Research. 2009; 24(2): p. 251-264.
[84] Ceradini DJ, Kulkarni AR, Callaghan MJ, et al. *Progenitor cell trafficking is regulated by hypoxic gradients through HIF-1 induction of SDF-1.* Nature Medicine. 2004; 10(8): p. 858-864.
[85] Bastian O, Pillay J, Alblas J, et al. *Systemic inflammation and fracture healing.* Journal of Leukocyte Biology. 2011; 89(5): p. 669-673.
[86] Schindeler A, McDonald MM, Bokko P, et al. *Bone remodeling during fracture repair: The cellular picture.* Seminars in Cell & Developmental Biology. 2008; 19(5): p. 459-466.

[87] Lienau J, Schmidt-Bleek K, Peters A, et al. *Differential regulation of blood vessel formation between standard and delayed bone healing.* Journal of Orthopaedic Research. 2009; 27(9): p. 1133-1140.
[88] Maes C, Kobayashi T, Selig MK, et al. *Osteoblast Precursors, but Not Mature Osteoblasts, Move into Developing and Fractured Bones along with Invading Blood Vessels.* Developmental Cell. 2010; 19(2): p. 329-344.
[89] Patel SR, Richardson JL, Schulze H, et al. *Differential roles of microtubule assembly and sliding in proplatelet formation by megakaryocytes.* Blood. 2005; 106(13): p. 4076-4085.
[90] Thon JN, Montalvo A, Patel-Hett S, et al. *Cytoskeletal mechanics of proplatelet maturation and platelet release.* The Journal of Cell Biology. 2010; 191(4): p. 861-874.
[91] Geddis AE. *The regulation of proplatelet production.* Haematologica. 2009; 94(6): p. 756-759.
[92] Patel SR, Hartwig JH, and Italiano JE, Jr. *The biogenesis of platelets from megakaryocyte proplatelets.* The Journal of Clinical Investigation. 2005; 115(12): p. 3348-3354.
[93] Kaushansky K. *The molecular mechanisms that control thrombopoiesis.* The Journal of Clinical Investigation. 2005; 115(12): p. 3339-3347.
[94] Geraldo RB, Sathler PC, Lourenço AL, et al. *Platelets: Still a Therapeutical Target for Haemostatic Disorders.* International Journal of Molecular Sciences. 2014; 15(10): p. 17901-17919.
[95] Eckly A, Heijnen H, Pertuy F, et al. *Biogenesis of the demarcation membrane system (DMS) in megakaryocytes.* Blood. 2014; 123(6): p. 921-930.
[96] Rendu F and Brohard-Bohn B. *The platelet release reaction: granules' constituents, secretion and functions.* Platelets. 2001; 12(5): p. 261-273.
[97] Fitch-Tewfik J and Flaumenhaft R. *Platelet Granule Exocytosis: A Comparison with Chromaffin Cells.* Frontiers in Endocrinology. 2013; 4(77).
[98] Dzieciatkowska M, D'Alessandro A, Burke TA, et al. *Proteomics of apheresis platelet supernatants during routine storage: Gender-related differences.* Journal of Proteomics. 2015; 112: p. 190-209.
[99] MAYNARD DM, HEIJNEN HFG, HORNE MK, et al. *Proteomic analysis of platelet α-granules using mass spectrometry.* Journal of Thrombosis and Haemostasis. 2007; 5(9): p. 1945-1955.
[100] Blair P and Flaumenhaft R. *Platelet α-granules: Basic biology and clinical correlates.* Blood Reviews. 2009; 23(4): p. 177-189.
[101] ADAMS RLC and BIRD RJ. *Review article: Coagulation cascade and therapeutics update: Relevance to nephrology. Part 1: Overview of coagulation, thrombophilias and history of anticoagulants.* Nephrology. 2009; 14(5): p. 462-470.
[102] GAILANI D and RENNÉ T. *The intrinsic pathway of coagulation: a target for treating thromboembolic disease?* Journal of Thrombosis and Haemostasis. 2007; 5(6): p. 1106-1112.
[103] Maguire PB and Fitzgerald DJ. *Platelet proteomics.* Journal of Thrombosis and Haemostasis. 2003; 1(7): p. 1593-1601.
[104] Furie B and Furie BC. *Thrombus formation in vivo.* The Journal of Clinical Investigation. 2005; 115(12): p. 3355-3362.
[105] Kereiakes DJ and Gurbel PA. *Peri-Procedural Platelet Function and Platelet Inhibition in Percutaneous Coronary Intervention.* JACC: Cardiovascular Interventions. 2008; 1(2): p. 111-121.

[106] Turnbull G, Clarke J, Picard F, et al. *3D bioactive composite scaffolds for bone tissue engineering.* Bioactive Materials. 2018; 3(3): p. 278-314.
[107] Lichte P, Pape HC, Pufe T, et al. *Scaffolds for bone healing: Concepts, materials and evidence.* Injury. 2011; 42(6): p. 569-573.
[108] Burg KJL, Porter S, and Kellam JF. *Biomaterial developments for bone tissue engineering.* Biomaterials. 2000; 21(23): p. 2347-2359.
[109] Schwartz I, Robinson BP, Hollinger JO, et al. *Calvarial Bone Repair with Porous D,L-Polylactide.* Otolaryngology–Head and Neck Surgery. 1995; 112(6): p. 707-713.
[110] O'Brien FJ. *Biomaterials & scaffolds for tissue engineering.* Materials Today. 2011; 14(3): p. 88-95.
[111] Stevens MM. *Biomaterials for bone tissue engineering.* Materials Today. 2008; 11(5): p. 18-25.
[112] Shin M, Yoshimoto H, and Vacanti JP. *In Vivo Bone Tissue Engineering Using Mesenchymal Stem Cells on a Novel Electrospun Nanofibrous Scaffold.* Tissue Engineering. 2004; 10(1-2): p. 33-41.
[113] Rohner D, Hutmacher DW, Cheng TK, et al. *In vivo efficacy of bone-marrow-coated polycaprolactone scaffolds for the reconstruction of orbital defects in the pig.* Journal of Biomedical Materials Research Part B: Applied Biomaterials. 2003; 66B(2): p. 574-580.
[114] Schimming R and Schmelzeisen R. *Tissue-engineered bone for maxillary sinus augmentation.* Journal of Oral and Maxillofacial Surgery. 2004; 62(6): p. 724-729.
[115] Ji W, Sun Y, Yang F, et al. *Bioactive Electrospun Scaffolds Delivering Growth Factors and Genes for Tissue Engineering Applications.* Pharmaceutical Research. 2011; 28(6): p. 1259-1272.
[116] Das K, Bose S, and Bandyopadhyay A. *TiO2 nanotubes on Ti: Influence of nanoscale morphology on bone cell–materials interaction.* Journal of Biomedical Materials Research Part A. 2009; 90A(1): p. 225-237.
[117] Kapanen A, Ilvesaro J, Danilov A, et al. *Behaviour of Nitinol in osteoblast-like ROS-17 cell cultures.* Biomaterials. 2002; 23(3): p. 645-650.
[118] MacDonald DE, Rapuano BE, Deo N, et al. *Thermal and chemical modification of titanium–aluminum–vanadium implant materials: effects on surface properties, glycoprotein adsorption, and MG63 cell attachment.* Biomaterials. 2004; 25(16): p. 3135-3146.
[119] S.S. J, A. L, M. S, et al. *EFFECTS OF AS-CAST AND WROUGHT COBALT-CHROME-MOLYBDENUM ANDTITANIUM-ALUMINIUM-VANADIUM ALLOYS ON CYTOKINE GENE EXPRESSIONAND PROTEIN SECRETION IN J774A.1 MACROPHAGES.* European Cells and Materials. 2017; 14: p. 45-55.
[120] Hu Y, Cai K, Luo Z, et al. *Regulation of the differentiation of mesenchymal stem cells in vitro and osteogenesis in vivo by microenvironmental modification of titanium alloy surfaces.* Biomaterials. 2012; 33(13): p. 3515-3528.
[121] Ramires PA, Romito A, Cosentino F, et al. *The influence of titania/hydroxyapatite composite coatings on in vitro osteoblasts behaviour.* Biomaterials. 2001; 22(12): p. 1467-1474.
[122] Wen CE, Yamada Y, Shimojima K, et al. *Processing and mechanical properties of autogenous titanium implant materials.* Journal of Materials Science: Materials in Medicine. 2002; 13(4): p. 397-401.
[123] Witte F, Ulrich H, Palm C, et al. *Biodegradable magnesium scaffolds: Part II: Peri-implant bone remodeling.* Journal of Biomedical Materials Research Part A. 2007; 81A(3): p. 757-765.

[124] Luo J, Ajaxon I, Ginebra MP, et al. *Compressive, diametral tensile and biaxial flexural strength of cutting-edge calcium phosphate cements.* Journal of the Mechanical Behavior of Biomedical Materials. 2016; 60: p. 617-627.
[125] Rezwan K, Chen QZ, Blaker JJ, et al. *Biodegradable and bioactive porous polymer/inorganic composite scaffolds for bone tissue engineering.* Biomaterials. 2006; 27(18): p. 3413-3431.
[126] Xynos ID, Edgar AJ, Buttery LDK, et al. *Ionic Products of Bioactive Glass Dissolution Increase Proliferation of Human Osteoblasts and Induce Insulin-like Growth Factor II mRNA Expression and Protein Synthesis.* Biochemical and Biophysical Research Communications. 2000; 276(2): p. 461-465.
[127] A, Gupta V, Bains V, et al. *Clinical and cone beam computed tomography comparison of NovaBone Dental Putty and PerioGlas in the treatment of mandibular Class II furcations.* Indian Journal of Dental Research. 2014; 25(2): p. 166-173.
[128] Fielding GA, Bandyopadhyay A, and Bose S. *Effects of silica and zinc oxide doping on mechanical and biological properties of 3D printed tricalcium phosphate tissue engineering scaffolds.* Dental Materials. 2012; 28(2): p. 113-122.
[129] J. S, F. T, V. W, et al. *Development of porous powder printed high density polyethylene for personalized bone implants.* Journal of Porous Materials. 2012; 19(5): p. 623-632.
[130] Schoof H, Apel J, Heschel I, et al. *Control of pore structure and size in freeze-dried collagen sponges.* Journal of Biomedical Materials Research. 2001; 58(4): p. 352-357.
[131] Zander NE. *Formation of melt and solution spun polycaprolactone fibers by centrifugal spinning.* Journal of Applied Polymer Science. 2015; 132(2).
[132] Yoshimoto H, Shin YM, Terai H, et al. *A biodegradable nanofiber scaffold by electrospinning and its potential for bone tissue engineering.* Biomaterials. 2003; 24(12): p. 2077-2082.
[133] Katsogiannis KAG, Vladisavljević GT, and Georgiadou S. *Porous electrospun polycaprolactone (PCL) fibres by phase separation.* European Polymer Journal. 2015; 69: p. 284-295.
[134] Um IC, Fang D, Hsiao BS, et al. *Electro-Spinning and Electro-Blowing of Hyaluronic Acid.* Biomacromolecules. 2004; 5(4): p. 1428-1436.
[135] Mai Y and Eisenberg A. *Self-assembly of block copolymers.* Chemical Society Reviews. 2012; 41(18): p. 5969-5985.
[136] Williams JM, Adewunmi A, Schek RM, et al. *Bone tissue engineering using polycaprolactone scaffolds fabricated via selective laser sintering.* Biomaterials. 2005; 26(23): p. 4817-4827.
[137] Kundu J, Shim J-H, Jang J, et al. *An additive manufacturing-based PCL–alginate–chondrocyte bioprinted scaffold for cartilage tissue engineering.* Journal of Tissue Engineering and Regenerative Medicine. 2015; 9(11): p. 1286-1297.
[138] Pok S, Myers JD, Madihally SV, et al. *A multilayered scaffold of a chitosan and gelatin hydrogel supported by a PCL core for cardiac tissue engineering.* Acta Biomaterialia. 2013; 9(3): p. 5630-5642.
[139] Bezwada RS, Jamiolkowski DD, Lee I-Y, et al. *Monocryl® suture, a new ultra-pliable absorbable monofilament suture.* Biomaterials. 1995; 16(15): p. 1141-1148.
[140] Labet M and Thielemans W. *Synthesis of polycaprolactone: a review.* Chemical Society Reviews. 2009; 38(12): p. 3484-3504.
[141] Kweon H, Yoo MK, Park IK, et al. *A novel degradable polycaprolactone networks for tissue engineering.* Biomaterials. 2003; 24(5): p. 801-808.

[142] Casper CL, Stephens JS, Tassi NG, et al. *Controlling Surface Morphology of Electrospun Polystyrene Fibers: Effect of Humidity and Molecular Weight in the Electrospinning Process.* Macromolecules. 2004; 37(2): p. 573-578.
[143] Badrossamay MR, McIlwee HA, Goss JA, et al. *Nanofiber Assembly by Rotary Jet-Spinning.* Nano Letters. 2010; 10(6): p. 2257-2261.
[144] Yang Y, Li X, Qi M, et al. *Release pattern and structural integrity of lysozyme encapsulated in core–sheath structured poly(dl-lactide) ultrafine fibers prepared by emulsion electrospinning.* European Journal of Pharmaceutics and Biopharmaceutics. 2008; 69(1): p. 106-116.
[145] Moghadasi Boroujeni S, Mashayekhan S, Vakilian S, et al. *The synergistic effect of surface topography and sustained release of TGF-β1 on myogenic differentiation of human mesenchymal stem cells.* Journal of Biomedical Materials Research Part A. 2016; 104(7): p. 1610-1621.
[146] Ohtake S, Martin RA, Saxena A, et al. *Formulation and Stabilization of Francisella tularensis Live Vaccine Strain.* Journal of Pharmaceutical Sciences. 2011; 100(8): p. 3076-3087.
[147] Tian L, Prabhakaran MP, Ding X, et al. *Emulsion electrospun vascular endothelial growth factor encapsulated poly(l-lactic acid-co-ε-caprolactone) nanofibers for sustained release in cardiac tissue engineering.* Journal of Materials Science. 2012; 47(7): p. 3272-3281.
[148] Nie H, Soh BW, Fu Y-C, et al. *Three-dimensional fibrous PLGA/HAp composite scaffold for BMP-2 delivery.* Biotechnology and Bioengineering. 2008; 99(1): p. 223-234.
[149] Schneider A, Wang XY, Kaplan DL, et al. *Biofunctionalized electrospun silk mats as a topical bioactive dressing for accelerated wound healing.* Acta Biomaterialia. 2009; 5(7): p. 2570-2578.
[150] Yin L, Yang S, He M, et al. *Physicochemical and biological characteristics of BMP-2/IGF-1-loaded three-dimensional coaxial electrospun fibrous membranes for bone defect repair.* Journal of Materials Science: Materials in Medicine. 2017; 28(6): p. 94.
[151] Li H, Zhao C, Wang Z, et al. *Controlled Release of PDGF-bb by Coaxial Electrospun Dextran/Poly(L-lactide-co-ε-caprolactone) Fibers with an Ultrafine Core/Shell Structure.* Journal of Biomaterials Science, Polymer Edition. 2010; 21(6-7): p. 803-819.
[152] Jiang H, Hu Y, Zhao P, et al. *Modulation of protein release from biodegradable core–shell structured fibers prepared by coaxial electrospinning.* Journal of Biomedical Materials Research Part B: Applied Biomaterials. 2006; 79B(1): p. 50-57.
[153] Choi JS, Leong KW, and Yoo HS. *In vivo wound healing of diabetic ulcers using electrospun nanofibers immobilized with human epidermal growth factor (EGF).* Biomaterials. 2008; 29(5): p. 587-596.
[154] Kim HS and Yoo HS. *MMPs-responsive release of DNA from electrospun nanofibrous matrix for local gene therapy: In vitro and in vivo evaluation.* Journal of Controlled Release. 2010; 145(3): p. 264-271.
[155] Kim S-S, Sun Park M, Jeon O, et al. *Poly(lactide-co-glycolide)/hydroxyapatite composite scaffolds for bone tissue engineering.* Biomaterials. 2006; 27(8): p. 1399-1409.
[156] Liu H, Slamovich EB, and Webster TJ. *Less harmful acidic degradation of poly(lacticco-glycolic acid) bone tissue engineering scaffolds through titania nanoparticle addition.* International journal of nanomedicine. 2006; 1(4): p. 541-545.

[157] Chu C, Xue X, Zhu J, et al. *Fabrication and characterization of titanium-matrix composite with 20 vol% hydroxyapatite for use as heavy load-bearing hard tissue replacement.* Journal of Materials Science: Materials in Medicine. 2006; 17(3): p. 245-251.
[158] Chu C, Xue X, Zhu J, et al. *Mechanical and biological properties of hydroxyapatite reinforced with 40 vol. % titanium particles for use as hard tissue replacement.* Journal of Materials Science: Materials in Medicine. 2004; 15(6): p. 665-670.
[159] Inzana JA, Olvera D, Fuller SM, et al. *3D printing of composite calcium phosphate and collagen scaffolds for bone regeneration.* Biomaterials. 2014; 35(13): p. 4026-4034.
[160] Lei Y, Xu Z, Ke Q, et al. *Strontium hydroxyapatite/chitosan nanohybrid scaffolds with enhanced osteoinductivity for bone tissue engineering.* Materials Science and Engineering: C. 2017; 72: p. 134-142.
[161] Carragee EJ, Hurwitz EL, and Weiner BK. *A critical review of recombinant human bone morphogenetic protein-2 trials in spinal surgery: emerging safety concerns and lessons learned.* The Spine Journal. 2011; 11(6): p. 471-491.
[162] Barr T, McNamara AJA, Sándor GKB, et al. *Comparison of the osteoinductivity of bioimplants containing recombinant human bone morphogenetic proteins 2 (Infuse) and 7 (OP-1).* Oral Surgery, Oral Medicine, Oral Pathology, Oral Radiology, and Endodontology. 2010; 109(4): p. 531-540.
[163] Gomar F, Orozco R, Villar JL, et al. *P-15 small peptide bone graft substitute in the treatment of non-unions and delayed union. A pilot clinical trial.* International Orthopaedics. 2007; 31(1): p. 93-99.
[164] Lee YJ, Lee J-H, Cho H-J, et al. *Electrospun fibers immobilized with bone forming peptide-1 derived from BMP7 for guided bone regeneration.* Biomaterials. 2013; 34(21): p. 5059-5069.
[165] Lock J and Liu H. *Nanomaterials enhance osteogenic differentiation of human mesenchymal stem cells similar to a short peptide of BMP-7.* International journal of nanomedicine. 2011; 6: p. 2769-2777.
[166] Moore NM, Lin NJ, Gallant ND, et al. *Synergistic enhancement of human bone marrow stromal cell proliferation and osteogenic differentiation on BMP-2-derived and RGD peptide concentration gradients.* Acta Biomaterialia. 2011; 7(5): p. 2091-2100.
[167] Roy K, Wang D, Hedley ML, et al. *Gene delivery with in-situ crosslinking polymer networks generates long-term systemic protein expression.* Molecular Therapy. 2003; 7(3): p. 401-408.
[168] Soffer E, Ouhayoun JP, and Anagnostou F. *Fibrin sealants and platelet preparations in bone and periodontal healing.* Oral Surgery, Oral Medicine, Oral Pathology, Oral Radiology, and Endodontology. 2003; 95(5): p. 521-528.
[169] Dohan Ehrenfest DM, Doglioli P, de Peppo GM, et al. *Choukroun's platelet-rich fibrin (PRF) stimulates in vitro proliferation and differentiation of human oral bone mesenchymal stem cell in a dose-dependent way.* Archives of Oral Biology. 2010; 55(3): p. 185-194.
[170] Burnouf T, Strunk D, Koh MBC, et al. *Human platelet lysate: Replacing fetal bovine serum as a gold standard for human cell propagation?* Biomaterials. 2016; 76: p. 371-387.
[171] Bardsley K, Wimpenny I, Wechsler R, et al. *Defining a turnover index for the correlation of biomaterial degradation and cell based extracellular matrix synthesis using fluorescent tagging techniques.* Acta Biomaterialia. 2016; 45: p. 133-142.

[172] Rai B, Oest ME, Dupont KM, et al. *Combination of platelet-rich plasma with polycaprolactone-tricalcium phosphate scaffolds for segmental bone defect repair.* Journal of Biomedical Materials Research Part A. 2007; 81A(4): p. 888-899.
[173] Sarkar MR, Augat P, Shefelbine SJ, et al. *Bone formation in a long bone defect model using a platelet-rich plasma-loaded collagen scaffold.* Biomaterials. 2006; 27(9): p. 1817-1823.
[174] Chang S-H, Hsu Y-M, Wang YJ, et al. *Fabrication of pre-determined shape of bone segment with collagen-hydroxyapatite scaffold and autogenous platelet-rich plasma.* Journal of Materials Science: Materials in Medicine. 2009; 20(1): p. 23-31.
[175] Cerruti HF, Kerkis I, Kerkis A, et al. *Allogenous Bone Grafts Improved by Bone Marrow Stem Cells and Platelet Growth Factors: Clinical Case Reports.* Artificial Organs. 2007; 31(4): p. 268-273.
[176] Middleton KK, Barro V, Muller B, et al. *Evaluation of the effects of platelet-rich plasma (PRP) therapy involved in the healing of sports-related soft tissue injuries.* The Iowa orthopaedic journal. 2012; 32: p. 150-163.
[177] Kasten P, Vogel J, Beyen I, et al. *Effect of Platelet-rich Plasma on the in vitro Proliferation and Osteogenic Differentiation of Human Mesenchymal Stem Cells on Distinct Calcium Phosphate Scaffolds: The Specific Surface Area Makes a Difference.* Journal of Biomaterials Applications. 2008; 23(2): p. 169-188.
[178] M. K, H. K, A. SK, et al. *The effect of the platelet concentration in platelet-rich plasma gel on the regeneration of bone.* The Journal of Bone and Joint Surgery. British volume. 2008; 90-B(7): p. 966-972.
[179] Arpornmaeklong P, Kochel M, Depprich R, et al. *Influence of platelet-rich plasma (PRP) on osteogenic differentiation of rat bone marrow stromal cells. An in vitro study.* International Journal of Oral and Maxillofacial Surgery. 2004; 33(1): p. 60-70.
[180] Herrera BS, Coimbra LS, Bastos AS, et al. *Platelet-rich plasma stimulates cytokine expression and alkaline phosphatase activity in osteoblast-derived osteosarcoma cells.* Archives of Oral Biology. 2012; 57(9): p. 1282-1289.
[181] Shi X, Wang Y, Varshney RR, et al. *Microsphere-based drug releasing scaffolds for inducing osteogenesis of human mesenchymal stem cells in vitro.* European Journal of Pharmaceutical Sciences. 2010; 39(1): p. 59-67.
[182] Kim H, Kim HW, and Suh H. *Sustained release of ascorbate-2-phosphate and dexamethasone from porous PLGA scaffolds for bone tissue engineering using mesenchymal stem cells.* Biomaterials. 2003; 24(25): p. 4671-4679.
[183] Kim H, Suh H, Jo SA, et al. *In vivo bone formation by human marrow stromal cells in biodegradable scaffolds that release dexamethasone and ascorbate-2-phosphate.* Biochemical and Biophysical Research Communications. 2005; 332(4): p. 1053-1060.
[184] Yoon JJ, Kim JH, and Park TG. *Dexamethasone-releasing biodegradable polymer scaffolds fabricated by a gas-foaming/salt-leaching method.* Biomaterials. 2003; 24(13): p. 2323-2329.
[185] Martins A, Duarte ARC, Faria S, et al. *Osteogenic induction of hBMSCs by electrospun scaffolds with dexamethasone release functionality.* Biomaterials. 2010; 31(22): p. 5875-5885.
[186] Langer R and Vacanti J. *Tissue engineering.* Science. 1993; 260(5110): p. 920-926.
[187] Bonassar LJ and Vacanti CA. *Tissue engineering: The first decade and beyond.* Journal of Cellular Biochemistry. 1998; 72(S30–31): p. 297-303.
[188] Griffith LG and Naughton G. *Tissue Engineering--Current Challenges and Expanding Opportunities.* Science. 2002; 295(5557): p. 1009-1014.

[189] Billiet T, Vandenhaute M, Schelfhout J, et al. *A review of trends and limitations in hydrogel-rapid prototyping for tissue engineering.* Biomaterials. 2012; 33(26): p. 6020-6041.
[190] OPTN (2010) Donation and transplantation. Online. Available from URL: http://optn.transplant.hrsa.gov/about/.
[191] Wolfe RA, Roys EC, and Merion RM. *Trends in Organ Donation and Transplantation in the United States, 1999–2008.* American Journal of Transplantation. 2010; 10(4p2): p. 961-972.
[192] Yoon E, Dhar S, Chun DE, et al. *In Vivo Osteogenic Potential of Human Adipose-Derived Stem Cells/Poly Lactide-Co-Glycolic Acid Constructs for Bone Regeneration in a Rat Critical-Sized Calvarial Defect Model.* Tissue Engineering. 2007; 13(3): p. 619-627.
[193] Shao XX, Hutmacher DW, Ho ST, et al. *Evaluation of a hybrid scaffold/cell construct in repair of high-load-bearing osteochondral defects in rabbits.* Biomaterials. 2006; 27(7): p. 1071-1080.
[194] Lü L-X, Zhang X-F, Wang Y-Y, et al. *Effects of Hydroxyapatite-Containing Composite Nanofibers on Osteogenesis of Mesenchymal Stem Cells In vitro and Bone Regeneration In vivo.* ACS Applied Materials & Interfaces. 2013; 5(2): p. 319-330.
[195] Schofer MD, Roessler PP, Schaefer J, et al. *Electrospun PLLA Nanofiber Scaffolds and Their Use in Combination with BMP-2 for Reconstruction of Bone Defects.* PloS One. 2011; 6(9): p. e25462.
[196] Fu S, Ni P, Wang B, et al. *In vivo biocompatibility and osteogenesis of electrospun poly(ε-caprolactone)–poly(ethylene glycol)–poly(ε-caprolactone)/nano-hydroxyapatite composite scaffold.* Biomaterials. 2012; 33(33): p. 8363-8371.
[197] Wang H, Li Y, Zuo Y, et al. *Biocompatibility and osteogenesis of biomimetic nano-hydroxyapatite/polyamide composite scaffolds for bone tissue engineering.* Biomaterials. 2007; 28(22): p. 3338-3348.
[198] Nie H, Ho M-L, Wang C-K, et al. *BMP-2 plasmid loaded PLGA/HAp composite scaffolds for treatment of bone defects in nude mice.* Biomaterials. 2009; 30(5): p. 892-901.
[199] M. AL, T. S, S. S, et al. *Centrifugal spun ultrafine fibrous web as a potential drugdelivery vehicle.* eXPRESS Polymer Letters. 2012; 17(3): p. 238-248.
[200] Nair LS and Laurencin CT. *Biodegradable polymers as biomaterials.* Progress in Polymer Science. 2007; 32(8): p. 762-798.
[201] Blakeney BA, Tambralli A, Anderson JM, et al. *Cell infiltration and growth in a low density, uncompressed three-dimensional electrospun nanofibrous scaffold.* Biomaterials. 2011; 32(6): p. 1583-1590.
[202] Thibault RA, Baggett LS, Mikos AG, et al. *Osteogenic Differentiation of Mesenchymal Stem Cells on Pregenerated Extracellular Matrix Scaffolds in the Absence of Osteogenic Cell Culture Supplements.* Tissue Engineering Part A. 2010; 16(2): p. 431-440.
[203] Mitsak AG, Kemppainen JM, Harris MT, et al. *Effect of Polycaprolactone Scaffold Permeability on Bone Regeneration In Vivo.* Tissue Engineering Part A. 2011; 17(13-14): p. 1831-1839.
[204] Lam CXF, Hutmacher DW, Schantz J-T, et al. *Evaluation of polycaprolactone scaffold degradation for 6 months in vitro and in vivo.* Journal of Biomedical Materials Research Part A. 2009; 90A(3): p. 906-919.

[205] Wu Y-C, Shaw S-Y, Lin H-R, et al. *Bone tissue engineering evaluation based on rat calvaria stromal cells cultured on modified PLGA scaffolds.* Biomaterials. 2006; 27(6): p. 896-904.
[206] Cukierman E, Pankov R, Stevens DR, et al. *Taking Cell-Matrix Adhesions to the Third Dimension.* Science. 2001; 294(5547): p. 1708-1712.
[207] CHIMELI TBC, D'ALPINO PHP, PEREIRA PN, et al. *Effects of solvent evaporation on water sorption/solubility and nanoleakage of adhesive systems.* Journal of Applied Oral Science. 2014; 22: p. 294-301.
[208] Diaz-Gomez L, Alvarez-Lorenzo C, Concheiro A, et al. *Biodegradable electrospun nanofibers coated with platelet-rich plasma for cell adhesion and proliferation.* Materials Science and Engineering: C. 2014; 40: p. 180-188.
[209] Hulbert SF, Young FA, Mathews RS, et al. *Potential of ceramic materials as permanently implantable skeletal prostheses.* Journal of Biomedical Materials Research. 1970; 4(3): p. 433-456.
[210] Roosa SMM, Kemppainen JM, Moffitt EN, et al. *The pore size of polycaprolactone scaffolds has limited influence on bone regeneration in an in vivo model.* Journal of Biomedical Materials Research Part A. 2010; 92A(1): p. 359-368.
[211] Park K, Ju YM, Son JS, et al. *Surface modification of biodegradable electrospun nanofiber scaffolds and their interaction with fibroblasts.* Journal of Biomaterials Science, Polymer Edition. 2007; 18(4): p. 369-382.
[212] Ma Z, Gao C, Gong Y, et al. *Cartilage tissue engineering PLLA scaffold with surface immobilized collagen and basic fibroblast growth factor.* Biomaterials. 2005; 26(11): p. 1253-1259.
[213] Jin Yoon J, Ho Song S, Sung Lee D, et al. *Immobilization of cell adhesive RGD peptide onto the surface of highly porous biodegradable polymer scaffolds fabricated by a gas foaming/salt leaching method.* Biomaterials. 2004; 25(25): p. 5613-5620.
[214] Jia X, Zhao C, Li P, et al. *Sustained Release of VEGF by Coaxial Electrospun Dextran/PLGA Fibrous Membranes in Vascular Tissue Engineering.* Journal of Biomaterials Science, Polymer Edition. 2011; 22(13): p. 1811-1827.
[215] Zhang H, Liang J, Ding Y, et al. *The controlled release of growth factor via modified coaxial electrospun fibres with emulsion or hydrogel as the core.* Materials Letters. 2016; 181: p. 119-122.
[216] Rubert M, Dehli J, Li Y-F, et al. *Electrospun PCL/PEO coaxial fibers for basic fibroblast growth factor delivery.* Journal of Materials Chemistry B. 2014; 2(48): p. 8538-8546.
[217] Ju Y-E, Janmey PA, McCormick ME, et al. *Enhanced neurite growth from mammalian neurons in three-dimensional salmon fibrin gels.* Biomaterials. 2007; 28(12): p. 2097-2108.
[218] Zhang Y, Heher P, Hilborn J, et al. *Hyaluronic acid-fibrin interpenetrating double network hydrogel prepared in situ by orthogonal disulfide cross-linking reaction for biomedical applications.* Acta Biomaterialia. 2016; 38: p. 23-32.
[219] Durmuşlar MC, Ballı U, Öngöz Dede F, et al. *Evaluation of the effects of platelet-rich fibrin on bone regeneration in diabetic rabbits.* Journal of Cranio-Maxillofacial Surgery. 2016; 44(2): p. 126-133.
[220] Wang Z, Hu H, Li Z, et al. *Sheet of osteoblastic cells combined with platelet-rich fibrin improves the formation of bone in critical-size calvarial defects in rabbits.* British Journal of Oral and Maxillofacial Surgery. 2016; 54(3): p. 316-321.
[221] Sadeghi-Ataabadi M, Mostafavi-pour Z, Vojdani Z, et al. *Fabrication and characterization of platelet-rich plasma scaffolds for tissue engineering applications.* Materials Science and Engineering: C. 2017; 71: p. 372-380.

[222] M.B. H, N. G, and A. G. *Rheological Properties and Reverse Micelles Conditions of PEO-PPO-PEO Pluronic F68: Effects of Temperature and Solvent Mixtures.* Journal of Polymers. 2013; 7.
[223] Lee HJ, McAuley A, Schilke KF, et al. *Molecular origins of surfactant-mediated stabilization of protein drugs.* Advanced Drug Delivery Reviews. 2011; 63(13): p. 1160-1171.
[224] Yeung CK, Chan KP, Chan CKM, et al. *Cytotoxicity of Triamcinolone on Cultured Human Retinal Pigment Epithelial Cells: Comparison with Dexamethasone and Hydrocortisone.* Japanese Journal of Ophthalmology. 2004; 48(3): p. 236-242.
[225] Chen Q, Zielinski D, Chen J, et al. *A validated, stability-indicating HPLC method for the determination of dexamethasone related substances on dexamethasone-coated drug-eluting stents.* Journal of Pharmaceutical and Biomedical Analysis. 2008; 48(3): p. 732-738.
[226] Friedrich RB, Ravanello A, Cichota LC, et al. *Validation of a simple and rapid UV spectrophotometric method for dexamethasone assay in tablets.* Química Nova. 2009; 32: p. 1052-1054.
[227] Sill TJ and von Recum HA. *Electrospinning: Applications in drug delivery and tissue engineering.* Biomaterials. 2008; 29(13): p. 1989-2006.
[228] Zeng J, Yang L, Liang Q, et al. *Influence of the drug compatibility with polymer solution on the release kinetics of electrospun fiber formulation.* Journal of Controlled Release. 2005; 105(1): p. 43-51.
[229] Gandhi M, Srikar R, Yarin AL, et al. *Mechanistic Examination of Protein Release from Polymer Nanofibers.* Molecular Pharmaceutics. 2009; 6(2): p. 641-647.
[230] Dallari D, Fini M, Stagni C, et al. *In vivo study on the healing of bone defects treated with bone marrow stromal cells, platelet-rich plasma, and freeze-dried bone allografts, alone and in combination.* Journal of Orthopaedic Research. 2006; 24(5): p. 877-888.
[231] Kanthan SR, Kavitha G, Addi S, et al. *Platelet-rich plasma (PRP) enhances bone healing in non-united critical-sized defects: A preliminary study involving rabbit models.* Injury. 2011; 42(8): p. 782-789.
[232] Wiltfang J, Kloss FR, Kessler P, et al. *Effects of platelet-rich plasma on bone healing in combination with autogenous bone and bone substitutes in critical-size defects.* Clinical Oral Implants Research. 2004; 15(2): p. 187-193.
[233] Dallari D, Savarino L, Stagni C, et al. *Enhanced Tibial Osteotomy Healing with Use of Bone Grafts Supplemented with Platelet Gel or Platelet Gel and Bone Marrow Stromal Cells.* JBJS. 2007; 89(11): p. 2413-2420.
[234] Kim T-H, Kim S-H, Sándor GK, et al. *Comparison of platelet-rich plasma (PRP), platelet-rich fibrin (PRF), and concentrated growth factor (CGF) in rabbit-skull defect healing.* Archives of Oral Biology. 2014; 59(5): p. 550-558.
[235] Anitua E, Sánchez M, Nurden AT, et al. *New insights into and novel applications for platelet-rich fibrin therapies.* Trends in Biotechnology. 2006; 24(5): p. 227-234.
[236] Nam D, Mau E, Wang Y, et al. *T-Lymphocytes Enable Osteoblast Maturation via IL-17F during the Early Phase of Fracture Repair.* PloS One. 2012; 7(6): p. e40044.
[237] Mehta M, Schmidt-Bleek K, Duda GN, et al. *Biomaterial delivery of morphogens to mimic the natural healing cascade in bone.* Advanced Drug Delivery Reviews. 2012; 64(12): p. 1257-1276.
[238] Kurane A, Simionescu DT, and Vyavahare NR. *In vivo cellular repopulation of tubular elastin scaffolds mediated by basic fibroblast growth factor.* Biomaterials. 2007; 28(18): p. 2830-2838.

[239] Schmidmaier G, Wildemann B, Ostapowicz D, et al. *Long-term effects of local growth factor (IGF-I and TGF-β1) treatment on fracture healing: A safety study for using growth factors.* Journal of Orthopaedic Research. 2004; 22(3): p. 514-519.
[240] NODA M and CAMILLIERE JJ. *In Vivo Stimulation of Bone Formation by Transforming Growth Factor-β.* Endocrinology. 1989; 124(6): p. 2991-2994.
[241] Allori AC, Sailon AM, and Warren SM. *Biological Basis of Bone Formation, Remodeling, and Repair—Part I: Biochemical Signaling Molecules.* Tissue Engineering Part B: Reviews. 2008; 14(3): p. 259-273.
[242] Liu Y-C, Kao Y-T, Huang W-K, et al. *CCL5/RANTES is important for inducing osteogenesis of human mesenchymal stem cells and is regulated by dexamethasone.* BioScience Trends. 2014; 8(3): p. 138-143.
[243] Van Vlasselaer P, Borremans B, van Gorp U, et al. *Interleukin 10 inhibits transforming growth factor-beta (TGF-beta) synthesis required for osteogenic commitment of mouse bone marrow cells.* The Journal of Cell Biology. 1994; 124(4): p. 569-577.
[244] Cai Y, Yu J, Kundu SC, et al. *Multifunctional nano-hydroxyapatite and alginate/gelatin based sticky gel composites for potential bone regeneration.* Materials Chemistry and Physics. 2016; 181: p. 227-233.
[245] Hu J-X, Ran J-B, Chen S, et al. *Carboxylated Agarose (CA)-Silk Fibroin (SF) Dual Confluent Matrices Containing Oriented Hydroxyapatite (HA) Crystals: Biomimetic Organic/Inorganic Composites for Tibia Repair.* Biomacromolecules. 2016; 17(7): p. 2437-2447.
[246] Chu S-F, Huang M-T, Ou K-L, et al. *Enhanced biocompatible and hemocompatible nano/micro porous surface as a biological scaffold for functionalizational and biointegrated implants.* Journal of Alloys and Compounds. 2016; 684: p. 726-732.
[247] Stevenson G, Rehman S, Draper E, et al. *Combining 3D human in vitro methods for a 3Rs evaluation of novel titanium surfaces in orthopaedic applications.* Biotechnology and Bioengineering. 2016; 113(7): p. 1586-1599.
[248] Hejazi F and Mirzadeh H. *Novel 3D scaffold with enhanced physical and cell response properties for bone tissue regeneration, fabricated by patterned electrospinning/electrospraying.* Journal of Materials Science: Materials in Medicine. 2016; 27(9): p. 143.
[249] C. P, M. S, T. T, et al. *Characterization of Osteosarcoma Cell Lines MG-63, Saos-2 and U-2 OS in Comparison to Human Osteoblasts.* Anticancer Research. 2004; 24(6): p. 3743-3748.
[250] Bilbe G, Roberts E, Birch M, et al. *PCR phenotyping of cytokines, growth factors and their receptors and bone matrix proteins in human osteoblast-like cell lines.* Bone. 1996; 19(5): p. 437-445.
[251] Rampichová M, Buzgo M, Chvojka J, et al. *Cell penetration to nanofibrous scaffolds.* Cell Adhesion & Migration. 2014; 8(1): p. 36-41.
[252] Ilmer M, Karow M, Geissler C, et al. *Human Osteoblast–Derived Factors Induce Early Osteogenic Markers in Human Mesenchymal Stem Cells.* Tissue Engineering Part A. 2009; 15(9): p. 2397-2409.
[253] Tsai M-T, Li W-J, Tuan RS, et al. *Modulation of osteogenesis in human mesenchymal stem cells by specific pulsed electromagnetic field stimulation.* Journal of Orthopaedic Research. 2009; 27(9): p. 1169-1174.
[254] Park J-B. *The Effects of Dexamethasone, Ascorbic Acid, and β-Glycerophosphate on Osteoblastic Differentiation by Regulating Estrogen Receptor and Osteopontin Expression.* Journal of Surgical Research. 2012; 173(1): p. 99-104.

[255] Coelho MJ and Fernandes MH. *Human bone cell cultures in biocompatibility testing. Part II: effect of ascorbic acid, β-glycerophosphate and dexamethasone on osteoblastic differentiation.* Biomaterials. 2000; 21(11): p. 1095-1102.
[256] Mikami Y, Omoteyama K, Kato S, et al. *Inductive effects of dexamethasone on the mineralization and the osteoblastic gene expressions in mature osteoblast-like ROS17/2.8 cells.* Biochemical and Biophysical Research Communications. 2007; 362(2): p. 368-373.
[257] Nishimura I, Hisanaga R, Sato T, et al. *Effect of osteogenic differentiation medium on proliferation and differentiation of human mesenchymal stem cells in three-dimensional culture with radial flow bioreactor.* Regenerative Therapy. 2015; 2: p. 24-31.
[258] Peter SJ, Liang CR, Kim DJ, et al. *Osteoblastic phenotype of rat marrow stromal cells cultured in the presence of dexamethasone, β-glycerolphosphate, and L-ascorbic acid.* Journal of Cellular Biochemistry. 1998; 71(1): p. 55-62.
[259] Jaiswal N, Haynesworth SE, Caplan AI, et al. *Osteogenic differentiation of purified, culture-expanded human mesenchymal stem cells in vitro.* Journal of Cellular Biochemistry. 1997; 64(2): p. 295-312.

8 RELEVANT PUBLICATIONS

International Journal of Nanomedicine

Dovepress
open access to scientific and medical research

Open Access Full Text Article

ORIGINAL RESEARCH

Platelet-functionalized three-dimensional poly-ε-caprolactone fibrous scaffold prepared using centrifugal spinning for delivery of growth factors

Michala Rampichová[1,2]
Matej Buzgo[1]
Andrea Míčková[1,2]
Karolína Vocetková[2]
Věra Sovková[2]
Věra Lukášová[2]
Eva Filová[2]
Franco Rustichelli[2]
Evžen Amler[1,2]

[1]Indoor Environmental Quality, University Center for Energy Efficient Buildings, Czech Technical University in Prague, Buštěhrad, [2]Laboratory of Tissue Engineering, Institute of Experimental Medicine, Czech Academy of Sciences, Prague, Czech Republic

Abstract: Bone and cartilage are tissues of a three-dimensional (3D) nature. Therefore, scaffolds for their regeneration should support cell infiltration and growth in all 3 dimensions. To fulfill such a requirement, the materials should possess large, open pores. Centrifugal spinning is a simple method for producing 3D fibrous scaffolds with large and interconnected pores. However, the process of bone regeneration is rather complex and requires additional stimulation by active molecules. In the current study, we introduced a simple composite scaffold based on platelet adhesion to poly-ε-caprolactone 3D fibers. Platelets were used as a natural source of growth factors and cytokines active in the tissue repair process. By immobilization in the fibrous scaffolds, their bioavailability was prolonged. The biological evaluation of the proposed system in the MG-63 model showed improved metabolic activity, proliferation and alkaline phosphatase activity in comparison to nonfunctionalized fibrous scaffold. In addition, the response of cells was dose dependent with improved biocompatibility with increasing platelet concentration. The results demonstrated the suitability of the system for bone tissue.

Keywords: centrifugal spinning, 3D scaffold, platelets, growth factors, cytokines, PCL

Introduction

In order to fulfill the goals of tissue engineering, scaffolding materials that support cell adhesion and proliferation are in demand. These materials should attract cells to infiltrate inside the scaffold and stimulate them to differentiate to the desired cell type. Proper cell differentiation is crucial for tissue-specific extracellular matrix (ECM) synthesis and could create newly formed fully functionalized tissue. To fulfill such expectations, tissue-engineered scaffolds are combined with drug delivery carriers and serve as a mechanical support not only for cells but also for their stimulation.

Among the wide spectrum of scaffolding materials used in tissue engineering, nanofibers and microfibers raise much attention. With diameters similar to the compounds of ECM, the fibers mimic the natural environment for cells and enhance their adhesion and proliferation.[1,2] The most commonly used technology for producing ultrafine fibers for tissue engineering applications is electrospinning. To overcome electrospinning limitations, such as low production capacity and sheet structure with limited layer thickness, alternative methods such as melt-blown and centrifugal spinning have been used.[3]

Centrifugal spinning (Forcespinning™) is a technology that uses centrifugal force to produce ultrafine fibers from melts and solutions.[4] The polymeric solution or melt is placed in a rotating chamber with a thin orifice. The applied centrifugal speed has to be strong enough to overcome surface tension of the solution. The polymer solution is ejected from the orifice,

Correspondence: Michala Rampichová
Indoor Environmental Quality, University Center for Energy Efficient Buildings, Czech Technical University in Prague, Trinecka 1024, 273 43, Buštěhrad, Czech Republic
Tel/fax +420 296 442 387
Email michala.rampichova@cvut.cz

submit your manuscript | www.dovepress.com
Dovepress
http://dx.doi.org/10.2147/IJN.S120206

and emerged jets are stretched and deposited on a collector. The Forcespinning technology has been used for fabricating tissue engineering scaffolds from various polymers, such as poly-ε-caprolactone (PCL),[4–6] gelatin,[5] poly(L-lactic acid) (PLLA),[7] and poly-lactic-co-glycolic acid (PLGA).[8] Loordhuswamy et al[5] used in their study PCL in combination with gelatin to produce fibrous meshes and tested them in vitro and in vivo for wound healing. Zander[4] used a rotating collector to deposit aligned PCL fibers and used them to culture neuronal PC12 cells. It was shown that the cells extended their neurites along the fibers.

However, the structure of the scaffold alone is often not sufficient to promote tissue healing. In order to simulate the physiological gradients of signaling molecules regulating cellular fate, the scaffolds are often combined with drug delivery systems. Platelets are frequently used in tissue engineering and regenerative medicine as a source of natural cytokines and growth factors. Platelets play an important role in wound healing and regeneration and inflammatory response. Alfa granules of platelets contain a wide range of growth factors, including PDGF, TGF-β, PDAF, VEGF, EGF, PDEGF, ECGF and IGF.[9] It has been reported that the use of platelets is beneficial for healing of bone,[10] cartilage,[11] tendon,[12] hernia[13] and skin[14] defects. One of the main advantages of using platelets as a source of growth factor is the possibility of autologous use, which reduces the immune reaction.

In our previous experiment, platelets were used to make electrospun PCL nanofibers functional.[11] Platelets adhered effectively to nanofibers, and the released growth factors enhanced the adhesion and proliferation of chondrocytes. The system of electrospun PCL nanofibers with adhered platelets was also tested in a study by Plencner et al.[13] The nanofibrous samples with adhered platelets were tested with fibroblast as a potential chirurgical mesh. The study showed that the platelets improved the properties of PCL nanofibers. In a study by Diaz-Gomez et al,[15] PCL nanofibers prepared using electrospinning were soaked in platelet-rich plasma (PRP) and subsequently lyophilized. It was shown that growth factors were released from the scaffold-enhanced adhesion and proliferation of mesenchymal stem cells (MSCs). No effect of MSC differentiation was detected.

In the current study, PCL three-dimensional (3D) fibrous meshes prepared via centrifugal spinning (Forcespinning) were combined with adhered platelets. The adhered platelets were used as a natural source of cytokines and growth factors for stimulating cell adhesion, proliferation and osteogenic differentiation. The fibers prepared using centrifugal spinning were expected to possess the same adhesive capacity as electrospun fibers, with the advantage of a 3D mesh structure. A 3D structure is essential for bone tissue engineering.

Materials and methods

Fibrous scaffold preparation using centrifugal spinning technology

Fibrous meshes were prepared using a centrifugal spinning device (Cyclone 1000 L/M Forcespinning® device; FibeRio, McAllen, TX, USA). PCL (Sigma-Aldrich, St Louis, MO, USA) was dissolved in a mixture of chloroform and ethanol in a volume ratio of 9:1 to make 40% solution. An orifice G30 at a rotation speed of 6,000× *g* was used to prepare the fibrous meshes. Fibers were deposited on spunbond textile using vacuum-assisted deposition.

Characterization of fibrous scaffolds prepared using centrifugal spinning

The prepared fibers were visualized using a scanning electron microscope (SEM), and fiber diameter was determined. Samples were coated with a thin layer of platinum using a Quorum Q 150R S device (3 cycles; Quorum Technologies, Lewes, UK) and visualized using SEM (Vega 3; Tescan, Brno, Czech Republic). The acceleration voltage for all samples was 10 kV. Fiber diameter and pore size were analyzed in the ImageJ program.

Adhesion of platelets on fibrous scaffolds

Leukocyte-depleted platelets derived from buffy coat in additive solution were purchased from the Transfusion Station at Šumperk hospital. The bag contained platelets from 4 donors. According to the Czech legislation of blood transfusion, blood products not used for therapy can be used for scientific purposes. Therefore, approval from an ethics committee was not necessary for this study. All donors signed an informed consent, agreeing to the use of their blood for scientific purposes. Platelets were centrifuged at 120× *g* for 7 min for sedimentation and removal of residual erythrocytes. Subsequently, the supernatant was transferred into a new tube and centrifuged (2,200× *g*; 10 min) to retrieve the pellet of platelets, which was resuspended in Platelet Additive Solution SSP+ (Macopharma, Tourcoing, France). Platelets were then diluted to required concentrations in SSP solution: $3{,}000\times10^9$/L (corresponds to 10× concentrated physiological concentration (PC); P1), 900×10^9/L (corresponds to 3× concentrated PC; P2), 300×10^9/L (corresponds to PC; P3), 100×10^9/L (3× diluted PC; P4) and 30×10^9/L (10× diluted PC; P5).

Quantification of selected growth factors released from platelets

To quantify the concentrations of pro- and anti-inflammatory cytokines and growth factors, a Bio-Plex 200 Multiplex

System (Bio-Rad Laboratories, Hercules, CA, USA) and enzyme-linked immunosorbent assay (ELISA, DuoSet®; R&D Systems, Minneapolis, MN, USA) were used. Platelet lysate was prepared by the freeze/thaw method. Platelets at a concentration of 900×10^9/L were lysed using 3 freeze/thaw cycles (−80°C and 37°C) and subsequently centrifuged at 3,422× *g* for 10 min to remove the cell membranes. To analyze the cytokine content of the platelet lysate, the commercially available cytokine panel (Bio-Plex ProTM Human Cytokine 27-plex Assay; Bio-Rad Laboratories) was used in accordance with the manufacturer's instructions. The assay allows multiple cytokines to be quantified simultaneously in 1 well. Briefly, the platelet lysate was incubated with a set of color-coded magnetic beads, each conjugated with an antibody directed against a specific mediator. Biotinylated detection antibody was added and allowed to bind to streptavidin–phycoerythrin. To remove the unbound protein, thorough washing series were performed in between each step by an automatic wash station (Bio-Plex ProTM II). Finally, the data were analyzed using a BioPlex 200 instrument fitted with BioManager analysis software (5-parameter curve fitting).

To observe the distribution of growth factors released from platelets, a sandwich ELISA was used. SDF-1α and bFGF were determined according to the guidelines (Peprotech, Rocky Hill, NJ, USA). P-Selectin, EGF, HGF, KGF, IGF-1, TGF-β, thrombospondin and VEGF were quantified according to the manufacturer's instructions (DuoSet).

Release of thrombospondin from platelets adhered on fibers

Thrombospondin was used as a model molecule to determine the release profile of growth factors from the platelet-functionalized samples. Scaffolds of 11 mm diameter were punched out of the prepared fibrous samples. The scaffolds were functionalized with different concentrations of platelets and incubated in phosphate-buffered saline (PBS; 500 µL) at 37°C. At given time points, the PBS was collected, replaced with a fresh one and the samples were stored at −20°C until analysis. To quantify the released thrombospondin, ELISA was conducted according to the manufacturer's instructions (DuoSet).

Release of proteins from platelets adhered on fibers

Overall protein quantification was used to analyze the kinetics of growth factor release from platelets. Scaffolds of 11 mm diameter were punched out of the prepared fibrous samples. The scaffolds were functionalized with different concentrations of platelets and incubated in PBS (500 µL) at 37°C. At given time points, the PBS was collected, replaced with a fresh one and the samples were stored at −20°C until analysis. To quantify the released protein, the QuantIT Protein assay (Life Technologies, Carlsbad, CA, USA) was used according to the manufacturer's instructions. Briefly, 10 µL of the sample was mixed with 200 µL of fluorescent probe. The fluorescence intensity was measured using a multimode reader (Synergy H1; Biotek, Winooski, VT, USA) at excitation wavelength (λ_{ex}) =470 nm and emission wavelength (λ_{em}) =570 nm. Samples were analyzed in 4 independent measurements.

Cell seeding of the scaffold and adhesion of platelets

Before cell seeding, PCL nanofibers were cut into round patches of 6 mm diameter and sterilized using ethylene oxide. Samples were seeded with 10×10^3 MG-63 cells (Cell Lines Service GmbH, Eppelheim, Germany) per well of a 96-well plate. Cells adhered to the scaffolds for 2 h in 30 µL of culture medium (Dulbecco's Modified Eagle's Medium [DMEM] supplemented with 2% fetal bovine serum and penicillin/streptomycin; Sigma-Aldrich). Subsequently, 20 µL of platelet suspensions in different concentrations (P1–P5 as mentioned earlier) were added and left to adhere for another hour. Finally, 250 µL of culture medium was added. Culture medium was not changed during the experiment. Six different samples were prepared. Five groups with different concentrations of platelets adhered on fibrous scaffolds (PCL/P1–P5), and fibrous scaffold without any platelets as a control (PCL). Scaffolds with adhered platelets in different concentrations (P1–P5) without cells were used as a control. The results acquired from these samples were used as a control of the interaction of platelets with the used methods and were deducted from the values measured on the cell-seeded samples.

Cell viability analysis

The metabolic activity of cells was measured using an MTS assay (CellTiter 96® AQueous One Solution Cell Proliferation Assay; Promega, Madison, WI, USA). Twenty microliters of MTS solution were added to 100 µL of the sample medium and incubated for 2 h at 37°C. Subsequently, 100 µL of the cultured solution was transferred to a new clean well. The absorbance of the medium was detected using spectrophotometry at 490 nm (reference wavelength: 690 nm).

Cell proliferation analysis

The proliferation of chondrocytes on the scaffold was determined from the amount of DNA (Quant-iT™ dsDNA

Assay Kit; Life Technologies). The proliferation of chondrocytes on scaffolds was tested on days 1, 3, 7 and 14. The scaffolds were put into a vial with 200 µL of cell lysis solution (0.2% v/v Triton X-100, 10 mM Tris [pH 7.0] and 1 mM EDTA) and processed through 3 freeze/thaw cycles; the scaffold was first frozen at −70°C and thawed at room temperature. Between each freeze/thaw cycle, the scaffolds were roughly vortexed. A sample (10 µL) was mixed with 200 µL of reagent solution, and fluorescence intensity was detected using a multiplate fluorescence reader (Synergy HT; Winooski, VT, USA; λ_{ex} =485 nm and λ_{em} =525 nm). The DNA content was determined according to the calibration curve using the standards in the kit.

Visualization of cell adhesion and proliferation on scaffolds

3,3′-Diethyloxacarbocyanine iodide, DiOC6(3), staining was used to detect cell adhesion on the scaffolds on days 1, 7 and 14 (Molecular Probes, Eugene, OR, USA). The samples were fixed with frozen methyl alcohol (−20°C) for 10 min. Fluorescent probe DiOC6(3) (1 µg/mL in PBS, pH 7.4; Thermo Fisher Scientific, Waltham, MA, USA) was added and incubated with the samples for 45 min at room temperature. Subsequently, the samples were rinsed with PBS, and propidium iodide (PI; 5 µg/mL in PBS; Sigma-Aldrich) was added for 10 min, followed by rinsing with PBS. The samples were visualized using a ZEISS LSM 5 DUO confocal microscope (PI: λ_{ex} =561 nm, λ_{em} =630–700 nm and DiOC6(3): λ_{ex} =488 nm, λ_{em} =505–550 nm).

Detection of alkaline phosphatase (ALP) activity

ALP activity was measured using a 1-Step™ PNPP kit (Thermo Fisher Scientific). A total of 100 µL of p-nitrophenyl phosphate (PNPP) was added to each well and incubated for 30 min. Subsequently, the reaction was stopped with 2N NaOH. Absorbance was measured using a spectrophotometer at 405 nm (Synergy HT).

Detection of osteogenic marker using indirect immunofluorescence staining

The presence of osteocalcin (OCN), a marker typical for osteogenic differentiation, was confirmed using indirect immunofluorescence staining on days 1, 7 and 14. Samples were fixed with 4% formaldehyde for 10 min, washed with PBS and incubated in 3% fetal bovine serum (FBS) in PBS/0.1% Triton for 30 min at room temperature. Primary monoclonal antibody against OCN (OCG3; Abcam, Cambridge, UK; dilution 1:20) was added, and the samples were incubated overnight at 2°C–8°C. After 3 washes with PBS/0.05% Tween, the samples were incubated with secondary antibody, Alexa Fluor 488-conjugated antimouse antibody, for 45 min. Subsequently, a solution of PI was added for 10 min (5 µg/mL in PBS) to visualize the cellular nuclei. Finally, the samples were washed 3 times with PBS/0.05% Tween. A confocal microscope (ZEISS LSM 5 DUO) was used to detect the present OCN (Alexa Fluor 488: λ_{ex}=488 nm, λ_{em} =505–550 nm and PI: λ_{ex} =561 nm, λ_{em} =630–700 nm).

Statistical analysis

Quantitative data are presented as mean values ± standard deviation (SD). The averaged values were determined from at least 3 independently prepared samples. Results were evaluated statistically using one-way analysis of variance and Student–Newman–Keuls test (SigmaStat 12.0; Systat, San Jose, CA, USA).

Results

Characterization of the prepared scaffolds

Six different scaffold types were prepared. Fibrous meshes were combined with 5 different concentrations of platelets: maximum concentration of platelets ($3{,}000\times10^9$ platelets/L; PCL/P1), 3× diluted concentration of platelets (PCL/P2), 10× diluted concentration of platelets (PCL/P3), 30× diluted concentration of platelets (PCL/P4) and 100× diluted concentration of platelets (PCL/P5). Plain PCL fibers were used as a control.

PCL fibers were prepared successfully and showed nano/microfibrous morphology. The mean diameter of microfibers was ~1,380±427 nm. The mean diameter of the dominant nanofibrous fraction was 504±148 nm. The mean pore size was 7.11±11.9 µm^2, and 20% of pores were bigger than 10 µm^2. In addition, from the micrograph it is apparent that platelets successfully adhered to the PCL samples (Figure 1). Platelets were partially activated and formed a fibrin network on the scaffolds. Platelets were visible on the scaffolds even after 14 days of the experiment (Figure 1B). The mean diameter of platelets on day 1 was 1,080±178 nm and on day 14 was 2,465±370 nm.

Growth factors content in platelets and their release

Platelets used in the experiment were analyzed using a multiplexed protein assay (X-MAP assay; BioPlex, Bio-Rad, Hercules, CA, USA), and the content of cytokines, chemokines and growth factors was evaluated (Table 1). The analysis showed a higher presence of pro-inflammatory cytokines compared to

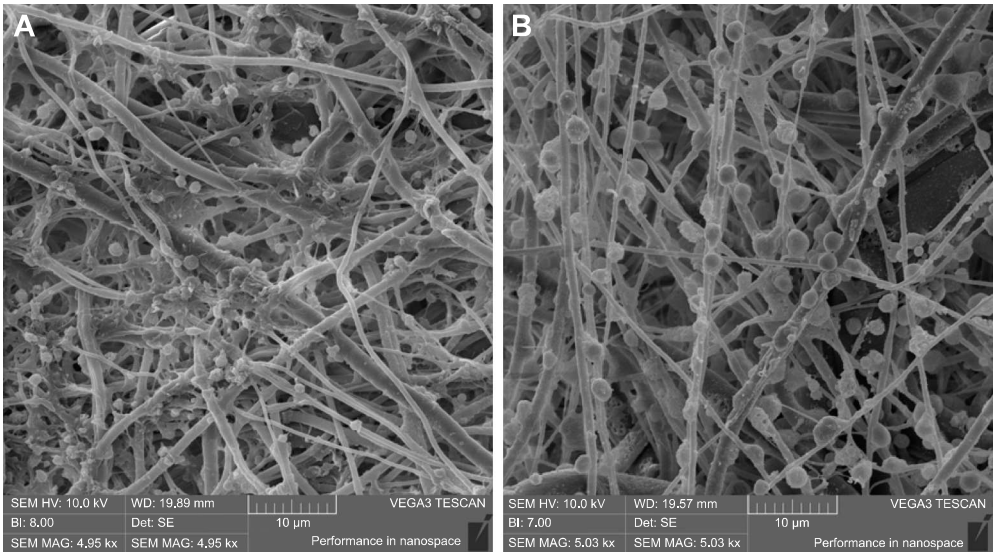

Figure 1 SEM visualization of platelet adhesion on PCL fibers.
Notes: Platelets were partially activated and formed a fibrin net 24 h after adhesion (**A**). Platelets were visibly adhered on fibers even after 14 days of the experiment (**B**).
Abbreviations: SEM, scanning electron microscope; PCL, poly-ε-caprolactone.

anti-inflammatory cytokines such as IL-1ra (340±4 pg/mL) and IL-10 (109±7 pg/mL). The IL-4 and IL-13 were detected in concentrations <50 pg/mL. The pro-inflammatory cytokines were present in higher concentration: IL-17 (1,774±10 pg/mL), IL-8 (133±30 pg/mL), IL-9 (139±12 pg/mL), IL-15 (108±6 pg/mL), INF-γ (299±11 pg/mL) and TNF-α (204±9 pg/mL). The concentrations of IL-1b, IL-2, IL-5, IL-6 and IL-7 were <50 pg/mL. RANTES was the dominant chemokine present in platelets (14,721±239 pg/mL). In addition, MIP-1b (176±68 pg/mL), eotaxin (122±8 pg/mL), IP-10 (383±22 pg/mL) and MCP-1 (113±7 pg/mL) were present in concentrations >100 pg/mL. However, from the tissue engineering point of view, the growth factors have the highest importance in stimulating cell proliferation and differentiation. PDGF-bb was the most abundant growth factor identified by X-MAP assay (9,218±313 pg/mL). VEGF (750±24 pg/mL) and bFGF (379±10 pg/mL) were present in higher concentrations. G-CSF and GM-CSF were also present in concentrations >100 pg/mL. In addition, ELISA was performed for quantification of additional growth factors. TGF-β (76,817±6,384 pg/mL), EGF (403±32 pg/mL) and HGF (530±16 pg/mL) had the highest concentration. In addition, ELISA confirmed a high concentration of thrombospondin as an antiangionetic factor (94,200±10,575 pg/mL) and P-selectin (4,667±80 pg/mL) as a marker of alpha-granule release.

To visualize the release kinetic of growth factors (GFs) from the platelets adhered on fibers, thrombospondin was used as a model protein. Thrombospondin is an inhibitor of neovascularization, which is contained in platelets at high concentrations. The thrombospondin concentration was detected in samples collected at selected time points, and its cumulative release was evaluated. The concentration of thrombospondin in the samples collected from the PCL/P4 (30× diluted maximum platelet concentration) and PCL/P5 (100× diluted maximum platelet concentration) scaffolds was below the limit of detection of the thrombospondin ELISA kit, therefore only the acquired data from the PCL/P1 (maximum platelet concentration), PCL/P2 (3× diluted maximum platelet concentration) and PCL/P3 (10× diluted maximum platelet concentration) are listed in the graph (Figure 2A). As is visible from Figure 2A, thrombospondin was released through the first 7 days of the experiment from the PCL/P1 sample (the highest concentration of adhered platelets). With decreasing concentration of the adhered platelets, the plateau phase was reached earlier in the experiment (day 3 for the PCL/P2 sample and day 1 for the PCL/P3 sample).

Besides thrombospondin release, the overall protein was measured by sensitive fluorescence probe (Figure 2B). The overall protein release overcomes the detection limit of ELISA, as all proteins released from platelets are measured in a single reaction. In addition, the detection limit of the fluorometric assay is improved compared to colorimetric determination. Therefore, the release pattern from all samples was measurable. The results are in accordance with ELISA. The amount of released proteins showed dose-dependent release in higher concentrations (10× PC, 3× PC). In this case, the release time was prolonged compared to lower platelet concentrations. On the other hand, in less

Table 1 Growth factors content in platelets measured using multiplexed protein assay and ELISA

Mediator	Concentration (pg/mL)	SD
Anti-inflammatory cytokines		
IL-1ra	340	4
IL-4	168	15
IL-10	109	7
IL-13	13	4
Pro-inflammatory cytokines		
IL-1b	12	6
IL-2	33	5
IL-5	29	6
IL-6	31	9
IL-7	53	6
IL-8	134	30
IL-9	139	12
IL-12 (p70)	229	4
IL-15	108	6
IL-17	1,774	10
IFN-γ	299	11
TNF-α	204	9
Chemokines		
RANTES	14,722	239
MIP-1a	25	4
MIP-1b	177	68
Eotaxin	122	8
IP-10	383	22
MCP-1 (MCAF)	114	7
Growth factors		
VEGF	750	24
PDGF-bb	9,218	313
FGF basic	379	10
G-CSF	219	1
GM-CSF	164	6
Growth factors measured using ELISA		
KGF	128	11
EGF	403	32
HGF	530	16
IGF-1	283	20
TGFb1	76,817	6,384
SDF-1α	67	27
Thrombospondin	94,200	10,575
P-Selectin	4,667	80

Abbreviations: ELISA, enzyme-linked immunosorbent assay; SD, standard deviation.

concentrated samples, results were influenced by proteins obtained in plasma, which were comparable in all samples. Concentrations of plasma proteins were so high compared to proteins contained in platelets that differences between samples were minimal.

Cell metabolic activity and proliferation on scaffolds

Cell metabolic activity and cell proliferation on scaffolds were examined using MTS test and DNA amount analysis on days 1, 3, 7, 10 and 14 (Figure 3). Cell adhesion was similar on all the scaffolds 24 h after seeding (Figure 3A). Cells started to proliferate faster on samples with higher platelet concentrations. The most visible proliferation was on scaffolds with the largest number of platelets (PCL/P1 and PCL/P2) on day 3. Cells continuously proliferated until day 7, where the highest number of cells was detected on PCL/P1. Lower proliferation was shown on PCL/P2 and PCL/P3 and the lowest on PCL/P4, PCL/P5 and PCL. Although the cell numbers started to decrease in PCL/P1, PCL/P2 and PCL/P3 samples from day 7, the highest number of cells was still detected in the PCL/P1 on days 10 and 14. No statistical difference was seen between the other groups.

The metabolic activity of the cells was highest in the sample with the most concentrated platelets (PCL/P1) as early as 1 day after the seeding (Figure 3B). The metabolic activity continuously increased and was highest in the PCL/P1 and PCL/P2 samples on days 10 and 14. On the other hand, relating the metabolic activity to the DNA content offered a different point of view (Figure 3C). The highest metabolic activity was seen in PCL/P1 24 h after the seeding. Although the metabolic activity significantly decreased in the samples with the most concentrated platelets (PCL/P1-P3) on days 3 and 7, afterward it started to increase again. The highest metabolic activity was seen in the PCL/P2 scaffold on day 14. The samples with lower platelet number and the control PCL sample showed stable or slightly increased metabolic activity during the whole experiment.

Cells in the samples with a higher concentration of platelets (PCL/P1–P3) started to proliferate noticeably from day 3 to day 7. The fast increase in the cell numbers resulted in a decrease in the cell metabolic activity, when related to the DNA content. The cell growth started to slow down in these samples on day 10, which corresponded with an increase in metabolic activity. The decrease in cell proliferation was probably caused by the depletion of nutrients, since the culture medium was not changed during the experiment. Fast growing cells on the scaffolds with higher concentrations of platelets (PCL/P1–P3) exhausted the nutrients faster than the cells on the scaffolds with lower concentrations of platelets or no platelets (PCL/P4, PCL/P5 and PCL).

Osteogenic activity of MG-63 cells

The activity of ALP and immunodetection of OCN were used to measure the stimulation of osteogenic differentiation by platelets. Figure 3D shows that the higher concentrations of platelets increased the ALP activity. PCL/P1 showed the highest ALP activity compared to all the other samples on days 7 and 14. Lower ALP activity was detected in the PCL/

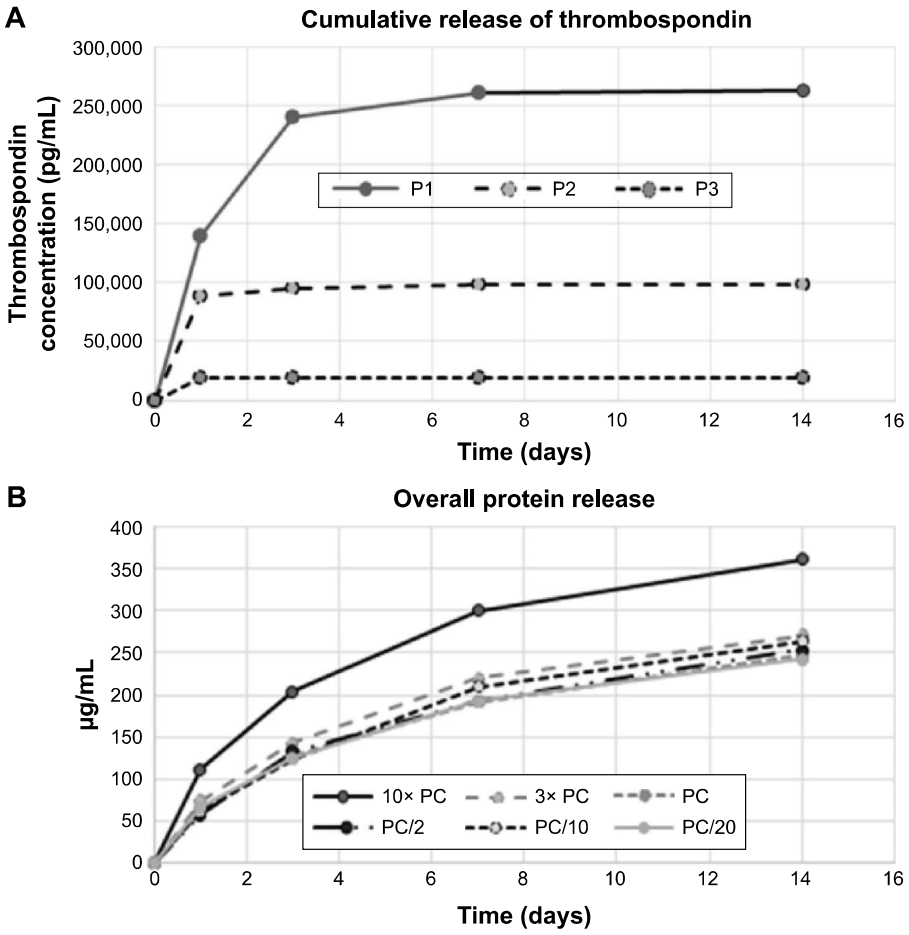

Figure 2 Release kinetics of protein from platelets.
Notes: Thrombospondin was used as a model protein to detect the release kinetics from platelets (**A**). Release of thrombospondin was dose dependent and was detectable only for higher concentrations of platelets (P1–P3). Samples with lower platelet concentrations were below the ELISA kit detection limit (P4 and P5). Total protein release was measured using fluorescence probe (**B**). Dependence on platelet concentrations was shown only for the highest concentration (10× PC = P1). In lower concentrations, results were influenced by the presence of plasma proteins.
Abbreviations: P, platelets; ELISA, enzyme-linked immunosorbent assay; PC, physiological concentration.

P2 sample, although the ALP activity was higher than in all the samples with lower platelet concentration or no platelets (PCL/P3–P4, PCL).

Visualization of OCN via confocal microscopy did not confirm the osteogenic stimulation of platelets. There were only small, sporadic islands of OCN. The largest amount of OCN was visible on the PCL/P1 and PCL/P2 scaffolds, respectively, on day 14 (data not shown).

Morphology of cells in samples analyzed by microscopy

The morphology and spreading of the cells on the scaffolds were visualized using both confocal microscope and SEM. The cells on the scaffolds were visualized using DiOC6 (internal cell membranes, green color) and PI (cell nuclei, red color) staining (Figure 4). The confocal microscopy showed good adhesion of cells to the PCL fibers. Cells adhered similarly on all the tested scaffolds. Besides the cells, adhered platelets were visible on day 1. The cells on the scaffolds were well spread, and during the culture their number was rising. The highest number of cells was visible on day 7. The microscope confirmed the trend from MTS and Picogreen assay, where cells showed higher proliferation with the increase in platelet concentration. The highest number of cells was detected in the PCL/P1 sample and the lowest in PCL/P5 and control PCL sample. On day 14, the cell number was decreasing. The numbers of cells on the scaffolds with a low concentration of platelets (PCL/P3, PCL/P4) and control sample (PCL) were constant during the experiment. The results correlate well with the data from DNA analysis. The results of SEM analysis confirmed that the cells were adhered to the fibers and showed a well-spread morphology.

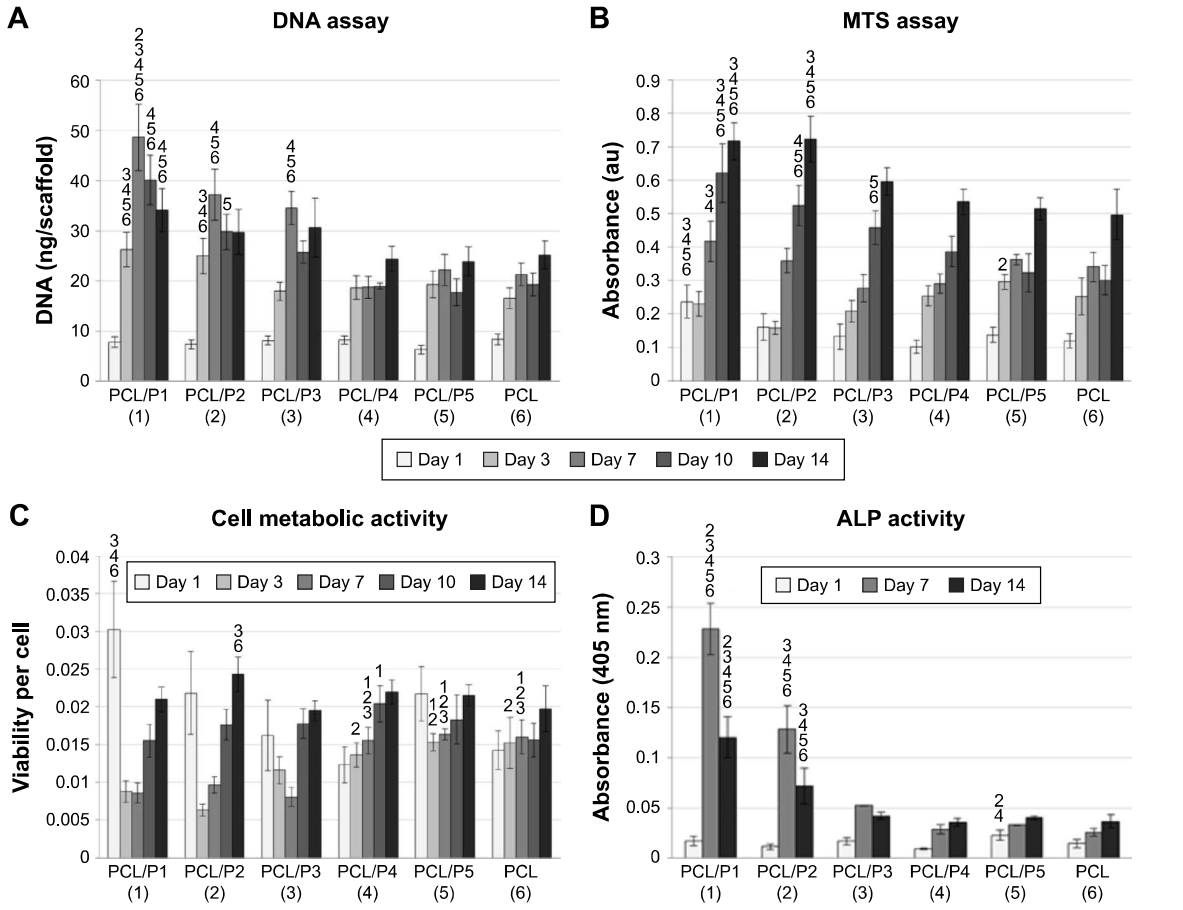

Figure 3 MG-63 cell proliferation, metabolic activity and ALP activity.
Notes: Cell proliferation was measured using quantification of DNA (**A**). Cell metabolic activity was measured using MTS assay (**B**). Both cell proliferation and metabolic activity were highest in samples with the highest platelet concentrations (PCL/P1 and PCL/P2). Metabolic activity was subsequently related to the DNA content (**C**). ALP activity was highest in samples with the highest platelet concentrations (PCL/P1 and PCL/P2; **D**). The numbers above the columns in the graphs represent the numbers of the samples (corresponding to numbers in parentheses on the *x*-axis) to show statistically significant differences.
Abbreviations: PCL, poly-ε-caprolactone; P, platelets; ALP, alkaline phosphatase.

In addition, due to higher pore size compared to electrospun scaffolds,[16] the cells penetrated into the scaffold. In all groups, the penetration depth was ~80–90 µm, and only on the PCL/P1 group, the penetration was deeper (120 µm; Figure 5).

Samples were also visualized using an SEM to detect cell morphology and adhesion in more detail (Figure 6). Cells adhered well on polymeric fibers and were well spread. No difference was seen between the groups.

Discussion

Bone and cartilage defects are among the most prevalent reasons for disability in the population worldwide. Due to the 3D nature of bone and cartilage tissue, the scaffolds for their regeneration should support cell growth in all 3 dimensions. Three-dimensional scaffolding systems are in high demand in tissue engineering. In order to address this challenge, a system with high porosity and open pores is needed. Different strategies have been used to prepare fibrous scaffolds for tissue engineering applications. Currently, the most popular method is electrospinning. A classical electrospinning device layout gives rise to sheet-like layers of fibers. These layers have large porosity and a big surface to volume ratio, with excellent adhesive capacity. A disadvantage of the electrospun layers is a 2D-like structure with small pores. Most tissue engineering applications demand 3D-structured scaffolds with open pores to enable cell infiltration. Different strategies such as special collectors[17] and salt leaching[18] were used to enhance the pore size and thickness of nanofibrous layers. Currently, alternative methods to prepare nano- and microfibers, such as melt-blown or centrifugal spinning, are being tested for tissue engineering applications. In our previous work, we have shown that PCL scaffolds prepared by centrifugal spinning technology, unlike electrospinning

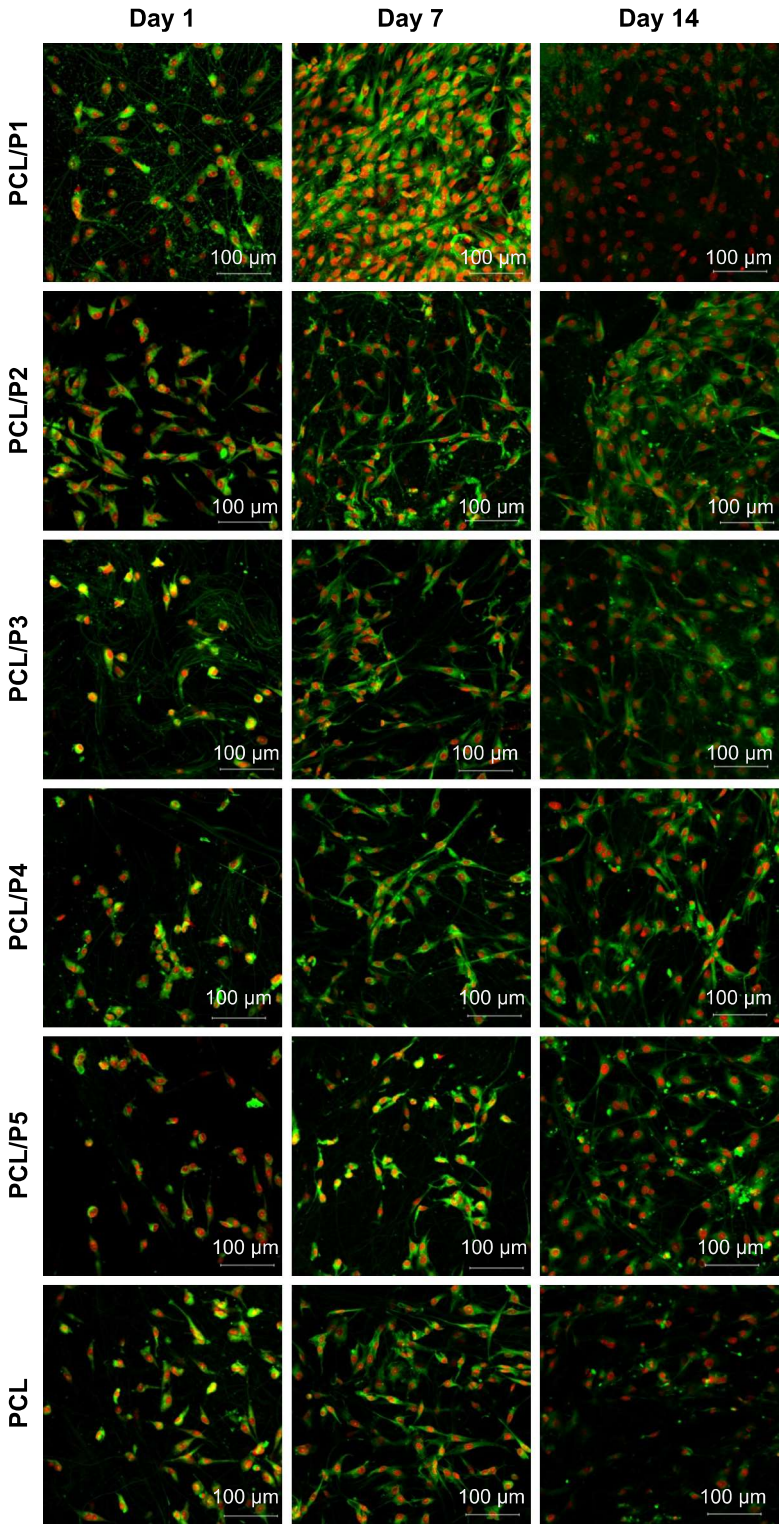

Figure 4 Visualization of MG-63 cells on scaffolds prepared using centrifugal spinning.
Notes: Cells were stained using DiOC6 (internal cell membranes, green color) and propidium iodide (cell nuclei, red color) and visualized using a confocal microscope. Cells adhered similarly on all the tested scaffolds. The highest number of cells was visible on the PCL/P1 on day 7. On day 14, the cell number was decreasing. The numbers of cells on the scaffolds with low concentrations of platelets (PCL/P3, PCL/P4) and control sample (PCL) were constant during the experiment. The results correspond well with the data from DNA analysis.
Abbreviations: DiOC6, 3,3′-diethyloxacarbocyanine iodide; PCL, poly-ε-caprolactone; P, platelets.

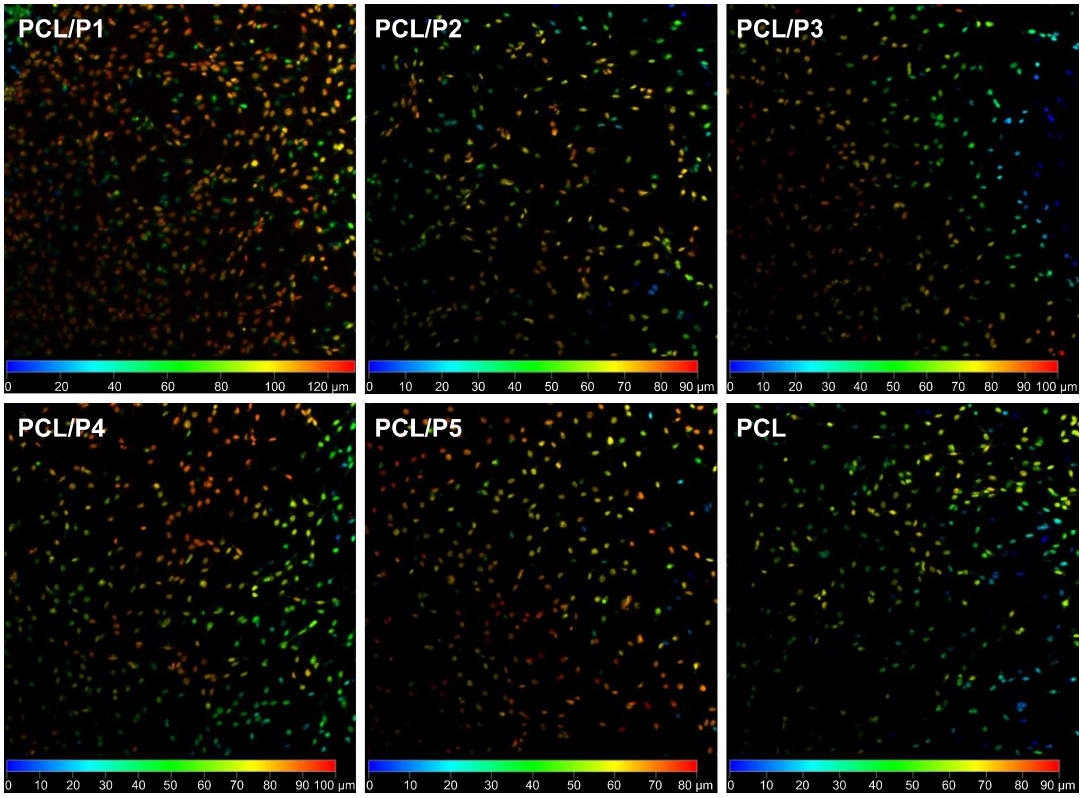

Figure 5 Cell infiltration into the scaffolds.
Notes: Cell nuclei visualized using confocal microscope were labeled based on their position inside fibrous scaffolds. The color scale shows cells in different depths of the scaffold. Cell infiltration was similar on all the scaffolds (80–90 µm) except for the PCL/P1, where cells penetrated to the depth of 120 µm.
Abbreviations: PCL, poly-ε-caprolactone; P, platelets.

scaffolds, show morphology favoring cell penetration.[16] The results of the current study confirmed that the cells were able to penetrate as deep as 120 µm in the PCL/P1 sample.

Stimulation of cell migration inside the scaffold and their differentiation toward the required cell type is essential for successful tissue regeneration. Only correctly differentiated cells can produce proteins of ECM of the right composition and ratio for the particular tissue. The cellular differentiation is regulated by numerous stimuli including the mechanical properties of the surrounding tissue, tension of oxygen, small molecular weight signaling molecules and protein-based morphogens (ie, growth factors). The differentiation process is an interplay of these stimuli. A wide range of bioactive stimulating molecules has been studied for bone tissue engineering.

Bone tissue healing upon injury is a complex process involving a number of cytokines, chemokines and growth factors. The early phases of bone regeneration are associated with hemostasis and inflammation in the fracture site. Platelets play a pivotal role in these early phases of healing. IL-1[19] and IL-6[20] as pro-inflammatory cytokines play a role in macrophage activation. IL-17 was shown to be one of the key regulators in the early phases of bone healing via osteoblast maturation.[21,22] IL-17 was found in high levels in platelets. In addition, IL-1, TNF-α, SDF-1 and GCSF stimulate mesenchymal progenitor cell activation.[23] The multiplex analysis confirmed that TNF-α, IL-1ra and GCSF were present in the platelets adhered to the proposed scaffold. Delivery of these stimuli may help initiate the regeneration process. In later phases, growth factors play a pivotal role in the regulation of tissue regeneration. The most prominent growth factors efficient in the early phases of bone healing include SDF-1α recruiting the progenitor cells to the site of injury, bFGF promoting proliferation of progenitor cells, IGF-I acting as an antiapoptotic and pro-osteogenic factor and TGF-β stimulating osteogenic differentiation. In the middle and late phases, the roles of BMP-2, BMP-7 and IGF-I become the most dominant.[23] The presence of PDGF was also observed to have a positive effect on bone repair.[24] Bone tissue neovascularization is regulated by VEGF and is essential for bone tissue integrity restoration. In order to develop a successful scaffold, the system should deliver these growth factors.

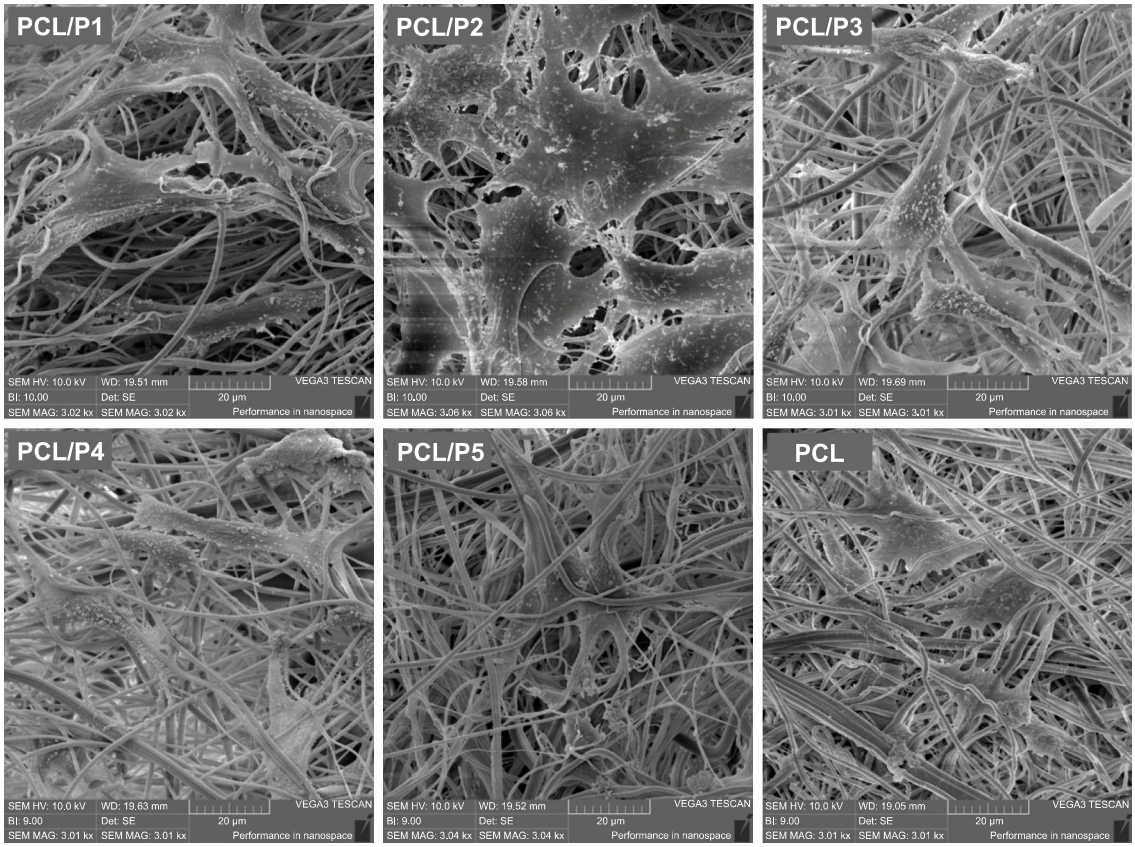

Figure 6 Visualization of the adhered cells using SEM.
Notes: Cells were uniformly distributed and well spread on the scaffolds. A similar picture was seen on all the samples. Day 7, magnification 3,000×.
Abbreviations: SEM, scanning electron microscope; PCL, poly-ε-caprolactone; P, platelets.

The multiplex assay identified the presence of PDGF-bb, VEGF, bFGF and other growth factors. Analysis by ELISA confirmed the presence of TGF-β, IGF-I and EGF. However, the other active molecules identified by multiplex assay also have relevance for bone tissue engineering. RANTES was identified in high concentration and was shown to play a role in the osteogenic differentiation of MSCs.[25]

Besides a stimulatory role, the released molecules may inhibit the progress of the bone healing process. In biomaterials research, TNF-α and IL-1 are the best known mediators of the foreign body reaction. Lange et al[19] observed the positive effect of IL-1β on the proliferation of osteoblasts and the negative effect on the proliferation and differentiation of MSCs. Similarly, TNF-α was shown to inhibit the progress of bone healing by inducing osteoblast and chondrocyte apoptosis.[26,27] However, some reports show that some level of TNF-α signalizing is necessary for bone resorption during the repair process.[28] Thrombospondin is one of the most abundant platelet proteins. Thrombospondin is an inhibitor of vascularization, and several studies also showed its negative influence on bone healing. Hsu et al[29] showed in his study that thrombospondin (TSHB) negatively influences the proliferation of different cell types (periodontal ligament cells [PDL], osteoblasts and endothelial cells) in concentrations >2.5 μg/mL. The mean level of thrombospondin in our samples was ~94 ng/mL, and the inhibitory effect therefore may be lower.[29]

Nevertheless, the current study employed multiplexed immunoassays and ELISA, which have limited capacity and sensitivity. Therefore, we have identified and quantified only part of the proteins present in the platelets. A complex proteomic analysis showed >500 proteins in platelet proteome.[30] A study of thrombin-induced release showed >90 proteins in platelet releasate.[31] In addition, the platelet protein content highly fluctuates in donors depending on gender, age and physiological state.[30] In a recent study, Mussano et al[32] performed a similar X-MAP multiplex assay on male and female platelets. The result showed differences with our results. In our case, IL-17, VEGF and PDGF-bb concentration was higher and INF-γ concentration was lower compared to the described study. In addition, the multiplexed assay

was more sensitive than standard ELISA. For instance, bFGF in our sample was not measurable using the standard ELISA protocol.

Platelets are, for their regenerative potential, currently often used in regenerative medicine.[33] The key strategies for platelet preparation include buffy coat and apheresis methods.[34–37] The buffy coat method, which was used in this manuscript, is based on centrifugation of the whole blood to separate platelets, leukocytes, erythrocytes and plasma. The excess erythrocytes and leukocytes are removed via specific filtration. The key advantage of the buffy coat method is the possibility to prepare large batches of platelets from mixed donors. On the other hand, apheresis is based on online platelet separation from a single donor. Although the platelet concentrates are less contaminated by leukocytes and erythrocytes, the method is rather time-consuming and requires complex apparatuses. In clinical practice, the platelets for chirurgical application could be isolated on site by specific concentrators. The systems are based on diverse modifications of the buffy coat method and commercialized under trade names such as Plateltex, SmartPReP, PCCS and Magellan.[34,35] From application point of view, the commercial methods enable isolation of autologous platelets. The key advantages of autologous platelets are elimination of disease transmission, possible immune reaction and high compatibility with the patient. On the other hand, allogenic platelet formulations enable rapid donation even to patients in life-threatening states. The allogenic preparations based on buffy coat also enable elimination of donor-to-donor variations by preparing mixed platelet isolates from multiple donors. The importance of the problem was highlighted by Lohmann et al,[38] who observed relationship between patient age and proliferation of MSCs.

The isolated platelet formulation highly differs in its properties. According to Dohan Ehrenfest et al,[34,35] the platelet formulations may be divided into pure PRP (P-PRP), leukocyte and PRP (L-PRP), pure platelet-rich fibrin (P-PRF) and leukocyte and platelet-rich fibrin (L-PRF). The differences are the presence of leukocytes and activation state of platelets. In the current manuscript, we have used P-PRP for adhesion to fibers. On the other hand, activated platelets provide interesting properties for tissue engineering applications.

Platelets, when they are activated, create fibrin net and release various growth factors and cytokines. This natural process is used as a scaffolding material. To date, platelets have showed great promise mainly in the field of maxillofacial bone reconstruction. The fibrin gels made completely of platelets show high cell adhesion, proliferation[39] and bone repair.[40,41] However, the fibrin gel formed by activation of platelets is stable only for a few days. Rapid degradation of fibrin has been studied in various studies.[42–44] Bardsley et al[43] showed in his study high initial in vitro degradation of fibrin gel between 0 and 5 days. It was shown that the degradation rate can be slowed down by combining with hyaluronic acid and laminin[42] or polyethylenglycol.[45] While fibrin-only gel totally degrades after 14 days of cultivation, PEGylated fibrin stayed intact. In addition, the pore size of fibrin gel is lower due to the packed morphology of fibrin fibers.[46] Therefore, the cell penetration is connected with fibrin gel degradation.[43] On the other hand, PCL is a biocompatible and biodegradable polymer, which degrades after several months.[47] The material proposed in this study shows longer stability and is more suitable for reconstruction of critical defects, which need prolonged stabilization of the scaffolds. Slow degradation enables cells to synthesize the ECM and gradually form new tissue. Especially, the bone regeneration in critical bone defects (ie, long bones and large extractions) takes several months. In such indications, the fibrin gel cannot show sufficient stability. The material in the present study showed that the adhered platelets were able to form fibrin net on the fibers and showed improved initial cellular adhesion of model cells compared to the pure PCL scaffold. In addition, the centrifugal spinning technology enables formation of large fluffy fibrous scaffolds with interconnected pore morphology enabling cell penetration. From the drug release point of view, the addition of platelets is key for the delivery of active molecules. The effect of growth factor delivery improved the scaffold colonization both in vitro[48] and in vivo.[10]

The importance of the adhesion of the platelets to the surface of fibers is mainly in their immobilization. The results of SEM and the release study showed that platelets delivered active molecules for several days. The active molecules identified in platelets may therefore improve tissue regeneration. For comparison with fibrin gel, a study by Dohan Ehrenfest et al[49] showed that platelet fibrin gel released growth factors up to 7 days.The present study showed that platelets adhered on fibers release growth factors even after the 7th day. We believe that this phenomenon was observed because of fibrin net degradation upon colonization of deeper scaffold layer and liberation of the attached growth factors. The mechanism behind the release in this system may be connected with 2 phenomena. The intact platelets were shown on the scaffold even after 14 days of incubation, which indicates that they were viable and able to secrete their cargo. The second mechanism for sustained release is connected with

degradation of the fibrin net. The fibrin net binds growth factors and through degradation the attached proteins are liberated. After 14 days, both the decreased number of intact platelets on the scaffold and the degraded fibrin net were observed. Therefore, the release by both mechanisms was attenuated. The functionalization of fibrous scaffolds may be performed via encapsulation or surface binding of platelet derivatives. Only a limited number of studies report using scaffolds prepared via centrifugal electrospinning as a drug delivery system. In a study by Mary et al,[50] tetracycline-loaded PCL-blended polyvinylpyrrolidone (PVP) fibers were used as a drug delivery vehicle. The prepared fibers showed rapid drug release followed by a sustained release and good antimicrobial activity against pathogenic bacteria, which are commonly found in dermal infections. In the current study, we focused on the delivery of regeneration promoting substances. The platelets were adhered to the surface of fibers and provided bioactive molecules. The results of metabolic activity and proliferation assays showed that the factors stimulated MG-63 cell proliferation. The cell proliferation was dose dependent, and with an increase in the platelet concentration the cells showed a higher proliferation rate and increased metabolic activity.

MG-63 is a cell line derived from human osteosarcoma. These cells are frequently used in tissue engineering studies to study scaffold biocompatibility and bone tissue formation.[51–55] On the other hand, differences between osteosarcoma lines and primary osteoblast cells have been published.[56,57] Main differences have been found in proliferation kinetics, cell morphology and synthesis of ECM proteins. For this reason, further experiments using primary osteoblast cells or MSCs will be necessary to confirm the positive effect of the fibrous scaffold–platelet system on specific cell infiltration and osteogenic differentiation.

The results are similar to those of Diaz-Gomez et al,[15] who observed that adhesion of PRP to PCL nanofibers promotes proliferation of MSCs. Similarly, Buzgo et al[58] found that embedded alpha granules were able to stimulate the chondrogenic differentiation of MSCs. In addition, the stimulatory role of platelets in bone regeneration was confirmed by Anjana et al,[59] Getgood et al[60] and Prosecká et al.[10]

The additional advantage of surface functionalization by platelets, when compared to encapsulation, is the much simpler scaffold preparation. The system enables modification in the outpatient clinic and solves the problems associated with the long-term storage of the scaffolds. In addition, the utilized platelets may be autologous, thus minimizing the risks associated with the use of allogenous platelets, such as disease transmission and immune reaction. In the present study, the performance of the system was evaluated in the model of MG-63 osteoblasts. The samples functionalized by platelets showed improved proliferation, metabolic activity and ALP activity. Cell penetration is essential for bone tissue engineering scaffolds. Prosecká et al[10] recently produced a collagen/hydroxyapatite scaffold prepared using the freeze drying process. However, the foam scaffolds showed problems with pore interconnection. In the case of the fibrous scaffolds produced by centrifugal spinning, the pores are highly interconnected and allow efficient cell migration. Confocal microscopy showed that due to the 3D structure of the fibrous matrix the cells were able to penetrate deep into the scaffold. The biological properties of the system described in this work are therefore a simple and clinically translatable system for bone tissue engineering.

Conclusion

Centrifugal electrospinning is a simple method for producing 3D fibrous scaffolds. However, the complex osteogenic regeneration process requires stimulation by active molecules. Herein, we have introduced a simple composite scaffold based on platelet adhesion to PCL 3D fibers. The platelets are a source of growth factors and cytokines active in tissue repair. The multiplexed immunoassay showed the presence of a high concentration of IL-17, RANTES, PDGF-bb, TGF-β and other molecules active in the bone healing process. The immobilization on a fibrous scaffold prolonged the bioavailability of these active molecules. The biological evaluation in the MG-63 model showed improved metabolic activity, proliferation and ALP activity compared to nonfunctionalized fibrous scaffold. In addition, the response of cells was dose dependent with improved biocompatibility with increasing platelet concentration. The results demonstrated the suitability of the system for bone tissue engineering.

Acknowledgments

This research was supported by the Czech Science Foundation Grant No 15-15697S and the Ministry of Education, Youth and Sports of the Czech Republic (Research Programs NPU I:LO1508).

Disclosure

The authors report no conflicts of interest in this work.

References

1. Sill TJ, von Recum HA. Electrospinning: applications in drug delivery and tissue engineering. *Biomaterials*. 2008;29(13):1989–2006.

2. Agarwal S, Wendorff JH, Greiner A. Use of electrospinning technique for biomedical applications. *Polymer*. 2008;49(26):5603–5621.
3. Zhou F-L, Gong R-H, Porat I. Mass production of nanofibre assemblies by electrostatic spinning. *Polym Int*. 2009;58(4):331–342.
4. Zander NE. Formation of melt and solution spun polycaprolactone fibers by centrifugal spinning. *J Appl Polym Sci*. 2015;132(2).
5. Loordhuswamy AM, Krishnaswamy VR, Korrapati PS, Thinakaran S, Rengaswami GDV. Fabrication of highly aligned fibrous scaffolds for tissue regeneration by centrifugal spinning technology. *Mater Sci Eng C Mater Biol Appl*. 2014;42:799–807.
6. Rampichova M, Buzgo M, Chvojka J, Prosecka E, Kofronova O, Amler E. Cell penetration to nanofibrous scaffolds: Forcespinning®, an alternative approach for fabricating 3D nanofibers. *Cell Adh Migr*. 2014;8(1):36–41.
7. Ren L, Pandit V, Elkin J, Denman T, Cooper JA, Kotha SP. Large-scale and highly efficient synthesis of micro- and nano-fibers with controlled fiber morphology by centrifugal jet spinning for tissue regeneration. *Nanoscale*. 2013;5(6):2337–2345.
8. Wang L, Shi J, Liu L, Secret E, Chen Y. Fabrication of polymer fiber scaffolds by centrifugal spinning for cell culture studies. *Microelectron Eng*. 2011;88(8):1718–1721.
9. Blair P, Flaumenhaft R. Platelet alpha-granules: basic biology and clinical correlates. *Blood Rev*. 2009;23(4):177–189.
10. Prosecká E, Rampichova M, Litvinec A, et al. Collagen/hydroxyapatite scaffold enriched with polycaprolactone nanofibers, thrombocyte-rich solution and mesenchymal stem cells promotes regeneration in large bone defect in vivo. *J Biomed Mater Res A*. 2015;103(2):671–682.
11. Jakubova R, Mickova A, Buzgo M, et al. Immobilization of thrombocytes on PCL nanofibres enhances chondrocyte proliferation in vitro. *Cell Prolif*. 2011;44(2):183–191.
12. Wang X, Qiu Y, Triffitt J, Carr A, Xia Z, Sabokbar A. Proliferation and differentiation of human tenocytes in response to platelet rich plasma: an in vitro and in vivo study. *J Orthop Res*. 2012;30(6):982–990.
13. Plencner M, Prosecka E, Rampichova M, et al. Significant improvement of biocompatibility of polypropylene mesh for incisional hernia repair by using poly-epsilon-caprolactone nanofibers functionalized with thrombocyte-rich solution. *Int J Nanomedicine*. 2015;10:2635–2646.
14. Lacci KM, Dardik A. Platelet-Rich plasma: support for its use in wound healing. *Yale J Biol Med*. 2010;83(1):1–9.
15. Diaz-Gomez L, Alvarez-Lorenzo C, Concheiro A, et al. Biodegradable electrospun nanofibers coated with platelet-rich plasma for cell adhesion and proliferation. *Mater Sci Eng C Mater Biol Appl*. 2014;40:180–188.
16. Rampichova M, Buzgo M, Chvojka J, Prosecka E, Kofronova O, Amler E. Cell penetration to nanofibrous scaffolds. *Cell Adh Migr*. 2014;8(1):36–41.
17. Rampichova M, Chvojka J, Buzgo M, et al. Elastic three-dimensional poly (epsilon-caprolactone) nanofibre scaffold enhances migration, proliferation and osteogenic differentiation of mesenchymal stem cells. *Cell Prolif*. 2013;46(1):23–37.
18. Rnjak-Kovacina J, Weiss AS. Increasing the pore size of electrospun scaffolds. *Tissue Eng Part B Rev*. 2011;17(5):365–372.
19. Lange J, Sapozhnikova A, Lu CY, et al. Action of IL-1 beta during fracture healing. *J Orthop Res*. 2010;28(6):778–784.
20. Yang X, Ricciardi BF, Hernandez-Soria A, Shi Y, Camacho NP, Bostrom MPG. Callus mineralization and maturation are delayed during fracture healing in interleukin-6 knockout mice. *Bone*. 2007;41(6):928–936.
21. Nam D, Mau E, Wang YF, et al. T-lymphocytes enable osteoblast maturation via IL-17F during the early phase of fracture repair. *PLoS One*. 2012;7(6):e40044.
22. Ono T, Okamoto K, Nakashima T, et al. IL-17-producing gamma delta T cells enhance bone regeneration. *Nat Commun*. 2016;7:10928.
23. Mehta M, Schmidt-Bleek K, Duda GN, Mooney DJ. Biomaterial delivery of morphogens to mimic the natural healing cascade in bone. *Adv Drug Deliv Rev*. 2012;64(12):1257–1276.
24. Santo VE, Frias AM, Carida M, et al. Carrageenan-based hydrogels for the controlled delivery of PDGF-BB in bone tissue engineering applications. *Biomacromolecules*. 2009;10(6):1392–1401.
25. Liu YC, Kao YT, Huang WK, et al. CCL5/RANTES is important for inducing osteogenesis of human mesenchymal stem cells and is regulated by dexamethasone. *BioSci Trends*. 2014;8(3):138–143.
26. Zhou FH, Foster BK, Zhou XF, Cowin AJ, Xian CJ. TNF-alpha mediates p38 MAP kinase activation and negatively regulates bone formation at the injured growth plate in rats. *J Bone Miner Res*. 2006;21(7):1075–1088.
27. Sun MQ, Yang JL, Wang JZ, et al. TNF-alpha is upregulated in T2DM patients with fracture and promotes the apoptosis of osteoblast cells in vitro in the presence of high glucose. *Cytokine*. 2016;80:35–42.
28. Gerstenfeld LC, Cho TJ, Kon T, et al. Impaired intramembranous bone formation during bone repair in the absence of tumor necrosis factor-alpha signaling. *Cells Tissues Organs*. 2001;169(3):285–294.
29. Hsu CW, Yuan K, Tseng CC. The negative effect of platelet-rich plasma on the growth of human cells is associated with secreted thrombospondin-1. *Oral Surg Oral Med Oral Pathol Oral Radiol Endod*. 2009;107(2):185–192.
30. Dzieciatkowska M, D'Alessandro A, Burke TA, et al. Proteomics of apheresis platelet supernatants during routine storage: gender-related differences. *J Proteomics*. 2015;112:190–209.
31. van Holten TC, Bleijerveld OB, Wijten P, et al. Quantitative proteomics analysis reveals similar release profiles following specific PAR-1 or PAR-4 stimulation of platelets. *Cardiovasc Res*. 2014;103(1):140–146.
32. Mussano F, Genova T, Munaron L, Petrillo S, Erovigni F, Carossa S. Cytokine, chemokine, and growth factor profile of platelet-rich plasma. *Platelets*. 2016;27(5):467–471.
33. Kon E, Filardo G, Di Martino A, Marcacci M. Platelet-rich plasma (PRP) to treat sports injuries: evidence to support its use. *Knee Surg Sports Traumatol Arthrosc*. 2011;19(4):516–527.
34. Dohan Ehrenfest DM, Andia I, Zumstein MA, Zhang C-Q, Pinto NR, Bielecki T. Classification of platelet concentrates (Platelet-Rich Plasma-PRP, Platelet-Rich Fibrin-PRF) for topical and infiltrative use in orthopedic and sports medicine: current consensus, clinical implications and perspectives. *Muscles Ligaments Tendons J*. 2014;4(1):3–9.
35. Dohan Ehrenfest DM, Rasmusson L, Albrektsson T. Classification of platelet concentrates: from pure platelet-rich plasma (P-PRP) to leucocyte- and platelet-rich fibrin (L-PRF). *Trends Biotechnol*. 2009;27(3):158–167.
36. Gulliksson H. Platelets from platelet-rich-plasma versus buffy-coat-derived platelets: what is the difference? *Rev Bras Hematol Hemoter*. 2012;34(2):76–77.
37. Bock M, Rahrig S, Kunz D, Lutze G, Heim MU. Platelet concentrates derived from buffy coat and apheresis: biochemical and functional differences. *Transfus Med*. 2002;12(5):317–324.
38. Lohmann M, Walenda G, Hemeda H, et al. Donor age of human platelet lysate affects proliferation and differentiation of mesenchymal stem cells. *PLoS One*. 2012;7(5):e37839.
39. Dohan Ehrenfest DM, Doglioli P, de Peppo GM, Del Corso M, Charrier JB. Choukroun's platelet-rich fibrin (PRF) stimulates in vitro proliferation and differentiation of human oral bone mesenchymal stem cell in a dose-dependent way. *Arch Oral Biol*. 2010;55(3):185–194.
40. Durmuslar MC, Balli U, Ongoz Dede F, et al. Evaluation of the effects of platelet-rich fibrin on bone regeneration in diabetic rabbits. *J Craniomaxillofac Surg*. 2016;44(2):126–133.
41. Wang Z, Hu H, Li Z, et al. Sheet of osteoblastic cells combined with platelet-rich fibrin improves the formation of bone in critical-size calvarial defects in rabbits. *Br J Oral Maxillofac Surg*. 2016;54(3):316–321.
42. Arulmoli J, Wright HJ, Phan DT, et al. Combination scaffolds of salmon fibrin, hyaluronic acid, and laminin for human neural stem cell and vascular tissue engineering. *Acta Biomater*. 2016;43:122–138.

43. Bardsley K, Wimpenny I, Wechsler R, Shachaf Y, Yang Y, El Haj AJ. Defining a turnover index for the correlation of biomaterial degradation and cell based extracellular matrix synthesis using fluorescent tagging techniques. *Acta Biomater*. 2016;45:133–142.
44. Zhang Y, Heher P, Hilborn J, Redl H, Ossipov DA. Hyaluronic acid-fibrin interpenetrating double network hydrogel prepared in situ by orthogonal disulfide cross-linking reaction for biomedical applications. *Acta Biomater*. 2016;38:23–32.
45. Benavides OM, Quinn JP, Pok S, Petsche Connell J, Ruano R, Jacot JG. Capillary-like network formation by human amniotic fluid-derived stem cells within fibrin/poly(ethylene glycol) hydrogels. *Tissue Eng Part A*. 2015;21(7–8):1185–1194.
46. Sadeghi-Ataabadi M, Mostafavi-pour Z, Vojdani Z, Sani M, Latifi M, Talaei-Khozani T. Fabrication and characterization of platelet-rich plasma scaffolds for tissue engineering applications. *Mater Sci Eng C*. In press 2016.
47. Lam CX, Hutmacher DW, Schantz JT, Woodruff MA, Teoh SH. Evaluation of polycaprolactone scaffold degradation for 6 months in vitro and in vivo. *J Biomed Mater Res A*. 2009;90(3):906–919.
48. Santo VE, Duarte AR, Popa EG, Gomes ME, Mano JF, Reis RL. Enhancement of osteogenic differentiation of human adipose derived stem cells by the controlled release of platelet lysates from hybrid scaffolds produced by supercritical fluid foaming. *J Control Release*. 2012;162(1):19–27.
49. Dohan Ehrenfest DM, de Peppo GM, Doglioli P, Sammartino G. Slow release of growth factors and thrombospondin-1 in Choukroun's platelet-rich fibrin (PRF): a gold standard to achieve for all surgical platelet concentrates technologies. *Growth Factors*. 2009;27(1):63–69.
50. Mary LA, Senthilram T, Suganya S, et al. Centrifugal spun ultrafine fibrous web as a potential drug delivery vehicle. *Express Polym Lett*. 2013;7(3):238–248.
51. Cai Y, Yu J, Kundu SC, Yao J. Multifunctional nano-hydroxyapatite and alginate/gelatin based sticky gel composites for potential bone regeneration. *Mater Chem Phys*. 2016;181:227–233.
52. Hu J-X, Ran J-B, Chen S, Jiang P, Shen X-Y, Tong H. Carboxylated agarose (CA)-silk fibroin (SF) dual confluent matrices containing oriented hydroxyapatite (HA) crystals: biomimetic organic/inorganic composites for tibia repair. *Biomacromolecules*. 2016;17(7):2437–2447.
53. Chu S-F, Huang M-T, Ou K-L, et al. Enhanced biocompatible and hemocompatible nano/micro porous surface as a biological scaffold for functionalizational and biointegrated implants. *J Alloys Comp*. 2016;684:726–732.
54. Stevenson G, Rehman S, Draper E, Hernández-Nava E, Hunt J, Haycock JW. Combining 3D human in vitro methods for a 3Rs evaluation of novel titanium surfaces in orthopaedic applications. *Biotechnol Bioeng*. 2016;113(7):1586–1599.
55. Hejazi F, Mirzadeh H. Novel 3D scaffold with enhanced physical and cell response properties for bone tissue regeneration, fabricated by patterned electrospinning/electrospraying. *J Mater Sci Mater Med*. 2016;27(9):143.
56. Pautke C, Schieker M, Tischer T, et al. Characterization of osteosarcoma cell lines MG-63, Saos-2 and U-2 OS in comparison to human osteoblasts. *Anticancer Res*. 2004;24(6):3743–3748.
57. Bilbe G, Roberts E, Birch M, Evans DB. PCR phenotyping of cytokines, growth factors and their receptors and bone matrix proteins in human osteoblast-like cell lines. *Bone*. 1996;19(5):437–445.
58. Buzgo M, Jakubova R, Mickova A, et al. Time-regulated drug delivery system based on coaxially incorporated platelet alpha-granules for biomedical use. *Nanomedicine*. 2013;8(7):1137–1154.
59. Anjana J, Kuttappan S, Keyan KS, Nair MB. Evaluation of osteoinductive and endothelial differentiation potential of Platelet-Rich Plasma incorporated Gelatin-Nanohydroxyapatite Fibrous Matrix. *J Biomed Mater Res B Appl Biomater*. 2016;104(4):771–781.
60. Getgood A, Henson F, Brooks R, Fortier LA, Rushton N. Platelet-rich plasma activation in combination with biphasic osteochondral scaffolds-conditions for maximal growth factor production. *Knee Surg Sports Traumatol Arthrosc*. 2011;19(11):1942–1947.

Materials Science & Engineering C 97 (2019) 567–575

Contents lists available at ScienceDirect

Materials Science & Engineering C

journal homepage: www.elsevier.com/locate/msec

Needleless electrospun and centrifugal spun poly-ε-caprolactone scaffolds as a carrier for platelets in tissue engineering applications: A comparative study with hMSCs

V. Lukášová[a,b,c], M. Buzgo[a,b,f], K. Vocetková[b], V. Sovková[a,b,d], M. Doupník[a,f], E. Himawan[f], A. Staffa[a,b,f], R. Sedláček[e], H. Chlup[e], F. Rustichelli[b], E. Amler[a,b,d], M. Rampichová[a,b,*]

[a] University Center for Energy Efficient Buildings (UCEEB), Czech Technical University in Prague, Třinecká 1024, 273 43, Buštěhrad, Czech Republic
[b] Laboratory of Tissue Engineering, Institute of Experimental Medicine, Czech Academy of Sciences, Vídeňská 1083, 142 40 Prague, Czech Republic
[c] Department of Cell Biology, Faculty of Science, Charles University, Albertov 6, 128 43 Prague, Czech Republic
[d] Institute of Biophysics, 2nd Faculty of Medicine, Charles University in Prague, V Uvalu 84, Prague 5-Motol 150 06, Czech Republic
[e] Laboratory of Biomechanics, Faculty of Mechanical Engineering, Czech Technical University in Prague, Prague 6, Czech Republic
[f] InoCure s.r.o., Politických vězňů 935/13, Prague 1, Czech Republic

ARTICLE INFO

Keywords:
Platelets
Electrospinning
Centrifugal spinning
Mesenchymal stem cells
Growth factors

ABSTRACT

The biofunctionalization of scaffolds for tissue engineering is crucial to improve the results of regenerative therapies. This study compared the effect of platelet-functionalization of 2D electrospun and 3D centrifugal spun scaffolds on the osteogenic potential of hMSCs. Scaffolds prepared from poly-ε-caprolactone, using electrospinning and centrifugal spinning technology, were functionalized using five different concentrations of platelets. Cell proliferation, metabolic activity and osteogenic differentiation were tested using hMSCs cultured in differential and non-differential medium. The porous 3D structure of the centrifugal spun fibers resulted in higher cell proliferation. Furthermore, the functionalization of the scaffolds with platelets resulted in a dose-dependent increase in cell metabolic activity, proliferation and production of an osteogenic marker – alkaline phosphatase. The effect was further promoted by culture in an osteogenic differential medium. The increase in combination of both platelets and osteogenic media shows an improved osteoinduction by platelets in environments rich in inorganic phosphate and ascorbate. Nevertheless, the results of the study showed that the optimal concentration of platelets for induction of hMSC osteogenesis is in the range of 900–3000 × 10^9 platelets/L. The study determines the potential of electrospun and centrifugal spun fibers with adhered platelets, for use in bone tissue engineering.

1. Introduction

Nanofibers are established in the field of tissue engineering (TE) as a superior material for cell adhesion and proliferation. This is mainly due to their dimensions being comparable to the native extracellular matrix (ECM) and their porous structure, enabling good nutritional exchange. To date, various strategies have been used for the preparation of nanofibers; the most common method being electrospinning. Using this versatile method, a variety of polymers were processed for TE applications [1,2].

However, electrospinning has some disadvantages. In addition to the application of a dangerously high voltage during processing, further limitations comprise of small pore diameters and a sheet-like structure of the prepared layers; limiting the use of electrospun fibers in the TE applications. Primarily, a 3D structure, with sufficient pores for cell penetration, is usually required. A recently introduced fabrication method - centrifugal spinning, has presented a solution to this [3]. It is a simple method that uses centrifugal forces for the preparation of fibers with a diameter in the range of nano- to micrometers. Different polymers have been processed using this method from solutions or melts [3–6]. As previously published, fibers prepared using centrifugal spinning show a 3D structure with sufficient pore size to allow the penetration of cells [7].

One of the excellent properties of nanofibers is the huge surface-area-to-volume ratio, which enables the adhesion or adsorption of various molecules. The surface functionalization of nanofibers can be carried out by simple physical adsorption, such as: electrostatic interaction, hydrogen bonding, hydrophobic interaction, and van der Waals

* Corresponding author at: Institute of Experimental Medicine, Czech Academy of Sciences, Vídeňská 1083, 142 20 Prague, Czech Republic.
E-mail address: michala.rampichova@iem.cas.cz (M. Rampichová).

https://doi.org/10.1016/j.msec.2018.12.069
Received 25 January 2018; Received in revised form 20 December 2018; Accepted 20 December 2018
Available online 21 December 2018
0928-4931/

interaction [8,9]. Alternatively, biomolecules could be bound covalently [10,11]. This property was used in our previous study for the adhesion of platelets to fibers prepared using electrospinning [12] or centrifugal spinning [13].

Platelets contain a wide range of growth factors in their granules, such as: platelet-derived growth factor (PDGF), transforming growth factor-β (TGF-β), platelet-derived angiogenesis factor (PDAF), vascular endothelial growth factor (VEGF), epidermal growth factor (EGF), platelet-derived endothelial growth factor (PDEGF), epithelial cell growth factor (ECGF) and an insulin like growth factor (IGF) [14–16]. These molecules are employed in important processes in the human body, containing coagulation, immune response, angiogenesis and the healing of damaged tissues, and could also be beneficially used in TE applications [17,18].

The positive effect of platelets in combination with nanofibrous scaffolds, has been well documented in various studies including: culture of dermal cells [19,20], osteogenic differentiation of adipose-derived stem cells [21], chondrogenesis of bone marrow stem cells [22] and the enhanced effect on hernia repair [23].

In this study, scaffolds prepared from the same polymer poly-ε-caprolactone (PCL) but using different technologies; centrifugal spinning and electrospinning, were used in combination with platelets as a potential drug delivery system for tissue engineering applications. Fibrous scaffolds prepared from PCL, a fully biocompatible polymer, were covered with different concentrations of platelets. Furthermore, two different types of media were used for the culture; a growth medium without any supplements, and a differential medium containing supplements supporting osteogenic differentiation. The samples were seeded with human mesenchymal stem cells (hMSCs) and the effect of platelet concentration, scaffold morphology and composition of the culture media on cell proliferation, metabolic activity and alkaline phosphatase (ALP) activity was tested.

2. Materials and methods

2.1. The preparation and characterization of scaffolds using centrifugal spinning and electrospinning technology

Two different fibrous scaffolds were prepared from the same polymer poly-ε-caprolactone (45,000 Da; Sigma Aldrich St Louis, USA) using centrifugal spinning (CS), or electrospinning (ES). The principle of both methods is represented in the diagram (Fig. 1). Centrifugal spinning was performed using a Cyclone 1000 L/M Forcespinning® device (Fiberio, McAllen, TX, USA). Centrifugal spinning technology uses centrifugal forces; a reservoir is filled with polymer, which is then forced through thin orifices. The polymeric solution forms fiber jets when in contact with strong centrifugal forces; the polymeric liquid is elongated, the solvent evaporates and the fibers are placed on a collector. 40% (w/v) PCL was dissolved in a mixture of chloroform ethanol solution at a volume ratio of 9:1. An orifice G30 and rotation speed of 10,000 RPM were used to prepare the fibrous meshes. The fibers were deposited on a spunbond textile using vacuum-assisted deposition.

Electrospun scaffolds (ES) were prepared using a Nanospider device. Electrospinning technology uses electrostatic forces between the electrode and the collector. A polymer solution was extracted from a thin layer of polymer on the needleless electrode, a Taylor cone was formed, and fibers were progressively formed. As the solvent evaporated, the fibers were placed on the collector. 24% (w/v) PCL was dissolved in a mixture of chloroform ethanol solution at a volume ratio of 9:1. The electrospinning was performed using a needleless wire electrode on Nanospider NS500 (Elmarco, Czech Republic) at a potential difference of 50 kV. The process was performed at room temperature and the fibers were collected on a spunbond textile.

The prepared fibers were visualized using scanning electron microscopy (SEM) and the fiber diameter was determined. The samples were coated with a thin layer of platinum using a Quorum SC7620 device (1 cycle, Quorum Technologies, Lewes, GB). For non-coated analysis, the samples were placed into a Charge Reduction Holder and imaged without coating. All samples were visualized using SEM (Phenom G5 Pure, Eindhoven, Netherlands). The acceleration voltage for all the samples was 5 kV, and BSE was used in a 4 quadrant or 2 quadrant (TOPO) setting. The fiber diameter, porosity and pore size were analyzed using the DiameterJ plugin in the ImageJ program [24]. Image analyses were performed from three independent images sampled from different locations of the produced scaffold.

The mechanical properties were evaluated by conducting uniaxial tensile tests of rectangular strips of the layers (the average width of the samples was approximately 10 mm, resp. the thickness was 0.1–0.3 mm). During the test procedure, the ultimate tensile strength (the maximum stress at the beginning of sample failure), the modulus of elasticity I (the slope of the tangent made to a stress-strain relationship on the initial linear part), the modulus of elasticity II (the slope of the secant line made to a stress-strain relationship on the defined part) and the strain-energy density (which is equal to the area under the stress-strain diagram of a material) were determined. Tensile tests were conducted using a Zwick/Roell multipurpose testing machine equipped with a built-in video extensometer. With the use of contrasting marks on the surface of samples, the video extensometer automatically determined the reference length and elongation of the samples. Tensile experiments were conducted at a constant clamp velocity of 0.1 mm/s. The loading force was measured by a U9B (± 250 N, HBM, Germany) force transducer.

2.2. The preparation of platelet solutions and the cell seeding of scaffolds

Platelets derived from buffy coat in plasma and additive solution were purchased from the transfusion station at Šumperk Hospital. The bag contained platelets from 4 donors. The platelets were centrifuged at 120 ×*g* for 7 min for sedimentation and the removal of residual erythrocytes. Subsequently, the supernatant was transferred into a new tube and centrifuged (2200 ×*g*; 10 min) to retrieve the pellet of platelets which was re-suspended in a Platelet Additive Solution SSP+ (Macopharma, France). The platelets were then diluted to the required concentrations in SSP solution: 3000×10^9/L (corresponds to 10× concentrated physiological concentration (PC)), 900×10^9/L (corresponds to 3× concentrated PC), 300×10^9/L (corresponds to PC), 100×10^9/L (3× diluted PC) and 30×10^9/L (10× diluted PC).

PCL CS and ES nanofibers were sterilized using 70% ethanol. The samples were seeded with 25×10^3 human bone marrow-derived mesenchymal stem cells (hMSCs; ScienCell, San Diego, California, USA) per well of 96-well-plates in 30 μL of medium. After 2 hour adhesion to the scaffolds, 20 μL of the platelet solutions was added. After 1-hour adhesion of the platelets, the medium was filled to 300 μL per well. The samples were cultured in a non-differential or differential medium. A non-differential medium was composed from a Minimum Essential Medium (MEM; Sigma Aldrich), 5% fetal bovine serum (FBS; Sigma Aldrich) and antibiotics (PenStrep; Gibco). A differential medium was enriched with 10 mM β-glycerolphosphate, 100 nM dexamethasone and 40 μg/mL ascorbic acid-2-phosphate. The scaffolds were named as CS or ES (depending on the preparation of the fibers), numbered depending on the concentration of platelets (1: 3000×10^9/L; 2: 900×10^9/L; 3: 300×10^9/L, 4: 100×10^9/L; 5: 30×10^9/L, C: control without platelets) and the last letter of the name of the samples corresponded to whether it was cultivated in a differential (D) or non-differential (N) medium. The exact composition of the samples is summarized in Table 1.

2.3. Cell viability and proliferation analysis

The metabolic activity of the cells was measured using an MTS assay (CellTiter 96® AQueous One Solution Cell Proliferation Assay; Promega, Madison, WI, USA) according to the manufacturer's protocol. The

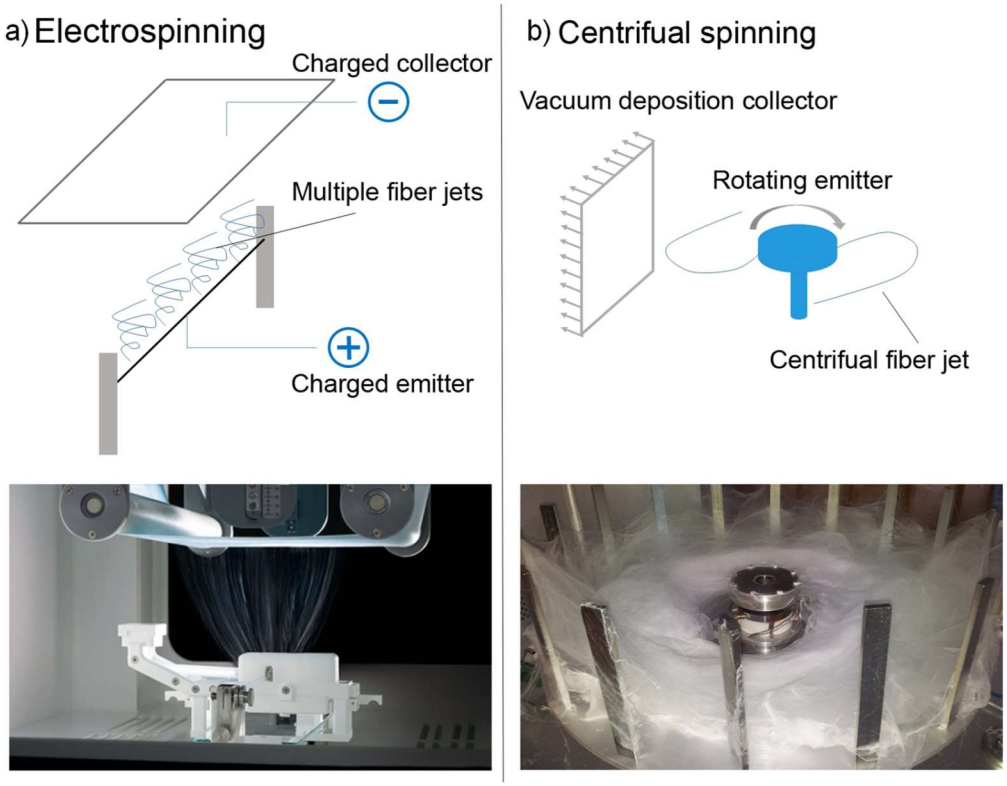

Fig. 1. Schema of the manufacturing of fibers using electrospinning and centrifugal spinning technology. While electrospinning uses electrostatic forces between a charged emitter and an oppositely charged collector (a), centrifugal spinning uses centrifugal forces (b).

proliferation of hMSCs on the scaffold was determined from the amount of DNA (Quant-iT™ dsDNA Assay Kit; Life Technologies, Carlsbad, CA, USA). The scaffolds seeded with cells were placed in 200 µL of cell lysis solution (0.2% v/v Triton X-100, 10 mM Tris (pH 7.0), and 1 mM EDTA) and processed through 3 freeze/thaw cycles with vortexing between each cycle. The samples were further processed according to the manufacturer's protocol and measured using a multiplate fluorescence reader (Synergy HT, Winooski, VT, USA; λex = 485 nm, λem = 525 nm).

To visualize cell distribution on the scaffolds, the cells were stained using DiOC6(3) and propidium iodide. The samples were fixed with frozen methylalcohol (− 20 °C) for 10 min and then incubated with 3,3′-dihexyloxacarbocyanine iodide (DiOC6(3), D273, Invitrogen, Molecular Probes 1 µg/mL in phosphate buffered saline (PBS); pH 7.4) for 45 min at room temperature to visualize the cell biomembranes. Subsequently, the samples were incubated with propidium iodide (PI; 5 µg/mL in PBS; Sigma Aldrich, USA) for 10 min to visualize the cell nuclei. The samples were scanned using a ZEISS LSM 5 DUO confocal microscope (PI: λex = 561 nm, λem = 630–700 nm; DiOC6(3): λex = 488 nm, λem = 505–550 nm).

2.4. The detection of alkaline phosphatase activity

Alkaline phosphatase activity was measured using a 1-Step™ PNPP kit (Thermo Scientific, Waltham, MA USA). 100 µL of PNPP was added to each well and incubated for 10 min. Subsequently, the reaction was stopped with 2 N NaOH. The absorbance was measured using a spectrophotometer at 405 nm (Synergy HT, Winooski, VT, USA).

2.5. Statistical analysis

Quantitative data are presented as mean values ± standard

Table 1
Overview of samples prepared using electrospinning (ES) and centrifugal spinning (CS) technology.

Sample	Fiber type	Platelet concentration [platelets/L]	Medium	Sample	Fiber type	Platelet concentration [platelets/L]	Medium
CS1D	CS	3000×10^9	Differential	ES1D	ES	3000×10^9	Differential
CS2D	CS	900×10^9	Differential	ES2D	ES	900×10^9	Differential
CS3D	CS	300×10^9	Differential	ES3D	ES	300×10^9	Differential
CS4D	CS	100×10^9	Differential	ES4D	ES	100×10^9	Differential
CS5D	CS	30×10^9	Differential	ES5D	ES	30×10^9	Differential
CSCD	CS	–	Differential	ESCD	ES	–	Differential
CS1N	CS	3000×10^9	Non-differential	ES1N	ES	3000×10^9	Non-differential
CS2N	CS	900×10^9	Non-differential	ES2N	ES	900×10^9	Non-differential
CS3N	CS	300×10^9	Non-differential	ES3N	ES	300×10^9	Non-differential
CS4N	CS	100×10^9	Non-differential	ES4N	ES	100×10^9	Non-differential
CS5N	CS	30×10^9	Non-differential	ES5N	ES	30×10^9	Non-differential
CSCN	CS	–	Non-differential	ESCN	ES	–	Non-differential

deviation (SD). The averaged values were determined from a minimum of 3 independently prepared samples. Results were evaluated statistically using One-Way Analysis of Variance and Student-Newman-Keuls test (SigmaStat 12.0, Systat).

The statistical analysis of mechanical testing data was performed using statistical software (STATGRAPHICS Centurion XV, StatPoint, USA). The normality of the data was primarily verified using the Shapiro-Wilk's and Chi-Squared tests; outliers were identified via either the Grubbs' or Dixon's tests. The mean values and variability of normally distributed numerical data were expressed as the arithmetical mean and the standard deviation (SD), while abnormally distributed numerical data was expressed as the median and interquartile range (IQR). Homoscedasticity was verified using the Levene's and Bartlett's tests. Non-parametric analysis was employed since either the assumption of normality or homoscedasticity were violated and, consequently, the Kruskal-Wallis test for multiple comparisons or the Mann-Whitney W test (as a post hoc test) was performed. Statistical significance was accepted at $p \leq 0.05$.

3. Results

3.1. The characterization of scaffolds

The fibrous scaffolds prepared by electrospinning and centrifugal spinning technology were used for the surface adsorption of platelets. Both types of scaffolds have high porosity, pore interconnection and a fibrous nature, mimicking the native ECM. Fibers are prepared from the same polymer – polycaprolactone with molecular weight 45,000 Da and using the same solvent system, based on chloroform and ethanol in the ratio 9:1. However, the fabrication and deposition methods have a different principle; resulting in the formation of meshes with different stereological properties. Complete image analysis of the scaffold characterization using DiameterJ validated fiber analysis algorithm can be seen in Table 2.

In general, the electrospun (ES) fibrous scaffold shows a more planar structure with more compacted fibers compared to scaffold obtained from centrifugal spinning (CS).

From Fig. 2A, the fiber diameter size distribution of ES PCL scaffold mostly lies in 200 nm size range. This is also reflected by its mean diameter of 232 ± 129 nm. On the other hand, the same scaffold also consisted of a microfibrous fraction with a fiber diameter of up to 2500 nm. The ES PCL scaffold end product, which has two fiber size fraction is typical for electrospinning from chloroform:ethanol solvent [25,26]. In the case of the fibers prepared by centrifugal spinning (CS), the samples showed a mean fiber diameter of 572 ± 330 nm. The CS PCL scaffold has wider diameter distribution and it contains significant fraction of fibers in microfibrous range.

From Fig. 2B, the scaffold pore size distribution showed that the ES scaffold has more compacted pore morphology compared to CS scaffolds ($p < 0.001$). This was reflected by the CS scaffold's much larger mean pore size of 13.36 ± 33.4 μm^2 while the ES scaffolds has mean pore size of 0.783 ± 1.521 μm^2. The porosity of ES and CS scaffolds were 46.0 ± 0.27% and 62.4 ± 3.67% respectively. The centrifugal spun scaffolds had a more open morphology which is more suitable for cell penetration.

Table 2
Summary of scaffold characterization results.

Parameter	ES fiber	CS fiber
Fiber diameter	0.232 ± 0.129 μm	0.572 ± 0.330 μm
Pore size	0.783 ± 1.521 μm^2	13.36 ± 33.4 μm^2
Porosity	46.0 ± 0.27%	62.4 ± 3.67%
Modulus of elasticity I	3.11 ± 1.70 MPa	2.71 ± 1.26 MPa
Modulus of elasticity II	3.19 ± 0.89 MPa	2.50 ± 0.98 MPa
Strain energy density	1500 ± 1.57 J/m	1100 ± 1.08 J/m

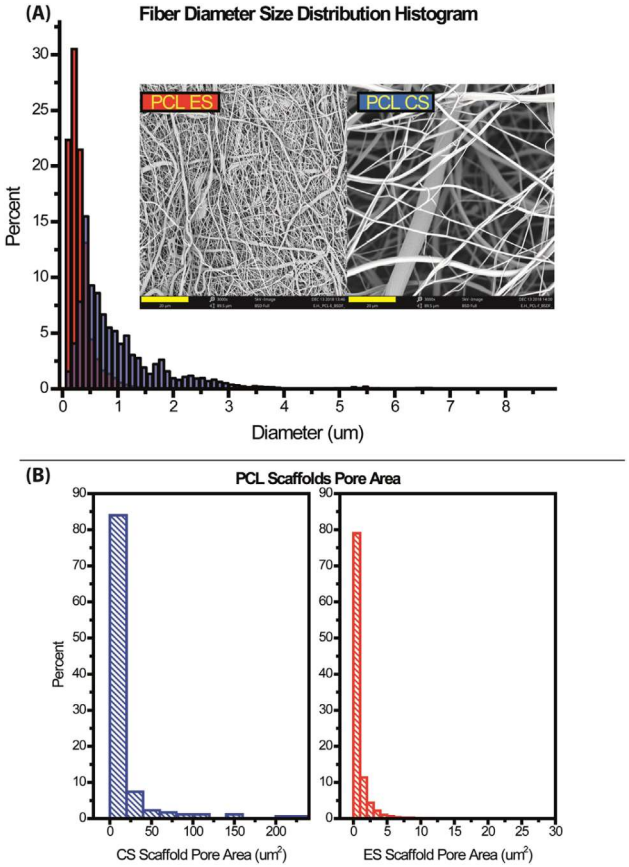

Fig. 2. PCL fibers diameter size (A) and pore size (B) distributions from electrospinning (ES) and centrifugal spinning (CS). Both scale bar in the inset images represent 20 μm.

The results obtained from the mechanical tests revealed no statistically significant differences ($p = 0.05$) in the modulus of elasticity I (tangent modulus) – ES 3.11 ± 1.70 MPa; CS 2.71 ± 1.26 MPa. However, with reference to the ultimate tensile strength, statistically significant differences ($p = 0.05$) were detected - ES 0.16 ± 0.03 MPa; CS 0.34 ± 0.04 MPa. Similarly to the previous results, statistically significant differences were detected in the modulus of elasticity II (secant line) – ES 3.19 ± 0.89 MPa; CS 2.50 ± 0.98 MPa and likewise in the strain-energy density - ES 1.50 ± 1.57 $J \cdot m^{-1}$; CS 1.10 ± 1.08 J/m. The results of the mechanical tests revealed that fibers prepared using centrifugal spinning have more elasticity but higher ultimate tensile strength than electrospun fibers.

Platelets were activated after adhesion to the scaffolds and formed a fibrin mesh, comparable on both the ES and CS scaffold (Fig. 3).

3.2. The cell adhesion and proliferation on scaffolds

Cell adhesion and proliferation were measured using DNA quantification. The results showed that the concentration of platelets was the main factor influencing cell proliferation (Fig. 4). The cell numbers increased with the increasing platelet concentration.

In the case of scaffolds prepared using centrifugal spinning, the highest cell adhesion was observed on the scaffolds with the two highest platelet concentrations cultured in differential and non-differential media (CS1N, CS1D, CS2N, CS2D). The cells on these scaffolds continuously increased their number during the experiment. Cell proliferation was higher on the CS3N, CS3D and CS4N, CS4D scaffolds compared to the controls. The scaffolds with the lowest platelet

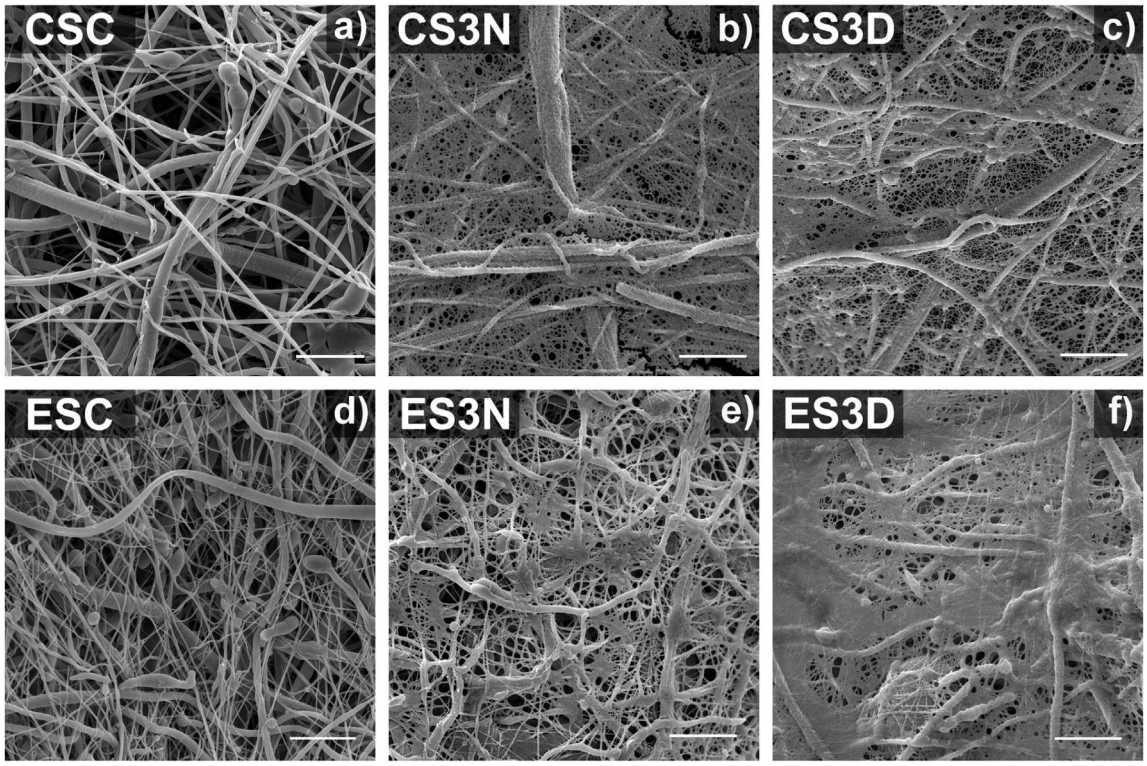

Fig. 3. Fibrous scaffolds prepared using ES and CS with adhered platelets visualized using scanning electron microscopy. Platelets activated after adhesion on the scaffolds and formed a fine fibrin network (platelets in physiological concentration - 300 × 10^9/L adhered on centrifugal spun fibers cultivated in differential (CS3D; b) and non- differential medium (CS3N; c) and on electrospun fibers cultivated in differential (ES3D; e) and non-differential medium (ES3N; f)). Scale 10 μm.

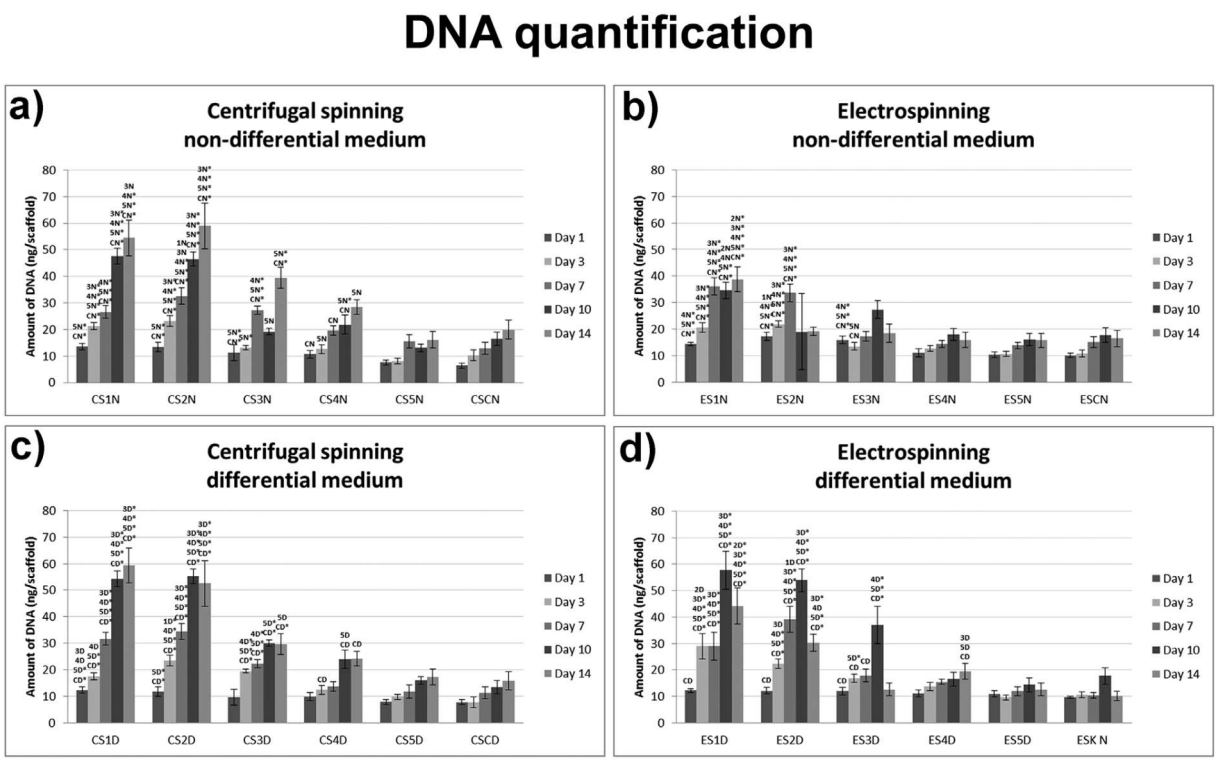

Fig. 4. Proliferation of hMSCs measured using DNA quantification. As is visible, proliferation was higher on scaffolds prepared using centrifugal spinning, when cultured in non-differential medium (a) compared to electrospinning cultured in non-differential medium (b). On the other hand, proliferation was comparable for CS and ES scaffolds cultured in differential medium (c) and d) respectively). The letters above the columns express statistical significance ($p < 0.05$, $*p < 0.001$).

concentrations (CS5N, CS5D) were comparable to the controls (CSCN, CSCD). There were no significant differences observed between the differential and non-differential medium.

On the scaffolds prepared using electrospinning, differences were observed between scaffolds cultured in the differential and non-differential medium. In the case of the non-differential medium, the adhesion to the samples was the highest and comparable on the samples with the three most concentrated platelets (ES1N, ES2N, ES3N). On days 3 and 7, the cell amount was gradually increasing on the ES1N and ES2N samples. Conversely, the cell proliferation stagnated on the ES3N sample. On days 10 and 14, the cells predominantly proliferated on the ES1N and the proliferation was the highest compared to all the samples. A decrease in the cell amount was shown on the ES2N. The platelets with a concentration lower than physiological (ES4N and ES5N) did not improve the scaffold properties and the cell proliferation on these samples was comparable to the control sample.

Electrospun nanofibers and fibers prepared using centrifugal spinning, were further compared. The best cell adhesion was shown on the electrospun fibers cultured in the non-differential medium with the three most concentrated platelets (ES1N, ES2N and ES3N). Additional proliferation was similar on the scaffolds with the two most concentrated platelets. Proliferation was comparable until day 7 on all the tested scaffolds. At this time point, the cells on the electrospun scaffolds in the non-differential medium (ES1N and ES2N) stopped proliferation and the cell number was the lowest on days 10 and 14. On day 14, the proliferation also discontinued on the electrospun scaffolds cultured in differential media (ES1D and ES2D). The highest number of cells was detected on the scaffolds prepared using centrifugal spinning, cultured in both media (CS1N, CS1D, CS2N, CS2D). The differences in cell proliferation on the scaffolds with a physiological concentration of platelets were not so distinct. However, apart from day 10, when the highest cell amount was detected on the ES3D, the cell proliferation was higher on the CS samples compared to the ES. In the lower concentration of platelets, the cell proliferation was lower on all the samples and the differences among the samples were less important.

The cell adhesion and distribution on the scaffolds were visualized using confocal microscopy (Fig. 5). Cells adhered well on all the scaffolds and were uniformly distributed. The cells were of elongated shape; the shape typical for mesenchymal stem cells.

3.3. Metabolic activity of cells

Fig. 6 shows that the cell metabolic activity was mainly influenced by supplements contained in the differential medium. Platelets supported cell metabolic activity in the three highest concentrations.

The results obtained on the CS and ES scaffolds were very similar. The supportive effect of platelets on cell metabolic activity was shown for the three most concentrated platelets in both the differential and non-differential medium. A slight increase on some experimental days was also shown on the scaffolds with 100×10^9 platelets/L (CS4D, CS4N, ES4D, ES4N).

A lower concentration of platelets did not influence the cell metabolic activity and was comparable to the control.

The samples prepared using both methods, CS and ES, and cultured in both media, differential and non-differential, were again compared. The results were similar on all the experimental days. A higher cell metabolic activity was shown on the scaffolds cultured in the differential medium compared to those cultured in the non-differential medium. There were no differences seen between the ES and CS scaffolds.

3.4. ALP activity

The ALP activity measurement was used to detect the potential of the functionalized scaffolds for the osteogenic differentiation of cells. Similarly to the metabolic activity of cells, the ALP activity of cells was mostly influenced by the osteogenic supplements in the differential medium (Fig. 7).

The results were similar on the scaffolds prepared using centrifugal spinning. A higher ALP activity, compared to the control, was detected on CS1, CS2 and CS4 in both the differential and non-differential medium. On day 7, the ALP activity stagnated on the samples cultured in the non-differential medium. On the other hand, the differential medium in combination with platelets stimulated the ALP activity. The highest activity was detected on the CS3D and then on the CS2D and CS4D samples. Interestingly, the ALP activity on the sample with the highest concentration of platelets (CS1D) stagnated and was comparable to the control. On day 14, the highest ALP activity of cells cultured in the non-differential medium was detected on the CS2N sample. On the samples cultured in the differential medium, the highest values were measured for the scaffolds with the three most concentrated platelets.

There were no visible differences in the ALP activity on the ES scaffolds cultured in the differential medium on day 1. The highest value from the group cultured in the non-differential medium was measured on ES2N. On day 7, the ALP activity only grew on the ES2D sample. Interestingly, on day 14, the highest ALP activity of the samples cultured in the non-differential medium was measured on the control sample (ESCN). On the contrary, on samples cultured in differential medium, the highest ALP activity was detected on the sample with the physiological concentration of platelets (ES3D), then on the ES2D and ES1D samples. The values were significantly higher compared to the lower concentration of platelets and the control sample.

The comparison of the scaffolds prepared using ES and CS and cultured in the differential and non-differential medium with different concentrations of platelets, provided similar results for the highest concentrations. On days 7 and 14, higher ALP activity was measured on the samples cultured in a differential medium (ESD, CSD) compared to the samples cultured in a non-differential medium (ESN, CSN). The values measured on CS and ES samples were comparable apart from day 7, where the CS4D sample was statistically higher than the ES4D. The ALP activity on the samples with the lowest platelet concentration (ES5, CS5) and control samples was the highest on the CSD on day 7 (CS5D, CSCD). On day 14, the lowest values were measured on the CSN (CS5N, CSCN); values detected on the other samples were comparable.

4. Discussion

In this study, the effects of three different scaffold parameters on MSCs behavior were tested: fibrous scaffold morphology, different concentrations of platelets and supplements in the culture media. The study highlights the importance of platelet concentration and proper scaffold morphology.

The biggest impact on cell proliferation and metabolic activity was caused by the presence of platelets. Platelets contain a cocktail of growth factors, cytokines and chemokines, which are released after their activation. Growth factors contained in platelets, such as platelet-derived growth factor (PDGF), transforming growth factor β1 (TGF-β1), hepatocyte growth factor (HGF) or vascular endothelial growth factor (VEGF), play an important role in cell communication and influence the cell fate [15,27]. Most of these growth factors are mitogens for hMSCs and also play a role in hMSCs osteogenic differentiation [28–30]. The proliferative effect of platelets on MSCs was proved for concentrations of 100×10^9/L and above. The cell proliferation increased with the concentration of platelets. The two highest concentrations (3000×10^9/L and 900×10^9/L) were comparable, showing the saturation of the pro-proliferative capacity of cells on the scaffolds. In the samples with platelets with a concentration lower than the physiological concentration (300×10^9/L), the influence on cell proliferation was small. The concentration 30×10^9 platelets/L did not influence cell proliferation in any way and was comparable to the control sample. A similar effect of platelets on MG-63 osteosarcoma cells was observed in

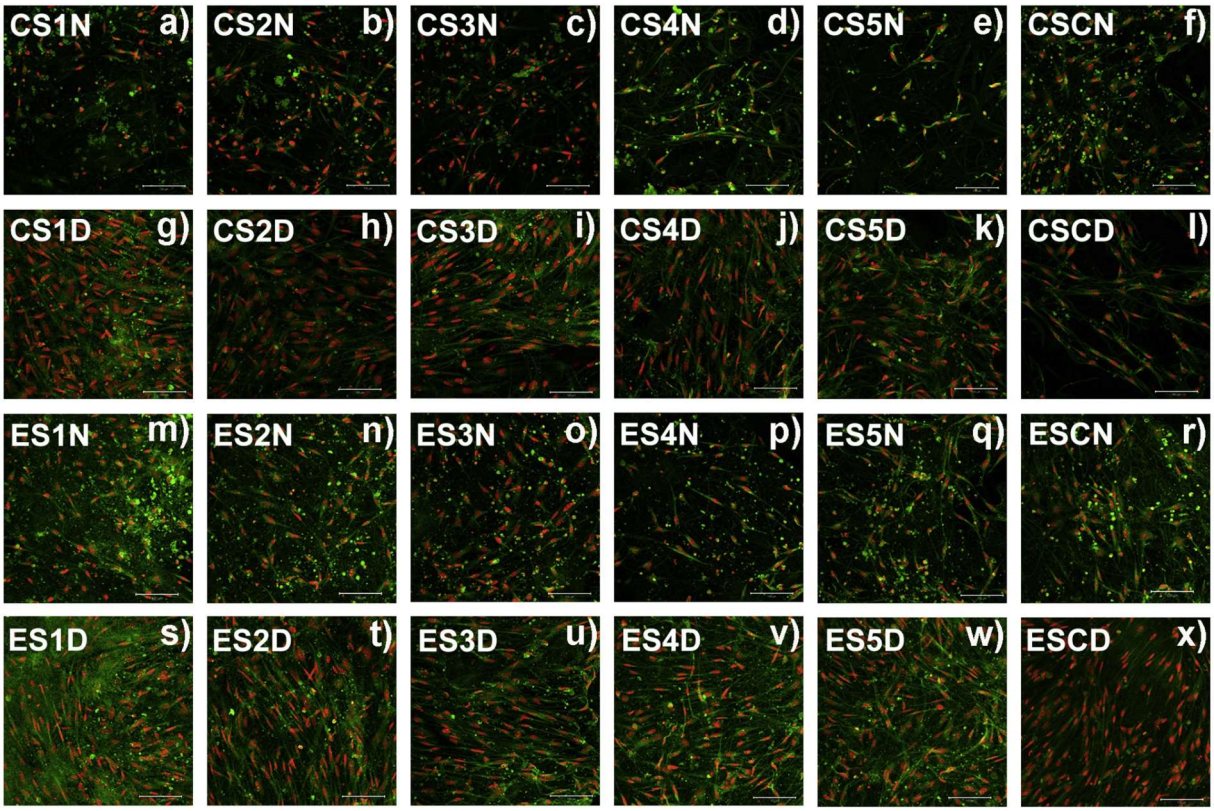

Fig. 5. Cell distribution on the scaffolds prepared using centrifugal spinning (CS) and electrospun scaffolds (ES) cultured in differentiation (D) and non-differentiation (N) media were visualized using confocal microscopy (Day 14). Cell nuclei were stained using propidium iodide (red color) and intracellular membranes using DioC6(3) (green color). Scale 200 μm. (For interpretation of the references to color in this figure legend, the reader is referred to the web version of this article.)

our previously published study [13]. The concentration of platelets, which supported cell proliferation and metabolic activity, was 300×10^9/L; lower concentrations did not affect MG-63 behavior.

In addition to proliferation, we have also evaluated metabolic activity. Cell metabolic activity was mainly influenced by supplements of the differential media. Cells in non-differential media showed a lower metabolic activity compared to cells in differential media. The addition of platelets had a significantly positive effect on the metabolic activity, indicating stimulation by the released biomolecules. However, co-administration of platelets and osteogenic supplements (differential medium was supplemented by β-glycerol phosphate (10 mM), dexamethasone (100 nM) and ascorbic acid-2-phosphate (40 μg/mL)) resulted in an increase of a three times higher value of metabolic activity. The platelets in concentrations higher than 300×10^9/L in combination with these supplements had a supportive effect on cell metabolic activity. The reason may be connected with the improved cellular proliferation and higher activity of ECM proteins and markers related to osteogenesis. This is supported by the results of the ALP activity assay.

In terms of the ALP activity, the addition of platelets further supported the effect of supplements contained in the differential medium. The effect was again visible for concentrations of 300×10^9/L and above. The increased alkaline phosphatase activity relates to osteogenic differentiation. Alternatively, the effect of platelets on ALP activity in the non-differential medium was not visible. This indicates that the cells cultured in the differential medium underwent osteogenic differentiation. Osteogenic supplements are widely used to stimulate the MSCs osteogenic differentiation [31,32]. It was shown that ascorbic acid-2-phosphate had a positive effect on hMSCs proliferation and preserved their differentiation ability [33]. Similarly, dexamethasone was shown to influence collagen formation and simultaneously support the MSCs proliferation [34]. Additionally, the synergic effect could be connected with an increased presence of calcium ions in the differential medium. The platelets are responsive to calcium levels and upon increased concentration of calcium and proper stimulation (i.e. by collagen), their activation and release of active molecules could be more intensive compared to a media with a normal calcium level [35]. However, in the differential medium, the addition of platelets had a highly stimulatory effect compared to the controls and it therefore illustrates the positive effect of the released biomolecules on both the proliferation and osteogenic differentiation of hMSCs.

Nevertheless, the scaffold morphology is an additional factor affecting the behavior of cells on scaffolds. ES and CS scaffolds were prepared from the same polymer and solvent system; however, the processing method resulted in different stereology and mechanical properties of fibers. Electrospinning resulted in a finer structure of fibers with high packing density and lower pore size. On the other hand, centrifugally spun fibers showed higher deviation of fiber diameter, higher mean fiber diameter and loose packing with a higher mean pore size. Therefore, the structure of CS is more flexible, as observed in mechanical testing, and open for cell penetration. However, the influence of the scaffold morphology on cell culture results was not so unequivocal. The differences between ES and CS were dependent on platelet concentration, and were visible on the samples with the three most concentrated platelets. In those cases, the best cell adhesion was visible on the electrospun scaffolds, cultured in the non-differentiated medium. Diversely, the best cell proliferation in the late phase of the experiment was detected on the scaffolds prepared using centrifugal spinning. The reason may be attributable to improved cell penetration to the deeper scaffold layers. The confluence of electrospun scaffolds was documented by confocal microscopy. After reaching confluence,

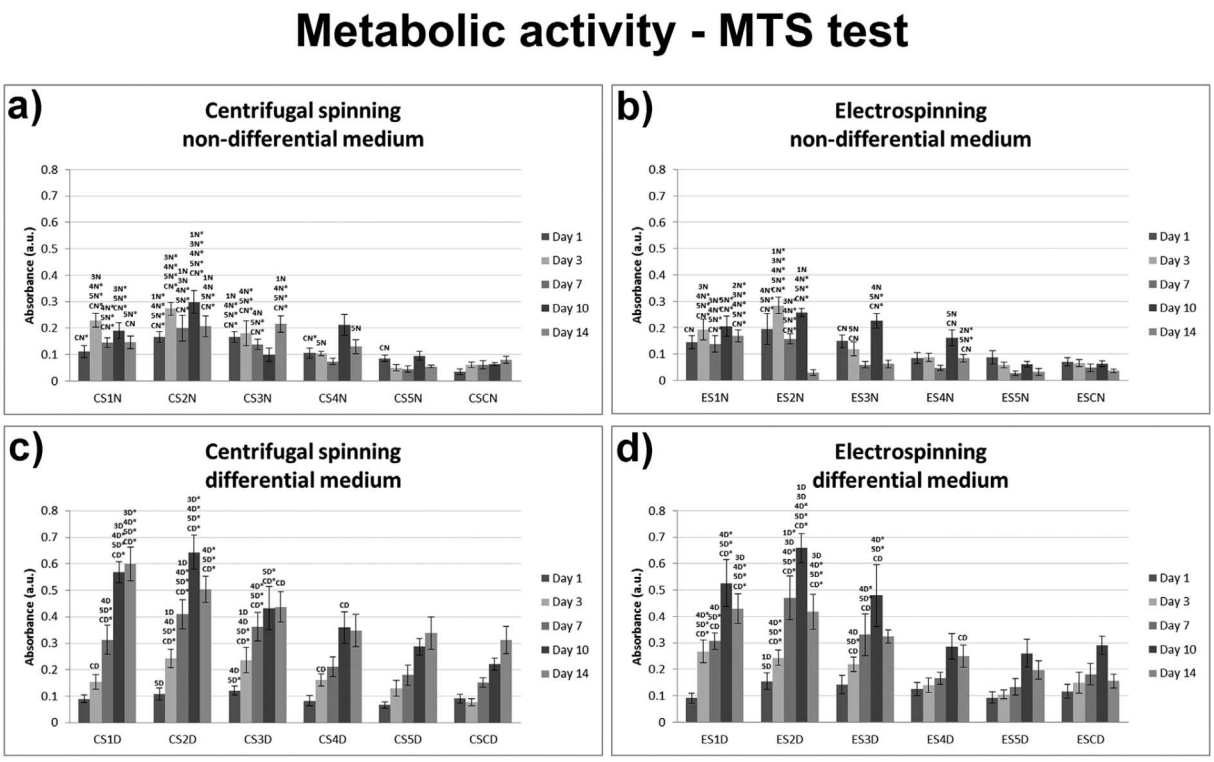

Fig. 6. Metabolic activity of hMSCs measured using MTS test. Metabolic activity was higher on scaffolds cultured in differential medium prepared with both centrifugal spinning (c) and electrospinning (d), compared to non-differential medium (CS – a), ES – b). The letters above the columns express statistical significance ($p < 0.05$, $*p < 0.001$).

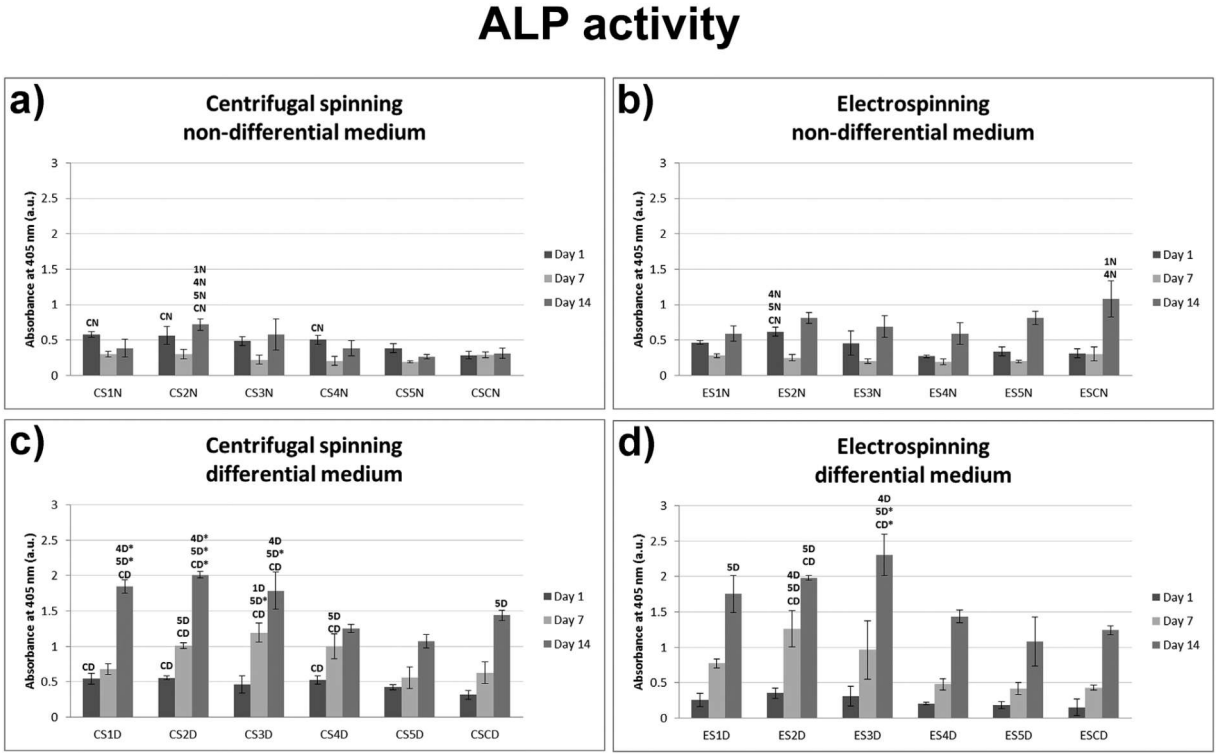

Fig. 7. ALP activity of hMSCs. ALP activity was higher on scaffolds cultured in differential medium prepared with both centrifugal spinning (c) and electrospinning (d), compared to non-differential medium (CS – a), ES – b). The letters above the columns express statistical significance ($p < 0.05$, $*p < 0.001$).

the cells on the ES scaffolds were unable to penetrate deeper into the scaffolds. On the other hand, the centrifugal spun PCL scaffolds were shown to have a more open morphology with a higher mean pore size, and in our previous studies were shown to better support cell infiltration [7]. Excellent cell adhesion on scaffolds prepared using electrospinning was proved in various studies. Fibrous scaffold prepared using centrifugal spinning contained fibers with diameters in the range of micrometers. This morphology did not seem so well suited for cell adhesion. However, the bigger pore size of the CS scaffold helped cell infiltration and provided more space for cell proliferation. This was visible on the 14th experimental day, where cell proliferation on the ES scaffolds started to decrease while it was increasing on the CS scaffolds. The results of the study showed that both scaffolds are suitable for bone-tissue engineering applications, and their use is further governed by the need for specific morphology requirements (i.e. defect size and locations).

5. Conclusion

In conclusion, the functionalization of scaffolds with platelets is beneficial for the improvement of cell adhesion, proliferation and osteogenic differentiation. The cells showed a dose-dependent stimulation by platelets with an optimal concentration in the range of 900–3000 × 10^9/L. Both the electrospun and centrifugal spun scaffolds showed properties beneficial for use in bone tissue engineering. Platelets, due to their efficacy, safety and regulatory compliance, will play an important role in future bone-regeneration therapies as a valuable source of growth factors. Their combination with scaffolds, prepared by needleless electrospinning and centrifugal spinning, provide advantages in the precise location and immobilization of these growth factor sources. Importantly, both methods are up-scaled to industrial quantities and qualities of production and the use of polycaprolactone enables simple certification, as it is approved both by the FDA and EMA. Therefore, the proposed functionalized systems have huge potential for practical application in bone tissue engineering.

Acknowledgements

This study was supported by the Czech Science Foundation (grants nos. 15-15697S, 16-14758S, 18-09306S), the Ministry of Education, Youth, and Sports of the Czech Republic (Research Programs NPU I:LO1309, NPU I:LO1508) and the Internal Grant Agency of the Ministry of Health of the Czech Republic (MZ-VES project no. 16-28637A, 17-32285A and 17-31276A).

References

[1] T.J. Sill, H.A. von Recum, Electrospinning: Applications in drug delivery and tissue engineering, Biomaterials vol. 29, (2008) 1989–2006.
[2] S. Agarwal, J.H. Wendorff, A. Greiner, Use of electrospinning technique for biomedical applications, Polymer vol. 49, (2008) 5603–5621.
[3] N.E. Zander, Formation of melt and solution spun polycaprolactone fibers by centrifugal spinning, J. Appl. Polym. Sci. 132 (2) (2015).
[4] A.M. Loordhuswamy, V.R. Krishnaswamy, P.S. Korrapati, S. Thinakaran, G.D.V. Rengaswami, Fabrication of highly aligned fibrous scaffolds for tissue regeneration by centrifugal spinning technology, Mater. Sci. Eng. C 42 (2014) 799–807.
[5] L. Ren, V. Pandit, J. Elkin, T. Denman, J.A. Cooper, S.P. Kotha, Large-scale and highly efficient synthesis of micro- and nano-fibers with controlled fiber morphology by centrifugal jet spinning for tissue regeneration, Nanoscale 5 (6) (2013) 2337.
[6] L. Wang, J. Shi, L. Liu, E. Secret, Y. Chen, Fabrication of polymer fiber scaffolds by centrifugal spinning for cell culture studies, Microelectronic Engineering, 2011, pp. 1718–1721.
[7] M. Rampichová, M. Buzgo, J. Chvojka, E. Prosecká, O. Kofronová, E. Amler, Cell penetration to nanofibrous scaffolds: Forcespinning®, an alternative approach for fabricating 3D nanofibers, Cell Adhes. Migr. vol. 8, (2014) 36–41.
[8] J.S. McGonigle, G. Tae, P.S. Stayton, A.S. Hoffman, M. Scatena, Heparin-regulated delivery of osteoprotegerin promotes vascularization of implanted hydrogels, Journal of Biomaterials Science, Polymer Edition, 2008.
[9] M. Rampichová, L. Martinová, E. Košťáková, E. Filová, A. Míčková, M. Buzgo, et al., A simple drug anchoring microfiber scaffold for chondrocyte seeding and proliferation, J. Mater. Sci. Mater. Med. 23 (2) (2012) 555–563.
[10] H.S. Koh, T. Yong, C.K. Chan, S. Ramakrishna, Biomaterials Enhancement of Neurite Outgrowth Using Nano-Structured Scaffolds Coupled With Laminin, 29 (2008), pp. 3574–3582.
[11] M. Buzgo, J. Greplová, M. Soural, D. Bezděková, A. Míčková, O. Kofroňová, et al., PVA immunonanofibers with controlled decay, Polymer 77 (2015) 387–398 (Guildf).
[12] R. Jakubova, A. Mickova, M. Buzgo, M. Rampichova, E. Prosecka, D. Tvrdik, et al., Immobilization of thrombocytes on PCL nanofibres enhances chondrocyte proliferation in vitro, Cell Prolif. 44 (2) (2011) 183–191.
[13] M. Rampichová, M. Buzgo, A. Míčková, K. Vocetková, V. Sovková, V. Lukášová, et al., Platelet-functionalized three-dimensional poly-ε-caprolactone fibrous scaffold prepared using centrifugal spinning for delivery of growth factors, Int. J. Nanomedicine 12 (2017) 347–361.
[14] A. Lubkowska, B. Dolegowska, G. Banfi, Growth factor content in PRP and their applicability in medicine, J. Biol. Regul. Homeost. Agents 26 (2 Suppl 1) (2012) 3S–22S.
[15] V. Sovkova, K. Vocetkova, M. Rampichova, A. Mickova, M. Buzgo, V. Lukasova, et al., Platelet lysate as a serum replacement for skin cell culture on biomimetic PCL nanofibers, Platelets (2017) 1–11.
[16] K. Vocetkova, M. Buzgo, V. Sovkova, M. Rampichova, A. Staffa, E. Filova, et al., A comparison of high throughput core-shell 2D electrospinning and 3D centrifugal spinning techniques to produce platelet lyophilisate-loaded fibrous scaffolds and their effects on skin cells, RSC Adv. 7 (85) (2017) 53706–53719.
[17] S.A. Sell, P.S. Wolfe, J.J. Ericksen, D.G. Simpson, G.L. Bowlin, Incorporating platelet-rich plasma into electrospun scaffolds for tissue engineering applications, Tissue Eng. Part A 17 (21 − 22) (2011) 2723–2737.
[18] L. Diaz-Gomez, C. Alvarez-Lorenzo, A. Concheiro, M. Silva, F. Dominguez, F.A. Sheikh, et al., Biodegradable electrospun nanofibers coated with platelet-rich plasma for cell adhesion and proliferation, Mater. Sci. Eng. C 40 (2014) 180–188.
[19] K. Vocetkova, M. Buzgo, V. Sovkova, D. Bezdekova, P. Kneppo, E. Amler, Nanofibrous polycaprolactone scaffolds with adhered platelets stimulate proliferation of skin cells, Cell Prolif. 49 (5) (2016) 568–578.
[20] V. Bertoncelj, J. Pelipenko, J. Kristl, M. Jeras, M. Cukjati, P. Kocbek, Development and bioevaluation of nanofibers with blood-derived growth factors for dermal wound healing, Eur. J. Pharm. Biopharm. 88 (1) (2014) 64–74.
[21] M. Kazem-Arki, M. Kabiri, I. Rad, N.H. Roodbari, H. Hosseinpoor, S. Mirzaei, et al., Enhancement of osteogenic differentiation of adipose-derived stem cells by PRP modified nanofibrous scaffold, Cytotechnology 70 (6) (2018) 1487–1498. Available from https://doi.org/10.1007/s10616-018-0226-4.
[22] J. Liu, H. Nie, Z. Xu, F. Guo, S. Guo, J. Yin, et al., Construction of PRP-containing nanofibrous scaffolds for controlled release and their application to cartilage regeneration, J. Mater. Chem. B 3 (4) (2015) 581–591.
[23] M. Plencner, E. Prosecká, M. Rampichová, B. East, M. Buzgo, L. Vysloužilová, et al., Significant improvement of biocompatibility of polypropylene mesh for incisional hernia repair by using poly-ε-caprolactone nanofibers functionalized with thrombocyte-rich solution, Int. J. Nanomedicine 10 (2015).
[24] N.A. Hotaling, K. Bharti, H. Kriel, C.G. Simon, DiameterJ: a validated open source nanofiber diameter measurement tool, Biomaterials 61 (2015) 327–338.
[25] E. Kostakova, M. Seps, P. Pokorny, D. Lukas, Study of polycaprolactone wet electrospinning process, Express Polym Lett 8 (8) (2014) 554–564.
[26] M. Rampichová, J. Chvojka, V. Jenčová, T. Kubíková, Z. Tonar, J. Erben, et al., The combination of nanofibrous and microfibrous materials for enhancement of cell infiltration and in vivo bone tissue formation, Biomed. Mater. 13 (2) (2018).
[27] S. Arora, V. Doda, U. Kotwal, M. Dogra, Quantification of platelets and platelet derived growth factors from platelet-rich-plasma (PRP) prepared at different centrifugal force (g) and time, Transfus. Apher. Sci. 54 (1) (2016) 103–110.
[28] A.M. Sotoca, J. Roelofs-Hendriks, S. Boeren, P.M. van der Kraan, J. Vervoort, E.J.J. van Zoelen, et al., Comparative proteome approach demonstrates that platelet-derived growth factor C and D efficiently induce proliferation while maintaining multipotency of hMSCs, Exp. Cell Res. 319 (17) (2013) 2649–2662.
[29] J. Murakami, M. Ishii, F. Suehiro, K. Ishihata, N. Nakamura, M. Nishimura, Vascular endothelial growth factor-C induces osteogenic differentiation of human mesenchymal stem cells through the ERK and RUNX2 pathway, Biochem. Biophys. Res. Commun. 484 (3) (2017) 710–718.
[30] G. D'Ippolito, P.C. Schiller, C. Perez-stable, W. Balkan, B.A. Roos, G.A. Howard, Cooperative actions of hepatocyte growth factor and 1,25-dihydroxyvitamin D3 in osteoblastic differentiation of human vertebral bone marrow stromal cells, Bone 31 (2) (2002) 269–275.
[31] X. Shi, Y. Wang, R.R. Varshney, L. Ren, Y. Gong, D.A. Wang, Microsphere-based drug releasing scaffolds for inducing osteogenesis of human mesenchymal stem cells in vitro, Eur. J. Pharm. Sci. 39 (1–3) (2010) 59–67.
[32] H. Kim, H.W. Kim, H. Suh, Sustained release of ascorbate-2-phosphate and dexamethasone from porous PLGA scaffolds for bone tissue engineering using mesenchymal stem cells, Biomaterials 24 (25) (2003) 4671–4679.
[33] K.-M. Choi, Y.-K. Seo, H.-H. Yoon, K.-Y. Song, S.-Y. Kwon, H.-S. Lee, et al., Effect of ascorbic acid on bone marrow-derived mesenchymal stem cell proliferation and differentiation, J. Biosci. Bioeng. 105 (6) (2008) 586–594.
[34] K. Szöke, J. Daňková, M. Buzgo, E. Amler, J.E. Brinchmann, E. Østrup, The effect of medium composition on deposition of collagen type 1 and expression of osteogenic genes in mesenchymal stem cells derived from human adipose tissue and bone marrow, Process Biochem. 59 (2017) 321–328.
[35] D. Varga-Szabo, A. Braun, B. Nieswandt, Calcium signaling in platelets, Journal of Thrombosis and Haemostasis vol. 7, (2009) 1057–1066.

RSC Advances

PAPER

View Article Online
View Journal | View Issue

Cite this: *RSC Adv.*, 2017, **7**, 1215

Emulsion centrifugal spinning for production of 3D drug releasing nanofibres with core/shell structure

Matej Buzgo,*[bc] Michala Rampichova,[ac] Karolina Vocetkova,[abc] Vera Sovkova,[ab] Vera Lukasova,[abc] Miroslav Doupnik,[c] Andrea Mickova,[ac] Franco Rustichelli[a] and Evzen Amler[abc]

Received 10th November 2016
Accepted 13th December 2016

DOI: 10.1039/c6ra26606a

www.rsc.org/advances

Herein we describe the core/shell centrifugal spinning process to deliver susceptible bioactive molecules. The fibres are produced from water-in-oil (W/O) emulsion, where poly-ε-caprolactone (PCL) dissolved in chloroform serves as the continuous phase and Pluronic F-68 (PF-68) dissolved in ethanol serves as the droplet phase. The successful core/shell fibre formation and discontinuous morphology of the core was identified by confocal microscopy. Encapsulation of a model enzyme resulted in protection of enzymatic activity and release during the first 7 days. The feasibility for tissue engineering applications was demonstrated by the incorporation of platelet lyophilisates as a source of growth factors. The cultivation of 3T3 fibroblasts and MG63 osteoblasts resulted in improved metabolic activity and fostered proliferation. Results of the study indicate that the proposed scaffold combines the 3D structure of scaffolds produced by centrifugal spinning with the drug delivery of growth factors.

Introduction

Tissue engineering has drawn much attention in recent years due to its potential to solve complex healthcare problems unsolvable using current methods.[1,2] The regeneration capacity of the adult body is limited and further decreases with ageing. In order to achieve tissue regeneration, tissue engineering employs diverse scaffolds and protocols. Scaffolding platforms may be based on hydrogels, foams, 3D printed matrices and fibrous materials. The key properties for tissue engineering scaffolds are biocompatibility, mechanical and stereological properties respecting the target tissue and the capacity to integrate into the surrounding tissues.[1,2]

Fibrous scaffolds have ideal properties for regeneration of a broad scale of target tissue. The nano- and microfibrous structure mimics the natural extracellular matrix and provides numerous contact points for cell adhesion. In addition, fibrous scaffolds have good mechanical properties, high porosity and pore interconnection.[3,4] Due to this unique property, nanofibrous scaffolds offer numerous contact points for cells. The key strategy in producing fibrous scaffolds is electrospinning. Electrospinning enables the formation of a submicron fibrous mesh with a random or ordered structure.[5] Electrospinning was successfully employed to encapsulate bioactive molecules for diverse tissue engineering applications. The release of encapsulated bioactive molecules stimulates and regulates cell recruitment, proliferation and differentiation in the site of injury. Sahoo *et al.*[6] prepared coaxial nanofibres poly(lactic-*co*-glycolic acid) (PLGA) loaded with basic fibroblast growth factor (bFGF), and blend nanofibres with PLGA and bFGF. Jia *et al.*[7] showed PLGA nanofibres loaded by dextran core with vascular endothelial growth factor (VEGF) for vascular tissue engineering applications. Tian *et al.*[8] prepared VEGF-loaded poly(lactic acid-*co*-caprolactone) PLCL nanofibres by emulsion electrospinning. The scaffold enabled the sustained release of VEGF and stimulated mesenchymal stem cell (MSC) metabolic activity in a 20 day *in vitro* assay. In a recent study, improved cardiac differentiation of MSC on VEGF loaded scaffolds was shown.[9]

However, electrospun layers suffer from poor cellular penetration caused by small pore size and limited thickness. Several attempts were made to improve cellular infiltration to electrospun scaffolds. Mean pore size could be increased by a combination of fibres with leachable particles *i.e.* sacrificial co-fibres,[10,11] salt[12] or ice crystals.[13] In addition, the organization of fibres highly depends on the collecting electrode.[14] Rampichova *et al.*[15] prepared a patterned 2D/3D collector, which produced a fibrous layer with loosely packed areas. The cells were able to penetrate through these areas and proliferate. Blakeney *et al.*[16] produced fluffy 3D fibres using a special collector. Cocoon-like structures showed higher mean pore size and efficient cell penetration. Despite the possibility to increase the mean pore size, the thickness of an electrospun fibrous layer is also limited.[33]

Centrifugal spinning technology is an alternative approach to produce fibrous scaffolds from polymeric solutions and

[a]*Institute of Experimental Medicine, Czech Academy of Sciences, v.v.i., Vídeňská 1083, 142 20 Prague 4, Czech Republic*

[b]*Department of Biophysics, 2nd Faculty of Medicine, Charles University in Prague, V Úvalu 84, 150 06 Prague 5, Czech Republic. E-mail: buzgo@labdemo.cz*

[c]*University Center of Energetically Efficient Buildings, Czech Technical University, Třinecká 1024, 273 43 Buštěhrad, Czech Republic*

melts.[17] In the centrifugal spinning process the polymeric solution or melt is placed in a rotating chamber with a thin orifice. When the applied centrifugal speed overcomes the surface tension of the solution, it is ejected from the orifice. Emerged jets are stretched and deposited on a collector. The produced fibres form fluffy meshes with a fibre diameter in the range from hundreds of nanometres to tens of micrometres. Centrifugal spinning was successfully applied for scaffold manufacturing from PLGA,[18] polylactic acid,[19] gelatin[20] and polycaprolactone (PCL).[20–22] However, the proposed scaffolds were rather a passive cell culture substrate. In order to stimulate cell proliferation and differentiation, bioactive molecules should be delivered using an optimal scaffold. So far, centrifugal spinning technology had been used for drug delivery applications only by Mary *et al.*[23] In the study of tetracycline loaded PCL blended polyvinyl pyrrolidone (PVP) fibres were used as a drug delivery vehicle. The results showed rapid release of tetracycline within 24 h. To the best of our knowledge, no studies on delivering protein-based active molecules have yet been performed.

The aim of the study is to develop a new technique for delivering growth factors based on centrifugal spinning. In order to protect the proteins from denaturation in organic solvents we will develop core/shell centrifugal spinning technology. The proposed technology is based on emulsion co-spinning, where a continuous phase will give rise to a shell and droplet phase to the core of the fibres. The combination of the 3D structure of scaffolds produced by centrifugal spinning with drug delivery function will result in the formation of novel bioactive and biomimicking scaffolds.

Results and discussion

Development and characterization of Pluronic F-68 based (W)/PCL (O) emulsions

The proposed approach is based on the formation of a protein water-in-oil (W/O) emulsion, which is subsequently processed *via* a centrifugal spinning process. The technology is based on utilizing Pluronic F-68 (PF-68) as a protein surfactant stabilizing the W/O emulsion and protecting the proteins from denaturation. The polar (W) droplet phase is based on PF-68 dissolved in ethanol. An analysis of dynamic surface tension showed that the addition of PF-68 to pure ethanol increases the surface tension. Upon the addition of 0.1% PF-68 and 0.5% PF-68 the surface tension increased, indicating incomplete occupation of the surface by PF-68 molecules. PF-68 is an amphiphilic polymer containing polar polyethylene oxide (PEO) segments and non-polar polypropylene oxide (PPO) segments.[24] Upon interaction with polar solvents, the polymer aggregates to thermodynamically stable particles with a minimal interaction of PPO with the polar solvent. The process therefore results in the self-assembly of particles with PEO coronas and PPO cores.[25] Above 1% PF-68 concentration the surface tension was not further changed (2.5% PF-68, 5% PF-68, 7.5 PF-68, 10% PF-68 and 20% PF-68) (Fig. 1a). The result indicates that all formulations above 1% PF-68 were above the critical micellar concentration (CMC). An analysis by laser scattering showed the formation of PF-68

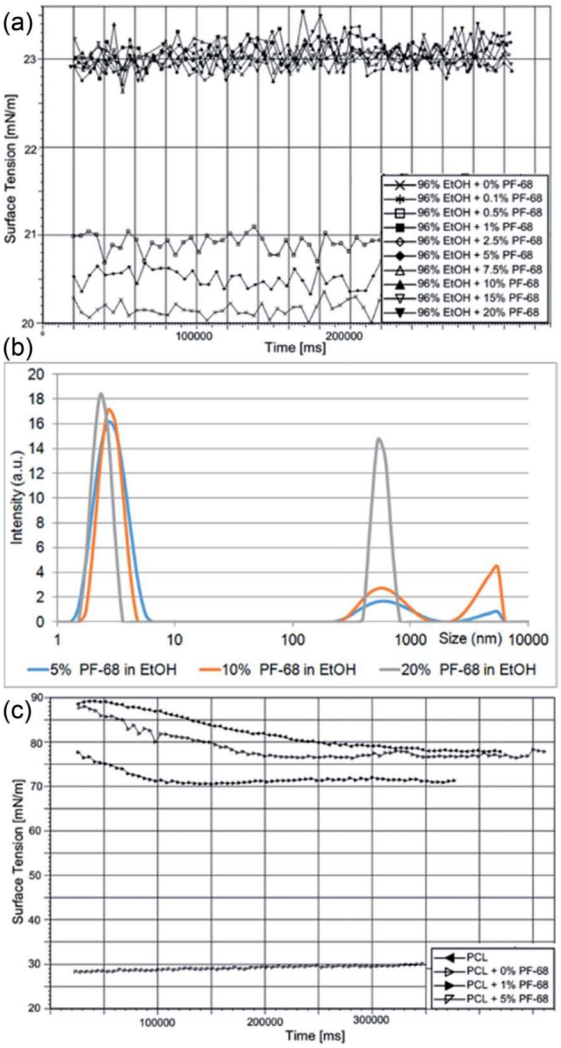

Fig. 1 Characterization of PF-68 (W)/PCL (O) emulsions. (a) Effect of PF-68 on surface tension of EtOH. (b) Size of PF-68 micelles in 70% EtOH. (c) Effect of W/O emulsification on surface tension of PCL solution.

micelles with a size of about 5 nm. An increase in the PF-68 concentration resulted in the formation of particles with a size of about 500 nm (Fig. 1b). The highest number of large PF-68 micelles was found in the 20% PF-68 sample. The average size for 5% PF-68 was 3.7 nm and polydispersity index was 0.2. For 10% PF-68 the average diameter was 86 nm and polydispersity index was 0.33. For 20% PF-68 the polydispersity index was very high (0.69) indicating multiple peaks and non-stable emulsion properties. The observed micelle distribution is in accordance with literature.[26,27] The small micelles correspond to pure PF-68 micelles. The large structures correspond to clusters containing aqueous components.

The continuous phase of W/O emulsion was formed by 40% polycaprolactone (MW 45 kDa) dissolved in chloroform. The emulsification with the PF-68 ethanol/water phase resulted in the formation of a W/O emulsion. The emulsification changed

the properties of the PCL solution. The addition of the polar phase containing 0% PF-68, 1% PF-68 and 5% PF-68 resulted in a decrease of surface tension (Fig. 1c). This decrease of surface tension is attributed to the accumulation of water/ethanol on the liquid surface. The decrease in case of 0% was low and decreased the tension from 80 mN m^{-1} to 77 mN m^{-1}. The addition of surfactant in a concentration of 1% ($w_{PF\text{-}68}/w_{PCL}$) resulted in a further decrease to values about 70 mN m^{-1}. The further increase in PF-68 concentration to 5% ($w_{PF\text{-}68}/w_{PCL}$) resulted in a significant decrease of surface tension (30 nN m^{-1}). Such decrease may be caused by the higher concentration of PF-68 than CMC. The excess PF-68 occupied the surface of the polymeric liquid and resulted in a decrease of surface tension.

The mixing of PF-68 dissolved in 70% ethanol with 40% PCL in chloroform resulted in the formation of an emulsion formed by PF-68 particles. Upon mixing the ethanolic solution of PF-68 with non-polar solvent, the ethanol is readily mixed with chloroform. Such particles expose hydrophobic PPO segments to the non-polar solvent and polar PEO segments minimize contact with the non-polar solvent. As a result, the hydrophilic segments of PF-68 form a polar cavity and stimulate the rearrangement of PF-68 to particles to inverse micellar particles. Ben Henda *et al.*[25] studied PF-68 micelles in polar and non-polar solvents. In case of binary mixtures, the hydrophobic solvents (phenol and *p*-xylene) resulted in the inhibition of micelle self-assembly or formation of various types of inverse micelles. However, in case of a ternary mixture with non-polar solvent and water the PF-68 behaviour became more complex. PF-68 was shown to form either inverse micelles or W/O emulsions with separated phases covered by surfactant molecules. Similar results were obtained for PF-127 in polar and non-polar solvents.[28] In our experiment, the laser scattering measurement showed that the W/O emulsion contained PF-68 particles. The sample emulsified without PF-68 contained a water phase (PCL + 0% PF-68) with a size of 787 nm and polydispersity index was 0.72. The sample containing 5% PF-68 as droplet phase showed a particle size of about 355 nm and polydispersity index 0.3. With a further increase of PF-68 concentration the size was lower (170 nm for 10% PF-68 and polydispersity index of 0.5). Highly concentrated 20% PF-68 showed higher particle size (1476 nm and polydispersity index 0.39). This observation may be related to the aggregation of PF-68 particles and the formation of flocculated particle clusters. The size of PF-68 indicated that the particles were rather formed by a separated aqueous phase and non-polar phase covered by PF-68. Nevertheless, the experimental conditions are further complicated by the presence of 40% (w/v) PCL in the continuous phase. Polycaprolactone is insoluble in water and the formation of an emulsion results in altered rheological properties. Phase separation is the result of PLC interacting with a non-solvent (*i.e.* water, DMSO). The polymer-rich segments are dispersed in solvent and the polymer poor phase is occupied by a non-solvent.[29] Similarly, phase separation occurs during the formation of W/O emulsions. The viscosity of polymeric liquids was measured in samples containing 40% PCL as a continuous phase and 0%, 1%, 5%, 10% and 20% PF-68 in 70% ethanol as an emulsion phase. The addition of an emulsion phase increased the viscosity of samples. The viscosity of 40% PCL without an emulsion phase was 790 ± 112 mPa s. The addition of an emulsion phase – 70% ethanol (PCL + 0% PF-68) resulted in an increase to 993 ± 92 mPa s. The addition of 5% PF-68 in 70% ethanol resulted in an increase to 1132 ± 112 mPa s. Nevertheless, the samples with 10% and 20% had even higher viscosity – 1370 ± 98 mPa s and 1610 ± 102 mPa s. The increase in viscosity may be caused by limited movement of PCL polymeric chains.

The centrifugal spinning process is connected with applying high centrifugal forces. The stabilization of the emulsion is therefore essential to obtain improved results of the encapsulation process. The stability of different formulations containing PF-68 were analysed by evaluating phase-separation during centrifugation. The emulsions were loaded to 2 ml tubes and centrifugation under 3000 × *g* was performed. The water phase was partially separated from the continuous nonpolar phase. The analysis by DLS showed that in case of a sample without PF-68 (PCL + 0% PF-68) the mean size was highly increased (from 787 nm to 1560 nm). The centrifugation of PCL + 5% PF solution resulted in an increase from 355 nm to 522 nm. Similarly, in case of PCL + 10% PF-68 the size increased from 170 nm to 332 nm. The increase of size was lower than a control sample without PF-68 and indicates the stabilization of the water phase by PF-68. Interestingly, for a PCL + 20% PF-68 solution, the size after centrifugation decreased from 1796 nm to 469 nm. This may be caused by the separation of aggregated particles after the partial separation of immiscible phases. The results clearly demonstrate that PF-68 was able to create water-phase particles upon mixing with PCL in chloroform. In addition, these particles were stable after centrifugation forces observed in the fibre preparation process.

Centrifugal spinning of coaxial fibres

The centrifugal spinning process was performed using Forcespinning™ technology (Fig. 2). Three experimental sets were performed by centrifugal core/shell technology: (1) core/shell fibres loaded with fluorescently labelled BSA, (2) core/shell fibres loaded with horseradish peroxidase and (3) core/shell fibres loaded with growth factors (platelet lyophylisates). All samples were prepared from W/O emulsions. First, the bioactive protein was mixed with PF-68 in 70% EtOH. When the concentration of PF-68 was above CMC (higher than wt 1%), PF-68 micelles were formed. The micelles had hydrophobic PPO cores and hydrophilic PEO coronas. Since the proteins are amphiphilic, part of the protein was probably embedded inside the PF-68 micelles. In the following step, PF-68 phase (W) was mixed with 40% PCL in chloroform as the oil phase (O). The samples were based on 40 ml of 40% PCL emulsified with 10 ml of PF-68 in 70% ethanol. The emulsification resulted in the formation of water/PF-68/protein droplets. The emulsion was further processed by centrifugal spinning to solid fibrous mesh. The fibres were spun using a rotating emitter with a G30 orifice. The rotation produces centrifugal force and draws the polymeric solution from the orifice in the form of a thin fibrous jet. The fibres are collected on the collector as a dry fibrous mesh.

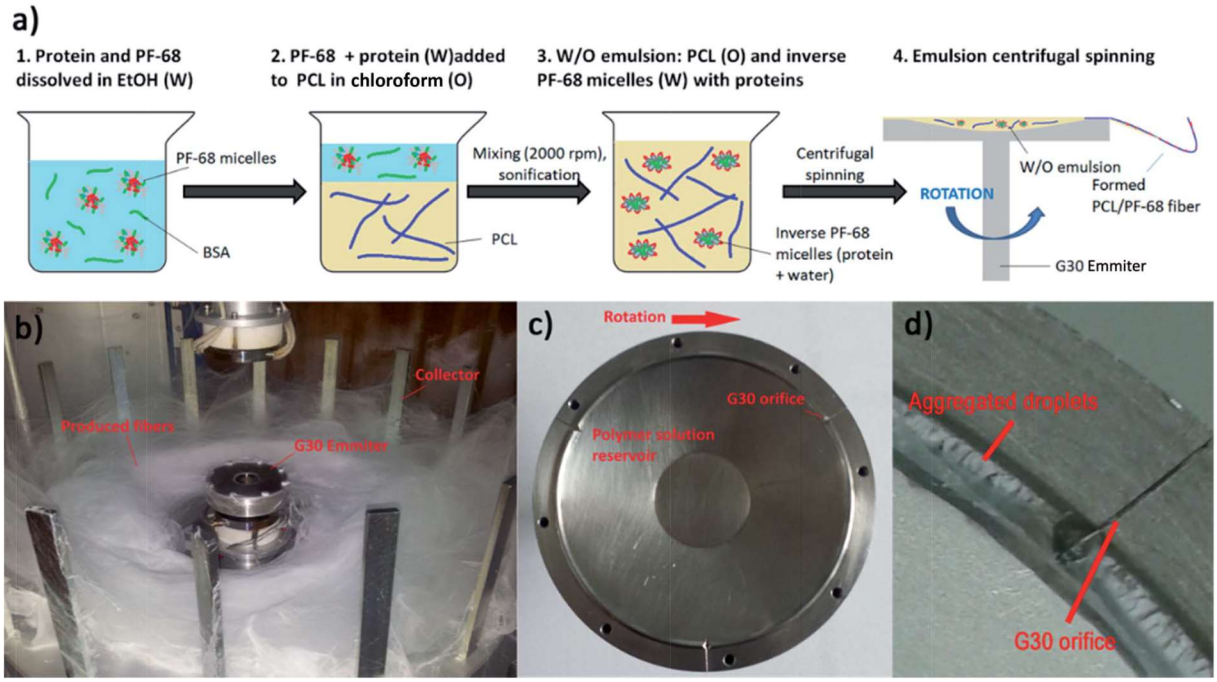

Fig. 2 Scheme of emulsion centrifugal spinning process. (a) Description of emulsification process (b) centrifugal spinning apparatus. (c) G30 emitter structure. (d) The emulsion in sites of G30 orifice is not forming creamed emulsion aggregates.

The yield of emulsion centrifugal spinning is 40 ± 7% as measured for basic PCL/10% PF-68 emulsions. However, the production yield is connected with emulsion stability and varies across formulations.

Scanning electron microscopic (SEM) analysis showed that the centrifugal spinning process resulted in the formation of a fibrous web (Fig. 3a–e). 40% PCL with blend encapsulated active molecules (LYO and FITC-BSA) showed fibrous morphology with microfibres (2.7 ± 1.5 μm) and nanofibres (338 ± 90 nm). Besides fibres, the mesh contained a large number of non-fibrous defects. The mean pore size is 47 ± 56 μm^2 and the pores larger than 10 μm^2 made up 36% of all pores. The samples based on emulsification by 70% ethanol (0% PF-68) showed more beaded morphology than blend PCL fibres. The fibrous mesh contained microfibres (1.6 ± 0.6 μm) and nanofibres (440 ± 110 nm) mixed with non-fibrous defects. The higher number of non-fibrous defects may be attributed to the separation of the hydrophobic PCL phase and the hydrophilic water based phase. The mean pore size was 38 ± 47 μm^2 and the pores larger than 10 μm^2 made up 32% of all pores. The sample based on emulsification with 5% PF-68 showed a lower number of non-fibrous droplets. The microfibres showed a higher mean size (2.4 ± 1.9 μm). The number of nanofibres was higher and showed a mean size of 470 ± 103 nm. The mean pore size was 30 ± 29 μm^2 and pores >10 μm^2 made up 24% of all pores. With a further increase of the PF-68 concentration the amount of defects was further lowered. The mean fibre size (2.1 ± 0.9 μm for microfibres and 453 ± 95 nm for nanofibres) and mean pore size (32 ± 21 μm^2) was higher. Similarly, the samples with the highest concentration of PF-68 (20%) had similar morphology. The number of defects was low and the mean fibre size was 2 ± 1.2 μm for microfibres and 537 ± 168 nm for nanofibres. The mean pore size was 29 ± 39 μm^2 and the number of pores larger than 10 μm^2 was 21%. The observed data are consistent with the fibre sizes measured in our previous article.[21]

In order to evaluate the internal morphology, the fluorescently labelled FITC-BSA was encapsulated to the fibres and the localization was detected by confocal microscopy (Fig. 3f–j). The analyses showed that the FITC-BSA was localized outside the fibres in the PCL blend mesh. The localization of fluorescence was predominantly in defects and non-fibrous areas. Similarly, the sample based on emulsion without PF-68 (PCL + 0% PF-68) showed distribution in non-fibrous areas. However, the protein was also localized along the fibres. In case of samples with PF-68 the localization was dominantly along the fibres. The localization of FITC-BSA was in the case of 5%, 10% and 20% PF-68 samples in distinct areas. As the concentration of PF-68 rises, the number of droplets along the fibres also rises. However, in case of 20% PF-68 the droplets were merged and formed bigger droplets. The localization indicates that the fibres with PF-68 were formed by regions containing zones with fluorescent molecules and zones without fluorescent signal. Such structure produces core/shell fibres with an island-in-the-see structure. The structure of the centrifugal spun fibres resembles the structure of core/shell fibres produced by emulsion electrospinning.[30–32] The chemical principle of both methods is similar. However, the fabrication process uses a different physical principle for fibre formation. Electrospinning is based on the steady-state drawing of fibres from the polymeric solution by electrostatic forces. On the other hand,

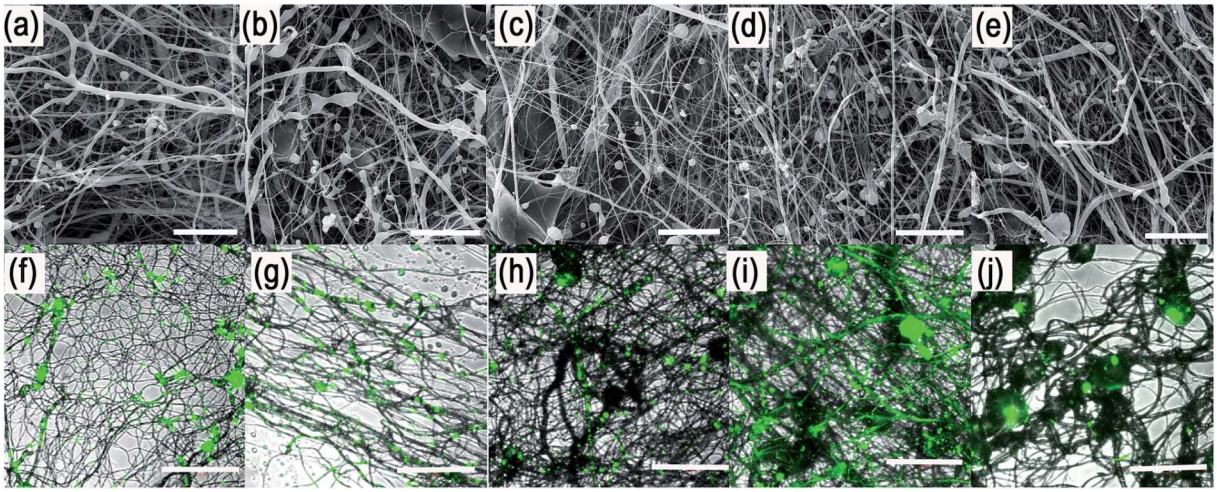

Fig. 3 Morphology of core/shell fibres. (a) SEM image of 40% PCL + 20% PF-68 + LYO. (b) SEM image of 40% PCL + 10% PF-68 + LYO. (c) SEM image of 40% PCL + 5% PF-68 + LYO. (d) SEM image of 40% PCL + 0% PF-68 + LYO. (e) SEM image of 40% PCL blend with LYO. (f) Confocal image of 40% PCL + 20% PF-68 + FITC-BSA. (g) Confocal image of 40% PCL + 10% PF-68 + FITC-BSA. (h) Confocal image of 40% PCL + 5% PF-68 + FITC-BSA. (i) Confocal image of 40% PCL + 0% PF-68 + FITC-BSA. (j) Confocal image of 40% PCL blend with FITC-BSA Scale bar in all SEM samples 50 μm and in all confocal samples 200 μm.

the proposed emulsion centrifugal spinning technique is a dynamic process. The centrifugation draws fibres from the polymeric solution and simultaneously changes the properties of the polymer solution. In the present study we employed the emulsification method with PF-68 as the core phase. PF-68 may form inverse micelles and protect the aggregation of micelles upon centrifugation, as indicated by our results from centrifugation of W/O emulsion and the structure of core droplets observed by confocal microscopy. On the other hand, the centrifugation process results in partial separation of the aqueous phase resulting in decreased efficacy of the process. Therefore, future research should be focused on increasing the stability of the emulsion to decrease this negative effect. Nevertheless, the G30 emitter morphology with only 3 orifices results in the aggregation of droplets on the walls of the emitter. A construction change to a linear form of emitter minimizing aggregation on the walls may be beneficial for improved fibre quality.

Encapsulation of HRP PF-68-based core/shell fibres improves protection of enzymatic activity during encapsulation

In order to evaluate the internal morphology, the fluorescently labelled FITC-BSA was encapsulated to the fibres and the localization was detected by confocal microscopy (Fig. 3f–j). The analyses showed that the FITC-BSA was localized outside the fibres in the PCL blend mesh. The localization of fluorescence was predominantly in defects and non-fibrous areas. Similarly, the sample based on emulsion without PF-68 (PCL + 0% PF-68) showed distribution in non-fibrous areas. However, the protein was also localized along the fibres. In case of samples with PF-68 the localization was dominantly along the fibres. The localization of FITC-BSA was in the case of 5%, 10% and 20% PF-68 samples in distinct areas. As the concentration of PF-68 rises, the number of droplets along the fibres also rises. However, in case of 20% PF-68 the droplets were merged and formed bigger droplets. The localization indicates that the fibres with PF-68 were formed by regions containing zones with fluorescent molecules and zones without fluorescent signal. Such structure produces core/shell fibres with an island-in-the-see structure. The structure of the centrifugal spun fibres resembles the structure of core/shell fibres produced by emulsion electrospinning.[30–32] The chemical principle of both methods is similar. However, the fabrication process uses a different physical principle for fibre formation. Electrospinning is based on the steady-state drawing of fibres from the polymeric solution by electrostatic forces. On the other hand, the proposed emulsion centrifugal spinning technique is a dynamic process. The centrifugation draws fibres from the polymeric solution and simultaneously changes the properties of the polymer solution. In the present study we employed the emulsification method with PF-68 as the core phase. PF-68 may form inverse micelles and protect the aggregation of micelles upon centrifugation, as indicated by our results from centrifugation of W/O emulsion and the structure of core droplets observed by confocal microscopy. On the other hand, the centrifugation process results in partial separation of the aqueous phase resulting in decreased efficacy of the process. Therefore, future research should be focused on increasing the stability of the emulsion to decrease this negative effect. Nevertheless, the G30 emitter morphology with only 3 orifices results in the aggregation of droplets on the walls of the emitter. A construction change to a linear form of emitter minimizing aggregation on the walls may be beneficial for improved fibre quality.

Encapsulation of HRP PF-68-based core/shell fibres improves protection of enzymatic activity during encapsulation

The classical approach for preparing nanofibre based drug delivery systems is blend spinning.[33] The polymer/drug

composite is prepared by a simple mixing of miscible solutions and is often enhanced by mechanical or ultrasound dispergation. The main constraint of using blend spinning for delivering protein-based therapeutics is their denaturation in organic solvents. Biocompatible polymers (such as PCL, PLGA, PU, *etc.*) supporting adhesion of cells are typically hydrophobic and soluble in organic solvents. Therefore, mixing proteins with organic solvents decreases their activity. Such a disadvantage could be overcome by eliminating the contact with non-polar solvents. In our previous research we have shown that the encapsulation of proteins to liposomes embedded in fibres produced by coaxial electrospinning eliminated the degradation and improved the bioactivity of HRP.[34] In addition, emulsion electrospinning is an alternative approach for producing core/shell fibres. Due to the high interfacial tension between the core and shell phases, the mobility of molecules is low and contact between susceptible bioactive molecules and nonpolar solvent is significantly reduced. In order to evaluate the hypothesis, the biological activity of a model enzyme – HRP was assessed. We prepared 5 samples with a distinct concentration of PF-68 in the emulsion phase. Blend encapsulation of HRP was used as a control to the emulsion approach. The morphology of fibres showed similar morphology as samples with embedded lyophilisates and BSA-FITC. The samples contained nano/microfibres with droplets. The detailed micrographs in Fig. 4 show the smooth surface of fibres in the case of 5%, 10% and 20% PF-68. The analysis of HRP activity was performed by analysing the activity of released HRP (Fig. 5a). The samples with 20%, 10% and 5% PF-68 (>60% activity) showed significantly higher activity compared with samples without PF-68 (<30% activity). The protective activity of PF-68 on the protein structure is well known.[35] Due to the amphiphilic structure and high flexibility, PF-68 interacts with both the hydrophilic and hydrophobic segments of polymers and stabilizes the protein structure in a harsh environment. For instance, PF-68 is used as a protein stabilization agent for vaccines.[36] The difference in protective activity between different concentrations of PF-68 may be related to phase transition during W/O emulsification. We hypothesize that in samples with a lower PF-68 concentration upon mixing with the chloroform phase the PF-68 molecules changed conformation. Upon transition from PPO-core micelles to PEO-core micelles the HRP may be in contact with chloroform. In samples with a higher PF-68 concentration, the phase transition may occur on the surface

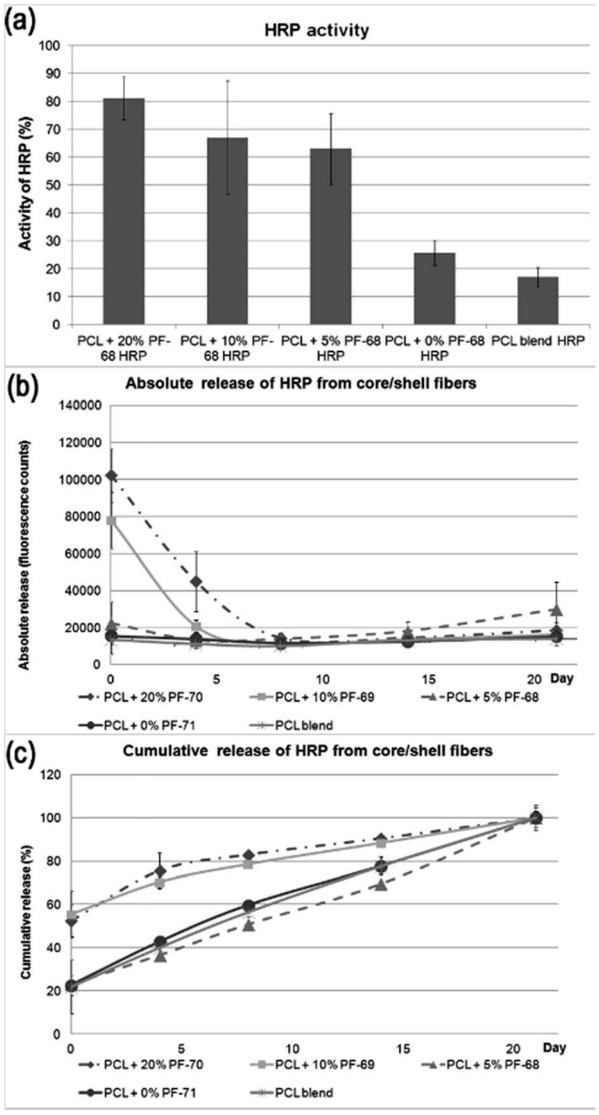

Fig. 5 Release kinetics of HRP from core/shell fibers. (a) Activity of HRP released from core/shell fibers. (b) Absolute release of HRP from core/shell fibers. (c) Cumulative release of HRP from core/shell fibers.

of the PF-68 particle structure and does not affect the structure inside the micelle. The protection of enzyme activity was observed in several works on emulsion electrospinning. Li

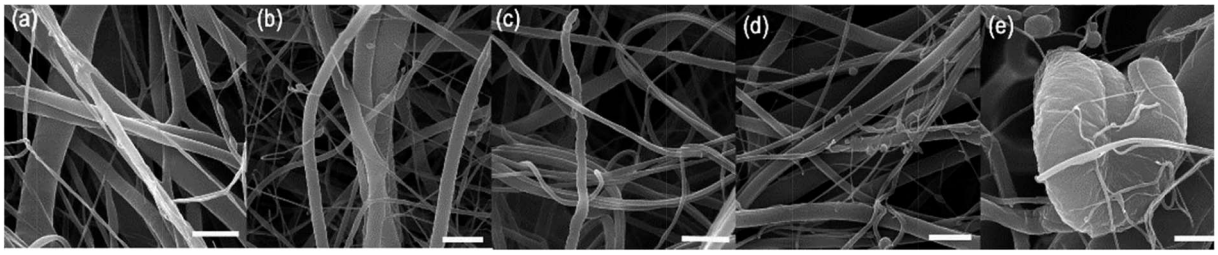

Fig. 4 Morphology of core/shell fibres visualized by SEM. (a) 40% PCL + 20% PF-68 + HRP. (b) 40% PCL + 10% PF-68 + HRP. (c) 40% PCL + 5% PF-68 + HRP. (d) 40% PCL + 0% PF-68 + HRP. (e) 40% PCL blend with HRP. Scale bar 5 μm.

et al.[37] prepared PLA–PEG composite nanofibres loaded by protease K by emulsion electrospinning. The released proteinase K accelerated the biodegradation of the scaffold. Briggs *et al.*[38] evaluated the effect of sonication and surfactant on lysozyme activity. The results showed that both addition of polar polymer to droplet and sonication lead to higher lysozyme activity after release from the nanofibres (Fig. 6).

Beside analysis of the enzyme activity, we focused on HRP release kinetics from fibres (Fig. 5b and c). The analysis of HRP release showed that release from core/shell fibres was faster compared to non-coaxial samples. The absolute release showed that in case of PF-68 the encapsulation efficacy was much higher with an increase in PF-68 concentration. The reason for such observation may be in the higher number of PF-68 micelles. The samples not exhibiting morphology with the droplet phase (PCL blend and PCL + 0% PF-68) showed slow release and a much lower concentration of the embedded HRP. The higher number of PF-68 micelles in 20% and 10% PF-68 was also detected by confocal microscopy of BSA-FITC loaded samples. The results indicate that with the increase of micelle content the encapsulation efficacy is improved and is demonstrated by a higher total release of the embedded protein. In addition, with the increase of PF-68 concentration, a higher number of micelles are exposed to the surface of fibres. Therefore, upon incubation with aqueous solution, the micelles dissolve in aqueous solution and support the release of proteins. These simultaneous effects may have important consequences for the biological applications of the system.

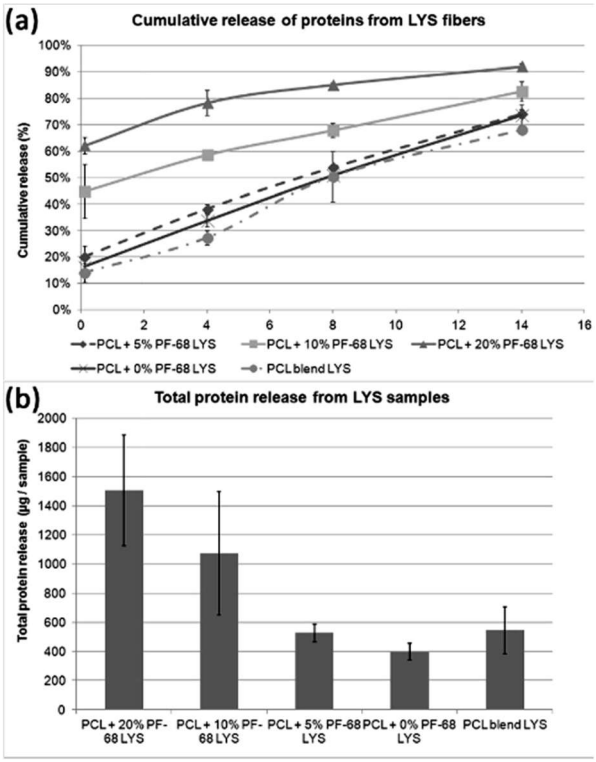

Fig. 6 Release kinetics of lyophilisate (LYO) from core/shell fibers. (a) Absolute release of proteins from LYO core/shell fibers. (b) Cumulative release of proteins from LYO core/shell fibers.

Growth factor release stimulates fibroblast metabolic activity and proliferation

Similarly, the release and encapsulation efficacy of samples containing platelet lyophilisates was evaluated. Platelet lyophilisates were harvested from human platelets and contained a broad spectrum of active agents. Multiplexed immunoassay was performed for quantification of bioactive proteins.

The content of cytokines, chemokines and growth factors was evaluated (Table 1). The analysis showed a higher presence of anti-inflammatory cytokines such as IL-1ra and IL-10. The IL-4 and IL-13 were detected in concentrations below 20 pg ml^{-1}. The pro-inflammatory cytokines were present in higher concentrations (IL-17, IL-8, IL-9, INF-γ) and TNF-α were detected in higher concentrations. The concentration of IL-1b, IL-2, IL-5, IL-6, IL-7 was below 50 pg ml^{-1}. RANTES was the dominant chemokine present in platelets. In addition, MIP-1b, eotaxin, IP-10 and MCP-1 were present in concentration above 50 pg ml^{-1}. However, from the tissue engineering point of view, the growth factors have the highest importance for stimulating cell proliferation and differentiation. PDGF-bb was the most abundant growth factor identified by X-MAP assay. In addition VEGF and bFGF were present in higher concentration. G-CSF and GM-CSF were also present in concentration above 100 pg ml^{-1}. In addition, ELISA was performed for quantification of additional growth factors. EGF, HGF, KGF and SDF-1α had the highest concentration.

The release was tested from samples containing embedded platelet lyophilisates (4.5 μg_{LYO} mg_{PCL}^{-1}) by either blend centrifugal spinning (PCL blend LYO) or emulsion centrifugal spinning. The emulsion centrifugal spinning was performed with 0%, 5%, 10% and 20% PF-68. The release was analysed by quantification of the released proteins. The results showed that similar to the case of HRP, the release from PF-68 containing fibres was fostered as the PF-68 concentration was higher. PCL + 20% PF-68 showed fast release during the first 7 days. In the case of PCL + 10% PF-68 the release was more sustained and showed release over the overall 14 day period. The samples with low PF-68 content (PCL + 5% PF-68 and PCL + 0% PF-68) showed slow release similar to the blend fibres. The reason may be in limited desorption from the core/shell fibres. In the case of lower PF-68 content the core droplets may be hidden in the non-degradable PCL structure. The release is then governed by limited diffusion from non-eroding PCL bulk polymeric matrix. The slower release is also demonstrated by low total release during the incubation period. The samples with LYO embedded in 10% and 20% PF-68 showed total release in order of 15 µg. On the other hand, release from samples with slow release showed only release of 5 µg of protein during the incubation period.

The bioactivity of samples was tested on a model of 3T3 murine fibroblasts in a 14 day experiment. Cells adhered similarly to all samples and also cell proliferation was similar on all samples. Differences were seen only on day 7, when the lowest cell number and metabolic activity was detected on the

Table 1 Concentration of proteins in platelet lysate

Mediator	Averaged value, pg mL^{-1}	SD, pg mL^{-1}
Anti-inflammatory cytokines		
IL-1ra	236	3.3
IL-4	15	0.3
IL-10	58	0.9
IL-13	9	0.5
Pro-inflammatory cytokines		
IL-1b	7	0.1
IL-5	8	0.1
IL-6	21	2.3
IL-7	46	1.2
IL-8	116	5.0
IL-9	130	3.6
IL-12	128	12.8
IL-17	1043	48.4
IFN-γ	165	6.8
TNF-α	145	8.5
Chemokines		
RANTES	11 132	939.5
MIP-1a	13	0.6
MIP-1b	157	3.9
Eotaxin	78	1.6
IP-10	315	1.8
MCP-1(MCAF)	58	16.9
Growth factors		
VEGF	510	5.2
PDGF-bb	14 656	247.1
FGF basic	274	6.9
G-CSF	139	18.1
GM-CSF	98	3.8
EGF	591	123.0
HGF	514	49.2
KGF	50	5.5
SDF1-a	339	55.9

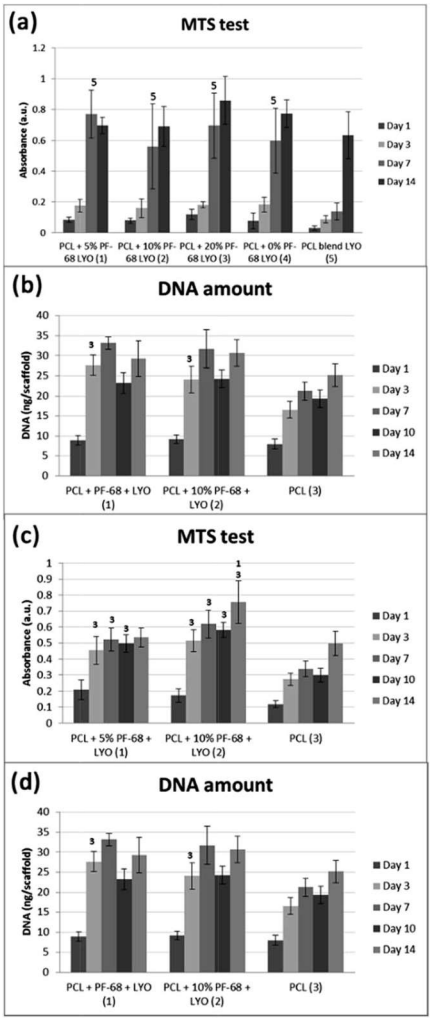

Fig. 7 Results of cell culture studies. (a) Cell metabolic activity of 3T3 fibroblasts detected using MTS assay. (b) Cell proliferation of 3T3 fibroblasts evaluated using quantification of DNA. (c) Cell metabolic activity of MG63 osteoblasts detected using MTS assay. (d) Cell proliferation of MG63 osteoblasts evaluated using quantification of DNA. * indicates significant differences ($p < 0.05$).

PCL blend sample. The results indicate that the release of platelet lyophilisates stimulated cell metabolic activity (Fig. 7a). However, the proliferation of cells on the blended sample was only slowed down and no significant difference was visible on day 14 (Fig. 7b). The measured data was confirmed using confocal microscopy (Fig. 8).

The cell culture study showed that release of platelet lyophilisates from core/shell fibres fosters cell proliferation and metabolic activity. However, the effect was rather transient and observed during the first 7 days. The reason may be connected with burst release from fibres, which was confirmed both in HRP and lyophilisates release experiments. The stability of proteins is rather limited and released proteins are rapidly degraded. For instance, the *in vivo* half-life of PDGF is only about 2 minutes (ref. 39) and EGF about 8 minutes.[40] Therefore, the effect of release in the first days is diminished. The release may be prolonged by utilizing a polymer with slower degradation[6] or by changing the ratio of degradable and non-degradable components.[41] In addition, the amount of released active molecules may not be sufficient. The embedded amount of the most abundant growth factor – PDGF was about 350 pg per sample. Therefore, the increase in protein concentration may improve the efficacy of cell stimulation. Platelet-derived formulations were shown as a source of growth factors stimulating wound regeneration. Barsotti *et al.*[42] showed platelet lyophilisates were able to promote proliferation of cells involved in wound healing in concentrations about 10–20% (v/v). However, we found in our previous study[43] that upon encapsulation the lower concentrations of released platelet growth factors are sufficient to promote cell response compared to non-encapsulated platelets. This effect might be caused by the proximity of released growth factors to cells and formed bioactive molecule gradients. Similarly, Sell *et al.*[44] prepared platelet lyophilisates-enriched nanofibres and showed improved cell colonization. Recombinant growth factors could be used to increase the loading of fibres and the amount of

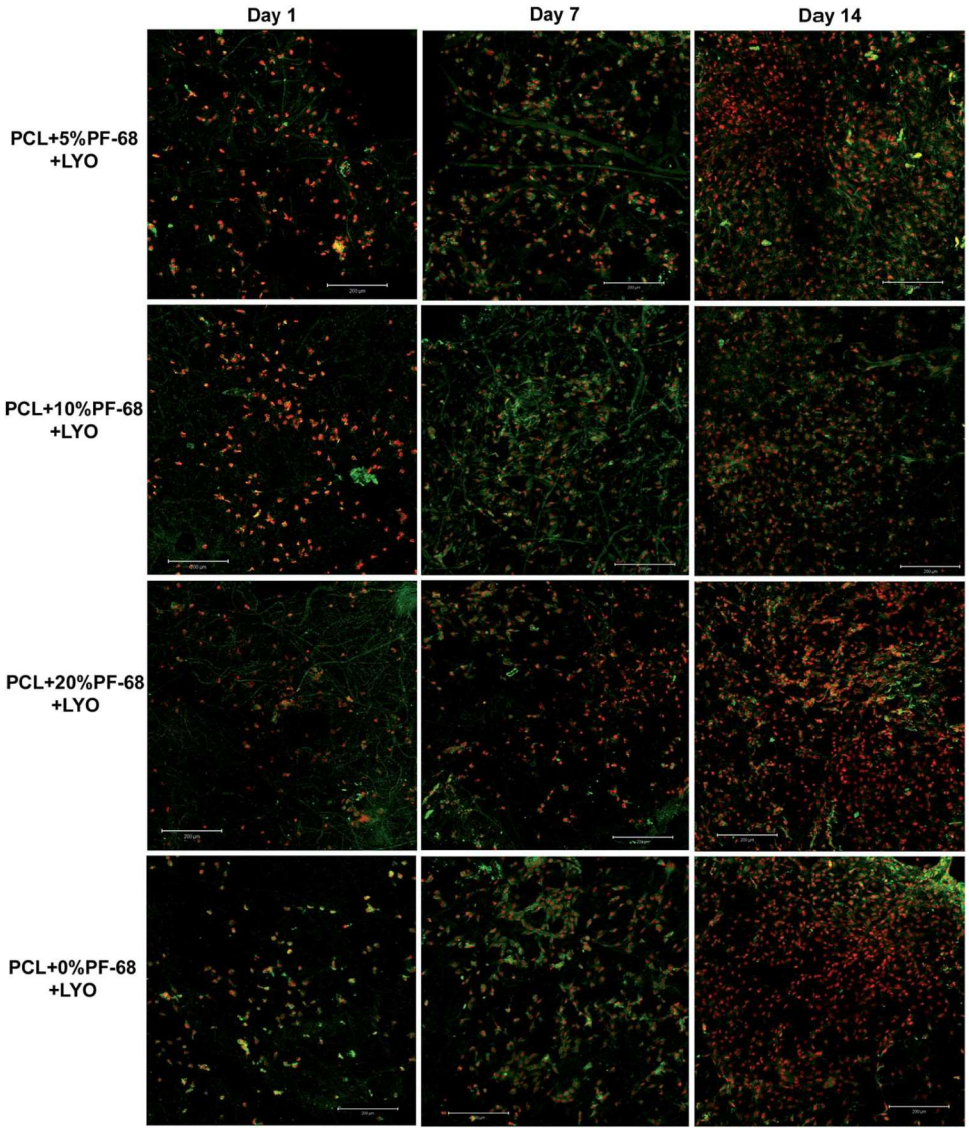

Fig. 8 Confocal microscopy of coaxial nanofibers seeded with 3T3 fibroblasts. Cells were stained with DiOC (green colour) and propidium iodide (red colour) and visualized using confocal microscopy on day 1, 7 and 14.

active molecules released. Yang *et al.*[45] prepared core/shell nanofibres loaded by bFGF. The fibrous dressing showed improved wound regeneration *in vivo* compared to control samples without bFGF delivery. Similarly, Choi *et al.* prepared EGF enriched electrospun nanofibres and showed improved regeneration of chronic wounds.[46] Up to date, only few growth factors are approved for clinical use, including bFGF, BMP-4 and BMP-7, which were successfully tested in clinical trials.[47] However, significant change in formulation results in further clinical tests and the produced growth factors are not easily accessible on the market. Therefore, we believe that natural sources of growth factors from clinically well characterized sources, such as platelets, are the most promising source of growth factors for tissue engineering applications. Autologous PRP has already been used in clinical applications for their stimulating effect on cells and tissue healing, even without cell therapy.[48]

The proposed scaffold is designed for tissue engineering applications. Fibres produced by centrifugal spinning have fibrous morphology mimicking the ECM and high pore interconnection. The key advantage of electrospun scaffolds is less compacted scaffold morphology with larger pores. The higher pore size allows cells to penetrate deeply into the scaffold. The importance of penetration was demonstrated by Pham *et al.*[49] Notably, the optimal pore size differs significantly for different types of cells. Pore sizes >300 μm have been recommended for vascularization in bone tissue engineering,[50] whereas fibroblasts have been demonstrated to prefer a pore size of 6–20 μm.[51]

The centrifugal spinning process produces fibrous scaffolds enabling efficient penetration of cells to the scaffold. Recently, we compared the penetration to PCL scaffolds prepared by electrospinning and centrifugal spinning.[21] The structure of the fibrous scaffold prepared by centrifugal spinning technology is optimal for application in skin tissue engineering. In the present work we have shown that the produced core/shell fibres fostered fibroblasts proliferation and enhanced metabolic activity. Nanofibrous scaffolds prepared by electrospinning have been shown as wound dressing.[52,53] In addition, Plencner *et al.*[54] recently showed the application of PCL fibres for stimulation of internal wound healing.

However, the application of the proposed system is not limited just to the field of skin tissue engineering. The platelet lyophilisates enriched core/shell fibres produced by centrifugal spinning have potential for bone tissue engineering. The potential for bone tissue engineering was evaluated by comparing core/shell samples (PCL with 5% and 10% PF-68 and embedded lyophilisates) with non-functionalized PCL fibres. The MTS assay showed significantly higher metabolic activity on samples functionalized by platelet lyophilisates than on non-functionalized samples during the first week (Fig. 7c). In the case of 5% PF-68 rapid growth of metabolic activity was observed between day 1–3. Similarly in the 10% PF-68 sample the rapid growth of metabolic activity was between days 1 and 3. However, the metabolic activity was further increased in subsequent days and steadily rose until day 14. Cell proliferation assay confirmed the trend in the MTS assay. However, the cell number was significantly higher on day 3 (Fig. 7d). The cell number on the following day was stable and control PCL achieved a comparable level on day 7. Confocal microscopy showed that cell number on day 7 was higher on samples with platelet lyophilisates and on day 14 similar on all scaffolds (Fig. 9).

The positive effect of platelet-based formulations on bone tissue regeneration has been presented in numerous publications.[55–57] The proposed technology of core/shell centrifugal spinning combines the advantages of 3D scaffolds with drug delivery structure. In addition, the soft-nature of the scaffold and degradation in time-frame of tissue regeneration ensures proper osteoinductive and osteoconductive properties.

The current study introduced novel core/shell centrifugal spinning technology. The results indicate that PF-68 based W/O emulsification is efficient in protecting bioactive proteins and enables the formation of stable emulsions processable to core/shell fibres by centrifugation spinning. In addition we have demonstrated the encapsulation of platelet lyophilisates to the core/shell fibres and biocompatibility with fibroblasts and osteoblasts. However, it is important to state that the presented results rather demonstrate the feasibility of core/shell centrifugal spinning technology. The new concept of core/shell centrifugal spinning is connected with numerous drawbacks. Work focusing on the stability of emulsion is essential for efficient encapsulation of diverse active molecules. The stabilization of the core phase and elimination of burst release will prolong the release times to achieve long-term protein release. Nevertheless, the biological properties of the system should be carefully validated on primary and stem cell models and relevant *in vivo* models.

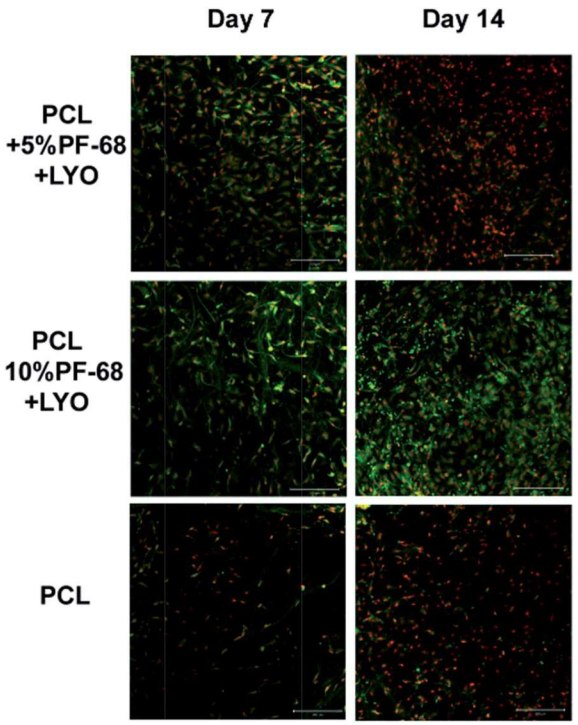

Fig. 9 Confocal microscopy of coaxial nanofibers seeded with MG-63 cells. Cells were stained with DiOC (green colour) and propidium iodide (red colour).

Experimental

Emulsion centrifugal spinning

The emulsion centrifugal spinning technology is based on a double emulsification procedure followed by centrifugal spinning processing. First, 30% (w/v) Pluronic F-68 (PF-68, Sigma-Aldrich) dissolved in 90% ethanol is mixed with encapsulated protein dissolved in 50% ethanol and pure ethanol to achieve solution of 0.1, 1, 5, 10 or 20% PF-68 and encapsulated protein in 70% ethanol. The emulsification process is performed by drop-wise mixing of components followed by sonification. The emulsion of PF-68 and proteins is subsequently emulsified with 50% polycaprolactone (PCL, 45 000 Da, Sigma-Aldrich) dissolved in chloroform to obtain 40% PCL dissolved in chloroform : ethanol. The ratio of the chloroform phase to the ethanol phase is 4 : 1. The ethanol phase is added drop-wise under stirring. The prepared emulsion is immediately processed by centrifugal spinning. The centrifugal spinning was performed by a Forcespinning process on a Cyclone L-1000 MD (Fiberio). All samples were processed using G30 needles at 11 000 rpm and collector distance 10 cm. The fibres were collected on a vacuum assisted deposition system to prepare more condensed samples.

Evaluation of PF-68 emulsified in PCL using tensiometry and laser scattering

The effect of Pluronic F-68 in ethanol on surface tension was evaluated using a bubble-pressure tensiometre (BP50, Kruss).

The samples with 0%, 1%, 5%, 10% and 20% PF-68 in ethanol or mixed with PCL were analysed using stable surface age mode. The results were interpreted as dependence of surface tension on time. The size distribution and zeta-potential of PF-68 droplets was analysed using a Zetasizer ZS (Malvern). The zeta-potential was evaluated using 40% PCL in chloroform as the continuous phase and PF-68 in 70% ethanol : water mixture as the droplet phase. Additional measurement focused on evaluating PF-68 in ethanol. The average droplet diameter was measured by dynamic light scattering (DLS) at 25 °C and an angle of 90° using a 5 mW He/Ne laser at 633 nm.

Centrifugal spinning of PCL/PF-68 coaxial samples for evaluation of core morphology

Coaxial fibers are based on mixture of two polymeric phases. The shell phase is supports cell adhesion and core is utilized for delivery of active molecules. In order to evaluate the possibility to prepare core/shell fibers by centrifugal spinning, morphology of the core phase, FITC-labelled bovine serum albumin (FITC-BSA) was used as a model drug. The samples were prepared as described previously and contained 300 μg ml^{-1} FITC-BSA in the core of the fibres. We prepared samples containing 0% PF-68 and FITC-BSA dispersed in 40% PCL (PCL/0% PF-68 (FITC-BSA)), 5% PF-68 and FITC-BSA dispersed in 40% PCL (PCL/0% PF-68 (FITC-BSA)), 10% PF-68 and FITC-BSA dispersed in 40% PCL (PCL/10% PF-68 (FITC-BSA)), 20% PF-68 and FITC-BSA dispersed in 40% PCL (PCL/20% PF-68 (FITC-BSA)). The control sample was prepared by directly dissolving a corresponding amount of FITC-BSA in 40% PCL solution (PCL blend FITC-BSA). The samples were centrifugally spun at 11 000 rpm using a G30 emitter and static voltage of 48 V.

The morphology of fibres was evaluated using scanning electron microscopy (SEM). Air-dried samples of electrospun nanofibres were mounted on aluminium stubs and sputter-coated with a layer of gold using a Quorum Q150R. The samples were examined in Vega 3 SBU (Tescan) scanning electron microscope in the secondary electron mode at 15 kV. Mean fibre diameter was calculated by image analysis in the ImageJ program.

In order to examine the morphology of the core phase of emulsion nanofibres, confocal microscopy of the fluorescently labelled core was utilized. The distribution of FITC-BSA within the prepared fibres was observed using a Zeiss LSM 5 DUO confocal laser scanning microscope (FITC fluorescence, λ_{ex} = 488 nm, λ_{em} = 520–560 nm).

Preparation of platelet lyophilisates

Fresh human leukocyte-depleted platelet concentrate derived from buffy coat in additive solution was obtained from a blood transfusion service (Sumperk, Czech Republic). The platelet concentration in the bag was 1020 × 10^9 platelets per l. The bag was prepared from the blood of 16 donors to minimize the inter-individual differences. The platelets were delivered on the day of production. Platelet lysate was prepared by the freeze–thaw method. The whole bag was frozen (−80 °C) and thawed (37 °C) three times in total to disrupt the cellular membranes. The solution was aliquoted and centrifuged (4100 g/15 min) to get rid of the cellular debris. Subsequently, the lysate was lyophilized under 480 mT (VirTis BenchTop Pro Freeze Dryer, SP Scientific, PA, USA) for 24 hours. The lyophilized platelet lysate was stored at −80 °C until use.

Characterization of growth factor content

To quantify the concentrations of pro- and anti-inflammatory cytokines and growth factors the Bio-Plex 200 Multiplex System (Bio-Rad Laboratories, CA, USA) and enzyme-linked immunosorbent assay (ELISA, DuoSet®, R&D systems, USA) were used. To analyse the cytokine content of the platelet lysate, the commercially available cytokine panel (Bio-Plex Pro™ Human Cytokine 27-plex Assay, Bio-Rad Laboratories, CA, USA) was used in accordance with the manufacturer's instructions. The assay allows multiple cytokines to be quantified simultaneously in one well. Briefly, the platelet lysate was incubated with set of colour-coded magnetic beads, each conjugated with an antibody directed against a specific mediator. Biotinylated detection antibody was added and allowed to bind to streptavidin–phycoerythrin. To remove the unbound protein, thorough washing series were performed in between each step by an automatic wash station (Bio-Plex Pro™ II). Finally, the data were analysed using a BioPlex 200 instrument fitted with Bio-Manager analysis software (5 parameter curve fitting). The concentration of growth factors (EGF, HGF, KGF and SDF1α) in the lyophilized platelet lysate was quantified by conducting the ELISA according to the manufacturer's instructions.

Preparation of emulsion centrifugal 3D fibres with embedded platelet lyophilisates

The samples were prepared as described previously and contained 2 mg ml^{-1} platelet lyophilisates (LYO) in the core of the fibres. We prepared samples containing 0% PF-68 and platelet lyophilisate dispersed in 40% PCL (PCL/0% PF-68–LYO), 5% PF-68 and lyophilisate dispersed in 40% PCL (PCL/5% PF-68–LYO), 10% PF-68 and lyophilisate dispersed in 40% PCL (PCL/10% PF-68–LYO), 20% PF-68 and lyophilisate dispersed in 40% PCL (PCL/20% PF-68–LYO). The control sample was prepared by directly dissolving the corresponding lyophilisate in 40% PCL solution (PCL blend LYO). The samples were centrifugally spun at 11 000 rpm using a G30 emitter and static voltage of 48 V.

Drug release studies on model of horseradish peroxidase (HRP) and platelet lyophilisates

The samples were prepared as described previously and contained 300 μg ml^{-1} HRP in the core of the fibres. We prepared samples containing 0% PF-68 and HRP dispersed in 40% PCL (PCL/0% PF-68 HRP), 5% PF-68 and HRP dispersed in 40% PCL (PCL/5% PF-68 HRP), 10% PF-68 and HRP dispersed in 40% PCL (PCL/10% PF-68 HRP), 20% PF-68 and HRP dispersed in 40% PCL (PCL/20% PF-68 HRP). The control sample was prepared by directly dissolving the corresponding HRP in 40% PCL solution (PCL blend HRP). The samples were centrifugally spun at 11 000 rpm using a G30 emitter and static voltage of 48 V.

The samples containing HRP and LYO were subjected to a release experiment. The samples were cut into pieces (~50 mg) and incubated with 1 ml of TBS buffer at room temperature. At specific intervals, the TBS buffer was withdrawn and replaced with fresh buffer. Release of HRP or platelet lyophilisates from the fibres was determined using a fluorescent Quant-IT Protein Assay Kit (Invitrogen). The assay was performed according to the manufacturer's guide. Briefly, 10 μl of sample or standard was mixed with 200 μl of fluorescent dye. The resulting fluorescence product was measured using a Synergy H1 multiplate fluorescence reader (Biotec, ex 470 nm, em. 570 nm). All values represent mean ± standard deviation of at least four independent samples.

The enzyme activity of the released HRP was measured on day 1 colorimetrically using tetramethylbenzidine (TMB, Sigma Aldrich) as the substrate. The enzyme substrate reaction was terminated with 50 μl of 2 N H_2SO_4 after 30 s. The enzyme activity was measured at 450 nm using an ELISA reader (Biotec, Synergy HT). The enzymatic activity was calculated as a percent ratio of enzyme concentration measured by the TMB assay (active enzyme, Sigma-Aldrich) and enzyme concentration measured by the Quant IT Protein Assay (overall protein, Life Technologies). All values represent mean ± standard deviation of at least ten independent experiments. Each experiment was performed from four independent samples.

Culture and seeding of human osteosarcoma cells (MG63) and murine 3T3 fibroblasts

Before cell seeding, scaffolds were cut into round patches of 6 mm diameter and sterilized using ethylene oxide. Samples were seeded with 10×10^3 MG-63 cells (Cell Lines Service GmbH, Germany) or alternatively with 3×10^3 3T3 fibroblasts (Sigma Aldrich, MO, USA) per well of the 96-well plate. Cells were left to adhere to the scaffolds for 2 hours in 30 μL of culture media (DMEM supplemented with 2% foetal bovine serum and penicillin/streptomycin). Subsequently, medium was added to the total volume of 300 μL per well.

Metabolic activity determination

Metabolic activity was determined using the CellTiter 96® Aqueous One Solution Cell Proliferation Assay (MTS assay, Promega). At 1, 3, 7, and 14 days, the scaffolds were transferred to a new 96-well plate containing 100 μL of fresh medium per well and 20 μL of CellTiter 96® Aqueous One Solution Reagent. The formazan absorbance in 100 μL of the solution was measured (λ_{sample} = 490 nm, $\lambda_{reference}$ = 690 nm) after a 2 h incubation at 37 °C and 5% CO_2 using an ELISA reader (Synergy HT; BioTek). The absorbance of the samples without cells was deducted from the cell-seeded samples.

Quantification of DNA amount in samples

DNA content was determined using a Quant-iT™ dsDNA Assay Kit (Life Technologies) on days 1, 3, 7, and 14. To process the samples for the analysis of DNA content, 500 μL of cell lysis solution (0.2% v/v Triton X-100, 10 mM Tris (pH 7.0), 1 mM EDTA) was added to each sample. To prepare the cell lysate, the samples were processed through a total of 3 freeze/thaw cycles, *i.e.*, the scaffold sample was first frozen at −70 °C and then thawed at RT. Between each freeze/thaw cycle, the scaffolds were roughly vortexed. The prepared samples were stored at −70 °C until analysis. Sample (10 μL) was mixed with 200 μL of reagent solution and the fluorescence intensity was measured on a multiplate fluorescence reader (Synergy HT, λ_{ex} = 485 nm, λ_{em} = 525 nm). The data were processed using the calibration curve of the standards in the kit.

Cell morphology determination by confocal microscopy

After 1, 7 and 14 days of culture, the scaffolds seeded with cells were fixed with frozen methanol (−20 °C), rinsed twice with PBS, incubated in 10 μg ml^{-1} 3,3′-dihexyloxacarbocyanine iodide ($DiOC_6$(3); Invitrogen) for 45 min at RT, and then incubated in 5 μg ml^{-1} propidium iodide in PBS for 10 min. The scaffold was rinsed twice with PBS and scanned the same day. DiOC6 staining was used to visualize mitochondria and inner membranes, while propidium iodide staining was used to visualize cell nuclei. A Zeiss LSM 5 DUO confocal microscope at λ_{ex} = 488 and 560 nm and λ_{em} = 505–550 and 575–650 nm was used for $DiOC_6$ and propidium iodide detection, respectively.

Statistical analysis

The quantitative data were presented as mean ± standard deviation (SD). The results were evaluated statistically using one-way analysis of variance (ANOVA) and the Student–Newman–Keuls test. The level of significance was set at 0.05.

Conclusions

Core/shell centrifugation spinning technology enables the formation of fibres with embedded growth factors. The water-in-oil emulsification is based on the behaviour of Pluronic F-68 micelles enabling the encapsulation and protection of susceptible proteins. The results of the study are the formation of core/shell fibres containing the core phase in the form of distinct droplets. The release studies showed that an increased number of droplets is connected with improved encapsulation efficacy and prolonged release. However, due to the aqueous solubility of the core phase high burst release was observed. Testing of core/shell fibres with embedded platelet lyophilisates showed improved fibroblast and osteoblast metabolic activity and proliferation. The effect of released proteins was dominant during the first week of cultivation. Altogether, centrifugal electrospinning is a suitable method for fabricating protein loaded scaffolds for tissue engineering applications.

Acknowledgements

This work has been supported by the Ministry of Education, Youth and Sports within the National Sustainability Programme I, projects No. LO1309, LO1508, and by project No. IPv6, and by the Czech Science Foundation, project No. 15-15697S, Operational Program – Prague Competitiveness CZ.2.16/3.1.00/21528,

and the Grant Agency of Charles University (projects No. 1246314, 1228214, 1262414).

References

1 R. Langer and J. Vacanti, *Science*, 1993, **260**, 920–926.
2 D. W. Hutmacher, J. T. Schantz, C. X. Lam, K. C. Tan and T. C. Lim, *J. Tissue Eng. Regener. Med.*, 2007, **1**, 245–260.
3 L. Susan, *et al.*, *Biomed. Mater.*, 2006, **1**, R45.
4 W. J. Li, C. T. Laurencin, E. J. Caterson, R. S. Tuan and F. K. Ko, *J. Biomed. Mater. Res.*, 2002, **60**, 613–621.
5 D. Lukáš, A. Sarkar, L. Martinová, K. Vodseďálková, D. Lubasová, J. Chaloupek, P. Pokorný, J. Chvojka and M. Komárek, *Text. Prog.*, 2009, **41**, 59–140.
6 S. Sahoo, L. T. Ang, J. C.-H. Goh and S.-L. Toh, *J. Biomed. Mater. Res., Part A*, 2010, **93**, 1539–1550.
7 X. Jia, C. Zhao, P. Li, H. Zhang, Y. Huang, H. Li, J. Fan, W. Feng, X. Yuan and Y. Fan, *J. Biomater. Sci., Polym. Ed.*, 2011, **22**, 1811–1827.
8 L. Tian, M. Prabhakaran, X. Ding, D. Kai and S. Ramakrishna, *J. Mater. Sci.*, 2012, **47**, 3272–3281.
9 L. Tian, M. Prabhakaran, X. Ding, D. Kai and S. Ramakrishna, *J. Mater. Sci.: Mater. Med.*, 2013, **24**, 2577–2587.
10 B. M. Baker, A. O. Gee, R. B. Metter, A. S. Nathan, R. A. Marklein, J. A. Burdick and R. L. Mauck, *Biomaterials*, 2008, **29**, 2348–2358.
11 A. Guimaraes, A. Martins, E. D. Pinho, S. Faria, R. L. Reis and N. M. Neves, *Nanomedicine*, 2010, **5**, 539–554.
12 J. Nam, Y. Huang, S. Agarwal and J. Lannutti, *Tissue Eng.*, 2007, **13**, 2249–2257.
13 M. Simonet, O. D. Schneider, P. Neuenschwander and W. J. Stark, *Polym. Eng. Sci.*, 2007, **47**, 2020–2026.
14 C. Vaquette and J. J. Cooper-White, *Acta Biomater.*, 2011, **7**, 2544–2557.
15 M. Rampichova, J. Chvojka, M. Buzgo, E. Prosecka, P. Mikes, L. Vyslouzilova, D. Tvrdik, P. Kochova, T. Gregor, D. Lukas and E. Amler, *Cell Proliferation*, 2013, **46**, 23–37.
16 B. A. Blakeney, A. Tambralli, J. M. Anderson, A. Andukuri, D. J. Lim, D. R. Dean and H. W. Jun, *Biomaterials*, 2011, **32**, 1583–1590.
17 N. E. Zander, *J. Appl. Polym. Sci.*, 2015, **132**, 41269.
18 L. Wang, J. Shi, L. Liu, E. Secret and Y. Chen, *Microelectron. Eng.*, 2011, **88**, 1718–1721.
19 L. Ren, V. Pandit, J. Elkin, T. Denman, J. A. Cooper and S. P. Kotha, *Nanoscale*, 2013, **5**, 2337–2345.
20 A. M. Loordhuswamy, V. R. Krishnaswamy, P. S. Korrapati, S. Thinakaran and G. D. V. Rengaswami, *Mater. Sci. Eng., C*, 2014, **42**, 799–807.
21 M. Rampichova, M. Buzgo, J. Chvojka, E. Prosecka, O. Kofronova and E. Amler, *Cell Adhes. Migr.*, 2014, **8**, 36–41.
22 N. E. Zander, *J. Appl. Polym. Sci.*, 2015, **132**, 41269.
23 L. A. Mary, T. Senthilram, S. Suganya, L. Nagarajan, J. Venugopal, S. Ramakrishna and V. R. G. Dev, *EXPRESS Polym. Lett.*, 2013, **7**, 238–248.
24 E. V. Batrakova and A. V. Kabanov, *J. Controlled Release*, 2008, **130**, 98–106.
25 M. Ben Henda, N. Ghaouar and A. Gharbi, *J. Polym.*, 2013, **2013**, 7.
26 W. Brown, K. Schillen and S. Hvidt, *J. Phys. Chem.*, 1992, **96**, 6038–6044.
27 W. Brown, K. Schillen, M. Almgren, S. Hvidt and P. Bahadur, *J. Phys. Chem.*, 1991, **95**, 1850–1858.
28 R. Ivanova, B. Lindman and P. Alexandridis, *Langmuir*, 2000, **16**, 9058–9069.
29 K. A. G. Katsogiannis, G. T. Vladisavljević and S. Georgiadou, *Eur. Polym. J.*, 2015, **69**, 284–295.
30 S. K. Murase, L. P. Lv, A. Kaltbeitzel, K. Landfester, L. J. del Valle, R. Katsarava, J. Puiggali and D. Crespy, *RSC Adv.*, 2015, **5**, 55006–55014.
31 Y. Yang, X. Li, L. Cheng, S. He, J. Zou, F. Chen and Z. Zhang, *Acta Biomater.*, 2011, **7**, 2533–2543.
32 J. Pal, S. Singh, S. Sharma, R. Kulshreshtha, B. Nandan and R. K. Srivastava, *Mater. Lett.*, 2016, **167**, 288–296.
33 T. J. Sill and H. A. von Recum, *Biomaterials*, 2008, **29**, 1989–2006.
34 A. Mickova, M. Buzgo, O. Benada, M. Rampichova, Z. Fisar, E. Filova, M. Tesarova, D. Lukas and E. Amler, *Biomacromolecules*, 2012, **13**, 952–962.
35 H. J. Lee, A. McAuley, K. F. Schilke and J. McGuire, *Adv. Drug Delivery Rev.*, 2011, **63**, 1160–1171.
36 S. Ohtake, R. A. Martin, A. Saxena, D. Lechuga-Ballesteros, A. E. Santiago, E. M. Barry and V. Truong-Le, *J. Pharm. Sci.*, 2011, **100**, 3076–3087.
37 X. Li, H. Zhang, H. Li, G. Tang, Y. Zhao and X. Yuan, *Polym. Degrad. Stab.*, 2008, **93**, 618–626.
38 T. Briggs and T. L. Arinzeh, *J. Biomed. Mater. Res., Part A*, 2014, **102**, 674–684.
39 D. F. Bowen-Pope, T. W. Malpass, D. M. Foster and R. Ross, *Blood*, 1984, **64**, 458–469.
40 D. P. Calnan, A. Fagbemi, J. Berlanga-Acosta, T. Marchbank, T. Sizer, K. Lakhoo, A. D. Edwards and R. J. Playford, *Gut*, 2000, **47**, 622–627.
41 E. Prosecka, M. Buzgo, M. Rampichova, T. Kocourek, P. Kochova, L. Vyslouzilova, D. Tvrdik, M. Jelinek, D. Lukas and E. Amler, *J. Biomed. Biotechnol.*, 2012, **2012**, 428503.
42 M. Chiara Barsotti, P. Losi, E. Briganti, E. Sanguinetti, A. Magera, T. Al Kayal, R. Feriani, R. Di Stefano and G. Soldani, *PLoS One*, 2013, **8**, e84753.
43 M. Buzgo, R. Jakubova, A. Mickova, M. Rampichova, E. Prosecka, P. Kochova, D. Lukas and E. Amler, *Nanomedicine*, 2013, **8**, 1137–1154.
44 S. A. Sell, P. S. Wolfe, J. J. Ericksen, D. G. Simpson and G. L. Bowlin, *Tissue Eng., Part A*, 2011, **17**, 2723–2737.
45 Y. Yang, T. Xia, W. Zhi, L. Wei, J. Weng, C. Zhang and X. Li, *Biomaterials*, 2011, **32**, 4243–4254.
46 J. S. Choi, K. W. Leong and H. S. Yoo, *Biomaterials*, 2008, **29**, 587–596.
47 K. Lee, E. A. Silva and D. J. Mooney, *J. R. Soc., Interface*, 2011, **8**, 153–170.
48 E. Kon, G. Filardo, B. Di Matteo, F. Perdisa and M. Marcacci, *Operat. Tech. Sports Med.*, 2013, **21**, 108–115.
49 Q. P. Pham, U. Sharma and A. G. Mikos, *Biomacromolecules*, 2006, **7**, 2796–2805.

50 V. Karageorgiou and D. Kaplan, *Biomaterials*, 2005, **26**, 5474–5491.
51 J. L. Lowery, N. Datta and G. C. Rutledge, *Biomaterials*, 2010, **31**, 491–504.
52 K. T. Shalumon, K. H. Anulekha, K. P. Chennazhi, H. Tamura, S. V. Nair and R. Jayakumar, *Int. J. Biol. Macromol.*, 2011, **48**, 571–576.
53 S. M. Jung, G. H. Yoon, H. C. Lee and H. S. Shin, *J. Biomater. Sci., Polym. Ed.*, 2015, **26**, 252–263.
54 M. Plencner, B. East, Z. Tonar, M. Otahal, E. Prosecka, M. Rampichova, T. Krejci, A. Litvinec, M. Buzgo, A. Mickova, A. Necas, J. Hoch and E. Amler, *Int. J. Nanomed.*, 2014, **9**, 3263–3277.
55 R. Simman, A. Hoffmann, R. J. Bohinc, W. C. Peterson and A. J. Russ, *Ann. Plast. Surg.*, 2008, **61**, 337–344.
56 A. Malhotra, M. H. Pelletier, Y. Yu and W. R. Walsh, *Arch. Orthop. Unfall-Chir.*, 2013, **133**, 153–165.
57 A. Oryan, S. Alidadi and A. Moshiri, *Expert Opin. Biol. Ther.*, 2016, **16**, 213–232.

RSC Advances

PAPER

View Article Online
View Journal | View Issue

Cite this: *RSC Adv.*, 2018, **8**, 21889

Osteoinductive 3D scaffolds prepared by blend centrifugal spinning for long-term delivery of osteogenic supplements

Lukasova Vera,[*abc] Buzgo Matej,[b] Vocetkova Karolina,[ab] Kubíková Tereza,[d] Tonar Zbyněk,[d] Doupnik Miroslav,[b] Blahnova Veronika,[ab] Litvinec Andrej,[a] Sovkova Vera,[ab] Voltrová Barbora,[a] Staffa Andrea,[b] Svora Petr,[b] Kralickova Milena,[d] Amler Evzen,[be] Filova Eva,[ae] Rustichelli Franco[a] and Rampichova Michala[ab]

Bone regeneration is a long-term process requiring proper scaffolding and drug delivery systems. The current study delivers a three-dimensional (3D) scaffold prepared by blend centrifugal spinning loaded with the osteogenic supplements (OS) β-glycerol phosphate, ascorbate-2-phosphate and dexamethasone. The OS were successfully encapsulated into a fibrous scaffold and showed sustained release for 30 days. Furthermore, biological testing showed the osteoinductive properties of the scaffolds on a model of human mesenchymal stem cells and stimulatory effect on a model of osteoblasts. The osteoinductive properties were further proved *in vivo* in critical size defects of rabbits. The amount of bone trabecules was bigger compared to control fibers without OS. The results indicate that due to its long-term drug releasing properties, single step fabrication process and 3D structure, the system shows ideal properties for use as a cell-free bone implant in tissue-engineering.

Received 29th March 2018
Accepted 6th June 2018

DOI: 10.1039/c8ra02735h

rsc.li/rsc-advances

1 Introduction

Over the last few years, bone tissue engineering has gained increased attention. Despite the high regeneration potential of bone itself, prevalent cases of traumatic injury, tumor, infection or osteoporosis result in the formation of critical bone defects. The treatment of these complications is connected with serious socioeconomic problems and the risk of long-term disability for patients.[1] In cases where the spontaneous healing of bones is often insufficient, reconstruction using natural or artificial grafts is necessary.[2,3] Today, plenty of bone grafting methods exist, with autologous bone widely used. However, there remain some drawbacks such as the risk of disease transmission, limited integration of the graft and complex storage conditions.[4,5] Thus, alternative routes for the treatment of defects are being investigated. Traditionally, non-degradable metals are used as materials for bone implants. Non-degradable scaffolds have limits in terms of bone ingrowth into the scaffold and the scaffold does not respond to changes in bone organization and shape.[6] As a consequence, attention has been centered on biodegradable scaffolds. A number of manufacturing methods for biodegradable implants have recently been described – *i.e.* scaffolds can take the form of foams, three-dimensional (3D) printed scaffolds, fibrous scaffolds or demineralized extracellular matrix (ECM).[7] Bone scaffolds should meet several criteria such as possessing proper mechanics to withstand stress and strain in bone tissue, osteoconductivity for the promotion of proper cellular differentiation and osteoinductivity to enable connection with the surrounding bone.[8,9]

In elderly patients the incidence of fractures has increased significantly.[1] Moreover, fracture healing in older patients is slower due to the decreased regeneration capacity of bone. The risks, connected with autologous graft transplantations or the aspiration of the proper amount of autologous cells for cellular based scaffolds are therefore higher with increased patient age. As a solution, non-cellular based scaffolds enriched with bioactive compounds stimulating bone regeneration are attractive alternatives for the treatment of bone fracture healing.[10] Since the regeneration process of bone is long, the supplementation of active molecules should be combined with systems prolonging drug delivery. The combination of drugs with drug delivery systems and scaffolds not only prolongs the bioavailability of the drugs, but also results in increased local

[a]*Laboratory of Tissue Engineering, The Czech Academy of Sciences, Institute of Experimental Medicine, Videnska 1083, 142 20 Prague 4, Czech Republic. E-mail: vera_lukasova@labdemo.cz; Fax: +420 2 9644 2387; Tel: +420 2 9644 2387*

[b]*University Center for Energy Efficient Buildings, Czech Technical University in Prague, Trinecka 1024, 273 43, Bustehrad, Czech Republic*

[c]*Department of Cell Biology, Faculty of Science, Charles University, Prague, Czech Republic*

[d]*Department of Histology and Embryology and Biomedical Center, Faculty of Medicine in Pilsen, Charles University, Karlovarská 48, 301 00, Pilsen, Czech Republic*

[e]*Institute of Biophysics, 2nd Faculty of Medicine, Charles University, V Uvalu 84, 150 06 Prague 5, Czech Republic*

concentration and stimulates bone healing in a spaciotemporal manner. Suitable bioactive compounds for osteogenesis promoting factors include widely used osteogenic supplements (OS)[11,12] *e.g.* β-glycerol phosphate, ascorbate-2-phosphate, dexamethasone and also growth factors such as bone morphogenetic protein-2 (BMP-2) and -7, insulin growth factor or fibroblast growth factor.[13–15]

An advantage of drug releasing scaffolds is their active stimulation of the bone healing process. Electrospinning is one of the most utilized technologies for producing biomimetic and drug releasing scaffolds in bone tissue engineering.[16] However, despite numerous advantages, electrospun scaffolds have a two-dimensional (2D) morphology, eliminating their practical application in healing large bone defects. For instance, the size of the pores is often insufficient to allow cell penetration.[17] The goal of this study is to overcome the inherent properties of fibrous scaffolds to improve the osteogenesis of seeded cells and subsequently to test the properties *in vivo*. This can be achieved by a centrifugal spinning method, which allows for the production of 3D scaffolds with higher pore diameters.[18] In the current work we aim to develop drug releasing 3D fibrous scaffolds by using a blend centrifugal spinning process. The technology of blend centrifugal spinning enables bioactive compounds to be encapsulated into the scaffold and their subsequent gradual release. The present work describes the fabrication, properties and osteoconductive potential of scaffolds prepared from poly-ε-caprolactone (PCL) with encapsulated OS. For *in vitro* testing of these scaffolds Saos2 osteosarcoma cell line as model of mature osteoblasts and hMSCs as multipotent stem cells were used.

2 Material and methods

2.1 Fibrous scaffold preparation using centrifugal spinning technology

Fibrous meshes were prepared using a centrifugal spinning device (Cyclone 1000 L/M Forcespinning® device, Fiberio, McAllen, TX, USA). 13% PCL (molecular weight 80 kDa, Sigma Aldrich, St. Louis, USA) and 16% PCL (molecular weight 45 kDa, Sigma Aldrich, St. Louis, USA) were dissolved in a mixture of acetic and formic acid in a volume ratio of 1 : 1 and blended with OS (β-glycerol phosphate, ascorbate-2-phosphate and dexamethasone). The spinneret was based on a flat disc with three orifices of G30 in size and a rotation speed of 10 000 rpm was used to prepare the fibrous meshes. The fibers were deposited on spunbond textile using vacuum-assisted deposition. Fibers with 4 different concentrations of OS were prepared: once concentrated OS (OS1), two times concentrated (OS2), five times concentrated (OS5) and ten times concentrated (OS10) (Table 1). Plain PCL fibers were used for control samples (CGM, COM). The spinning conditions for all groups were constant to evaluate the effect of polymeric blend properties on scaffold performance.

2.2 Characterization of fibrous scaffolds prepared using centrifugal spinning

The prepared fibers were visualized using scanning electron microscopy (SEM) and fiber diameter was determined. Samples were coated with a thin layer of platinum using a Quorum Q 150R S device (3 cycles, Quorum Technologies, Lewes, GB) and visualized using SEM (Tescan Vega 3, Brno, Czech Republic). The acceleration voltage for all samples was 10 kV. Fiber diameter and pore size was analyzed in the ImageJ program. The chemical composition of the scaffolds was analyzed using Fourier Transform Infrared-Attenuated Total Reflectance (FTIR-ATR) spectroscopy. Samples of plain PCL and PCL with OS were pelleted using a manual press. The pellets were analyzed using FTIR-ATR (IRAffinity-1, Shimazu with ZnS ATR). The measurement was performed with Happ-Ganzel apodization, at a resolution of 8 cm^{-1} and 20 scans per spectrum.

2.3 Determination of phosphate using HR-SEM

The samples were observed with a Zeiss scanning electron microscope Merlin equipped with an energy dispersive spectrometer (EDS) by Oxford Instruments with a silicon drifted detector X-Max 150. EDS measurements were carried out with charge compensator (injected medium was nitrogen), accelerating voltage 5 kV, beam current 1 nA, working distance – 8.5 mm. The EDS maps were analyzed with AZTEC software by Oxford Instruments. Samples were mounted on conductive carbon tape. The samples were not coated.

2.4 Characterization of phosphate release

To quantify the release of β-glycerol phosphate and ascorbate-2-phosphate from the fibrous scaffolds, we quantified the phosphate using ammonium molybdate. The release experiment was based on testing of samples with a size of 1 cm^2. The samples were placed in an Eppendorf tube and 1 mL of TBS was added to each sample. At specific time intervals, the supernatant was collected and frozen until analysis. 1 mL of Tris-buffered saline (TBS) was added to the scaffolds until the next time-interval. After completing the release experiment, the samples were dissolved in chloroform and resuspended in TBS for further analysis.

The analysis was performed in Eppendorf tubes. The samples were placed into Eppendorf tubes containing 0.25 mL

Table 1 Sample naming list and OS concentrations used for samples preparation by blend centrifugal spinning method[a]

Sample	asc-2-P (μg mL^{-1})	β-GP (mM)	dex (nM)	Sample	asc-2-P (μg mL^{-1})	β-GP (mM)	dex (nM)
OS1	40	10	100	OS5	200	50	500
OS2	80	20	200	OS10	400	100	1000

[a] asc-2-P, ascorbate-2-phosphate; β-GP, β-glycerol phosphate; dex, dexamethasone; OS, osteogenic supplement.

of 2.5% ammonium molybdate solution followed by 0.25 mL of 10% ascorbic acid solution (freshly prepared), mixed thoroughly, and heated for 5 min in a boiling water bath. After cooling the samples in a cold-water bath for 5 min, the optical density at 820 nm was measured using a Synergy H1 microplate reader. In each series of measurements, parallel determinations were made of the blank values of the reagent solution and a standard preparation. The release experiment was performed in 5 replicates and samples were analyzed as absolute release and cumulative release.

2.5 Saos2 and hMSC seeding of the scaffold

Before cell seeding, PCL nanofibers were cut into round patches 6 mm in diameter and sterilized using ethylene oxide. Samples were placed in the 96-well plate and pre-wet with 20 μL of growth media. Samples were seeded with 25×10^3 human bone marrow-derived mesenchymal stem cells (hMSCs; ScienCell, San Diego, California, USA) or with 10×10^3 Saos2 osteosarcoma cell line (Cell line service, Germany) per well in the 96-well plate. Samples (OS1, OS2, OS5, and OS10) with hMSCs were cultivated in growth medium (MEM supplemented with 10% fetal bovine serum (FBS) and Penicillin/Streptomycin; Sigma Aldrich, USA) and with Saos2, the same samples, were cultivated in growth medium (McCoy's 5A Medium supplemented with 15% FBS and Penicillin/Streptomycin; Sigma Aldrich, USA), without any other supplement. Two types of controls were used; plain PCL fibers cultivated in growth medium (CGM) and plain PCL fibers cultivated in osteogenic medium (COM). Osteogenic medium was growth medium supplemented with 10 mM β-glycerol phosphate, 100 nM dexamethasone and 40 μg mL^{-1} ascorbate-2-phosphate. One half of the culture medium was changed on days 7 and 14. Minimal changing of medium was used so as to not to wash out the OS released from the scaffolds to the medium.

2.6 Cell viability analysis

To determine the metabolic activity of the cells seeded on the prepared scaffolds, the MTS assay (CellTiter96® AQueous One Solution Cell Proliferation Assay, Promega, WI, USA) was used on days 1, 3, 7, 14 and 21 of the experiment. Briefly, the scaffolds were transferred into new wells to prevent the cells adhered to the tissue culture plastic to misrepresent the measured data. Subsequently, 100 μL of fresh media and 20 μL of the MTS substrate were added to each well. After 2 hour incubation at 37 °C, subsequently, 100 μL of the cultured solution was transferred to a new clean well. The absorbance of the media was detected at 490 nm using a microplate reader (Infinite® M200 PRO; Tecan, Switzerland). The background absorbance (690 nm) and the absorbance of the medium without cells were subtracted from the measured absorbance.

2.7 Cell proliferation analysis

The proliferation of cells on the scaffolds was determined using a Quant-iT™ dsDNA Assay Kit (Thermo Fisher Scientific, Waltham, MA, USA) from the amount of DNA on days 1, 3, 7, 14 and 21. The scaffolds were put into a vial with 200 μL of cell lysis solution (0.2% v/v Triton X-100, 10 mM Tris (pH 7.0), and 1 mM EDTA) and processed through 3 freeze/thaw cycles; the scaffolds were first frozen at −80 °C and thawed at room temperature. Between each freeze/thaw cycle, the scaffolds were roughly vortexed. A sample (10 μL) was mixed with 200 μL of reagent solution and fluorescence intensity was detected using a multiplate fluorescence reader (Infinite® M200 PRO; Tecan, Switzerland; $\lambda_{ex} = 485$ nm, $\lambda_{em} = 525$ nm). The DNA content was determined according to the calibration curve using the standards in the kit.

2.8 Visualization of cell adhesion and proliferation on scaffolds

DiOC6(3) (3,3′-diethyloxacarbocyanine iodide; Invitrogen, Molecular Probes) staining was used to detect cell adhesion on the scaffolds on days 1, 7, 14 and 21. The samples were fixed with frozen methyl alcohol (−20 °C) for 10 min and rinsed with phosphate buffered saline (PBS; pH 7.4). A fluorescent probe DiOC6(3) at a concentration of 1 μg mL^{-1} in PBS was added and incubated with the samples for 45 min at room temperature. Subsequently, the samples were rinsed with PBS, and propidium iodide (Sigma Aldrich, USA) at concentration of 5 μg mL^{-1} in PBS was added for 5 min, followed by rinsing with PBS. The samples were visualized using a ZEISS LSM 5 DUO confocal microscope. $\lambda_{ex} = 488$ and 560 nm and $\lambda_{em} = 520$ and 580 nm was used for DiOC6(3) and propidium iodide detection, respectively.

2.9 Cell visualization on scaffolds using scanning electron microscopy

The hMSC's morphology was evaluated by SEM on days 1 and 14. Scaffolds with hMSCs were washed in PBS and fixed in 2.5% glutaraldehyde for 2 hours at 4 °C. Then the samples were dehydrated in ethanol ranging from 35–100%. To dry the scaffolds hexamethyldisilazane (Sigma-Aldrich) was added. Scaffolds were analyzed using Vega 3 Tescan as described previously.

2.10 RNA isolation and qPCR analysis

The total RNA was isolated using a Qiagen RNA mini-kit (Qiagen, Hilden, Germany) according to the protocol provided by the manufacturer. Reverse transcription was performed using a RevertAid H Minus First Strand cDNA Synthesis Kit (Thermo Scientific, Waltham, MA, USA). Transcript levels were evaluated using quantitative PCR (qPCR). qPCR was performed using the Light Cycler 480 II real-time PCR system (Roche, Basel, Switzerland) with TaqMan Master Mix and TaqMan probes (Thermo Scientific, Waltham, MA USA) following the protocols from the manufacturer. The genes whose expression was analyzed by qPCR were RunX2 (86 bp, RUNX2, Hs01047973_m1, Thermo Scientific), osteocalcin (138 bp, BGLAP Hs01587814_g1, Thermo Scientific), type I collagen (66 bp, COL1A1 Hs00164004_m1, Thermo Scientific) and eukaryotic elongation factor (EEF1 Hs00265885_g1, Thermo Scientific). All samples were run in triplicates. The thermo cycling parameters were 95 °C for 10 min; 95 °C for 10 s, 60 °C for 10 s (45 cycles); and 40 °C for

1 min. All samples were scaled relative to the median of the EEF1 expression level, which was used as an endogenous control gene. Gene expression data were analyzed using the $2^{(-\Delta C_t)}$ method (relative quantification).

2.11 Detection of alkaline phosphatase activity

Alkaline phosphatase (ALP) activity was measured using a 1-Step™ PNPP kit (Thermo Scientific, Waltham, MA USA). 100 μL of PNPP was added to each well and incubated for 10 min. Subsequently, the reaction was stopped with 2 N NaOH. Absorbance was measured using a spectrophotometer at 405 nm (Infinite® M200 PRO; Tecan, Switzerland).

2.12 Detection of osteocalcin using indirect immunofluorescence staining

The presence of osteocalcin, a marker typical for osteogenic differentiation, was confirmed using indirect immunofluorescence staining on days 7, 14 and 21. Samples were fixed with frozen methanol (−20 °C) for 10 min, washed with PBS and incubated in 3% FBS in PBS/0.1% Triton X-100 for 30 min at room temperature. To detect osteocalcin, primary monoclonal antibody against osteocalcin (Rabbit anti-osteocalcin IgG, Peninsula Laboratories, dilution 1 : 20, San Carlos, CA USA) was added and the samples were incubated overnight at 2–8 °C. After three washes with PBS/0.05% Tween 20, the samples were incubated with secondary antibody, Alexa Fluor 488 conjugated anti-rabbit antibody (Thermo Scientific), at a dilution of 1 : 300 for 45 min. Subsequently, a solution of propidium iodide was added for 5 min (5 μg mL^{-1} in PBS) to visualize the cellular nuclei. Finally, the samples were washed three times with PBS/0.05% Tween 20. A confocal microscope (ZEISS LSM 5 DUO) was used to detect the present osteocalcin (Alexa Fluor 488: λ_{exc} = 488 nm, λ_{em} = 505–550 nm propidium iodide: λ_{exc} = 561 nm, λ_{em} = 630–700 nm).

2.13 Surgery and animal care

Scaffolds were implanted into the critical sized defects in the femur of New Zealand white rabbits. 22 male New Zealand white rabbits, 3 months old, weight approximately 3.0 kg, were obtained from a conventional breed (Velaz, Czech Republic) and bred in standard cages without bedding. The rabbits were fed ad libitum using standard granular mixture for rabbits (TM–MaK 1, Bergman, CZ). The Ethical Principles and Guidelines for Scientific Experiments on Animals were respected throughout the study. The maintenance and handling of the experimental animals followed EU Council Directive (86/609 EEC), and the animals were treated in accordance with the principles of Care and Use of Animals. The investigation was approved by the Expert Committee of the Institute of Physiology, The Czech Academy of Sciences, Prague, CZ, and conformed to Czech Animal Protection Law no. 246/92. The surgical procedure was conducted under general anesthesia using Narketan (0.5 mg kg^{-1}) and Xylapan (6 mg kg^{-1}) and subsequently inhalation of O_2 + 1.5–2.0% Halothane during surgery. In lateral femoral condyles, a critical size defect 6 mm in diameter and 10 ± 0.5 mm deep was made using a drill. Animals were divided into three groups. At group I (control group I, 7 animals) the defects were filled with PCL scaffolds. Defects of group II (control group II, 8 animals) were filled with PCL scaffolds with encapsulated OS. Defects of group III (tested group, 7 animals) were left empty, without any treatment. Scaffolds were cut into a cylinder shape with 6 mm in diameter and 10 mm in height and sterilized using ethylene oxide. Antibiotics (5 mg per kg per day i.m. of Marbocyl 2%) and analgesics (0.1 mg per kg per day s.c. of Meloxydil 5 ad us.vet.) were administered during the first 4 days. Rabbits were not limited in their movement after surgery. Euthanasia of the rabbits was performed 12 weeks after surgery, and the femoral condyles were examined. All of the harvested samples were fixed in 4% phosphate buffered formaldehyde.

2.14 Histological processing

Samples were demineralized in 5% solution of nitric acid (Merci, Brno, Czech Republic). After 7 days, nitric acid was neutralized by 5% solution of sodium sulfate for 1 hour and subsequently immersed in physiological solution for 24 hours. Every sample was cut in the center of the defect perpendicular to its longitudinal axis into two equal parts (13 × 13 × 5 mm). Tissue blocks were processed individually. Eight serial 5 μm thick histological sections were cut from the center of the healing defect from each paraffin-embedded tissue block. The sections were stained with haematoxylin–eosin, Verhoeff's haematoxylin with green trichrome[19] and picrosirius red (Direct Red 80, Sigma Aldrich, Munich, Germany) diluted in saturated picric acid solution was used to visualize the type I collagen (Rich and Whittaker, 2005). We used a circular polarizing filter (Hama, Monheim, Germany) crossed with a quarterwave λ/4 filter below the analyzer filter (U-GAN, Olympus, Tokyo, Japan) mounted on the Olympus CX41 microscope (Olympus, Tokyo, Japan). Methodology of the histological evaluation was described in detail elsewhere.[20,21]

2.15 Statistical analysis

Quantitative data are presented as mean values ± standard deviation (SD). The averaged values were determined from at least 3 independently prepared samples. Results were evaluated statistically using one-way analysis of variance and the Student–Newman–Keuls test (SigmaStat 12.0, Systat). The data from the histological analysis were processed with Statistica Base 9.1 (Stat-Soft, Inc., Tulsa, OK, USA). Testing of the randomness of bone distribution among compartments was based on the chi-squared distribution. The Mann–Whitney U test was used to test the quality of population medians among the groups in the study. All results were considered statistically significant if p was <0.05.

3 Results

3.1 Scaffold development and characterization

Scaffolds containing osteogenic supplements (OS) were prepared using blend centrifugal spinning technology. The technology is based on mixing a polymer solution with OS prior to the spinning process. Due to the substances mixing in

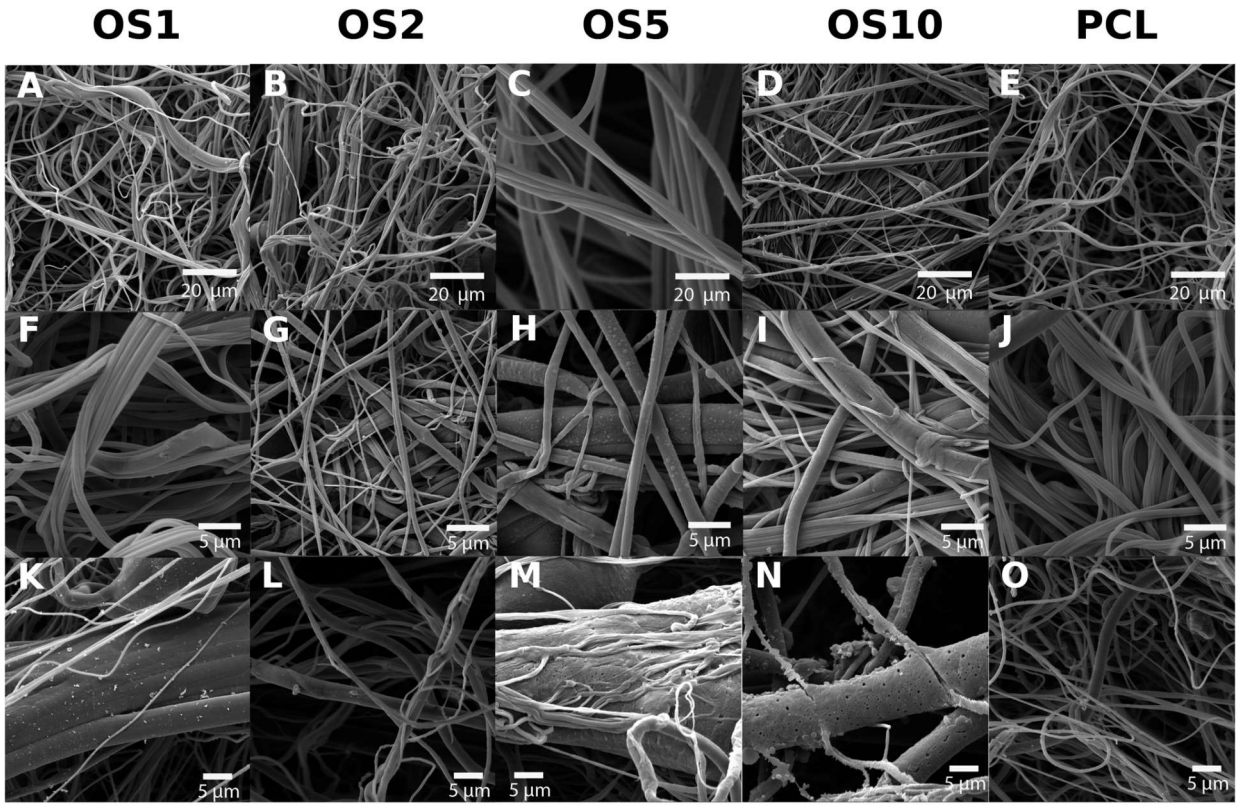

Fig. 1 Images from scanning electron microscopy of scaffolds. Micrograph of scaffold morphology with lower magnification (scale bar 20 μm) (A–E), detailed micrograph of fibers showing phosphate microdomains (scale bar 5 μm) (F–J), detailed fiber surface after 31 days washing in PBS (scale bar 5 μm) (K–O).

a liquid state, the OS are distributed along the fibers. The polymer selected for fiber development was PCL dissolved in acetic acid and formic acid. The acidic environment enabled the combination with high quantities of β-glycerol phosphate, ascorbate-2-phosphate and dexamethasone. The solutions were prepared containing different amounts of β-glycerol phosphate, ascorbate-2-phosphate and dexamethasone. Centrifugal spinning was performed using spinneret with G30 orifices and a rotation speed of 10 000 rpm.

The centrifugal spinning process resulted in the formation of a 3D fibrous mesh. The mesh was formed by fibers forming a porous structure with a thickness of about 3 mm. An analysis by SEM confirmed the fibrous character of all scaffolds (Fig. 1). A stereological analysis (Table 2) showed that with increase of OS concentration, the mean fiber diameter increased.

For the control PCL, the mean fiber diameter was 974.6 ± 299.1 nm (Table 2). Mean pore size was about 13.7 ± 29.8 μm^2 and maximum pore size was 326 μm^2. The scaffold contained polydisperse pores and the percentage of pores bigger than 5 μm^2 was 46.6%. For the OS1 sample with the lowest concentration of OS, the mean fiber thickness decreased to 739.7 ± 159.3 nm. The mean pore size decreased to 11.7 ± 20.5 μm^2. In case of OS2 group the fiber size further increased to 824.9 ± 271.2 nm. Similarly, in the group OS5 the mean fiber diameter increased to 1569.7 ± 1067.7 nm. The group showed high heterogeneity in fiber diameter, which may be related to change of solution properties. In case of OS10, the mean fiber diameter was 697.8 ± 527.7. Diameter of OS10 was lower compared to OS5, however the mesh contained higher presence of defects with non-fibrous morphology (Fig. 1N).

The encapsulation of OS was verified by FTIR-ATR spectroscopy (Fig. 2). The measurement showed the incorporation of β-glycerol phosphate, ascorbate-2-phosphate and dexamethasone into the scaffolds. The spectra of PCL without modification mainly contained a sharp peak corresponding to –C=O groups at 1700 cm^{-1} and C–H groups at 2800–2950 cm^{-1}. The addition

Table 2 Stereological characterization of prepared scaffolds[a]

	OS1	OS2	OS5	OS10	PCL
Fiber diameter (nm)	739.7	824.9	1569.7	697.8	974.6
Fiber diameter − SD (nm)	159.3	271.2	1067.7	527.7	299.1
Maximum pore size (μm^2)	205.0	157.9	204.5	33.3	326.0
Percentage of pores > 5 μm^2 (%)	51.1	43.3	58.0	39.3	46.6
Mean pore size (μm^2)	11.7	10.1	16.3	2.6	13.7
Mean pore size − SD (μm^2)	20.5	18.9	25.9	5.9	29.8

[a] asc-2-P, ascorbate -2-phosphate; β-GP, β-glycerol phosphate; dex, dexamethasone; OS, osteogenic supplement; PCL, poly-ε-caprolactone; SD, standard deviation.

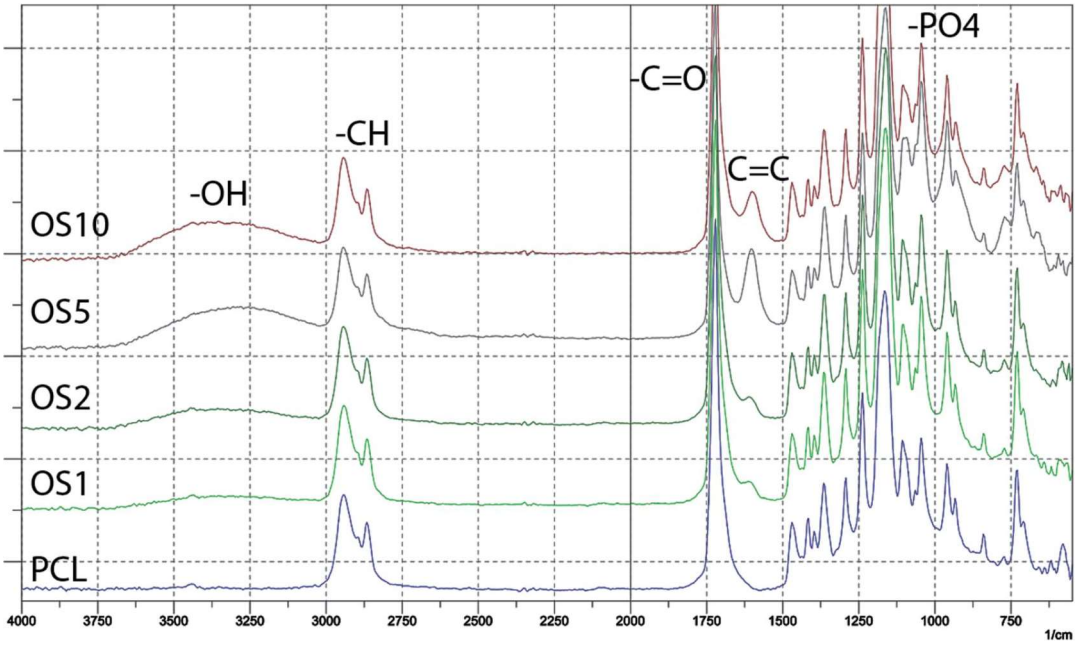

Fig. 2 Spectra of prepared scaffolds measured by FTIR-ATR spectroscopy.

of OS resulted in an increase of –O–H group resonance at 3200–3500 cm^{-1}. The hydroxyl group is present in all added supplements. The encapsulation of β-glycerol phosphate and ascorbate-2-phosphate was indicated by an increase in resonance of $-PO_4$ groups at 1000 cm^{-1}. The presence of dexamethasone was indicated by an increase of C=C resonance at 1600 cm^{-1}.

In addition, a high resolution-SEM (HR-SEM) with EDS detector was used to analyze the distribution of phosphate in the samples (Fig. 3). Phosphate was detected in all samples. The signal is distributed across all fibers. However, the phosphate was located in clusters, indicating the presence of β-glycerol phosphate and ascorbate-2-phosphate signals. In addition, in OS5 and OS10 samples, the phosphate and oxygen weight percentage (Table 3) was higher, indicating successful encapsulation of β-glycerol phosphate and ascorbate-2-phosphate.

Nevertheless, the release of phosphate contained in β-glycerol phosphate and ascorbate-2-phosphate was performed to analyze the bioavailability. The release was performed for 31 days (Fig. 4). The absolute release showed that the highest absolute amount of phosphate was released from the OS10 scaffold. A dose dependent total release was observed. The lowest amount was released from the OS1 and OS2 samples. The amount in OS5 was two times lower than in the OS10 samples. Interestingly, the cumulative release profile shows, that from the OS1 and OS2 samples, the release was more rapid than from the OS5 and OS10 samples. This indicates that the OS were located near the surface of the fibers, and after 10 days the depletion of OS leads to slower release. In the case of OS5 and

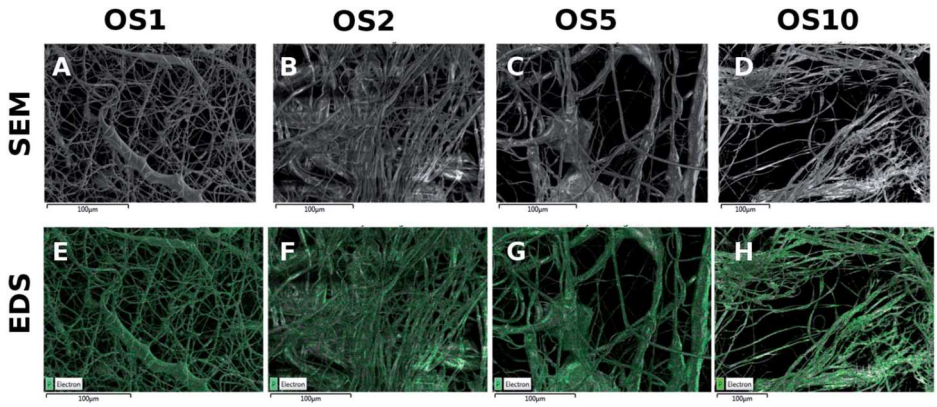

Fig. 3 HR-SEM analysis of PCL scaffolds. Images from scanning electron microscopy (A–D). Distribution of phosphate in PCL scaffolds with encapsulated OS, measured by HR-SEM with EDS detector (E–H).

Table 3 Weight percentage of carbon (C), phosphate (P) and oxygen (O) presented in PCL scaffold measured by HR-SEM

	C		P		O			C		P		O	
Sample	wt%	SD	wt%	SD	wt%	SD	Sample	wt%	SD	wt%	SD	wt%	SD
OS1	78.75	0.06	0.9	0.03	18.64	0.04	OS5	68.76	0.07	2.8	0.04	23.82	0.05
OS2	78.28	0.06	0.65	0.03	19.77	0.05	OS10	68.05	0.07	3.73	0.04	22.89	0.05

OS10, the release was sustained and showed near zero order kinetics. The half-time of release was fastest for the OS2 sample (8 days). OS1 showed a half time of 14.1 days and for the samples with the highest concentration of OS, OS5 and OS10, the half time of release was 23.8 and 23.2 days, respectively. The encapsulation efficiency calculated from total phosphate samples was highest for OS1 and reached 98.2 ± 62.1%. OS2 had lowest encapsulation efficiency reaching only 24.6 ± 10.8%. Samples OS5 and OS10 had 40.1 ± 22.4% and 35.9 ± 0.9% encapsulation efficiency.

Evaluation of dexamethasone release was problematic due to low concentration of dexamethasone in scaffolds. The maximal concentration of released dexamethasone was between 3.9 (OS1) and 39 ng (OS10). These values are under detection limit of both HPLC[22] and UV-Vis methods.[23] However, the effect of osteogenic supplements released from scaffolds was tested on model on Saos2 and hMSCs.

The results showed the successful encapsulation of OS to the fibrous structure and sustained release of factors for more than 10 days for OS1 and OS2 and for more than 30 days for OS5 and OS10.

3.2 Saos2 adhesion, proliferation and metabolic activity on scaffolds

In this study we tested fibers with 4 different concentrations of OS: once concentrated OS marked as OS1, two times concentrated (OS2), five times concentrated (OS5) and ten times concentrated (OS10). Two control samples were chosen, the

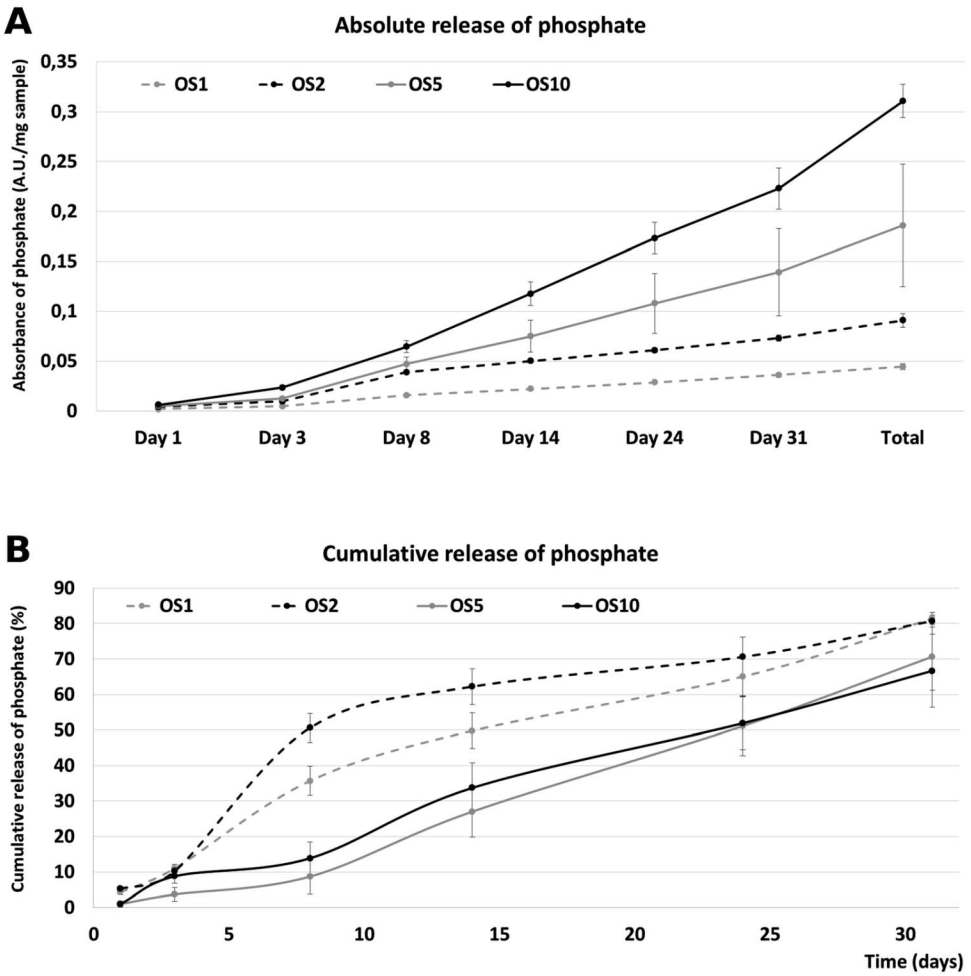

Fig. 4 Release of phosphate from fibers. Absolute release of phosphate over time (A). Cumulative release of phosphate from fibers (B).

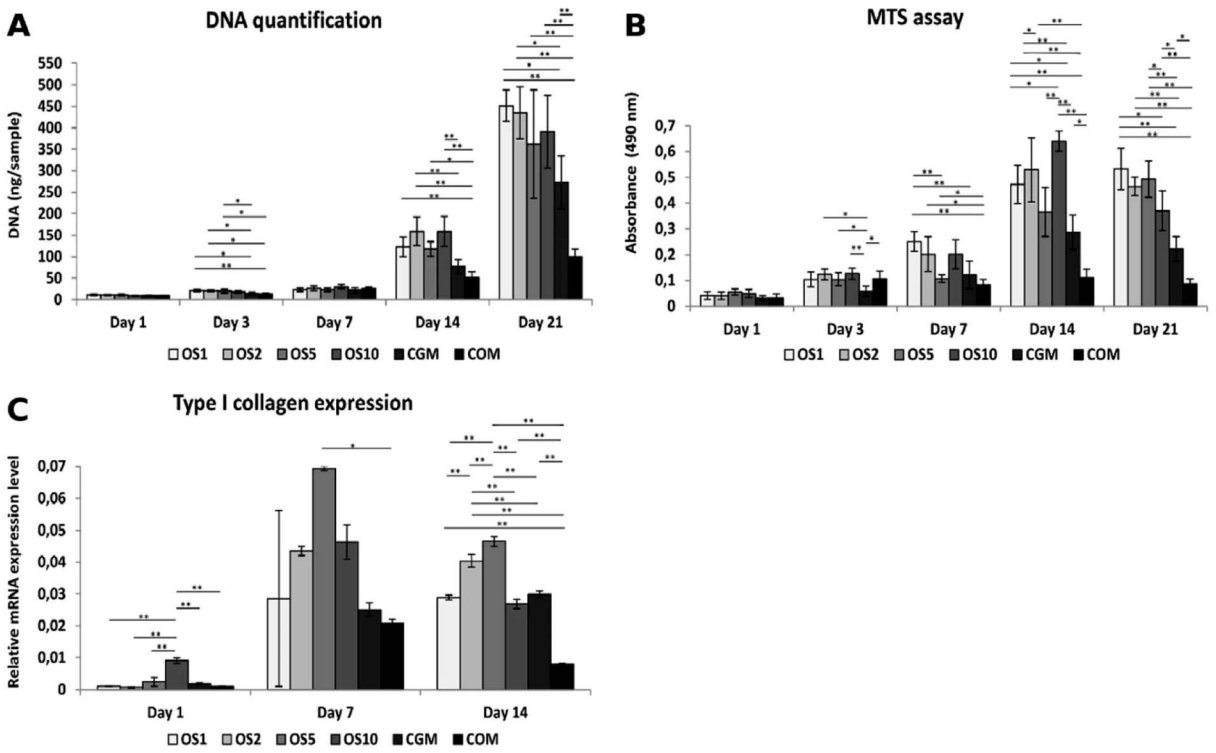

Fig. 5 Saos2 adhesion, proliferation, metabolic activity and type I collagen expression on scaffolds. Cell adhesion and proliferation was measured using quantification of DNA (A). Metabolic activity was determined from MTS assay (B). Relative expression of type I collagen was analyzed by qPCR (C). Statistical significance is shown above the columns (*$p < 0.05$; **$p < 0.01$).

cells seeded on plain PCL and cultivated in growth medium (CGM) and the cells seeded on plain PCL and cultivated in growth medium with OS (COM). To examine the effect of diverse concentrations of OS we tested the metabolic activity, proliferation and osteogenic differentiation of seeded cells.

The amount of DNA on scaffolds seeded with Saos2 was evaluated for DNA content (Fig. 5A), cells proliferated on all scaffolds as the amount of DNA was increasing. From day 7 we observed a huge growth of cells on the OS1–10 samples and CGM but on the COM samples cell ingrowth was slower. As Saos2 are normally cultured without OS, it possibly indicates that higher doses of OS work as inhibition agents on the Saos2 osteosarcoma cell line. The results are in agreement with confocal microscopy observation (data not shown).

Metabolic activity measured using an MTS metabolic assay (Fig. 5B) revealed a constant value of absorbance on the COM sample from day 3, although the gradual proliferation of cells was detected. Moreover, only on the OS1 and OS5 samples was the

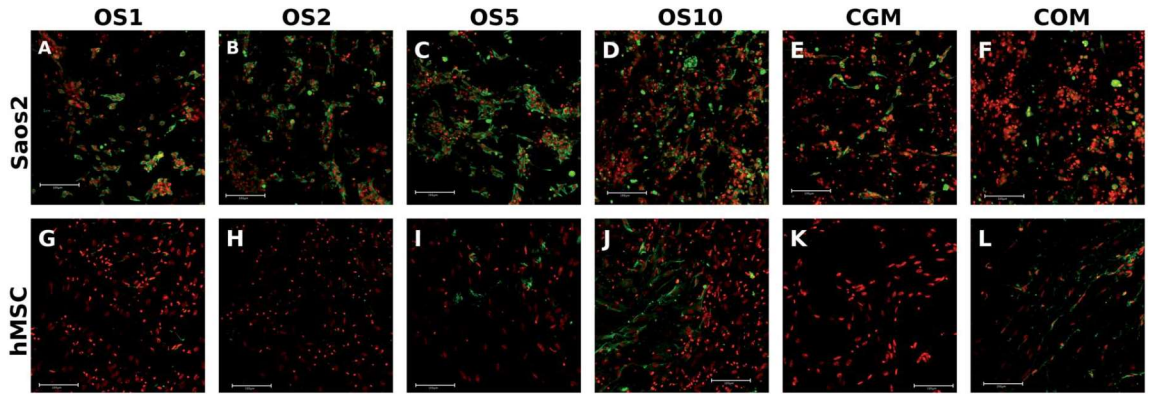

Fig. 6 Immunofluorescence staining of osteocalcin. Saos2 stained on day 21 (A–F) and hMSCs stained on day 14 (G–L). Osteocalcin was stained using indirect fluorescence (green color) and cell nuclei using propidium iodide (red color) and visualized using a confocal microscope. Magnification 200×, scale 100 μm.

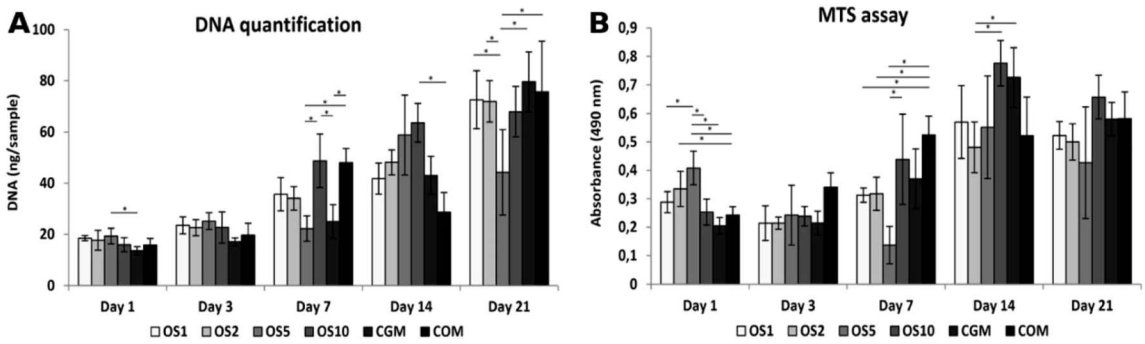

Fig. 7 hMSCs adhesion, proliferation and metabolic activity on scaffolds. Cell adhesion and proliferation was measured using quantification of DNA (A). Metabolic activity was determined from MTS assay (B). Statistical significance is shown above the columns (*$p < 0.05$; **$p < 0.01$).

continual increase in absorbance measured. On day 7, we detected the highest absorbance on the OS1 sample. On day 14, statistically higher absorbance was observed on the OS1–2 and –10 samples compared to the CGM and COM. Cells on the OS5 and CGM samples were more metabolically active compared to cells on the COM sample. On day 21, the absorbance detected on the OS1–10 samples were in all cases higher than the rate of absorbance measured on the CGM and COM samples.

3.3 Osteogenic marker expression of Saos2

Osteocalcin is an ECM protein associated with osteogenic differentiation. Indirect immunofluorescence staining was undertaken to visualize this protein (Fig. 6A–F). Clearly, on all samples on day 21 we observed osteocalcin, which was the most visible on the OS1–10 samples. However, even on both control groups we were able to detect high doses of osteocalcin as this protein is typically expressed by Saos2 cells.

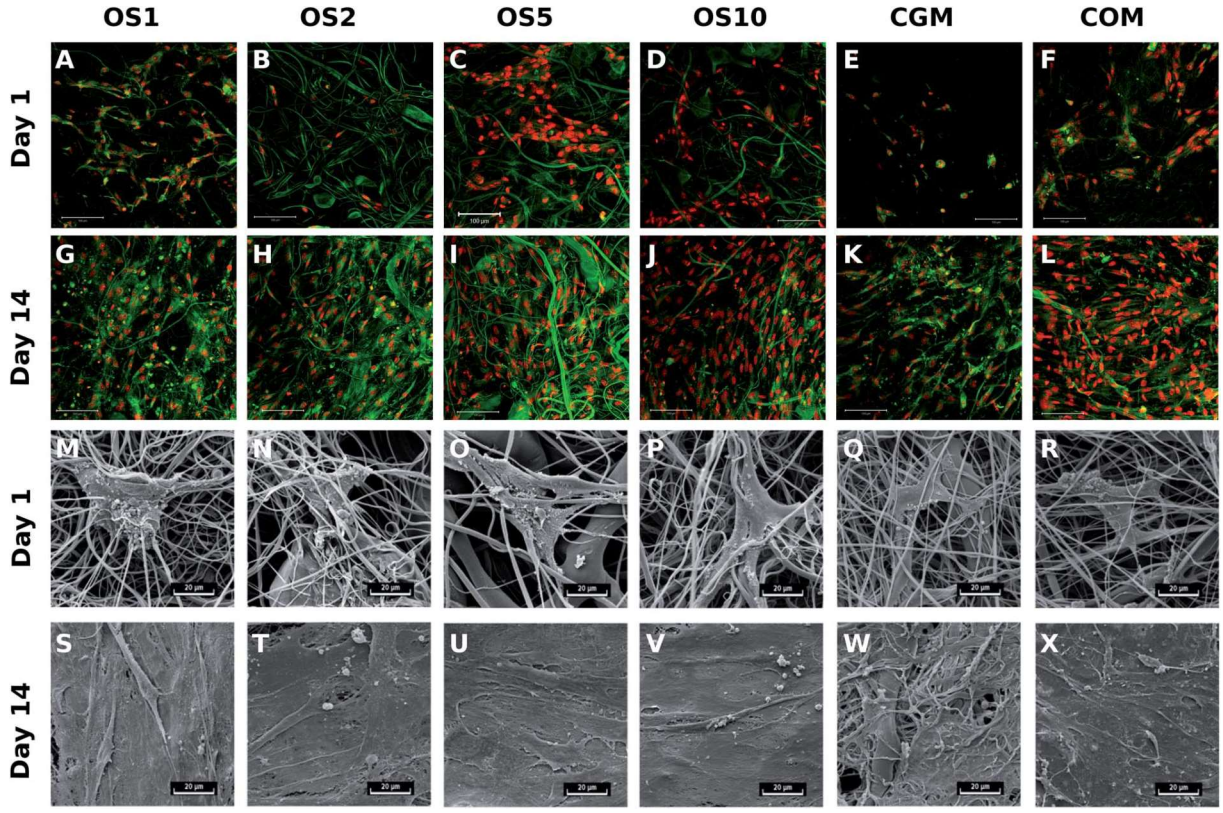

Fig. 8 Visualization of hMSCs adhesion and distribution on scaffolds using a confocal microscope. Cell nuclei were stained using propidium iodide (red color) and cell internal membranes using DiOC3 (green color). Magnification 200×, scale 100 μm (A–L). hMSCs adhesion and interaction on fibrous scaffolds visualized using scanning electron microscopy. Magnification 3000×, scale 20 μm (M–X).

Relative expression of type I collagen, an osteogenic marker, was evaluated on days 1, 7 and 14 (Fig. 5C). On day 1, cells on the OS10 sample expressed type I collagen statistically the most of all tested samples. On day 7 the normality test failed, thus one-way Anova on ranks revealed only that type I collagen expression on the OS5 sample was statistically significant in comparison to the COM sample. However, we can observe a trend that not only the OS5 samples induced higher expression but also the OS2 and OS10 samples promoted the expression of type I collagen in comparison to both control groups. On day 14, the highest expression of type I collagen was detected on the OS5 sample, followed by OS2 sample.

3.4 hMSCs adhesion, proliferation and metabolic activity on scaffolds

Cell proliferation was measured as the amount of DNA present on the scaffolds on days 1, 3, 7, 14, and 21 (Fig. 7A). On day 1, cells adhered similarly on all scaffolds. On the following days 7 and 14, the largest number of cells was seen on the OS10 sample. Moreover, on day 7, comparable amount of DNA was shown on COM. However, amount of cells decreased on COM on day 14. On day 21, the cell number decreased on all samples and was comparable to each other except for OS5, where the DNA amount was the lowest.

The metabolic activity of the cells was measured using an MTS assay (Fig. 7B). The highest absorbance was measured on OS5 on day 1. On the OS2 sample, measured absorbance was higher compared to the CGM. On day 3, metabolic activity was comparable on all samples. On day 7, absorbance was the highest on the COM. On day 14, the highest metabolic activity was measured on the OS10 and CGM samples. There was no difference measured in metabolic activity between the samples on day 21. As OS are standardly added into the hMSC's culture media for induction of osteogenic differentiation we observed no detrimental or strong positive effect of OS, released from scaffolds, on hMSCs proliferation and metabolic activity.

To visualize the adhesion and distribution of hMSC on scaffolds, cells were labeled using fluorescence staining and detected using confocal microscopy and also detected using SEM. As it is visible from Fig. 8, cells adhered on all scaffolds, but the best adhesion was shown on OS5. In the following days of the experiment, cell's density continuously increased. Results correlated well with data from DNA quantification.

3.5 Osteogenic differentiation of hMSCs

Osteogenic differentiation of hMSC was detected as an activity of ALP and qPCR analysis of osteogenic markers. ALP activity was similar in all samples on day 1 (Fig. 9A). On day 7, the highest activity was detected on the COM sample. The activity was higher on OS10 compared to OS1. On day 14 and 21, ALP activity was higher on the COM sample compared to CGM and OS2, but with other samples it was on the same statistical level.

qPCR was used to detect the expression of proteins typically associated with osteogenic differentiation. RunX2 was chosen as an early osteogenic marker (Fig. 8B). The highest expression was detected on the OS2 sample on day 1. On day 7, the highest expression was seen on the OS5 and OS10 samples. Last day, day

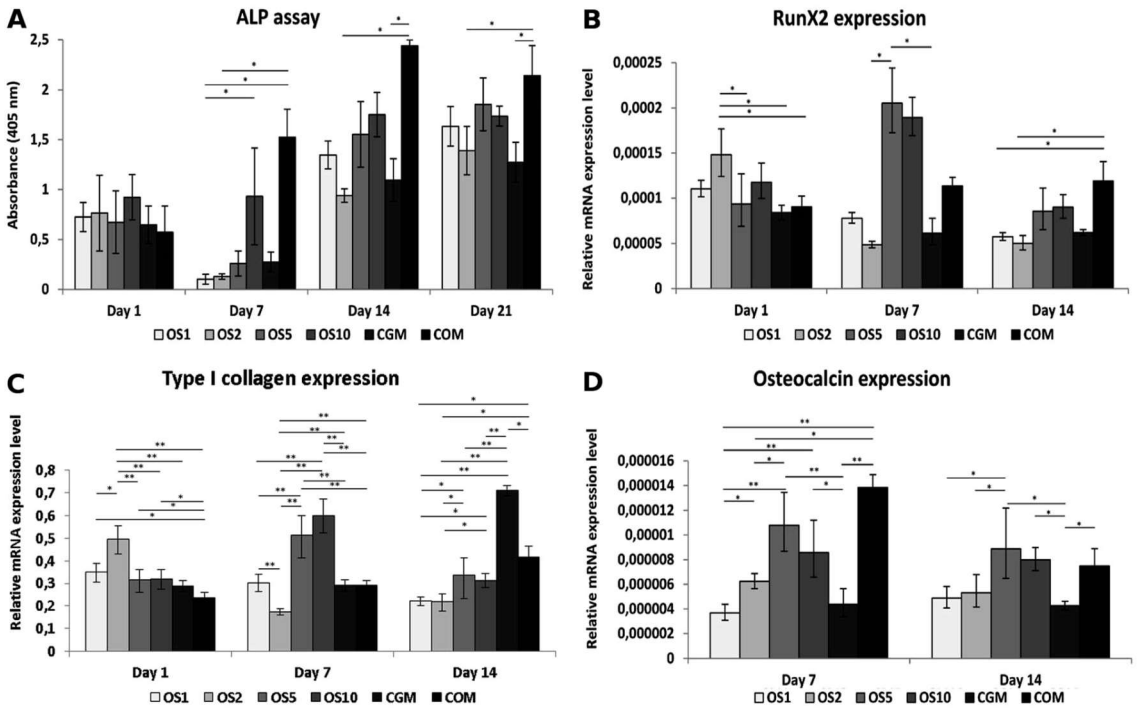

Fig. 9 Osteogenic differentiation of hMSCs was detected using ALP activity measurement and qPCR analysis of osteogenic markers. ALP activity of hMSCs (A), relative expression of RunX2 (B), type I collagen (C) and osteocalcin (D) was determined by qPCR analysis. Statistical significance is shown above the columns (*$p < 0.05$; **$p < 0.01$).

14, on the COM sample we observed highest expression of mRNA for RunX2. Similar to RunX2, type I collagen was the most expressed on OS2 on day 1 (Fig. 9C). On day 7, the highest expression was seen on the OS5 and OS10 samples. The expression of type I collagen decreased on these samples on day 14, when the most expressed protein was detected on the CGM sample. The expression of osteocalcin (Fig. 8D), the late osteogenic marker, was low, but there were still significant differences between the samples. The highest expression of osteocalcin was detected on the OS5, OS10 and COM samples respectively on day 7 and 14.

To visualize expressed osteocalcin on the samples, protein was stained using immunofluorescence staining and observed using confocal microscopy. Osteocalcin production was very low on day 7 (data not shown) as it is a late marker of osteogenic differentiation. On day 14, osteocalcin was visible mainly on the OS5, OS10 and COM samples (Fig. 6G–L).

3.6 *In vivo* regeneration of critical size bone defect using fibrous scaffold with OS

Scaffold OS5 (with 200 μg mL^{-1} ascorbate-2-phosphate, 50 mM β-glycerol phosphate, 500 nM dexamethasone) was further

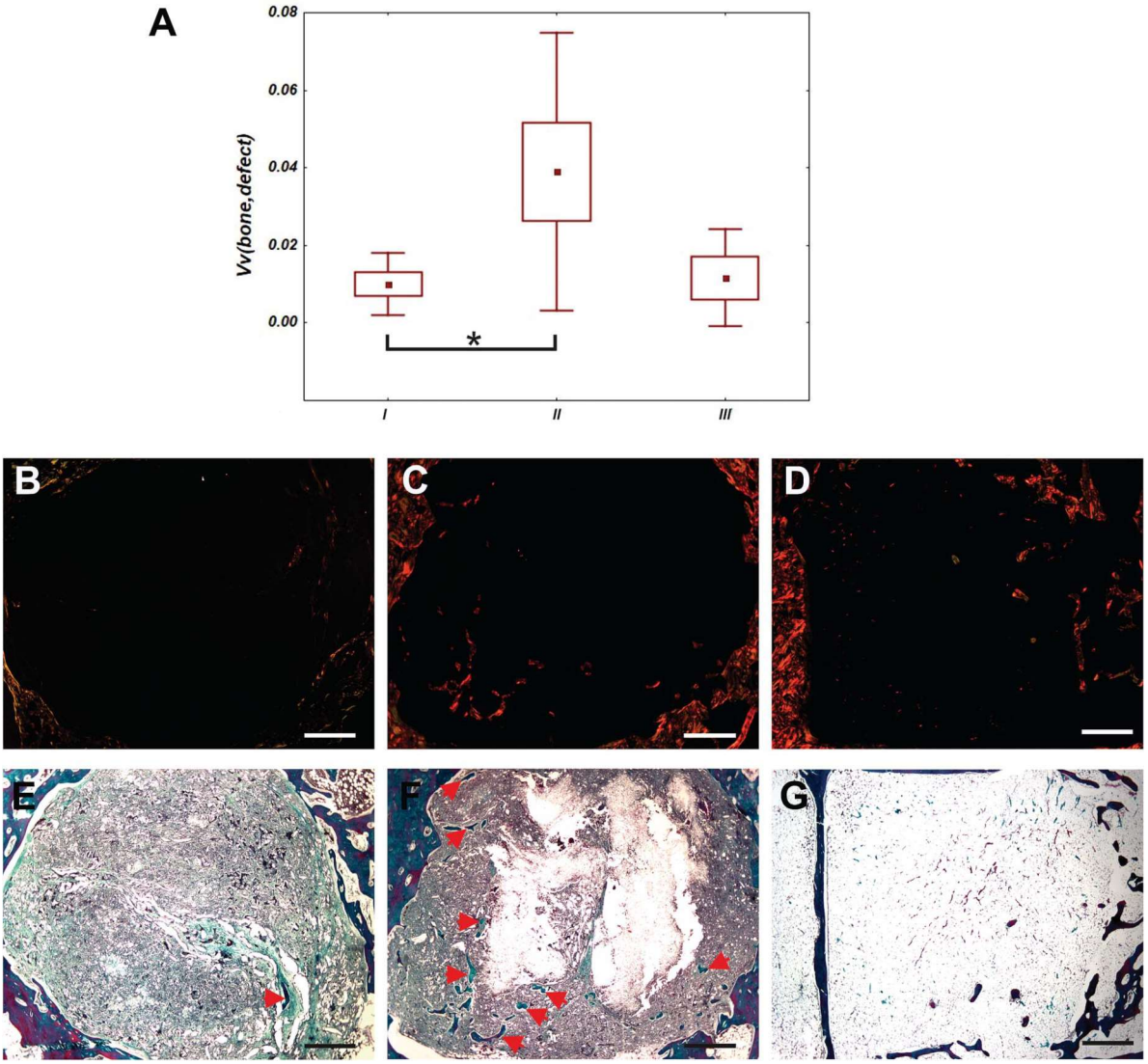

Fig. 10 Between-group comparison of bone volume. Bone quantity was expressed as volume fraction (V_v) of bone tissue within the whole reference volume of the defect (Box and Whisker plot showing mean, standard error, and standard deviation. The differences were considered statistically significant as $*p < 0.05$). Bone tissue and collagen connective tissue contain type I collagen were stained using picrosirius red (A). In group I (B) and II (C), newly formed bone trabecules were found in outer compartment of bone defect. In group III (D), there was mainly adipose tissue and small vessels in bone defect. Newly formed bone trabecules were stained using Verhoeff's haematoxylin with green trichrome. In group I (E) and II (F), a few newly formed bone trabecules (red arrows) were found in outer compartment of bone defect. In group III (G), there was mainly adipose tissue in bone defect. Scale 1000 μm.

tested *in vivo* on a rabbit model. Bone regeneration was tested in a critical sized defect in femur condyle for 12 weeks. The scaffold showed good manipulation during the surgical procedure. There was no evidence of any inflammation or any complication of healing. All defects in both groups were completely filled with newly formed tissue. Joint cavities were without any sign of inflammation. All animals survived to the date of scheduled euthanasia.

3.7 Histological evaluation of regenerated bone defects

Defects of control group were filled mainly with adipose tissue (Fig. 10). In defects filled with fibrous scaffolds, the newly formed bone trabecules were found preferentially in the outer compartment. Some bone trabecules were found also in the middle compartment, but none in the inner compartment. In group II, the total bone volume within the whole defect was greater than in group I ($p < 0.05$). There was no difference between bone volume within the whole defect in group I and group III ($p = 1$). There was no significant difference between bone volume within the whole defect in group II and group III ($p = 0.064$). Differences of bone volume in the outer, middle and central compartments were no significant. There were not found inflammation reaction for the scaffolds and their components. Occasionally, small deposit of inflammation white cells and multinucleated giant cells from foreign bodies were found.

4 Discussion

Centrifugal spinning technology enables the formation of nanostructured 3D scaffolds with fibrous morphology. As we have shown in our previous works, 3D nanofibers prepared by centrifugal spinning technology are beneficial for the stimulation of cell adhesion and proliferation.[18] The fibrous meshes were prepared from PCL – biocompatible and biodegradable polyester widely used in tissue engineering applications. PCL fibrous scaffolds were tested *in vitro* in various settings.[17,24–30] These studies demonstrate the potential of fibrous scaffolds for bone tissue engineering.

However, despite the bio mimicking properties of fibrous scaffolds, the improved osteoinductive properties could be achieved by release of active molecules. Fibrous scaffolds serve as drug delivery systems for encapsulated bioactive compounds and enable prolongation of their bioavailability. A variety of combinations of fibrous scaffolds with bioactive compounds like BMP-2, vascular growth factor or basic fibroblast growth factor was reported.[18,31–38] However, use of growth factors is problematic due to their price, stability and lack of medical approval (*i.e.* by the EMA or FDA). For instance, for bone tissue engineering only two growth factor formulations are approved to date – BMP-2 (Infuse) and BMP-7 (Osigraft).[39] Therefore, alternative osteoinductive supplements are applied in bone tissue engineering. Platelets are valuable sources of osteoinductive growth factors and their use as a natural product enable efficient combination with scaffolds for application in bone tissue engineering.[18,21,37] In addition, OS were shown to efficiently stimulate osteogenic differentiation of MSCs and stimulate osteogenic cells. Among these molecules, dexamethasone, ascorbic acid, vitamin D3, β-glycerol phosphate and L-proline are the most efficient molecules.

In the current work, we prepared novel 3D scaffolds by centrifugal spinning of a blend containing PCL as a matrix forming polymer and β-glycerol phosphate, ascorbate-2-phosphate and dexamethasone as pro-osteogenic drugs. The technology of blend centrifugal spinning was reported by Mary *et al.*[40] for short term delivery of tetracycline. When used as systems for bone tissue engineering, the scaffolds should be able to release the content for prolonged periods (weeks to months). The centrifugal spinning process enabled the formation of scaffolds with high loading of active molecules. The β-glycerol phosphate was dissolved in concentrations from 40 mg g^{-1} of PCL to 400 mg g^{-1} of PCL, ascorbate-2-phosphate in concentrations from 750 μg g^{-1} of PCL to 7500 μg g^{-1} of PCL. Dexamethasone was present in low concentrations due to the strong stimulation properties of transcription and potential toxic effect at higher concentration.[41] OS were dissolved in PCL solution and processed *via* centrifugal spinning. The loading of high concentrations of OS shows the low affection of centrifugal spinning *via* the presence of OS. The mean fiber size for low concentrations was smaller than in the case of plain PCL. This could be connected with the increased conductivity of the polymeric solution. However, in the case of the OS5 sample, the size was significantly higher due to the presence of microfibers. The increase is connected with the increased internal viscosity of the sample caused by the interaction of PCL chains and β-glycerol phosphate. Similarly, the number of pores bigger than 5 μm^2 was highest in the OS5 sample. Interestingly, sample OS10 showed a decreased mean fiber diameter and lower presence of pores bigger than 5 μm^2. However, the sample contained higher presence of defects indicating that increase of osteogenic additive concentration in OS10 group results in aberrant fiber formation. This could be caused by increased cohesion of polymeric solution and thus lower elongation of emitted polymeric droplet resulting in formation of non-fibrous defects. The results indicated that the blend centrifugal spinning process enables the incorporation of high concentrations of OS without the loss of the fibrous properties of the scaffolds, however the diameter and quality of fibers is decreasing with OS supplement concentration increase.

The presence of OS in the samples was confirmed by FTIR-ATR spectroscopy and RTG analysis of samples in HR-SEM. The infrared spectroscopy identified an increase in bands corresponding to OS, indicating the successful encapsulation of OS. The signal showed dose dependent behavior and with higher concentrations of added OS the signal was stronger. The RTG analysis of elements on the surface of fibers showed that with increased concentrations of drugs in solution, the amount of C decrease and amount of P and O increase. This indicates that O and P from β-glycerol phosphate, dexamethasone and ascorbate-2-phosphate are present in the structure of the scaffold. Nevertheless, the map of spatial distribution of phosphate shows distribution to distinct spots on the fibers. The spots are probably crystals of β-glycerol phosphate formed between PCL

chains. The number of spots increases with the concentration of OS and leads to the formation of a connected network of active molecule aggregates. The structure impacts the scaffold's release properties. The internal morphology of the fibers is among the most crucial variables affecting the release kinetics from emulsion nanofibers. As in other nanofiber types, release from osteogenic molecule loaded nanofibers is governed by diffusion or degradation mechanisms.[42] The degradation mechanism is dominant in fibers from degradable materials. Upon degradation, the drugs are liberated from the polymeric structure depending on the dissolution of the polymeric matrix.[43,44] Since PCL is a slowly degradable material, this type of release is less dominant in the case of our fibers. The release from materials that are non-degradable in the timeframe of drug release is governed by diffusion rate through the polymeric matrix.[45] In the case of the proposed scaffolds, the rate limiting factor is the diffusion rate of water and drugs through the polymeric matrix polymer. The rate is dependent on the internal structure of the fibers and the number of contact points available for the solvent to dissolve the core polymer. In the case of fibers with non-continuous islands of active molecule, the release depends on the interconnection of such aggregates.[37] The solvent dissolves first, and the aggregates on the surface of the fibers result in rapid release of their cargo. If the droplets are not interconnected or the solvent diffusion is slowed down, the availability of the drug decreases. The lower loading of OS in the OS1 and OS2 samples resulted in a lower number of aggregates along the fibers. However, the release data indicate that most of the drugs containing phosphate, β-glycerol phosphate and ascorbate-2-phosphate, were able to diffuse out of the fiber and 80% of the drug was released on day 31. On the contrary, the structure of the fibers with higher loading (OS5 and OS10) showed numerous contact points on the surface. In the case of aggregate interconnection, the solvent could reach aggregates deeper in the fibers and result in sustained release of high concentrations of OS. The release of OS5 and OS10 fibers was continuous over the release period and a higher total amount of OS was released, as illustrated by the model of measured phosphate release. The fibers were able to release high concentrations of OS over the 31 day period. Nevertheless, the release at day 31 was about 60% and the release rate was constant, without slowing down and achieving release plateau. Therefore, the scaffold seemed to further release the OS even after the release monitoring period. Such long-term releasing system is advantageous for bone tissue engineering applications. A similar microparticle-based system for the delivery of OS was shown to release β-glycerol phosphate for 25 days.[11] However, upon incomplete encapsulation, the small molecules due to their high solubility in aqueous solvents often show burst release.[12,46] For instance, dexamethasone loaded electrospun PCL scaffolds were able to release dexamethasone for 6 days, however, more than 50% of the drug was released during the first 24 hours. Despite fast release, system was able to stimulate osteogenic differentiation of hMSCs.[47] Lower encapsulation rate may be attributed to loss during centrifugal spinning process, where with increased concentration of active molecules, the number of defects and fiber morphology was decreased. Therefore, the non-fibrous defects had different trajectory after emission from spinerete resulting in lower accumulation on collector. This resulted in decreased encapsulation efficiency. However, the non-linearity of encapsulation efficiency still resulted in scaffold formation with different active molecule content.

The fibrous scaffolds with OS were further tested on relevant cell types – the Saos2 osteosarcoma cell line and hMSCs. The test on the Saos2 cell line showed improved proliferation and viability on OS loaded scaffolds compared to control scaffolds both in osteogenic and non-osteogenic medium. Similarly, the scaffolds with OS showed increased production of osteocalcin (protein production increase) and type I collagen (mRNA increase). The indirect immunostaining method of osteocalcin was performed on day 21 on cultivated Saos2 cells. We observed higher doses of osteocalcin on all samples with incorporated OS in comparison to both control groups. Type I collagen showed the highest mRNA expression on samples OS2–OS10, compared to both control groups in the case of cultivated Saos2 cells, meaning that higher doses of OS on the COM sample had a negative effect on the expression of type I collagen in cultured Saos2. The results clearly demonstrated the positive effect of released OS on Saos2 cells.

hMSCs that were seeded on the same scaffolds showed different trends during the culture period. The amount of DNA as well as metabolic activity were comparable for the whole time of the culture period, meaning that the incorporation of OS showed no positive as well as no detrimental effect on cell culture. Those results are in agreement with results obtained by confocal microscopy and SEM observation. Similar results were obtained by Shi *et al.* who tested the effect of released OS from microspheres on hMSC proliferation. The best cell proliferation was observed on the control group cultivated in growth medium.[11] Peter *et al.*[48] confirmed that after rat MSC reached confluency the ongoing exposure of cells to OS had no further positive effect on cell proliferation. However, experiments that study the effect of OS on hMSCs, seeded in lower cell density in comparison to our cell seeding density, indicate the positive effect of OS in culture medium on cell proliferation or metabolic activity,[49,50] meaning that in confluent cell layers there are other important factors that mainly affect cell differentiation. However, the results of the study show the osteoinductive properties of the prepared scaffolds. ALP activity was measured on the scaffold cultured with hMSCs to study the effect of released OS on the osteogenic differentiation of hMSCs. The trend in ALP activity of cells cultivated on scaffolds with incorporated OS was slightly lower in comparison to the COM samples, but higher compared to cell cultured in growth medium. Many studies have tested ALP activity in diverse cultivation conditions. However, the complete differentiation medium reaches the best ALP activity in cultured hMSCs.[48–50] Expression of mRNA for key osteogenic transcription factor – RunX2 was observed on the OS1–10 scaffolds. hMSCs cultivated on samples marked as OS5 and OS10 reached the peak in expression of mRNA for RunX2 on day 7. A higher amount of expressed mRNA for type I collagen was observed on day 7 on the OS5 and OS10 samples and on day 14 on the CGM sample.

In addition, the differentiation into osteogenic lineage was confirmed by the indirect immunostaining method of osteocalcin. On day 14 we observed stained osteocalcin on the OS5, OS10 and COM samples. Thus, we conclude that the presence of OS in higher doses influenced the osteogenic differentiation. Osteocalcin visualization on hMSCs is in agreement with the results obtained by qPCR. These findings again indicated that the OS5, OS10 and COM samples promoted the osteogenic differentiation the most of all tested groups. This means that the incorporation of OS in samples marked as OS5 and OS10 showed a comparable effect to OS freely added into growth medium at the concentration standardly used for the induction of osteogenic differentiation *in vitro*. Those results are in agreement with the study of Shi *et al.*[11] who observed the highest expression of mRNA for RunX2, type I collagen and osteocalcin on scaffolds releasing OS.

Osteoinductive properties of the centrifugal spun scaffold releasing OS were confirmed in *in vivo* study. While defects of the control group were filled dominantly with the adipose tissue, cells from surrounding tissues infiltrated the fibrous scaffolds and started to form bone trabecules. Fibers served to cells as a scaffolding material helping them to settle inside the defect and synthetized bone ECM. Bone trabecules were formed preferentially from the side of the defect, what is typical for cell-free scaffolds. OS released from the scaffolds induced osteoinduction, the amount of the bone trabecules was higher compared to PCL fibers without the OS.

The proposed scaffolds showed the osteoinductive properties and show high potential for application in cell-free tissue engineering. The use of the cell-free scaffolds possesses several advantages compared to scaffolds that are seeded with cells prior to implantation into the defect site. The aspiration of cells is connected with an extra surgical procedure that could lead on the donor side to morbidity, pain or inflammation. Moreover, during the *ex vivo* expansion and cultivation the cells can undergo unwanted phenotypic changes. Thus, cell-free scaffolds designated as drug delivery carriers can induce in the defect cell migration, proliferation and finally differentiation into the desired cell type.[16] Besides osteoinductive properties, the scaffolds based on centrifugal spinning technology are highly advantageous in the formation of the real 3D structure of the scaffolds. Classical electrospun scaffolds have limited thickness and pore size, which does not enable rapid cell penetration into the scaffolds.[17,51] Centrifugal spinning technology enables the penetration of cells thorough the fibrous scaffold without the need for additional components (*i.e.* like salt crystals).[51] Scaffold porosity is an important property in bone tissue engineering. Generally, pores of a size of less than 100 μm do not favor the ingrowth of mineralized extracellular matrix and also do not support cell migration.[52] Optimal pore size for bone tissue engineering ranges from 100–400 μm.[53] However, *in vivo* study where PCL scaffolds with the range of pore diameters from 350–800 μm were tested did not reveal differences in new bone formation.[54] In our case, the maximal pore size of the scaffolds was about 200 μm^2, which facilitated cell penetration thorough the scaffolds. It was proved in our previous study, where cells cultured in static conditions penetrated into the depth of 80–100 μm.[18] In the case of the OS10 sample, the pore size was lower, which may hamper *in vivo* bone formation using these scaffolds.

5 Conclusion

The above-mentioned properties of prepared OS releasing scaffolds clearly shows that the fibrous scaffolds prepared by blend centrifugal spinning technology are promising for application in bone tissue engineering. The materials prepared of PCL are biodegradable, biocompatible and the polymer is approved by the FDA for medical use. In addition, the utilized OS could be obtained in qualities applicable in medicine. Compared to growth factors, OS are longer lasting molecules with prolonged activity in solutions[11] and could be obtained at a lower price. Combined with the results of the *in vitro* study, the prepared scaffolds served as drug delivery systems releasing OS for a period of 31 days and were shown to have favorable morphological and osteoinductive properties for use in bone tissue engineering. These scaffolds, with incorporated OS, showed enhanced metabolic activity and cell proliferation while Saos2 cells were cultivated. According to the differentiation assays from the Saos2 and hMSCs cultivation, we conclude that the sample marked OS5 was the most potent one to induce osteogenic differentiation *in vitro* for both cell types. The obtained results were comparable or better than the sample, where the cells were cultivated in medium with added OS. Osteoinductive properties of OS5 scaffold were further confirmed in *in vivo* study on critical sized bone defect of rabbit. This scaffold, serving as drug delivery system, has great potential for bone tissue engineering as it is osteoinductive, porous, 3D and able to allow the sustained release of OS lasting for up to one month.

Conflicts of interest

There are no conflicts to declare.

Acknowledgements

This study has been supported by the Czech Science Foundation (grants no. 15-15697S, 16-14758S), the Ministry of Education, Youth, and Sports of the Czech Republic (Research Programs NPU I:LO1309, NPU I:LO1508) and the Internal Grant Agency of the Ministry of Health of the Czech Republic (MZ-VES project no. 16-29680A, 16-28637A, 17-32285A and 17-31276A) and MV projects no. VI20152018010, MOTOL 9775.

References

1 R. Lucas, A. Martins, M. Severo, P. Silva, T. Monjardino, A. R. Gaio, C. Cooper and H. Barros, *Sci. Rep.*, 2017, 7, 3754.
2 M. Mehta, K. Schmidt-Bleek, G. N. Duda and D. J. Mooney, *Adv. Drug Delivery Rev.*, 2012, **64**, 1257–1276.
3 J. Wiltfang, F. R. Kloss, P. Kessler, E. Nkenke, S. Schultze-Mosgau, R. Zimmermann and K. A. Schlegel, *Clin. Oral Implants Res.*, 2004, **15**, 187–193.

4 J. C. Banwart, M. A. Asher and R. S. Hassanein, *Spine*, 1995, **20**, 1055–1060.
5 R. Dimitriou, G. I. Mataliotakis, A. G. Angoules, N. K. Kanakaris and P. V. Giannoudis, *Injury*, 2011, **42**(suppl 2), S3–S15.
6 M. Saini, Y. Singh, P. Arora, V. Arora and K. Jain, *World J. Clin. Cases*, 2015, **3**, 52–57.
7 M. A. Velasco, C. A. Narváez-Tovar and D. A. Garzón-Alvarado, *BioMed Res. Int.*, 2015, **2015**, 729076.
8 P. V. Giannoudis, H. Dinopoulos and E. Tsiridis, *Injury*, 2005, **36**(suppl 3), S20–S27.
9 J. R. Woodard, A. J. Hilldore, S. K. Lan, C. J. Park, A. W. Morgan, J. A. Eurell, S. G. Clark, M. B. Wheeler, R. D. Jamison and A. J. Wagoner Johnson, *Biomaterials*, 2007, **28**, 45–54.
10 E. Filova, M. Rampichova, A. Litvinec, M. Drzik, A. Mickova, M. Buzgo, E. Kostakova, L. Martinova, D. Usvald, E. Prosecka, J. Uhlik, J. Motlik, L. Vajner and E. Amler, *Int. J. Pharm.*, 2013, **447**, 139–149.
11 X. Shi, Y. Wang, R. R. Varshney, L. Ren, Y. Gong and D.-A. Wang, *Eur. J. Pharm. Sci.*, 2010, **39**, 59–67.
12 H. Kim, H. Suh, S. A. Jo, H. W. Kim, J. M. Lee, E. H. Kim, Y. Reinwald, S.-H. Park, B.-H. Min and I. Jo, *Biochem. Biophys. Res. Commun.*, 2005, **332**, 1053–1060.
13 S. Srouji, I. Blumenfeld, A. Rachmiel and E. Livne, *Cell Tissue Banking*, 2004, **5**, 223–230.
14 X. Niu, Q. Feng, M. Wang, X. Guo and Q. Zheng, *J. Controlled Release*, 2009, **134**, 111–117.
15 P. Yilgor, K. Tuzlakoglu, R. L. Reis, N. Hasirci and V. Hasirci, *Biomaterials*, 2009, **30**, 3551–3559.
16 E. Amler, E. Filova, M. Buzgo, E. Prosecka, M. Rampichova, A. Necas, P. Nooeaid and A. R. Boccaccini, *Nanomedicine*, 2014, **9**, 1083–1094.
17 M. Rampichova, J. Chvojka, M. Buzgo, E. Prosecka, P. Mikes, L. Vyslouzilova, D. Tvrdik, P. Kochova, T. Gregor, D. Lukas and E. Amler, *Cell Proliferation*, 2013, **46**, 23–37.
18 M. Rampichová, M. Buzgo, A. Míčková, K. Vocetková, V. Sovková, V. Lukášová, E. Filová, F. Rustichelli and E. Amler, *Int. J. Nanomed.*, 2017, **12**, 347–361.
19 J. Kocova, *Folia Morphol.*, 1970, **15**, 293–295.
20 M. Rampichova, J. Chvojka, V. Jencova, T. Kubikova, Z. Tonar, j. Erben, M. Buzgo, j. Dankova, A. Litvinec, K. Vocetkova, M. Plencner, E. Prosecka, V. Sovkova, V. Lukasova, M. Kralickova, D. Lukas and E. Amler, *Biomed. Mater.*, 2018, **13**(2), 025004.
21 E. Prosecká, M. Rampichová, A. Litvinec, Z. Tonar, M. Králíčková, L. Vojtová, P. Kochová, M. Plencner, M. Buzgo, A. Míčková, J. Jančář and E. Amler, *J. Biomed. Mater. Res., Part A*, 2015, **103**, 671–682.
22 Q. Chen, D. Zielinski, J. Chen, A. Koski, D. Werst and S. Nowak, *J. Pharm. Biomed. Anal.*, 2008, **48**, 732–738.
23 R. B. Friedrich, A. Ravanello, L. C. Cichota, C. M. B. Rolim and R. C. R. Beck, *Quim. Nova*, 2009, **32**, 1052–1054.
24 K. Vocetkova, M. Buzgo, V. Sovkova, D. Bezdekova, P. Kneppo and E. Amler, *Cell Proliferation*, 2016, **49**, 568–578.
25 J. Venugopal, L. L. Ma, T. Yong and S. Ramakrishna, *Cell Biol. Int.*, 2005, **29**, 861–867.
26 Y. M. Ko, D. Y. Choi, S. C. Jung and B. H. Kim, *J. Nanosci. Nanotechnol.*, 2015, **15**, 192–195.
27 L. Koepsell, L. F. Zhang, D. Neufeld, H. Fong and Y. Deng, *Macromol. Biosci.*, 2011, **11**, 391–399.
28 H. Yoshimoto, Y. M. Shin, H. Terai and J. P. Vacanti, *Biomaterials*, 2003, **24**, 2077–2082.
29 R. A. Thibault, L. Scott Baggett, A. G. Mikos and F. K. Kasper, *Tissue Eng., Part A*, 2010, **16**, 431–440.
30 R. Kang, Y. Luo, L. Zou, L. Xie, H. Lysdahl, X. Jiang, C. Chen, L. Bolund, M. Chen, F. Besenbacher and C. Bunger, *RSC Adv.*, 2014, **4**, 5734–5739.
31 X. L. Jia, C. G. Zhao, P. Li, H. Zhang, Y. Huang, H. Li, J. Fan, W. Feng, X. Y. Yuan and Y. B. Fan, *J. Biomater. Sci., Polym. Ed.*, 2011, **22**, 1811–1827.
32 W. X. Cao, H. Zhang and X. Y. Yuan, *Chem. J. Chin. Univ.*, 2011, **32**, 1396–1400.
33 Y. Su, Q. Q. Su, W. Liu, J. R. Venugopal, X. M. Mo, S. Ramakrisha and C. T. Donghua Univ, *BMP2/ Dexamethasone Loaded and Release from Core-shell Nanofibers for Bone Tissue Engineering*, Donghua Univ Press, Shanghai, 2011.
34 L. H. Yin, S. H. Yang, M. M. He, Y. C. Chang, K. J. Wang, Y. D. Zhu, Y. H. Liu, Y. R. Chang and Z. H. Yu, *J. Mater. Sci.: Mater. Med.*, 2017, **28**, 15.
35 H. Zhang, J. Liang, Y. Ding and P. Li, *Mater. Lett.*, 2016, **181**, 119–122.
36 M. Rubert, J. Dehli, Y. F. Li, M. B. Taskin, R. D. Xu, F. Besenbacher and M. L. Chen, *J. Mater. Chem. B*, 2014, **2**, 8538–8546.
37 M. Buzgo, M. Rampichova, K. Vocetkova, V. Sovkova, V. Lukasova, M. Doupnik, A. Mickova, F. Rustichelli and E. Amler, *RSC Adv.*, 2017, **7**, 1215–1228.
38 M. D. Schofer, S. Fuchs-Winkelmann, C. Gräbedünkel, C. Wack, R. Dersch, M. Rudisile, J. H. Wendorff, A. Greiner, J. R. J. Paletta and U. Boudriot, *Sci. World J.*, 2008, **8**.
39 M. P. G. Bostrom and D. A. Seigerman, *HSS J.*, 2005, **1**, 9–18.
40 L. Amalorpava Mary, T. Senthilram, S. Suganya, L. Nagarajan, J. Venugopal, S. Ramakrishna and V. R. Giri Dev, *eXPRESS Polym. Lett.*, 2013, **7**, 238–248.
41 C. K. Yeung, K. P. Chan, C. K. M. Chan, C. P. Pang and D. S. C. Lam, *Jpn. J. Ophthalmol.*, 2004, **48**, 236–242.
42 R. Srikar, A. L. Yarin, C. M. Megaridis, A. V. Bazilevsky and E. Kelley, *Langmuir*, 2008, **24**, 965–974.
43 T. J. Sill and H. A. von Recum, *Biomaterials*, 2008, **29**, 1989–2006.
44 J. Zeng, L. Yang, Q. Liang, X. Zhang, H. Guan, X. Xu, X. Chen and X. Jing, *J. Controlled Release*, 2005, **105**, 43–51.
45 M. Gandhi, R. Srikar, A. L. Yarin, C. M. Megaridis and R. A. Gemeinhart, *Mol. Pharm.*, 2009, **6**, 641–647.
46 H. Kim, H. W. Kim and H. Suh, *Biomaterials*, 2003, **24**, 4671–4679.
47 A. Martins, A. R. C. Duarte, S. Faria, A. P. Marques, R. L. Reis and N. M. Neves, *Biomaterials*, 2010, **31**, 5875–5885.
48 S. J. Peter, C. R. Liang, D. J. Kim, M. S. Widmer and A. G. Mikos, *J. Cell. Biochem.*, 1998, **71**, 55–62.

49 M. J. Coelho and M. H. Fernandes, *Biomaterials*, 2000, **21**, 1095–1102.
50 N. Jaiswal, S. E. Haynesworth, A. I. Caplan and S. P. Bruder, *J. Cell. Biochem.*, 1997, **64**, 295–312.
51 M. Rampichova, M. Buzgo, J. Chvojka, E. Prosecka, O. Kofronova and E. Amler, *Cell Adhes. Migr.*, 2014, **8**, 36–41.
52 S. F. Hulbert, F. A. Young, R. S. Mathews, J. J. Klawitter, C. D. Talbert and F. H. Stelling, *J. Biomed. Mater. Res.*, 1970, **4**, 433–456.
53 S. H. Oh, I. K. Park, J. M. Kim and J. H. Lee, *Biomaterials*, 2007, **28**, 1664–1671.
54 S. M. M. Roosa, J. M. Kemppainen, E. N. Moffitt, P. H. Krebsbach and S. J. Hollister, *J. Biomed. Mater. Res., Part A*, 2010, **92A**, 359–368.